

**THE
PYROLYSIS OF SOME
METHYLCHLOROSILANES**

This thesis, by Christopher E. Dean, is submitted for
the degree of Doctor of Philosophy.

Department of Chemistry
Leicester University

March 1983

UMI Number: U334040

All rights reserved

INFORMATION TO ALL USERS

The quality of this reproduction is dependent upon the quality of the copy submitted.

In the unlikely event that the author did not send a complete manuscript and there are missing pages, these will be noted. Also, if material had to be removed, a note will indicate the deletion.



UMI U334040

Published by ProQuest LLC 2015. Copyright in the Dissertation held by the Author.
Microform Edition © ProQuest LLC.

All rights reserved. This work is protected against
unauthorized copying under Title 17, United States Code.



ProQuest LLC
789 East Eisenhower Parkway
P.O. Box 1346
Ann Arbor, MI 48106-1346

THESIS
666499
25 7. 83



x752920935

STATEMENT

The accompanying thesis submitted for the degree of Ph.D entitled "The Pyrolysis of Some Methylchlorosilanes" is based on work conducted by the author in the Department of Chemistry of the University of Leicester mainly during the period between October 1979 and September 1981.

All the work recorded in this thesis is original unless otherwise acknowledged in the text or by references. None of the work has been submitted for another degree in this or any other University.

Signed

C. E. Deas

Date

7th March 1983

ACKNOWLEDGEMENT

I wish to thank my supervisor, Dr. I. M. T. Davidson for all his help and encouragement throughout my post-graduate study at Leicester.

Thanks also to the S.E.R.C. for financial support, to Dow Corning (Europe) Ltd., for additional finances and an abundant supply of methylchlorosilanes, and to Messrs. J. A. Brivati and P. E. Acton for keeping the electronics in working order and for their help in interfacing the computer to the mass spectrometer.

Finally, thanks to Ms. K. A. Nuttall for typing this thesis.

TO MY MOTHER AND FATHER

CONTENTS

	Page No.
<u>CHAPTER ONE - INTRODUCTION</u>	1
1.2 Silylenes versus Silyl Radicals	3
1.3 Measurement of Bond Dissociation Energies -	
Kinetic Methods	11
Pyrolysis	11
Pyrolysis with a Chain Inhibitor	14
Very Low Pressure Pyrolysis	17
Kinetic Equilibrium Method	18
1.4 Measurement of Bond Dissociation Energies -	
From Appearance Potentials	20
1.5 Calculation of Heats of Formation - Additivity	
Schemes	25
Allen Scheme	25
Benson and Luria Model	30
1.6 Silaethene Intermediates	34
<u>CHAPTER TWO - EXPERIMENTAL</u>	37
2.1 Apparatus and Method	38
2.2 Data Logging Systems	40
Earlier Data Collection System	41
Data Logger Replaced by Micro Computer	41
Eight-channel PP2	42
Latest System	42
2.3 Computer Interface	43
Hardware	43
Software	44
2.4 Some Features of the Experimental System	44
Leak in and Leak out	44
Determination of Pyrolysis Rate Constants	45

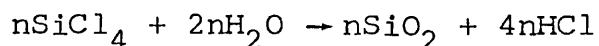
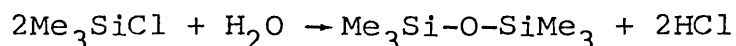
	Page No.
Determination of the Initial Amount of Reactant	47
Dead Space	47
Arrhenius Parameters	49
Product Formation	50
Fragmentation and Sensitivity Corrections	51
Interpolation of Data	51
<u>CHAPTER THREE - PYROLYSIS OF TRIMETHYLCHLOROSILANE</u>	52
3.1 Introduction	53
3.2 Pyrolysis of Trimethylchlorosilane	53
Summary of Earlier Work	54
Summary of Later Work	56
3.3 Pyrolysis Mechanism	57
Trimethylchlorosilane + Hydrogen Chloride	59
Trimethylchlorosilane + Oxygen	60
Trimethylchlorosilane + Hydrogen Bromide	62
3.4 Proposed Pyrolysis Mechanism	63
<u>CHAPTER FOUR - PYROLYSIS OF 1,1-DIMETHYL-1-SILACYCLO-</u> <u>BUTANE AND OF 1,1-DICHLORO-1-SILACYCLO-</u> <u>BUTANE</u>	65
4.1 Introduction	66
4.2 Initial Observations (Dimethyl- compound)	67
4.3 Dimethylsilacyclobutane + Hydrogen Chloride + Hydrogen Bromide	69
4.4 Dimethylsilacyclobutane + Hydrogen Chloride (3:1)	74
4.5 Test of Proposed Mechanism	77
4.6 Dimethylsilacyclobutane + Hydrogen Bromide	79

	Page No.
4.7 Pyrolysis of Dichlorosilacyclobutane	82
4.8 Decomposition Parameters for Dichlorosilacyclo- butane	83
<u>CHAPTER FIVE - PYROLYSIS OF DIMETHYLCHLOROSILANE AND OF</u> <u>METHYLDICHLOROSILANE</u>	87
5.1 Introduction	88
5.2 Pyrolysis of Dimethylchlorosilane	89
5.3 Formation of Products from Dimethylchlorosilane	91
5.4 Co-pyrolysis of Dimethylchlorosilane with Sulphur Hexafluoride	94
5.5 Proposed Pyrolysis Mechanism	95
5.6 Pyrolysis of Methyldichlorosilane	103
5.7 Formation of Products from Methyldichlorosilane	105
5.8 Co-pyrolysis of Methyldichlorosilane with Sulphur Hexafluoride	106
5.9 Proposed Pyrolysis Mechanism	106
5.10 Discussion of the proposed mechanisms for Dimethyl- chlorosilane and for Methyldichlorosilane	110
<u>CHAPTER SIX - DISCUSSION</u>	112
<u>APPENDIX - COMPUTER PROGRAMS</u>	134
<u>REFERENCES</u>	151

CHAPTER ONE

INTRODUCTION

1.1 The methylchlorosilanes are industrially important as precursors to siloxane (silicone) polymers. A simple hydrolysis reaction followed by heating with a catalyst is sufficient to achieve this conversion. On hydrolysis, trimethylchlorosilane can only produce hexamethyldisiloxane, whereas tetrachlorosilane produces silica.



Of the di- and tri- chloro- members of the series $\text{Me}_n\text{SiCl}_{(4-n)}$, $n=0-3$, the former produces straight chains and the latter a complex cross-linked polymer.

By starting with various mixtures of the four precursors, polymeric materials with "tailor made" physical properties can be produced. The siloxanes so prepared have a great many applications, including use in resins, rubbers, water-repellents, lubricants and release agents¹.

The methylchlorosilanes themselves are prepared industrially by the "Direct Synthesis", yielding a complex mixture of products. The process involves passing methylchloride vapour through a mixture of powdered silicon and metallic silver or copper at about 537K¹. As well as the fully substituted methylchlorosilanes, tetrachlorosilane, some unsubstituted chlorosilanes and some disilanes are produced. The products are separated by fractional distillation. The whole synthesis and separation processes are carried out under an excess pressure of nitrogen to prevent hydrolysis of the products.

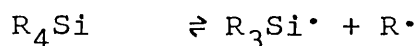
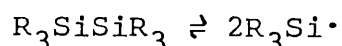
There is both industrial and fundamental interest

in the kinetics and mechanisms of thermal reactions involving methylchlorosilanes. In the decomposition of organosilicon compounds, silyl radicals $\text{H}_3\text{Si}\cdot$, analogous to alkyl radicals, silylenes $\text{H}_2\text{Si}:$, analogous to carbenes, and silaolefins eg. $\text{Me}_2\text{Si}=\text{CH}_2$ may be formed. Silylenes are easier to form thermally than carbenes and the interplay between silylene and silyl radical mechanisms in the pyrolysis of silicon compounds is of interest.

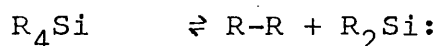
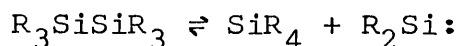
1.2 Silylenes versus Silyl Radicals.

Mono- or di- silanes may, on pyrolysis, dissociate to form either:-

(i) Two radical species



or (ii) A silylene and a stable molecule



The general factors which influence the formation of silylenes have been discussed by Davidson^{2,3}. A silylene will normally only be formed when the molecule formed with it contains a bond into which the silylene can readily insert. There is little quantitative information available, but silylenes insert rapidly into silicon-hydrogen bonds and into bonds between silicon and an atom with lone pairs of electrons eg. halogen, nitrogen and oxygen. Also, silylenes are known to insert into hydrogen chloride^{4,5}

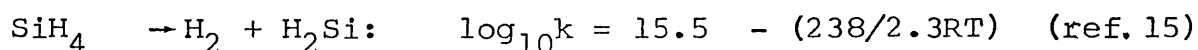
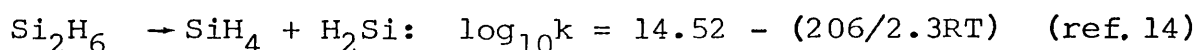
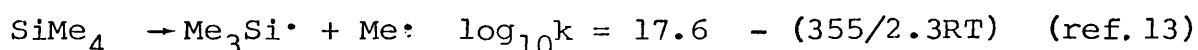
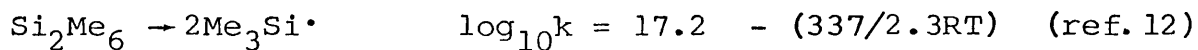
and into hydrogen^{6,7}. Insertion into silicon-carbon, carbon-carbon, or carbon-hydrogen bonds requires a relatively high activation energy^{8,9}. Some values for silylene insertions are shown in table 1.1.

Table 1.1.

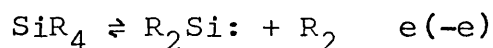
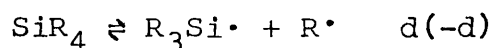
The activation energy (Ea) of some silylene insertion reactions.

Silylene	Inserting into	Ea/KJ mol ⁻¹	Ref.
Me ₂ Si:	Si-H	0	5
Me ₂ Si:	H-Cl	28	5
Me ₂ Si:	Me ₃ Si-CH ₃	79	10
H ₂ Si:	H-H	96	7,6
MeSiH	H-H	74	11

The following dissociate mainly as shown on thermolysis. Activation energies are in KJ mol⁻¹.



As shown by the examples above, for monosilanes, the two possible initial dissociation routes are:-²



The relationship between activation energy E, enthalpy change ΔH and bond dissociation energy D can be described thus:-

$$E(d) = \Delta H(d) + E(-d) \quad (i)$$

$$E(e) = \Delta H(e) + E(-e) \quad (ii)$$

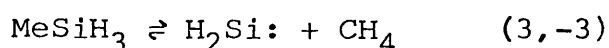
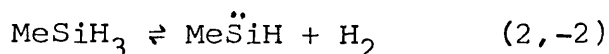
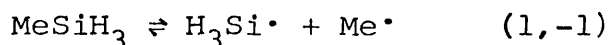
$$\Delta H(e) = D(R_3Si-R) + D(R_2\ddot{Si}-R) - D(R-R) \quad (iii)$$

$$\Delta H(d) = D(R_3Si-R) \quad (iv)$$

$$\Delta H(e) = \Delta H(d) - [D(R-R) - D(R_2\ddot{Si}-R)] \quad (v)$$

For silylene elimination to be thermodynamically favoured over radical production, a high value of $D(R-R)$ relative to $D(R_3Si-R)$ is required, thus reducing $\Delta H(e)$ compared with $\Delta H(d)$. The mechanisms of decomposition for trimethylsilane (Me_3SiH)¹⁶ and methylsilane ($MeSiH_3$)¹¹ have been determined and are compared below.

For methylsilane, the possible initial dissociation steps are:-



Using the following bond dissociation energies in $KJ\ mol^{-1}$
 $D(R_3Si-Me)=368$ ¹⁷, $D(R_3Si-H)=376$ ¹⁷, $D(R_2\ddot{Si}-H)=268$ ¹⁷,
 $D(H_3C-H)=435$ ¹⁹ and $D(H-H)=435$ ¹⁸,

$$\Delta H(1) = D(H_3Si-Me) = 368\ KJ\ mol^{-1}$$

$$\Delta H(2) = D(MeH_2Si-H) + D(MeHSi-H) - D(H-H) = 209\ KJ\ mol^{-1}$$

$$\Delta H(3) = D(H_3Si-Me) + D(H_2Si-H) - D(H_3C-H) = 201\ KJ\ mol^{-1}$$

Thermodynamically, the favoured decomposition route is the formation of a silylene and methane, closely followed by the formation of a silylene and hydrogen. The least favoured route thermodynamically is the dissociation into radicals.

The contribution by the A-factors must also be considered. The thermolysis of tetramethylsilane¹³ (TMS)

to give trimethylsilyl and methyl radicals proceeded with an A-factor of $10^{17.2} \text{ s}^{-1}$, whereas for the elimination of silylene from silane¹⁵, the A-factor was $10^{15.5} \text{ s}^{-1}$. Typically, A(d) is greater than A(e) by 10^2 - 10^3 s^{-1} . For the elimination rate constant to be bigger than that for dissociation, the forward activation energy E(e) must be low enough to out-weigh the greater A-factor expected for a radical mechanism.

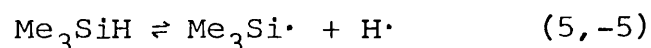
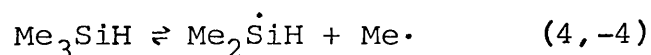
In practice, methylsilane produces mainly hydrogen and corresponding silylene ($\text{Me}\ddot{\text{Si}}\text{H}$). This illustrates that the vital factor determining the dissociation route is the size of the reverse activation energy E(-e) (eqn. ii). Davidson and Ring¹¹ determined E(2) to be 271 KJ mol^{-1} and E(3) to be approximately 290 KJ mol^{-1} . Combining these numbers with the above calculations of ΔH gives:-

$$E(-2) = (271-209) = 62 \text{ KJ mol}^{-1}$$

$$E(-3) = (290-201) = 89 \text{ KJ mol}^{-1}$$

At the low pressures (10^{-1} - 10^{-2} mm Hg) used by Davidson and Ring, no radical chain decomposition of methylsilane developed. The large error limits ($\pm 30 \text{ KJ mol}^{-1}$) quoted by the above workers in their estimation of E(3) are indicative of the problems encountered in obtaining an activation energy for a minor reaction.

For trimethylsilane, the possible initial steps are:-



Using the same bond dissociation values as above,

$$\Delta H(4) = D(\text{HMe}_2\text{Si-Me}) = 368 \text{ KJ mol}^{-1}$$

$$\Delta H(5) = D(\text{Me}_3\text{Si-H}) = 376 \text{ KJ mol}^{-1}$$

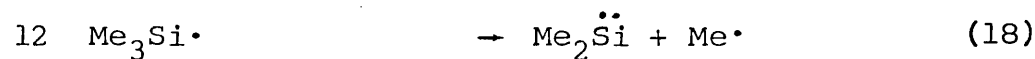
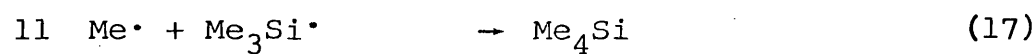
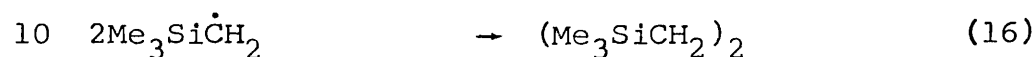
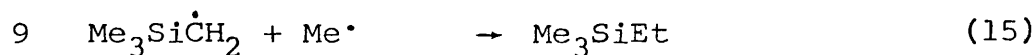
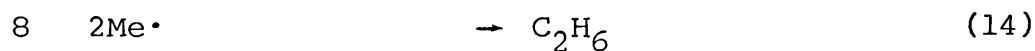
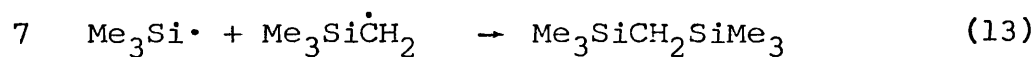
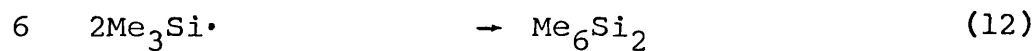
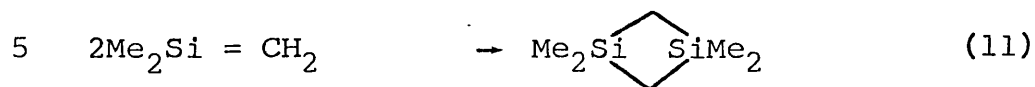
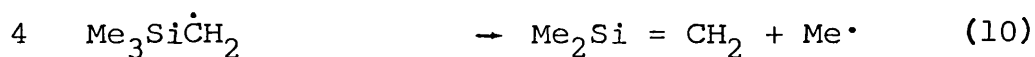
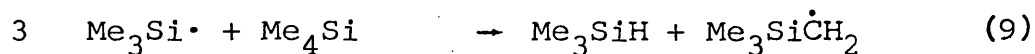
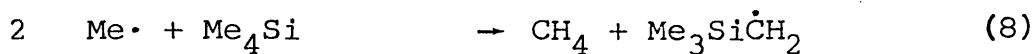
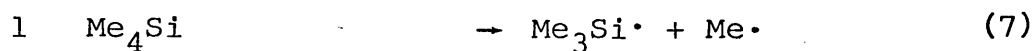
$$\Delta H(6) = D(\text{HMe}_2\text{Si-Me}) + D(\text{Me}_2\text{Si-H}) - D(\text{H}_3\text{C-H}) = 201 \text{ KJ mol}^{-1}$$

As for methylsilane, the favoured decomposition thermodynamically is the production of methane and corresponding silylene. Trimethylsilane has been shown to dissociate into radicals on thermolysis¹⁶, again illustrating that the value of $E(-e)$ (eqn. ii) determines the initial step of the pyrolysis mechanism.

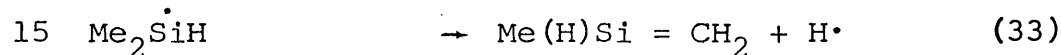
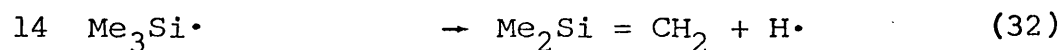
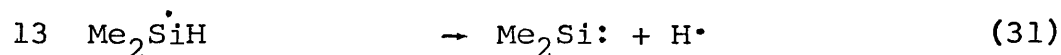
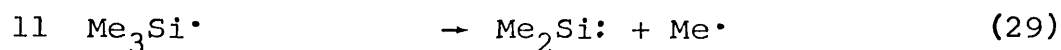
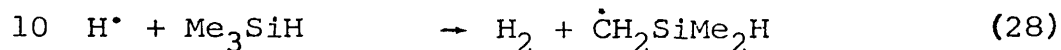
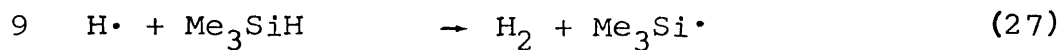
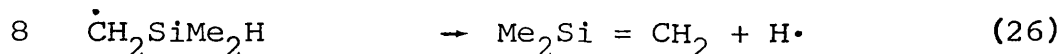
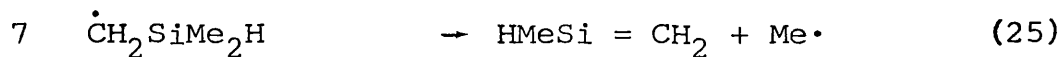
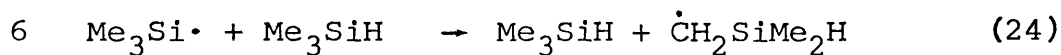
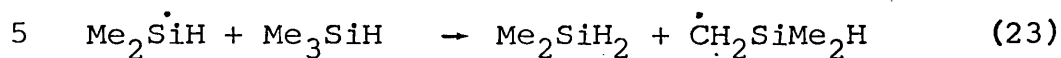
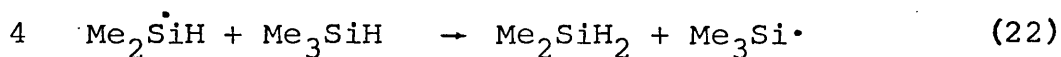
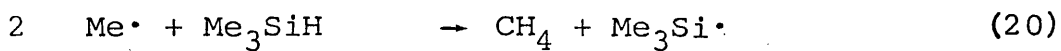
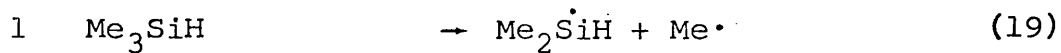
Work by Davidson et al¹³ on the pyrolysis of tetramethylsilane (TMS), produced a value of 355 KJ mol^{-1} for the silicon-methyl bond dissociation energy. The proposed pyrolysis mechanism involved a short radical chain. The value of 355 KJ mol^{-1} is less than the 368 KJ mol^{-1} derived by Walsh¹⁷, but maybe the chain had not been completely suppressed in the TMS experiments. The proposed mechanism is shown in scheme 1.1.

The silicon-methyl bond strength in trimethylsilane ought to be similar to that in TMS. It was therefore proposed¹³ that trimethylsilane pyrolyses by a radical chain mechanism analogous to that of TMS and not by the radical non-chain process suggested earlier¹⁶. The more recent mechanism is shown in scheme 1.2.

Scheme 1.1 Proposed pyrolysis mechanism of tetramethylsilane¹³.



Scheme 1.2 Proposed pyrolysis mechanism of trimethylsilane¹³.



The mechanism also includes all the possible termination steps involving the self- and cross-combination of all the radicals present and the self- and cross-dimerisation of the $\text{R}_2\text{Si} = \text{CH}_2$ species.

The experimental Arrhenius parameters for the production of methane from trimethylsilane were given by $\log_{10}k = 16.4 - 320 \text{ KJ mol}^{-1}/2.3RT^{13}$. From the work with methylsilane, E(6), by analogy with E(3) must be at least 290 KJ mol^{-1} , possibly more if dimethylsilylene ($\text{Me}_2\text{Si:}$) is assumed to be more stable than silylene ($\text{H}_2\text{Si:}$).

At the low pressures used, the methylsilane¹¹ was into the unimolecular fall off region such that the rate constants were calculated to be about $0.14k_x$, parameters from higher pressure work (40-400 mm Hg) by Neudorfl and Strausz²⁰ being taken as a measure of k_x . At low pressure, the formation of methane was given by $\log_{10}k = 13.6 - 290 \text{ KJ mol}^{-1}/2.3RT^{11}$.

The trimethylsilane, having more atoms than methylsilane, was not in the unimolecular fall off region, thus the A-factor A(6) could be given by $A(6) = 10^{13.6}/0.14 = 10^{14.5} \text{ s}^{-1}$. The experimental rate constants for the production of methane from trimethylsilane can thus be compared, in table 1.2, with the derived rate constants for reaction (6), i.e. $\text{Me}_3\text{SiH} \rightleftharpoons \text{CH}_4 + \text{Me}_2\text{Si:}$. The formation of a silylene and methane would be a minor process compared to the radical chain decomposition, especially if E(6) were 300 rather than 290 KJ mol^{-1} , which is not unreasonable.

Table 1.2 Comparison of experimental and derived rate constants for the production of methane from Me_3SiH .

$\log_{10}A$	E/KJ mol ⁻¹	k at 943K/s ⁻¹	k at 1031K/s ⁻¹	
14.5	290	2.73×10^{-2}	6.41×10^{-1}	Reaction 6
16.4	320	4.72×10^{-2}	1.54	Experiment
14.5	300	7.62×10^{-3}	2.00×10^{-1}	Reaction 6

1.3 Measurement of Bond Dissociation Energies-Kinetic Methods.

(i) Pyrolysis

The combination of two radicals is a process requiring zero activation energy. Therefore, the reverse of a gas-phase dissociation into radicals requires zero activation energy.

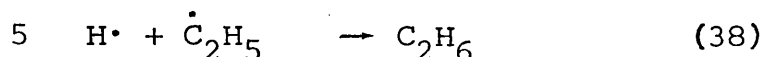
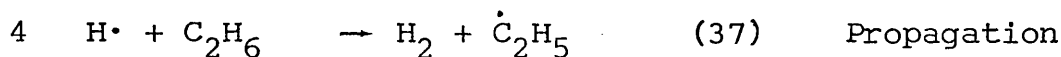
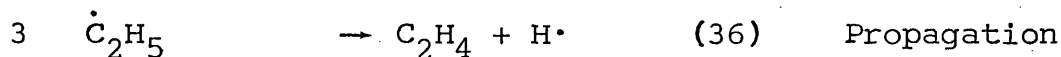
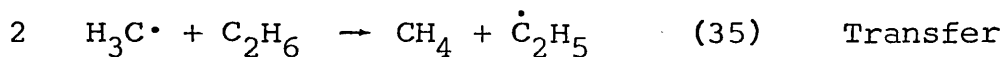


The bond dissociation energy D , activation energy E and enthalpy change ΔH are related simply by:-

$$E = \Delta H = D(R-R) \quad (vi)$$

If the rate of the above thermal dissociation can be measured, then the bond dissociation energy and hence ΔH for the process can be determined. This is not always a straight forward task however, as the radicals produced in the above manner generally interact with the reactant itself, setting up a chain reaction. The general form of the radical-reactant interaction involves the abstraction, by the radical, of an atom from the reactant. Alkyl radicals will normally abstract a hydrogen atom, whereas silyl radicals will abstract an atom with order of preference halide > hydrogen. The pyrolysis of TMS (scheme 1.1) is an example of a typical chain reaction following the Rice-Herzfeld type mechanism. This type of mechanism is common to hydrocarbon chemistry and can be illustrated by a simplified version of the complex pyrolysis of ethane²¹ (scheme 1.3).

Scheme 1.3 Pyrolysis mechanism of ethane²¹.



The initial slow dissociation of the reactant molecule into radicals is followed by rapid chain propagation steps, one of which (36) is the dissociation of a large radical into a smaller radical and a π -bonded species, in this case a stable olefin.

Reaction (34) is obviously analogous to the first step of the TMS pyrolysis scheme (reaction (7), scheme 1.1). The "transfer" process, reaction (35), is equivalent to the second and third steps (reactions (8) and (9)) of the TMS mechanism. The dissociative propagation reaction (36) corresponds to the fourth step of the TMS scheme. The energetics of this step illustrate a major difference between carbon and silicon chemistry.

Silicon does not form strong $P\pi - P\pi$ bonds, neither to itself, nor to carbon³, thus the formation of $\text{R}_2\text{Si} = \text{CH}_2$ is not an energetically favoured process, requiring an activation energy in the region of 190 kJ mol^{-1} ¹³. The hydrocarbon reaction (36) however, only requires an activation energy of about 137 kJ mol^{-1} ²². (A closer analogy to step four of the TMS scheme would involve the breaking of a carbon-methyl rather than carbon-hydrogen bond, a process requiring an even lower activation energy.)

Assuming the A-factors to be similar, then at 1000K, the rate constant for the hydrocarbon reaction (36) would be more than 500 times greater than for the analogous step in the TMS mechanism. This difference in activation energy requirement results in the chain length for hydrocarbon pyrolyses being very large (typically 10^6), whereas the chain length for organosilicon pyrolyses can be less than 10, that of TMS for example. An important implication of this short-chain feature is discussed below.

The highest activation energy step of any chain reaction is that of initiation. As the temperature is increased, the chain length decreases. If a reaction proceeds via a short chain at lower thermolysis temperatures, then at higher temperatures, the reaction may enter a non-chain region. This effect was demonstrated by Davidson et al¹³ for the pyrolysis of TMS.

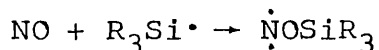
By following the first-order production of methane, it was found that the Arrhenius plot over the temperature range 840-1055K consisted of two distinct straight lines of different slope, a "high" (955-1055K) and a "low" (840-950K) temperature line, corresponding to 355 and 239 KJ mol^{-1} respectively. The slope of the line in the high temperature region was unaffected by packing the reaction vessel with quartz wool to increase the surface to volume ratio. This surface insensitivity, together with the higher activation energy found in this temperature region was evidence that the pyrolysis mechanism was very close to being a non-chain process. In the low temperature region however, the slope of the line was increased by increasing the surface to volume ratio, the measured activation energy being less than 355 KJ mol^{-1} (239-300 KJ mol^{-1}). The chain mechanism was thus proposed to operate in the low temperature region.

Chain suppression by increasing the temperature is only practicable for a short chain process such as was found in the example above. The very much greater chain lengths found in hydrocarbon reactions make this technique wholly unfeasible.

(ii) Pyrolysis with chain inhibitor.

A "chain inhibitor" can be added to the reaction mixture, its purpose being to remove reactive radicals from the system. Not all inhibitors work in all systems, but there are several to try. Some common inhibitors for alkyl radical reactions are nitric oxide (NO) and compounds with an easily-abstracted hydrogen atom eg. toluene or propene. Ethene is sometimes useful to identify radicals present in a system.

Nitric oxide adds to silyl radicals, forming a strong silicon-oxygen bond.



As an inhibitor for silyl radical reactions however, nitric oxide is not useful, as the resulting $\dot{\text{N}}\text{OSiR}_3$ radical can go on to react further. The non-chain photosensitised decomposition of trimethylsilane was determined²⁴ as scheme 1.4. In the presence of nitric oxide, the complex chain mechanism as shown by scheme 1.5 occurred.

The silicon-silicon bond dissociation energy in hexamethyldisilane was determined with the aid of m-xylene¹² as a chain inhibitor. Like toluene, m-xylene has an easily-abstracted hydrogen atom, a resonance stabilised (and therefore relatively unreactive) radical being left behind. Without added m-xylene, the hexamethyldisilane (HMDS) pyrolysed via a complex chain mechanism, the chain

products trimethylsilane (3MS), 1,1,3,3-tetramethyl-1,3-disilacyclobutane (TMDS) and the chain isomerisation product trimethylsilyl (dimethylsilyl) methane (ISO) being formed with orders greater than one. The proposed mechanism is shown by scheme 1.6.

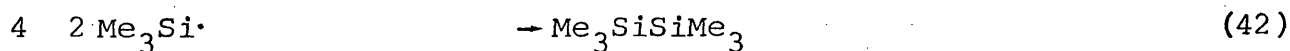
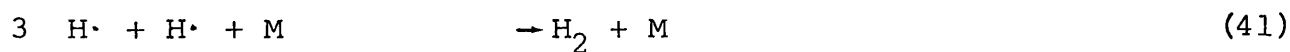
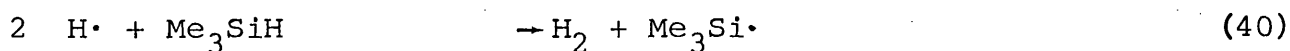
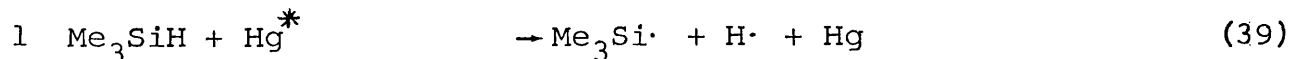
When excess m-xylene was added, chain isomerisation of HMDS continued, but by a different sequence of reactions, xylene and xylyl radicals being involved, resulting in different kinetic behaviour. The proposed thermolysis mechanism with added m-xylene is shown by scheme 1.7. The formation of 3MS was now a non-chain process with the rate equalling $2k_{48} [\text{HMDS}]$. The experimental rate constant for the formation of 3MS was thus equal to $2k_{48}$, hence Arrhenius parameters for reaction (48) could be obtained.

Chain inhibitors such as ethene simply add to a reactive radical to form a larger, less reactive radical. Addition of ethene to a silyl radical leaves the odd electron on a carbon atom rather than on the silicon, thus the species behaves as an alkyl rather than a silyl radical. Alkyl radicals behave in a predictable way by abstracting a hydrogen atom, either from some other species present in the system or from the walls of the reaction vessel.

It should be remembered that any alkyl radicals present in the system may also add to or react with the chain inhibitor and this possibility must be taken account of when assessing any changes in the observed chemistry brought about by the inclusion of an inhibitor in the reaction mixture.

Scheme 1.4

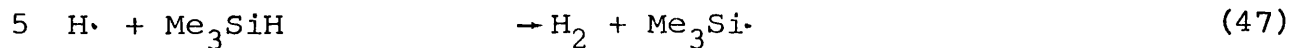
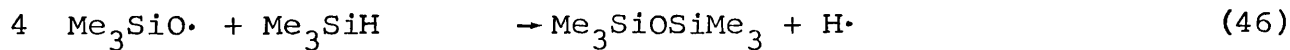
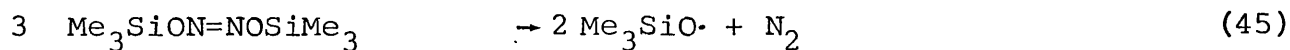
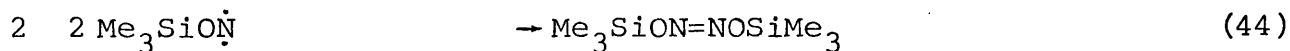
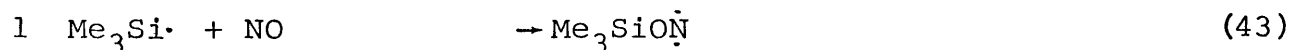
The photosensitised decomposition of Me₃SiH.²⁴



* - ... Excited "hot" Species.

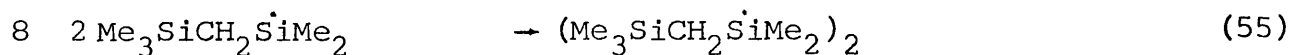
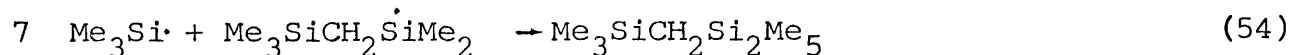
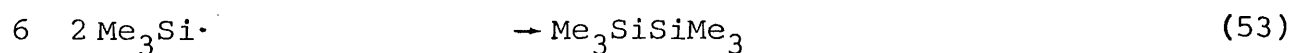
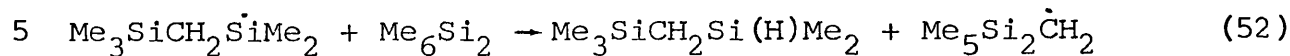
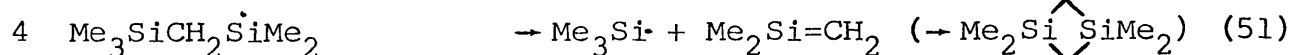
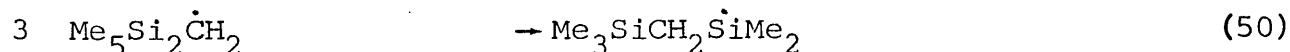
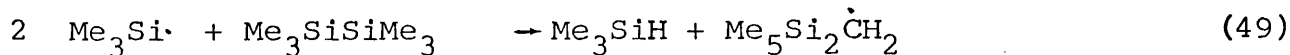
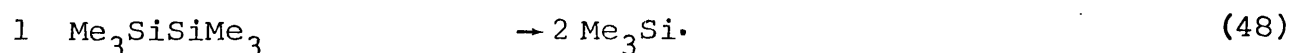
Scheme 1.5

Photosensitised decomposition of Me₃SiH in the presence of NO

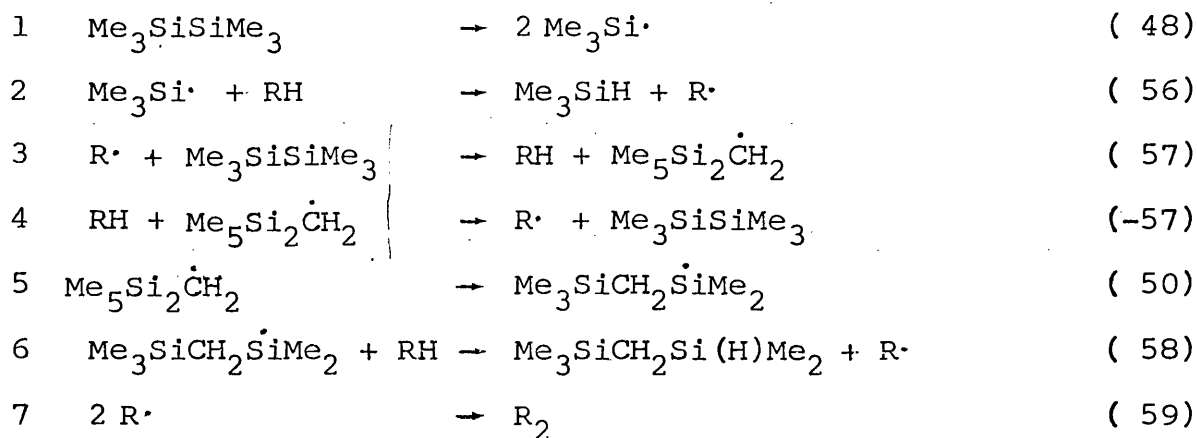


Scheme 1.6

The thermolysis of HMDS without added m-xylene.



Scheme 1.7 Pyrolysis of HMDS with added m-xylene (RH).



(iii) Very Low Pressure Pyrolysis (VLPP).

Carrying out the pyrolysis reaction at low pressure minimises the rate of the bimolecular processes, the radicals tending to be lost to the walls of the reaction vessel. Lowering the pressure however, can put the reaction into the unimolecular fall off region. The fewer atoms a molecule has, the further into "fall off" it will be. The effects of this phenomenon are maybe a slight lowering of the activation energy ($\sim 5 \text{ kJ mol}^{-1}$) and a more significant lowering of the A-factor. For methylsilane, $\log_{10} A = 14.1$ at about 10^{-1} mm Hg (ref. 11) and 14.5 at 40 mm Hg²⁰.

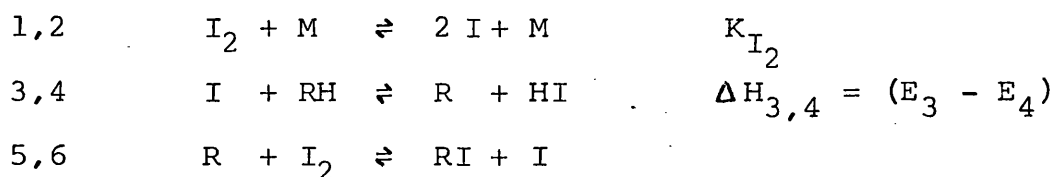
The VLPP technique developed by Benson²³ is an extension of the pyrolysis method. The VLPP experimental system involves allowing a steady state flow of reactant molecules to pass through a thermostatted reaction vessel under conditions of such low pressure that most collisions of reactant or product molecules take place with the vessel walls and not in the gas-phase. At the low pressures used ($\ll 10^{-2}$ mm Hg) it is likely that most unimolecular decompositions will be in the fall off region. The high pressure limiting Arrhenius parameters for a given reaction are estimated from a "best fit" of the results of RRK calculations to the

experimental data.

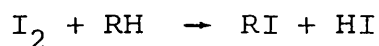
(iv) Kinetic Equilibrium Method.

The bond dissociation energy $D(R-H)$ can be measured by an "iodine equilibrium" reaction. The experimental technique, originally devised by Benson²⁵, has been applied to a series of silicon-centred molecules¹⁷.

The reaction between iodine and a hydrogen-containing molecule RH proceeds thus:-



The overall stoichiometry, in the early stages at least, is:-



In the early stages of the reaction, when step 6 is not important, the rate of change of iodine concentration is given by:-

$$-d[I_2]/dt = k_3 \cdot K_{I_2}^{1/2} [I_2]^{1/2} \cdot [RH]$$

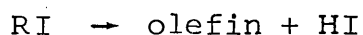
Using spectrophotometric techniques, the concentration of iodine was monitored as a function of time, the results being fitted to an integrated form of the rate equation to yield $k_3 \cdot K_{I_2}^{1/2}$. Values of $K_{I_2}^{1/2}$ were known, hence k_3 could be calculated and from its temperature dependence the activation energy for step 3 was determined. The activation energy E_4 was estimated, but in any case believed to be small (0-8 KJ mol⁻¹). The measured E_3 and estimated E_4 were then used to calculate $\Delta H_{3,4}$. This enthalpy change related to bond energies thus:-

$$\Delta H_{3,4} = D(R-H) - D(H-I)$$

The value of $D(H-I)$ was known, hence $D(R-H)$ could be

determined, with an estimated accuracy of $\pm 8 \text{ KJ mol}^{-1}$.

If $R\cdot$ were a carbon centred radical, then the overall iodination reaction would be highly reversible owing to the importance of step 6 in the mechanism. The species RI could also be unstable and undergo the elimination:-

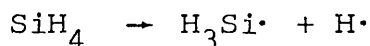


These complications did not arise for a silicon centred radical $R\cdot$ because the silicon-iodine bond is stronger than carbon-iodine and silicon does not form strong π -bonds to itself or to carbon.

The measured silicon-hydrogen bond dissociation energies were then combined with the literature heats of formation of some silicon compounds, enabling other bond energies to be derived. For example, the silicon-silicon bond dissociation energy in disilane was derived.

The bond energy $D(\text{H}_3\text{Si-H})$ was measured¹⁷ as 378 KJ mol^{-1} . The literature values of $\Delta H_f^0(\text{SiH}_4) = 34 \text{ KJ mol}^{-1}$ ²⁶ and $\Delta H_f^0(\text{H}\cdot) = 218 \text{ KJ mol}^{-1}$ ¹⁸ were used to calculate $\Delta H_f^0(\text{H}_3\text{Si}\cdot)$.

For



$$\Delta H_f^0(\text{H}_3\text{Si}\cdot) = \Delta H_f^0(\text{SiH}_4) - \Delta H_f^0(\text{H}\cdot) + D(\text{H}_3\text{Si-H})$$

hence

$$\Delta H_f^0(\text{H}_3\text{Si}\cdot) = 194 \text{ KJ mol}^{-1}$$

Having derived $\Delta H_f^0(\text{H}_3\text{Si}\cdot)$, then assuming the reaction



$$\Delta H^0 = D(\text{H}_3\text{Si-SiH}_3) = (2 \times \Delta H_f^0(\text{H}_3\text{Si}\cdot)) - \Delta H_f^0(\text{Si}_2\text{H}_6)$$

Thus, the literature value of $\Delta H_f^0(\text{Si}_2\text{H}_6) = 80 \text{ KJ mol}^{-1}$ ²⁶ was used to derive that $D(\text{H}_3\text{Si-SiH}_3) = 308 \text{ KJ mol}^{-1}$.

1.4 Measurement of Bond Dissociation Energies -

From Appearance Potentials.

Besides the kinetic methods outlined above, bond dissociation energies may also be determined, though with rather less certainty, from electron impact experiments in the ion source of a mass spectrometer. Under electron impact, a molecule may dissociate, one of its fragments possibly becoming ionized. Should the ionized fragment be the one of lower ionization potential, and if it and the other fragment are produced in their ground states from a ground state molecule, then the appearance potential of the ion produced is simply related to the ionization potential of the fragment and the dissociation energy of the bond broken to form it³. For the process,



the appearance potential (AP) of R^{1+} is given by,

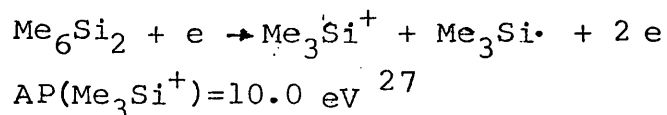
$$\text{AP}(\text{R}^{1+}) = D(\text{R}^1\text{-R}^2) + \text{IP}(\text{R}^1) \quad (\text{vii})$$

where $\text{IP}(\text{R}^1)$ is the ionization potential of fragment R^1 .

A direct determination of $\text{IP}(\text{R}^1)$ would be extremely difficult, no values being available for silicon compounds. Appearance potential measurements alone are not sufficient to yield bond dissociation energies, the additional information necessary being either (i) a bond dissociation energy obtained kinetically or (ii) molecular heats of formation obtained from calorimetric measurements.

(i) The appearance potential of the trimethylsilyl ion

(Me₃Si⁺) from hexamethyldisilane was determined as



The silicon-silicon bond dissociation energy in hexamethyldisilane has been determined by kinetic methods to be $D(\text{Me}_3\text{Si-SiMe}_3) = 337 \text{ kJ mol}^{-1}$ ¹² (3.5 eV.molecule⁻¹). By substitution into equation (vii), the ionisation potential of the trimethylsilyl radical can thus be calculated.

$$\text{IP}(\text{Me}_3\text{Si}\cdot) = 10.0 - 3.5 = 6.5 \text{ eV.}$$

This value of IP(Me₃Si·) may then be used to deduce bond dissociation energies in a series of trimethylsilyl compounds, Me₃Si-R, from the appearance potentials of the trimethylsilyl ions from these compounds. The necessary appearance potentials have been measured for some compounds and the resulting bond dissociation energies are shown in table 1.3.

Table 1.3 Bond Dissociation energies derived from Appearance Potential measurements.

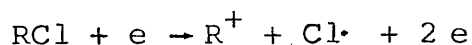
Me ₃ Si-R	R·	AP(Me ₃ Si ⁺) /eV	Ref.	D(Me ₃ Si-R) /eV (kJ mol ⁻¹)
Me ₃ SiSiMe ₃		10.0	27	3.5 (337)
Me ₃ Si-Me	Me·	10.25	28b	3.75 (362)
Me ₃ SiH	H·	10.5	28b	4.0 (386)
Me ₃ SiC ₂ H ₅	·C ₂ H ₅	10.0	28b	3.5 (338)
Me ₃ SiSiMe ₂ H	·SiMe ₂ H	10.2	28b	3.7 (357)
Me ₃ SiSiH ₃	·SiH ₃	9.7	28b	3.2 (309)
Me ₃ SiCl	Cl·	11.6	28b	5.1 (492)

Davidson et al¹³ obtained by kinetic means 355 KJ mol⁻¹ for the Si-Me bond dissociation energy in tetramethylsilane. The value of 362 KJ mol⁻¹ derived from appearance potential measurements is not too different.

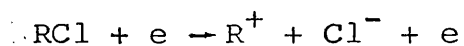
Some of the difficulties encountered in the kinetic determination of bond dissociation energies have been outlined above. The values of all the bond energies derived in table 1.3 rely, in part at least, on the accuracy of one kinetic determination. There may also be considerable errors in the appearance potentials themselves due to technical difficulties of measurement or because of misinterpretation of the ionization efficiency curves³.

Usually, when assessing appearance potentials, the lowest values obtained for a given process are favoured, because these represent the minimum energy for that process.

Gowenlock and Stephenson²⁹ have pointed out however, that this generalisation does not apply to the appearance potential of R⁺ from a molecule RCl. The desired measurement is for the process,



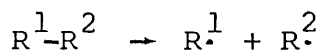
A lower energy process involving ion pair formation can occur,



The ion R⁺ can be produced in differing degrees of excitation, thus the ion-pair process itself can lead to various values for AP(R⁺).

(ii) Bond dissociation energies are related to molecular heats of formation as follows.³

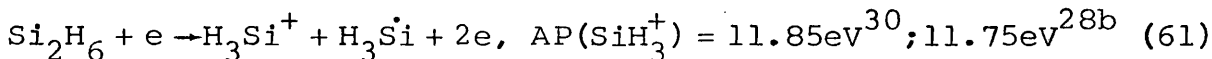
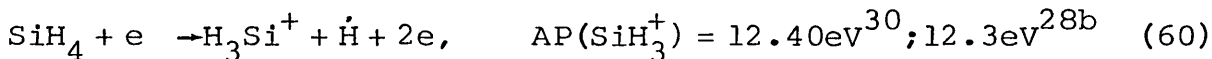
For a molecule R¹-R² with bond dissociation energy D(R¹-R²), the enthalpy change for the dissociation



is given by

$$\Delta H^0 = D(R^1-R^2) = \Delta H_f^0(R^{\cdot 1}) + \Delta H_f^0(R^{\cdot 2}) - \Delta H_f^0(R^1-R^2) \quad (\text{viii})$$

The following appearance potentials for (H_3Si^+) have been determined from electron impact studies of silane and disilane.



$$AP(60) - AP(61) = .55\text{eV} \quad (53 \text{ KJ mol}^{-1}) \text{ in both cases.}$$

The heat of formation of the $H_3Si\cdot$ radical is given by³⁰

$$\Delta H_f^0(H_3Si\cdot) = AP(61) - AP(60) + \Delta H_f^0(Si_2H_6) - \Delta H_f^0(SiH_4) + \Delta H_f^0(H\cdot) \quad (\text{ix})$$

assuming the SiH_3^+ ions are energetically identical in both reactions.

The heat of formation of a hydrogen atom is well established as 218 KJ mol^{-1} ¹⁸, so if the heats of formation of silane and disilane are known, then the heat of formation of the $H_3Si\cdot$ radical can be calculated from eqn. (ix) above. The value of $\Delta H_f^0(H_3Si\cdot)$ thus obtained can then be substituted into eqn. (viii) for calculation of the bond dissociation energies $D(H_3Si-SiH_3)$ and $D(H_3Si-H)$.

The heats of formation of silane and disilane were determined by Gunn and Green³¹ to be 30.5 and 71.5 KJ mol^{-1} respectively. Substitution into eqn. (ix) gives that

$$\Delta H_f^0(H_3Si\cdot) = 206 \text{ KJ mol}^{-1}$$

From eqn. (viii), $D(H_3Si-SiH_3) = 340 \text{ KJ mol}^{-1}$ and $D(H_3Si-H) = 393 \text{ KJ mol}^{-1}$.

The value of 340 KJ mol^{-1} for $D(H_3Si-SiH_3)$ is in very good agreement with Davidson's¹² kinetically determined value of 337 KJ mol^{-1} for $D(Me_3Si-SiMe_3)$, although Walsh¹⁷

has suggested that $D(\text{H}_3\text{Si}-\text{SiH}_3)$ could be about 24 KJ mol^{-1} less than $D(\text{Me}_3\text{Si}-\text{SiMe}_3)$ due to a strengthening effect of a methyl group over a hydrogen atom of 4 KJ per methyl. The value 393 KJ mol^{-1} for $D(\text{H}_3\text{Si}-\text{H})$ however, seems a little high, indeed Potzinger et al²⁸ themselves determined $D(\text{R}_3\text{Si}-\text{H})$ to be $372 \pm 17 \text{ KJ mol}^{-1}$ from the same set of appearance potential measurements as above, but by the application of an "additivity" method of analysis (section 1.5). Recent measurements of $D(\text{R}_3\text{Si}-\text{H})$ by Walsh¹⁷ using the "iodine equilibrium" technique gave a figure of about 376 KJ mol^{-1} , supporting the Potzinger et al²⁸ value.

The "CATCH" tables²⁶ give $\Delta H_f^0(\text{SiH}_4)$ as 34.3 KJ mol^{-1} . If this value is used in conjunction with the above appearance potentials^{28b,30}, then $\Delta H_f^0(\text{H}_3\text{Si}\cdot) = 202 \text{ KJ mol}^{-1}$, $D(\text{H}_3\text{Si}-\text{SiH}_3) = 333 \text{ KJ mol}^{-1}$ and $D(\text{H}_3\text{Si}-\text{H}) = 386 \text{ KJ mol}^{-1}$. There is still reasonable agreement between the kinetic¹² and electron impact values of $D(\text{R}_3\text{Si}-\text{SiR}_3)$ (337 and 332 KJ mol^{-1} respectively) and the value of $D(\text{H}_3\text{Si}-\text{H})$ now lies just within the error limits quoted by Potzinger et al²⁸. The same bond strength (386 KJ mol^{-1}) was derived in table 1.3.

In this type of calculation, as in (i), there is a considerable dependence on the reliability of the supporting data. In the example above for instance, the heats of formation of silane and disilane were required. In contrast to hydrocarbons, there are many difficulties encountered in the evaluation of heats of formation of silicon compounds. The established calorimetric techniques of obtaining heats of formation through measurement of heats of combustion, are unsatisfactory for silicon compounds due to the involatility of silica,

a product of combustion, the formation of solid films over uncombusted material and the tendency of many silanes to explode. Consequently, some earlier heats of formation measurements are not reliable. Modern rotating bomb and fluorine bomb calorimetry and in some cases heats of hydrolysis measurements could lead to more reliable data.

1.5 Calculation of Heats of Formation-Additivity Schemes.

As stated above, direct measurement of heats of formation of silicon compounds by calorimetric methods is unreliable. Various additivity schemes have been devised from which the heats of formation of a series of compounds can be calculated. Two such schemes, that of Allen³² and that of Benson and Luria³³ have been applied to series of silicon compounds.

(i) The Allen scheme assumes that bond energies are constant in all molecules. For example, the carbon-hydrogen bonds in methane each have the same energy as the carbon-hydrogen bonds in say iso-butane. Similarly, carbon-carbon bonds are assumed to always have the same energy. An additive "interaction energy", α , between each pair of non-bonded nearest neighbour atoms in the molecule is then introduced.

In the original work, using alkanes, interactions involving hydrogen atoms were found to be unimportant. The carbon-hydrogen bond energy (denoted $B(C-H)$ rather than $D(C-H)$, as the scheme requires an average, rather than a specific bond energy) was calculated as the heat of atomisation (ΔH_A^0) of methane divided by four, the number of carbon-hydrogen bonds, there being no neighbour interactions in methane.

$$B(\text{C-H}) = \Delta H_{\text{A}}^0(\text{CH}_4) / 4 \quad (\text{x})$$

A value for B(C-C) could then be calculated from the heat of atomisation of ethane, no neighbour interactions being involved.

$$B(\text{C-C}) = \Delta H_{\text{A}}^0(\text{C}_2\text{H}_6) - 6 B(\text{C-H})$$

It was shown that the heat of formation of a molecule could be calculated from the sum of the bond energies and the nearest neighbour interactions.

The heat of atomisation is related to the heat of formation by

$$\begin{aligned} & \text{C}_n\text{H}_{2n+2} \rightarrow n\text{C}\cdot + (2n+2)\text{H}\cdot \\ \Delta H_{\text{A}}^0 &= n\Delta H_{\text{f}}^0(\text{C}\cdot) + (2n+2)\Delta H_{\text{f}}^0(\text{H}\cdot) - \Delta H_{\text{f}}^0(\text{C}_n\text{H}_{2n+2}) \end{aligned} \quad (\text{xi})$$

It was proposed that

$$\Delta H_{\text{A}}^0 = \sum B(\text{C-H}) + \sum B(\text{C-C}) + X\alpha \quad (\text{xii})$$

where there are X nearest neighbour interactions α .

The heats of formation of carbon and hydrogen atoms were known, thus $\Delta H_{\text{f}}^0(\text{C}_n\text{H}_{2n+2})$ could be calculated.

The Allen scheme, in common with other additivity methods, requires a "base" or reference compound with known heat of formation, from which the enthalpies of formation of other, related compounds can be derived. In the example above, methane was the reference. In order to calculate B(C-H) in eqn. (x), the heat of atomisation was needed. This could be calculated from eqn. (xi), a value for $\Delta H_{\text{f}}^0(\text{CH}_4)$ being required.

This bond additivity procedure has been applied to a series of methylsilanes by Potzinger and Lampe²⁸. Silane was chosen as the reference compound, using the heat of formation measured by Gunn and Green³¹. The experimental data consisted of a series of appearance potential measurements for various fragment ions from compounds

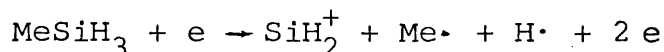
in the series $\text{Me}_n\text{SiH}_{4-n}$, $n = 0-4$.

The appearance potential of the SiH_2^+ ion from silane was used to calculate the enthalpy of formation of the ion.



$$\Delta H_f^0(\text{SiH}_2^+) = \text{AP}(\text{SiH}_2^+) - \Delta H_f^0(\text{H}_2) + \Delta H_f^0(\text{SiH}_4)$$

This value for $\Delta H_f^0(\text{SiH}_2^+)$ was then used along with the appearance potential of SiH_2^+ from methylsilane to calculate $\Delta H_f^0(\text{MeSiH}_3)$.



$$\Delta H_f^0(\text{MeSiH}_3) = \Delta H_f^0(\text{SiH}_2^+) + \Delta H_f^0(\text{Me}\cdot) + \Delta H_f^0(\text{H}\cdot) - \text{AP}(\text{SiH}_2^+)$$

The Allen bond interaction scheme was then used to calculate the heats of formation of the methylsilanes $\text{Me}_n\text{SiH}_{4-n}$, $n = 2-4$. In addition to $B(\text{C-H})$, which was assumed to be the same as in methane, the bond energies $B(\text{Si-H})$ and $B(\text{Si-C})$, and the interaction energy $\alpha(\text{CSiC})$ were required.

$B(\text{Si-H})$ was calculated in an analogous way to $B(\text{C-H})$ above. $B(\text{Si-C})$ could then be calculated using the derived values of $\Delta H_f^0(\text{MeSiH}_3)$ and $B(\text{Si-H})$. The interaction energy term $\alpha(\text{CSiC})$ was determined from the appearance potentials of the ions MeSiH^+ and MeSiH_2^+ from methylsilane and dimethylsilane.

The consistency of the calculated heats of formation was checked by deriving the enthalpies of formation of the various fragment ions. The standard deviation between these enthalpies was calculated. The heat of formation of methylsilane was then allowed to vary slightly and the whole calculation repeated until the standard deviation of the checking procedure had been minimised.

A minimum standard deviation of $\pm 12.5 \text{ KJ mol}^{-1}$ was achieved.

The additive term $\alpha(\text{CSiC})$ was calculated by comparing methylsilane with dimethylsilane. The fact that consistent results were obtained when the same value was applied to the ΔH_F^0 calculations of trimethylsilane and tetramethylsilane demonstrated that methylsilanes follow additivity rules and that the application of additivity schemes can generate internally consistent data sets.

Using the electron impact data acquired by Potzinger and Lampe^{28a} for the methylsilanes, along with the measured heats of combustion of some methylchlorosilanes³⁴, Quane³⁵ has recalculated the bond energy and bond interaction terms needed to apply the Allen interaction scheme to silicon compounds.

For each set of data, electron impact and calorimetric, an initial value for each energy term was calculated. Silane was used as the base compound for the methylsilanes, but a different value for its enthalpy of formation was chosen to that used by Potzinger and Lampe. (34.3 ³⁶ rather than 30.5 KJ mol^{-1} ³¹) The parameters for the chlorosilanes were based on a calculated value for the heat of formation of tetrachlorosilane.

A least squares procedure was used to separately fit each set of data to the Allen bond interaction scheme, yielding new, calculated values for the bond and interaction energy terms. The corresponding derived parameters for each set of data were considered to be the same within the combined limits of experimental error. The two series of experimental results were therefore combined and again fitted to the Allen scheme using the least squares procedure. A final set of values for the bond and

interaction energy terms was thus derived, and the enthalpies of formation of the compounds calculated.

The derived heats of formation of the chlorosilanes were found to agree with the experimental values with a standard deviation of 8.8 KJ mol⁻¹. With regard to the electron impact data, appearance potentials for the relevant ions were derived based on the calculated heats of formation of the parent compounds. Differences between these appearance potentials were compared with the corresponding experimental differences. A closer fit to the experimental results was found than when similar calculations were done using the heats of formation deduced by Potzinger and Lampe. It was proposed that this was because the least squares procedure used by Quane allowed the bond energy B(Si-H) to vary, whereas it was kept constant and equal to B(Si-H) in silane by Potzinger and Lampe. A comparison between the calculated heats of formation of the methylsilanes is shown in table 1.4.

Table 1.4. Derived Enthalpies of formation of methylsilanes.

Compound	$\Delta H_f^0 / \text{KJ mol}^{-1}$		
	Potzinger ^{28a} & Lampe	Quane ³⁵	PRK ^{28b}
SiH ₄	30.5 ³¹	23.8	34.3
MeSiH ₃	4.2	-16.7	-18.0
Me ₂ SiH ₂	-32.6	-63.5	-70.2
Me ₃ SiH	-75.2	-117.0	-123.7
Me ₄ Si	-137.9	-176.4	-177.2

The heat of formation of silane, the base compound, derived from the Quane bond and interaction energies is 23.8 KJ mol⁻¹.

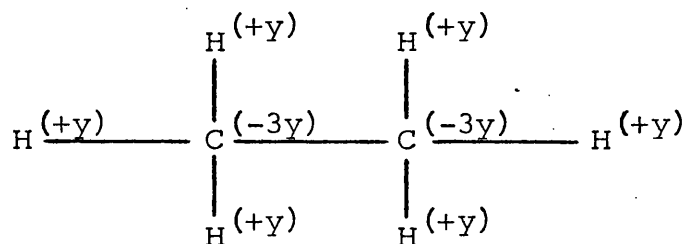
The reference value taken at the start was 34.3 KJ mol⁻¹, which corresponds to the CATCH tables value, a "best result" from independent experimental determinations of the heat of formation.

The Quane results demonstrate that the calorimetric heats of formation of the chlorosilanes investigated follow additivity rules, but the absolute value of each enthalpy is subject to the same uncertainty as the experimentally determined values for other silicon compounds. A systematic error in the calorimetric determinations could lead to a set of internally consistent, though absolutely incorrect heats of formation. The results would still fit an additivity scheme and in the treatment above the additivity features would be passed on to the methylsilanes, but any enthalpies calculated would only be correct relative to each other. Thus the comparison of appearance potentials only demonstrates the additivity properties of the methylsilanes and does not imply an absolute determination of an enthalpy of formation. More recently, using updated appearance potentials in a reassessment of the earlier work, Potzinger, Ritter and Krause^{28b} (PRK) have used the Allen interaction scheme to derive heats of formation for the methylsilanes which are more consistent with the values derived by Quane.

(ii) The Benson and Luria model proposes that the enthalpy of formation of a given molecule is related to the sum of the electrostatic and non-electrostatic energies within that molecule, the non-electrostatic term being an additive property³³.

$$\Delta H_F^0(\text{molecule}) = \left[\begin{array}{c} \text{Total Electrostatic} \\ \text{Energy} \end{array} \right] + \left[\begin{array}{c} \text{Total non-electrostatic} \\ \text{Energy} \end{array} \right]$$

For a series of alkanes, it was proposed that the carbon-hydrogen bond had a polarity, which was represented by assigning a formal charge of $-y$ to carbon and the opposite $+y$ to hydrogen. This led to a model of the methane molecule in which each hydrogen atom had a charge $+y$ and the central carbon atom a charge $-4y$. Similarly, the charge distribution in ethane was represented thus:



It followed that the CH_2 groups of a straight chain alkane would carry a charge of $-2y$ on each carbon atom and $+y$ on each hydrogen atom, while in branched chains, a tertiary carbon atom would be charged $-y$ and a quaternary carbon atom would have no charge at all.

The electrostatic energy (E_{el}) was then defined for any molecule as being the energy which arises from the interaction of all the formal charges present in the molecule. Generally,

$$E_{el} = \sum_{i=j}^n \cdot \sum_{j=i+1}^n \cdot q_i \cdot q_j / r_{i,j}$$

where q_i and q_j are the charges on the i^{th} and j^{th} atoms and $r_{i,j}$ is their distance apart. This expression can be applied to any molecule providing that the necessary parameters are known.

The heat of formation of any hydrocarbon was written as the sum of the electrostatic and non-electrostatic energies thus,

$$\Delta H_f^0 = E_{el} + \sum_i m_i \cdot \Delta H_{fi}^0 \text{ (bond)}$$

where m_i is the number of bonds of type i and ΔH_{fi}^0 represents the additive contribution of that bond to the heat of formation of the compound. This is a general expression for any molecule.

The above electrostatic model for calculating enthalpies of formation, has been applied in silicon chemistry to test the reliability of two existing but mutually exclusive data sets, those comprising the CATCH tables²⁶ and those obtained by Potzinger et al²⁸ from appearance potential measurements.

Davidson³⁷ applied the scheme to the methylsilanes and to some disilanes. As none of the available heat of formation data were known to be reliable, the charge separations about silicon-hydrogen and silicon-carbon were estimated from the dipole moment of methylsilane. The electrostatic energy terms for silane, disilane and the methylsilanes were then calculated. The values of ΔE_{el} , the change in electrostatic energy between successive members of the series, were found to vary little compared with similar calculations in an alkane series, which supported the conclusions of Potzinger et al²⁸ and of Quane³⁵ that the enthalpies of formation of the silanes closely followed bond additivity rules, only small interaction corrections being necessary.

By calculating values of $\Delta\Delta H_f^0$, the differences in enthalpy of formation between successive members of the methylsilane series, and comparing these values with $\Delta\Delta H_f^0$ from the results of Potzinger et al and from CATCH, Davidson concluded that the former were the more internally consistent of the two.

In their derivation of heats of formation from appearance potentials followed by the application of an additivity scheme, Potzinger et al^{28b} (PRK) calculated the standard heat of formation of methylsilane to be $-18.0 \text{ KJ mol}^{-1}$. The value quoted in CATCH is $-33.4 \text{ KJ mol}^{-1}$.

A more recent comparison between the heats of formation quoted in CATCH and those derived by Potzinger et al^{28b} was made by O'Neal and Ring³⁸, again by applying the Benson & Luria electrostatic model. Two sets of heats of formation values were calculated for a series of silanes, one set being standardised to the CATCH value for $\Delta H_f^0(\text{MeSiH}_3)$ and the other to the PRK value. The standardisation was achieved by choosing a value for the additivity of the carbon-silicon bond consistent with $\Delta H_f^0(\text{MeSiH}_3)$ for the data set concerned.

The results of the calculations indicated that both the CATCH and the PRK enthalpies showed good internal consistency. This conclusion was independent of the choice of charge dipole values. Any set of charges which produced good agreement between the calculated and recommended heats of formation for one set, produced comparably good agreement for the other.

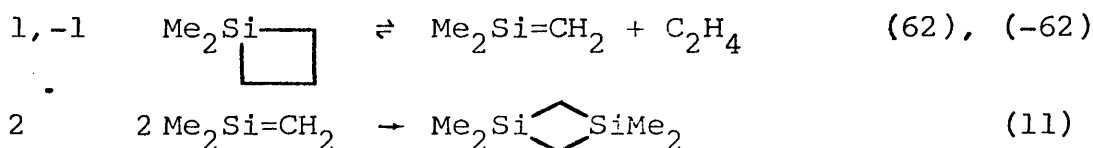
Ring and O'Neal favoured the use of the CATCH values on the grounds that they were all independently and experimentally determined, their internal consistency being a measure of reliability. There were however large differences between CATCH and calculated enthalpies of formation for some compounds, diethylsilane, tetraethylsilane and tetrakis(trimethylsilyl)silane being examples. It had been pointed out by Benson³³ that for some highly branched hydrocarbons, the electrostatic model

calculated heats of formation which were too negative. Steric repulsions amounting to around 4 KJ mol⁻¹ between non-bonded hydrogen atoms less than 2.5Å apart were given as the reason. The observed and calculated enthalpies of formation of tetraethyl- and tetrakis(trimethylsilyl)- silane could be brought into agreement when account was taken of close non-bonded hydrogen-hydrogen interactions. The calculated heat of formation of diethylsilane could not be corrected in this way and it was suggested that the experimental determination of ΔH_f^0 was in need of checking.

1.6 Silaethene Intermediates - R₂Si=CH₂ .

Evidence for the formation of silicon to carbon π bonds was first presented by Flowers and Gusel'nikov³⁹. The decomposition of 1,1-dimethyl-1-silacyclobutane (DMSCB) was proposed to follow scheme 1.8, involving the π -bonded reactive intermediate Me₂Si=CH₂, which had no counterpart in carbon chemistry.

Scheme 1.8 Pyrolysis of 1,1-dimethyl-1-silacyclobutane³⁹.



The Arrhenius parameters for step 1 were given as

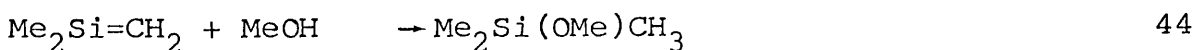
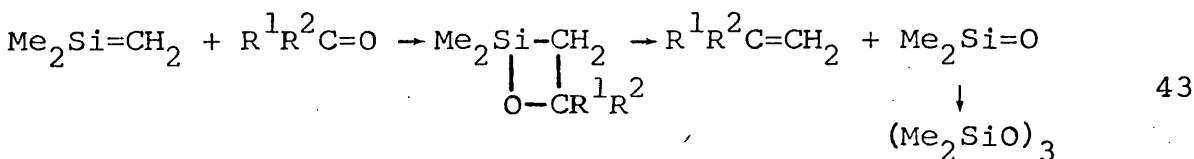
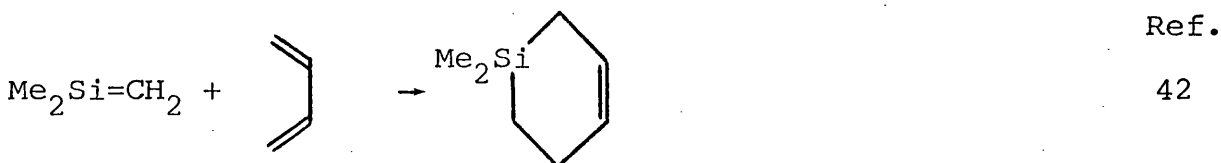
$$\log_{10} k_1 = (15.64 \pm 0.20) - (261.5 \pm 2.1 \text{ KJ mol}^{-1}) / 2.303RT .$$

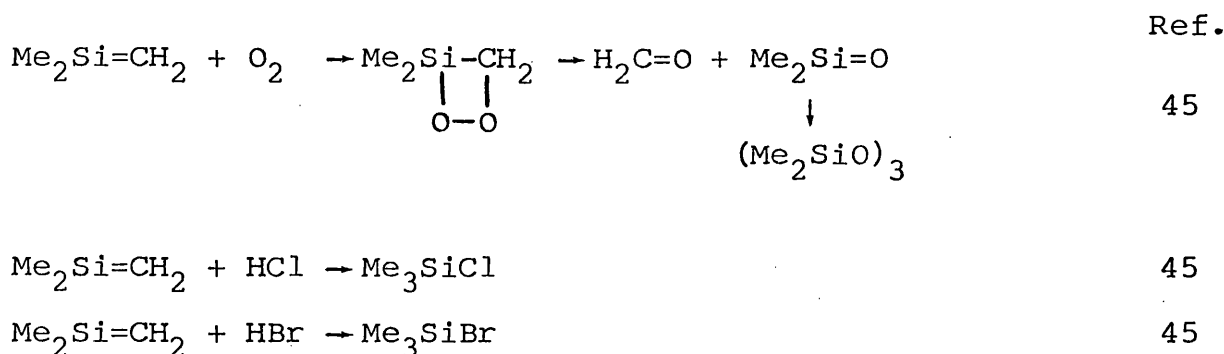
The value ($E_{-1} - \frac{1}{2}E_2$) was estimated to be 60.7 ± 16.7 KJ mol⁻¹. By assuming E₋₁ to be 84 KJ mol⁻¹, E₂ was calculated to be about 46 KJ mol⁻¹. More recently however, Gusel'nikov et al⁴⁰ have pyrolysed DMSCB in a flow system, analysing the

reaction mixture by mass spectrometry after it had passed along a tube of variable length and temperature. Assuming that scheme 1.8 accounted for all the processes involved, the concentrations of dimethylsilaethene (DMSE) were calculated under various conditions from the observed amounts of ethene and dimeric product. The second order rate constant k_2 , between 298 and 673 K, was calculated and given as $\log_{10} k_2 / \text{dm}^3 \text{mol}^{-1} \text{s}^{-1} = 6.55 \pm 0.03$ with zero activation energy. Hence E_{-1} was 60.7 KJ mol^{-1} .

The formation of other silaethene species have been reported in both the gaseous and liquid phases. The photolysis of 1,1-diphenyl-1-silacyclobutane at 328K in cyclohexane/MeOD⁴¹ generated $\text{Ph}_2\text{Si}=\text{CH}_2$, which added to MeOD to form $\text{Ph}_2\text{Si}(\text{OMe})\text{CH}_2\text{D}$.

As demonstrated by Gusel'nikov et al⁴⁰, silaethenes readily undergo dimerisation reactions (step 2 of scheme 1.8). They will also add to carbon-carbon and carbon-oxygen π bonds, to oxygen-hydrogen bonds, to oxygen itself, to hydrogen chloride and to hydrogen bromide, the following reactions having been observed. They will also add readily to radicals⁴⁶.





The results of theoretical calculations on the simplest "silaethene" SiCH_4 ^{47,48} suggested that the lower energy configuration was that of the π -bonded singlet $\text{H}_2\text{Si}=\text{CH}_2$, the 1,2-biradical triplet being estimated to be at least 117 KJ mol⁻¹⁴⁷ higher in energy. Calculations of the relative stability of $\text{H}_2\text{Si}=\text{CH}_2$ and its isomers, $\text{CH}_3\ddot{\text{Si}}\text{H}$ and $\text{H}_3\text{Si}\ddot{\text{C}}\text{H}$, concluded that the silaethene was the more stable and the silylcarbene the least stable⁴⁹. Other evidence as to the structure of silaethenes had been obtained from matrix spectroscopy experiments^{50,51} involving the photolytic generation of 1,1,2-trimethyl-1-silaethene in an argon matrix from trimethylsilyldiazomethane at 8 K. The spectroscopic data were consistent with a planar structure for the silaethene, with a significant barrier to internal rotation⁵⁰, factors favouring a π -bonded structure.

Attempts have been made to estimate the π -bond energy of silaethenes. Walsh¹⁷ has derived a value of 163 KJ mol⁻¹ for $D\pi(\text{Me}_2\text{Si}=\text{CH}_2)$. A recent estimate by Davidson et al⁵², obtained from the mercury-photosensitized decomposition of hexamethyldisilane, put the value at 188 KJ mol⁻¹.

CHAPTER TWO

EXPERIMENTAL

2.1 Apparatus and Method

The experimental set-up provided the means of carrying out low pressure pyrolysis reactions in a static system. Initial reactant pressures in the range 10^{-2} to 10^{-1} mm Hg could be studied.

A data-logging system enabled quantitative measurements to be made on both reactants and products.

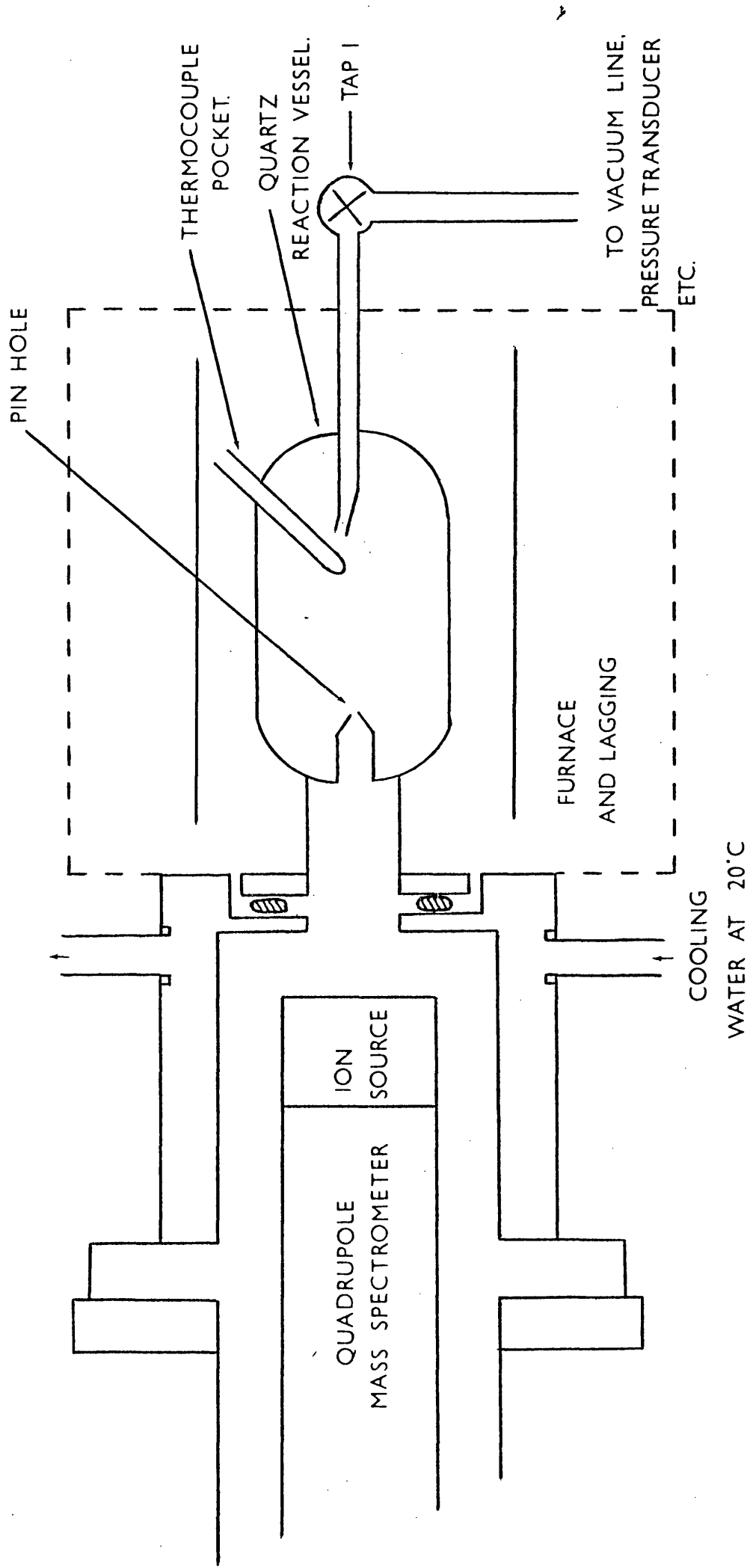
Several modifications to the experimental system were made during the period of the project, so a general description will be given here and the modifications noted in due course.

The pyrolyses were carried out in a quartz reaction vessel which was housed in an electrically heated furnace (see fig. 2.1). A 10 μ pin hole in the vessel, which led directly into the ion source of a quadrupole mass spectrometer, allowed for the continuous sampling of the reaction mixture, thus the progress of reactant and products could be followed.

Adjacent to the reaction vessel was a section of vacuum line fitted with a pressure transducer. Known pressures of material could be measured into this region and then expanded into the reaction vessel via tap 1 to start the pyrolysis.

The temperature inside the reaction vessel was measured using a single junction chromel alum thermocouple linked to a digital meter reading directly in degrees centigrade. The thermocouple junction was placed into a pocket in the quartz vessel, enabling the temperature at the centre of the reaction zone to be measured. The position of the thermocouple pocket also caused the sample to mix as it flowed into the reaction vessel.

Fig. 2.1 Low Pressure Pyrolysis Apparatus



The furnace consisted of a quartz cylinder just large enough in diameter to fit easily around the reaction vessel. A graded electrical heating element was wound around the outside of the quartz tube and the whole assembly surrounded by fire brick. The vacuum-line end of the furnace unit was packed with quartz wool to reduce heat losses.

The heating element was tapped in two places along its length, dividing it into three sections. The relative current passing through each section could be adjusted by rheostats 1, 2 and 3 (see fig. 2.2). These were set to give the most even temperature profile along the length of the reaction vessel. The overall heating current was controlled by the variac.

The quadrupole mass spectrometer, a V.G. Q801k, when used in a conventional way to record a spectrum, could cover any sections in the range $m/e=1-300$. The instrument could also be tuned in to monitor several (initially four, later eight) specific mass peaks within the working range. A V.G. "PP2" four (eight) channel recorder was used for this.

The PP2 could be set to repetitively scan its four (eight) channels at regular rates (1, 3, 10, 30 seconds etc). The heights of the chosen mass peaks could thus be monitored during an experiment by using some sort of data-logging system. During the course of the project, the data collection mechanism was improved from a relatively slow mechanical device to a much faster computer system. The two data collection mechanisms will be fully described below.

Fig.2.2a

Furnace heating circuit

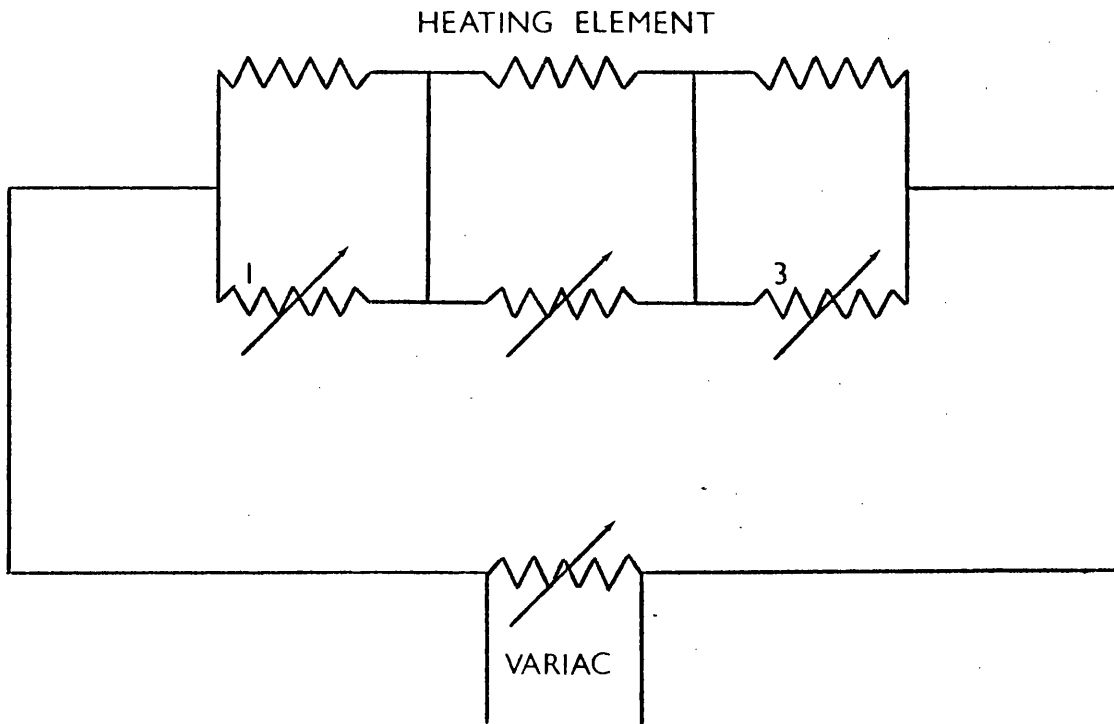
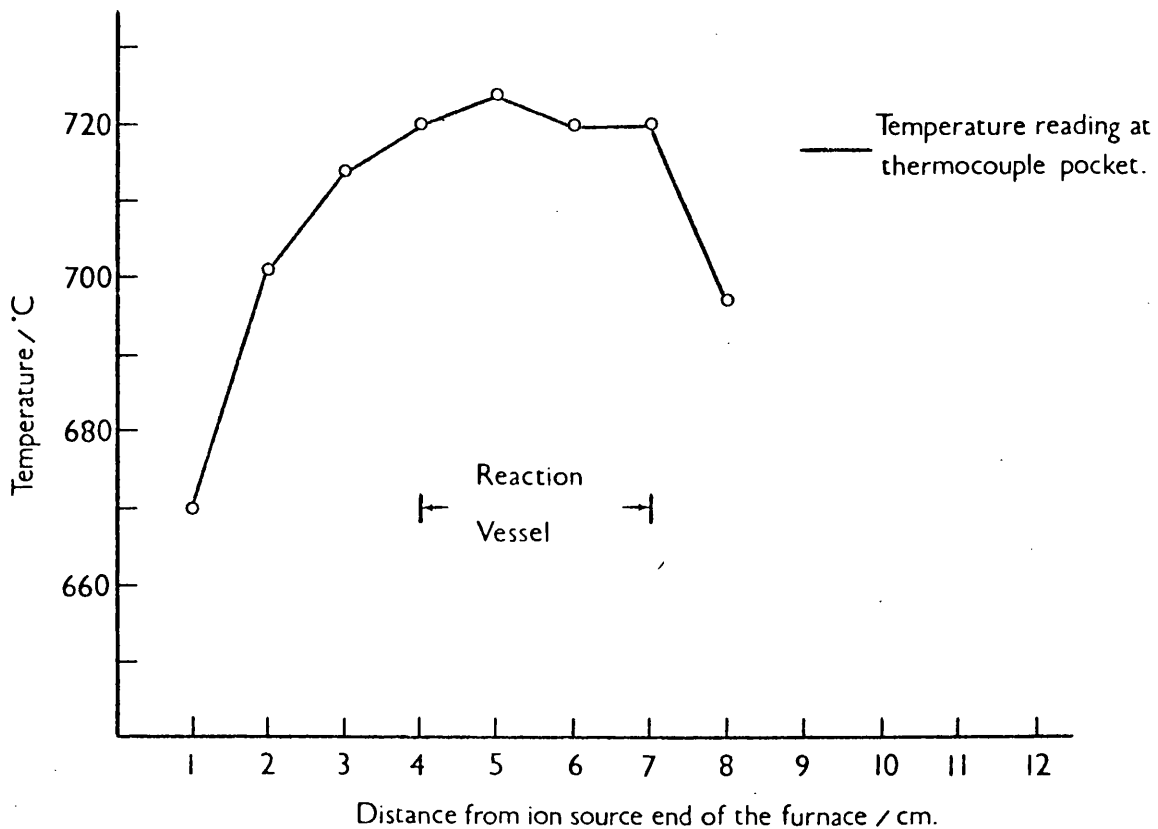


Fig.2.2b

Temperature profile along furnace



In all cases, the general experimental procedure was as follows:-

- (1) Tune in the PP2 to the desired mass peaks.
- (2) Prepare a known amount of sample in the "transducer region" of the vacuum line.
- (3) Start the PP2 scanning and record several "base line" readings.
- (4) Open tap 1 (fig. 2.1) long enough to allow the sample to expand into the reaction vessel.
- (5) Continue recording the heights of the selected mass peaks until sufficient data have been collected.

At the data processing stage, the average base line for each channel was subtracted from the corresponding "reaction" peak heights.

2.2 Data Logging Systems

Peak height information was put out from the PP2 as a DC voltage in analogue form, the voltage being directly proportional to the peak height (see fig. 2.3a). A digital volt meter (DVM), which was also an analogue to digital converter, was used to measure this voltage (and hence the peak height), presenting the value in a more useful form. As the PP2 scanned the top of each of the selected peaks, a pulse was sent to the DVM instructing it to take a reading, the digitised result being sent on to the next link in the chain, the data collection system. The latter was modified in several stages and a description of each now follows, starting with the "original" version.

(1) Earlier Data Collection System (fig. 2.3b)

This used a four-channel PP2 linked via a DVM to a four-channel data logger and mechanical tape punch.

The data collected on the punch tape were processed using the University main-frame computer. The main limitations of the system were:-

(i) No accurate time measurements could be made. The times, relative to tap 1 (fig. 2.1) being opened, at which the peak heights were read were based on the scan rate of the PP2, which was assumed to be regular. For example, at a 10s scan rate, a channel would be read every 2.5s. The "start time", or the point at which tap 1 was opened, was difficult to determine precisely.

(ii) The fastest the system could operate was at a PP2 scan rate of 3s, a channel being read every 0.75s.

(2) Data logger replaced by micro computer (fig. 2.3c)

The first modification was the replacement of the data logger and tape punch by a "Research Machines 380Z" micro computer with dual mini disk system. The interface between the computer and the DVM will be described in section 2.3.

The whole of the data collection procedure as performed by the computer was controlled by a Basic program. The data, once recorded, were written onto magnetic disk for processing later. Incorporated into the computer was a real-time clock, which was used to record accurately the relative time at which each peak height was read.

The system could operate at up to a PP2 scan rate of 1s, a channel being read every 0.25s. The limiting factor

Data logging systems.

Fig. 2.3a

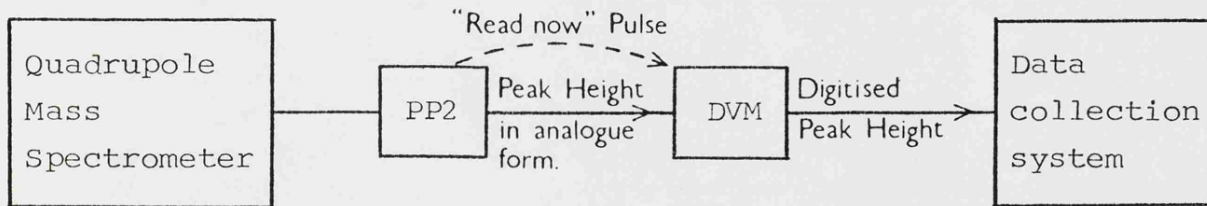


Fig. 2.3b

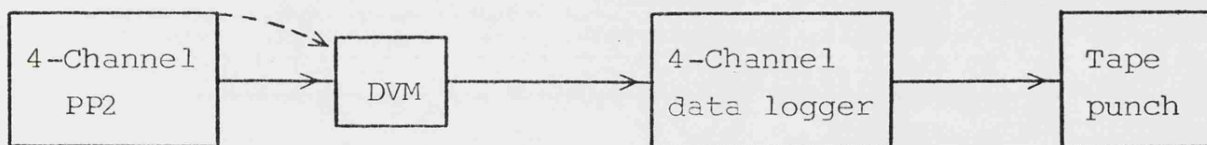


Fig. 2.3c

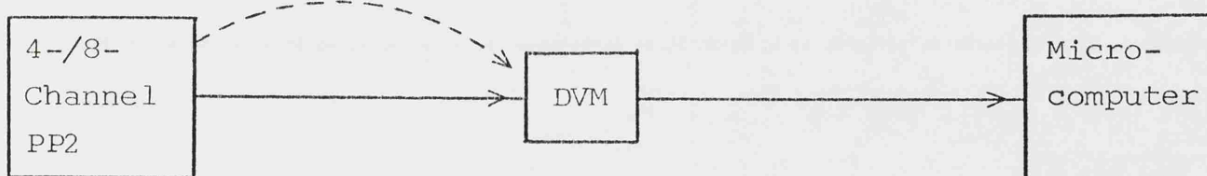
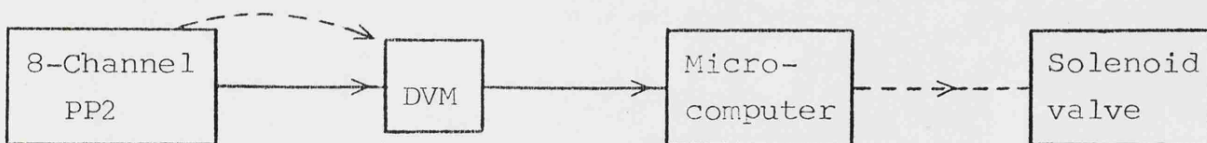


Fig. 2.3d



The transfer from the PP2 to the DVM, and the output from the DVM, was of the same form for all versions of the apparatus, thus only fig. 2.3a is labelled.

to the operating speed was the DVM, which could not handle more than 10 readings per second.

(3) Eight-channel PP2 (fig. 2.3c)

The four-channel PP2 amplifier was replaced by an eight-channel one. Some modifications were made to the new PP2 to enable finer adjustment of the peak tuning.

The DVM was replaced by one which could handle up to 50 readings per second.

Tap 1 (see fig. 2.1) was replaced by a manually operated solenoid valve.

The whole data collection procedure as carried out by the computer was still controlled by a Basic program as in version 2.

The maximum speed that the system could operate at was a PP2 scan rate of 3s, a channel being read every 0.375s. The limiting factor was the computer, the Basic interpreter not allowing quick enough access to the incoming data.

(4) Latest System (fig. 2.3d)

Two changes were made from version 3.

(i) The data collection software was rewritten using machine code routines to access the incoming data. This greatly improved the response time of the computer, enabling data to be read much more quickly.

(ii) The solenoid valve was opened under computer control after a pre-set number of base line readings. The length of time the valve remained open was under external hardware control, and adjustable by the operator.

The system could now operate at a PP2 scan rate of 1s, a channel being read every 0.125s. Faster scanning speeds were possible, but were found to be unnecessary.

2.3 Computer Interface.

(i) Hardware

The computer was supplied with an "Interface Development Board", which basically consisted of three standard Z80 PIO chips and a standard Z80 CTC (clock) chip set up for use in timer mode. The interface between the computer and the DVM was wired as described below.

The DVM took a reading in response to a trigger pulse being generated by the PP2. Such pulses were electronically timed to occur as the PP2 scanned the top of a peak. The peak height thus read (as a DC voltage) was digitised and subsequently copied to the computer.

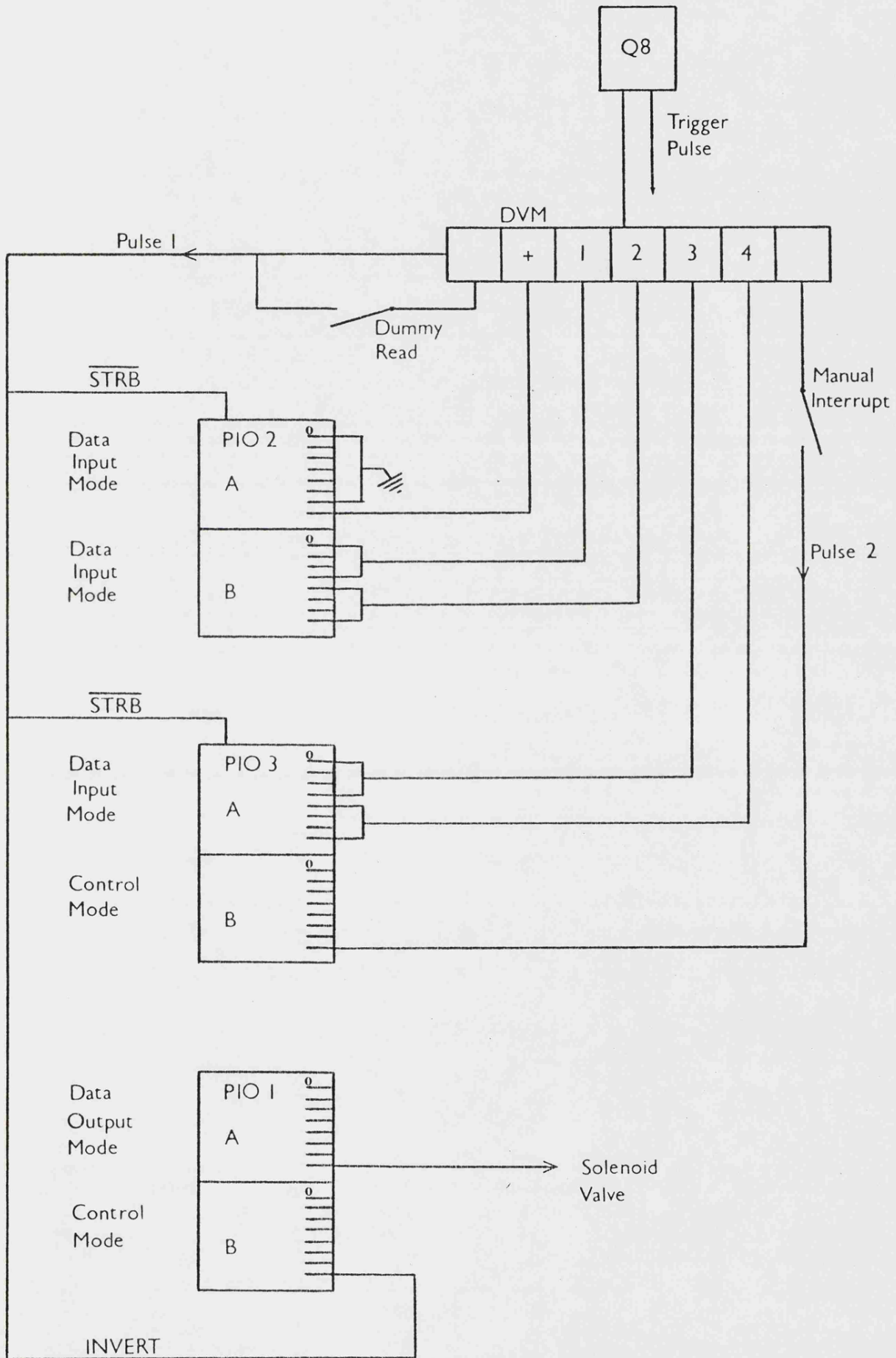
On completion of the digitisation process, the DVM immediately generated pulse 1 (see fig. 2.4), which was sent to the STRB lines of the PIO ports wired to receive the DVM's data, causing the transfer to occur. The same pulse was used (after being inverted) via PIO 1B to generate an interrupt, initiating a software port-reading routine.

The DVM displayed a four digit number with its sign. Each digit was put out as four bit binary and the sign as one bit, high for positive.

As each digit was represented by four bits, then one eight bit PIO port could store two digits. Thus, the number recorded by the DVM, from the PP2, was put onto the computer PIO ports as packed binary coded decimal (BCD), the number of ones and number of tens being sent to one PIO port, the number of hundreds and number of thousands to a second and the sign to a third.

Fig. 2.4

Computer Interface



(ii) Software

Data collection by the computer in the final experimental system, version 4, was controlled by a machine code routine, accessed from a high level Basic program. A listing of both appear in Appendix (1), and a general description of them is given below.

The controlling Basic program, after setting up data storage space within the computer memory, initiated the machine code routine, passing through to it the location of the start of the data storage space and the maximum number of readings to take. An outline of the low level program is shown in fig. 2.5. Standard Z80 interrupt mechanisms were used (see fig. 2.6) to both initiate the actual reading of the data ports by the computer and also to exit from the routine, returning control to the Basic program. The latter was achieved "automatically" on the maximum number of data points being read, or was brought about by the operator using the "manual interrupt" facility (fig. 2.4).

On return to the Basic program, the data which had been read were copied onto magnetic disk for processing later.

2.4 Some Features of the Experimental System.

(i) Leak in and Leak out.

A pyrolysis reaction was started by opening tap 1 (see fig. 2.1), which allowed the reactant to flow from the "transducer region" of the vacuum line into the hot reaction vessel. Fig. 2.7 shows, for the apparatus described above, the appearance of a typical peak height vs time curve for a reactant, the initial build up being due to this flow or "leak in" process. For practical purposes, leak in was assumed to be a first order process,

Fig. 2.5

Diagram of low level program

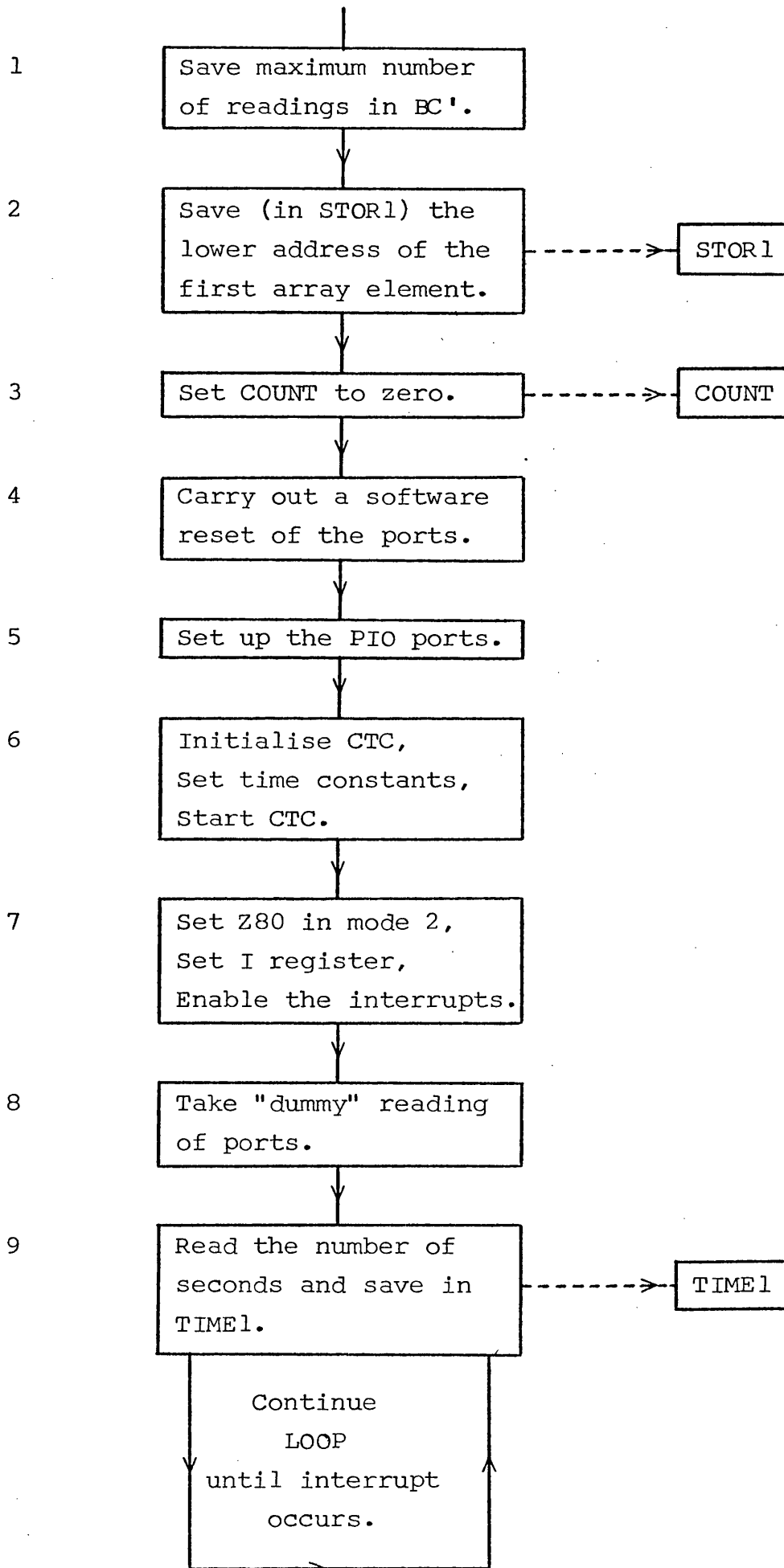
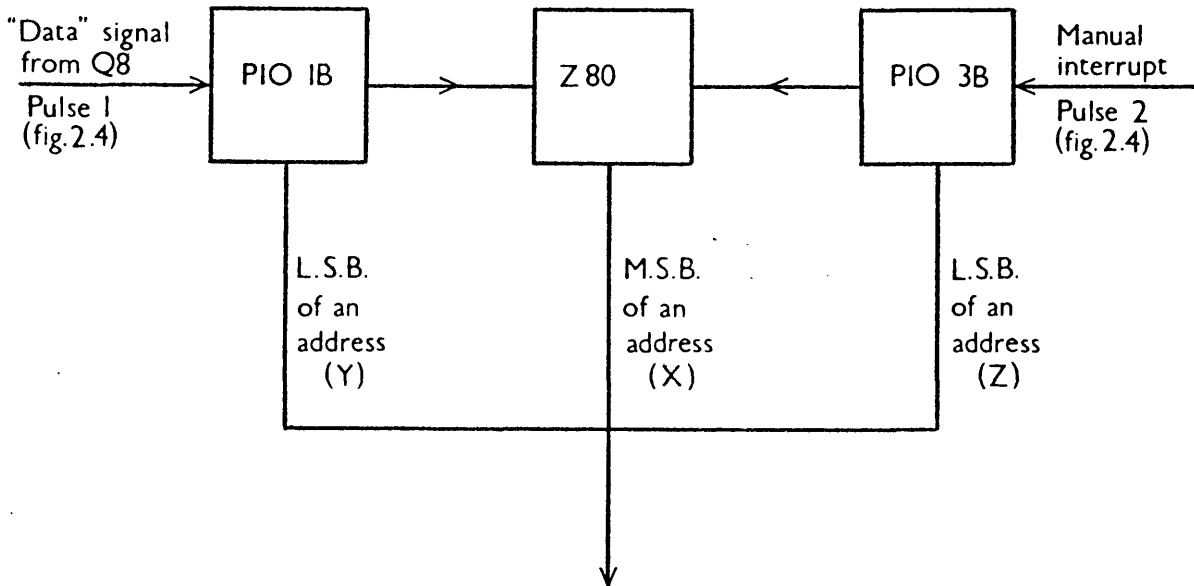


Fig. 2.6

Interrupt Mechanism.

An interrupt causes the computer to stop its current task and to proceed with a different one, usually returning to the first job at the end of the interrupt procedure.



Arrival of the "data ready" pulse (from the DVM) at PIO 1B generates an interrupt. The address XY is put together, the two halves having previously been stored on the appropriate chip. Program execution is transferred to the address found at location XY.

Similarly, for the "manual interrupt" program execution is transferred to the address found at location XZ. (In the Q8 program, X is the same for both interrupts.)

Fig.2.7 Typical Shape of a Peak Height vs Time Plot for a Reactant

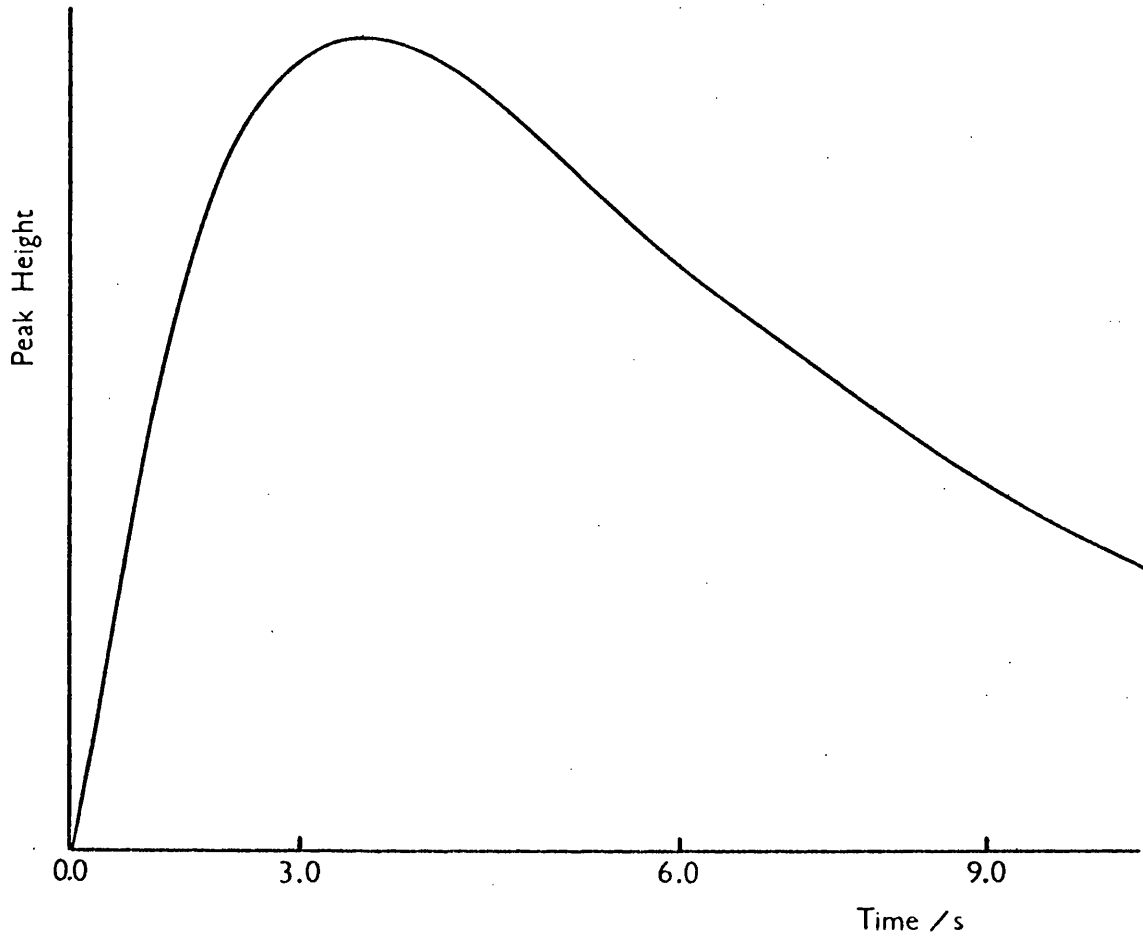


Table 2.1. Effect on Arrhenius parameters of changing the leak out rate constant from .001 - .002 s⁻¹.

Temp /K	Measured Rate Constant for loss reactant (k)/s ⁻¹	k-0.001 =k ₁ /s ⁻¹	ln k ₁	k-0.002 =k ₂ /s ⁻¹	ln k ₂
760	.007	.006	-5.116	.005	-5.298
830	.180	.179	-1.720	.178	-1.726
Arrhenius parameters /s ⁻¹ and KJ mol ⁻¹		k ₁ = 10 ^{15.3} e ^{$\frac{-254}{RT}$} s ⁻¹		k ₂ = 10 ^{16.1} e ^{$\frac{-268}{RT}$} s ⁻¹	

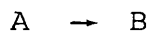
though recent work has shown it to be more complicated than this.

Material also "leaked out" of the reaction vessel, via the pin hole, into the ion source of the mass spectrometer. Therefore, some reactant was lost "unchanged" from the system, necessitating a small correction to be made when determining a decomposition rate constant. The leak out process was assumed to be first order, so a rate constant measured for the unimolecular loss of a reactant from the system was in fact the sum of two first order rate constants, that for the pyrolysis and that for leak out.

The leak out correction was important at lower pyrolysis temperatures, when the decomposition and leak out rate constants were of similar size. At higher pyrolysis temperatures it was less important. Table 2.1 demonstrates the effect of a small change in the leak out rate constant on calculated decomposition Arrhenius parameters.

(ii) Determination of Pyrolysis Rate Constants.

For a first order reaction



then

$$\ln(a-x) = -kt + \ln a$$

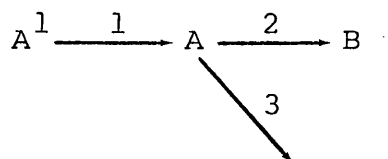
where a is the initial amount of A and x is the amount which has reacted with rate constant k at time t .

A plot of $\ln(a-x)$ vs t ought to give a straight line of slope $-k$ and intercept $\ln a$. In the experimental system $(a-x)$ was measured directly as the peak height of the reactant.

The up-date of the apparatus to version 4, which involved the introduction of a micro computer to collect and process the mass spectrometer data, enabled a new

"computer comparison" method of rate constant determination to be attempted.

The pyrolysis process was described thus,



where species A^1 represented the reactant in the "transducer region" of the vacuum line. When tap 1 (see fig. 2.1) was opened, the reactant flowed, with rate constant k_1 , into the reaction vessel, where it decomposed with rate constant k_2 and leaked out with rate constant k_3 .

The full mathematical equation which describes the concentration of species A is⁵³,

$$A = A_0^1 k_1 \left[\frac{e^{-k_1 t}}{((k_2+k_3)-k_1)} + \frac{e^{-(k_2+k_3)t}}{(k_1-(k_2+k_3))} \right]$$

thus,

$$A = A_0^1 k_1 / (k_1 - (k_2 + k_3)) \left[e^{-(k_2+k_3)t} - e^{-k_1 t} \right] \quad \text{(xiii)}$$

An interactive computer program was written to display the experimental peak height vs time curve for a reactant and to superimpose onto it a curve calculated by the above expression. The values of the rate constants used in the calculation could be independently varied to obtain the best fit of the calculated curve to the experiment, though normally, for any series of pyrolyses, k_1 and k_3 were kept constant. A value for k_3 could be measured experimentally and a value for k_1 , which was also temperature independent, was chosen by fitting a calculated curve to the experimental data from a relatively low temperature run. The value of A^1 used in the calculation was determined from the experimental data by substitution of the maximum reactant peak height into the following expression.

$$A_0^1 = R_{\max} / (K/k_1)^K / (k_1 - K) \quad \text{ref. 54}$$

where $K=k_2+k_3$ and R_{\max} was the maximum peak height of the reactant.

The above computer comparison method for determining decomposition rate constants was used with varying success. For some compounds the calculation was a very good fit to a large portion of the experimental curve, for others the calculation could only be fitted to the top of the experimental curve.

(iii) Determination of the initial amount of reactant.

Accurate determination of the initial amount of reactant (A_0) was difficult. The simple mathematical equations which describe the loss of a reactant by a first order process state that a plot of $\ln(A_0-x)$ vs time will have an intercept of $\ln A_0$.

This was not true however for the experimental system described here, owing to the initial build up or leak of material into the reaction vessel. The standard theory assumes an "instantaneous" initial amount of reactant in the reaction vessel.

However, the extrapolation of plots of $\ln(\text{peak height})$ vs time back to zero time was generally the method used to estimate A_0 , since there was no better way. The value of A_0 tended to be over estimated towards higher pyrolysis temperatures.

(iv) Dead Space.

The reaction vessel essentially consisted of two sections, the cylindrical pyrolysis region enclosed by the furnace, and the inlet tube through which the reactant had to flow to get to the pyrolysis region. This inlet into the reaction zone could not be heated all along its length, resulting in a cold region or "dead space" within

the reaction vessel. In a pyrolysis reaction which proceeded with an increase in pressure, reactant would tend to be pushed out of the reaction zone into the dead space. The opposite would happen if there were a decrease in pressure. A significant dead space effect would lead to a deviation from true first order kinetic behaviour and plots of \ln (concentration) vs time would be curved. For version 1 of the apparatus, the dead space was estimated to be about 10% of the total volume of the reaction vessel. The significance of this was investigated as outlined below.

An alternative way of determining the rate constant for a first order decomposition has been described by Swinbourne⁵⁵ thus,

$$\phi_n = \phi \left[1 - \exp(k \cdot \Delta t) \right] + \phi'_n \exp(k \cdot \Delta t)$$

where ϕ_n is the value of a time dependent property of reactant n at time t and ϕ'_n is the value of the same property at time (t+ Δt). The interval Δt should be about 2.5 half lives.

Thus a plot of reactant peak height at time t vs the peak height at time (t+ Δt) ought to give a straight line of slope $\exp(k \cdot \Delta t)$, where k is the rate constant for the loss of the reactant.

Using 1,1-dimethylsilacyclobutane (DMSCB) as a test compound, the above "Swinbourne" method was compared with the conventional "logs" method for determining pyrolysis rate constants. A mixture of DMSCB and hydrogen chloride (3:1) was pyrolysed over the temperature range 743-855K. The decomposition mechanism and the significance of the hydrogen chloride will be discussed in chapter 4. The

well established literature rate constants for the decomposition of DMSCB were given by $\log_{10} k = 15.64 - 261.5 \text{ KJ mol}^{-1} / 2.303 \text{ RT}^{39}$.

For each experimental "run", the decomposition rate constant was calculated both by the conventional "logs" way and by the "Swinbourne" method. The results are shown in table 2.2. The Arrhenius plot from the "Swinbourne" data is in fig. 2.8 and that from the "logs" data in fig. 2.9.

It is clear, both from table 2.2 and from each Arrhenius plot, that rate constants above about 0.06 s^{-1} were not estimated correctly by either method, though the "Swinbourne" values were closer to those from the literature. Up to 0.06 s^{-1} both methods returned rate constants which approximately matched the literature values.

A least squares fit over the "Swinbourne" data up to 814K gave $\log_{10} k = (15.23 \pm .19) - (255.7 \pm 2.8 \text{ KJ mol}^{-1}) / 2.303 \text{ RT}$. Likewise for the "logs" data gave $\log_{10} k = (15.45 \pm .24) - (259.2 \pm 3.7 \text{ KJ mol}^{-1}) / 2.303 \text{ RT}$, though without the anomalous point at 813K, the Arrhenius parameters were the same as those from the "Swinbourne" data.

As there was no significant difference between the two methods of determining decomposition rate constants it was concluded that dead space was not a serious problem.

In version 4 of the apparatus, the dead space only amounted to about 4% of the total reaction vessel volume and was therefore even less important than in version 1.

(v) Arrhenius parameters.

The Arrhenius parameters obtained above for the decomposition of DMSCB were less than the literature values, giving rate constants of about 90% the literature. Other

Table 2.2. Comparison between "Swinbourne" and "logs"
rate constants.

Temp/K	Literature Rate Constant /s ⁻¹	"Swinbourne" Rate Constant k _s /s ⁻¹	lnk _s	"Logs" Rate Constants k/s ⁻¹	lnk
743	.0018	.0019	-6.266	.0019	-6.226
753	.0032	.0031	-5.776	.0028	-5.878
754	.0033	.0031	-5.776	.0028	-5.878
763	.0055	.0054	-5.221	.0052	-5.259
763	.0055	.0047	-5.360	.0048	-5.339
773	.0093	.0092	-4.689	.0089	-4.722
774	.0098	.0091	-4.700	.0083	-4.792
774	.0098	.0095	-4.657	.0091	-4.700
782	.0149	.0140	-4.269	.0134	-4.313
782	.0149	.0140	-4.269	.0131	-4.335
783	.0157	.0126	-4.374	.0135	-4.305
792	.0247	.0243	-3.717	.0236	-3.747
792	.0247	.0252	-3.681	.0237	-3.742
793	.0260	.0248	-3.697	.0233	-3.759
802	.0405	.0397	-3.226	.0359	-3.327
802	.0405	.0388	-3.249	.0395	-3.232
802	.0405	.0383	-3.262	.0364	-3.313
813	.0689	.0604	-2.807	.0586	-2.837
813	.0689	.0593	-2.825	.0595	-2.822
813	.0689	.0639	-2.750	.0775	-2.558
814	.0723	.0638	-2.752	.0602	-2.810
814	.0723	.0647	-2.738	.0629	-2.766
814	.0723	.0651	-2.732	.0618	-2.784

(Table 2.2 continued).

Temp/K	Literature Rate Constant /s ⁻¹	"Swinbourne" Rate Constant k _s /s ⁻¹	lnk _s	"Logs" Rate Constants k/s ⁻¹	lnk
833	.1744	.1287	-2.050	.1141	-2.171
833	.1744	.1327	-2.020	.1161	-2.153
834	.1825	.1357	-1.997	.1211	-2.111
844	.2853	.2093	-1.564	.1701	-1.771
844	.2853	.2020	-1.600	.1585	-1.842
845	.2982	.2077	-1.572	.1698	-1.773
853	.4228	.3001	-1.204	.2338	-1.432
855	.4609	.3133	-1.161	.2265	-1.485
855	.4609	.3060	-1.184	.2265	-1.485

Fig. 2.8 Arrhenius plot for the decomposition of DMSCB from "Swinbourne" data.

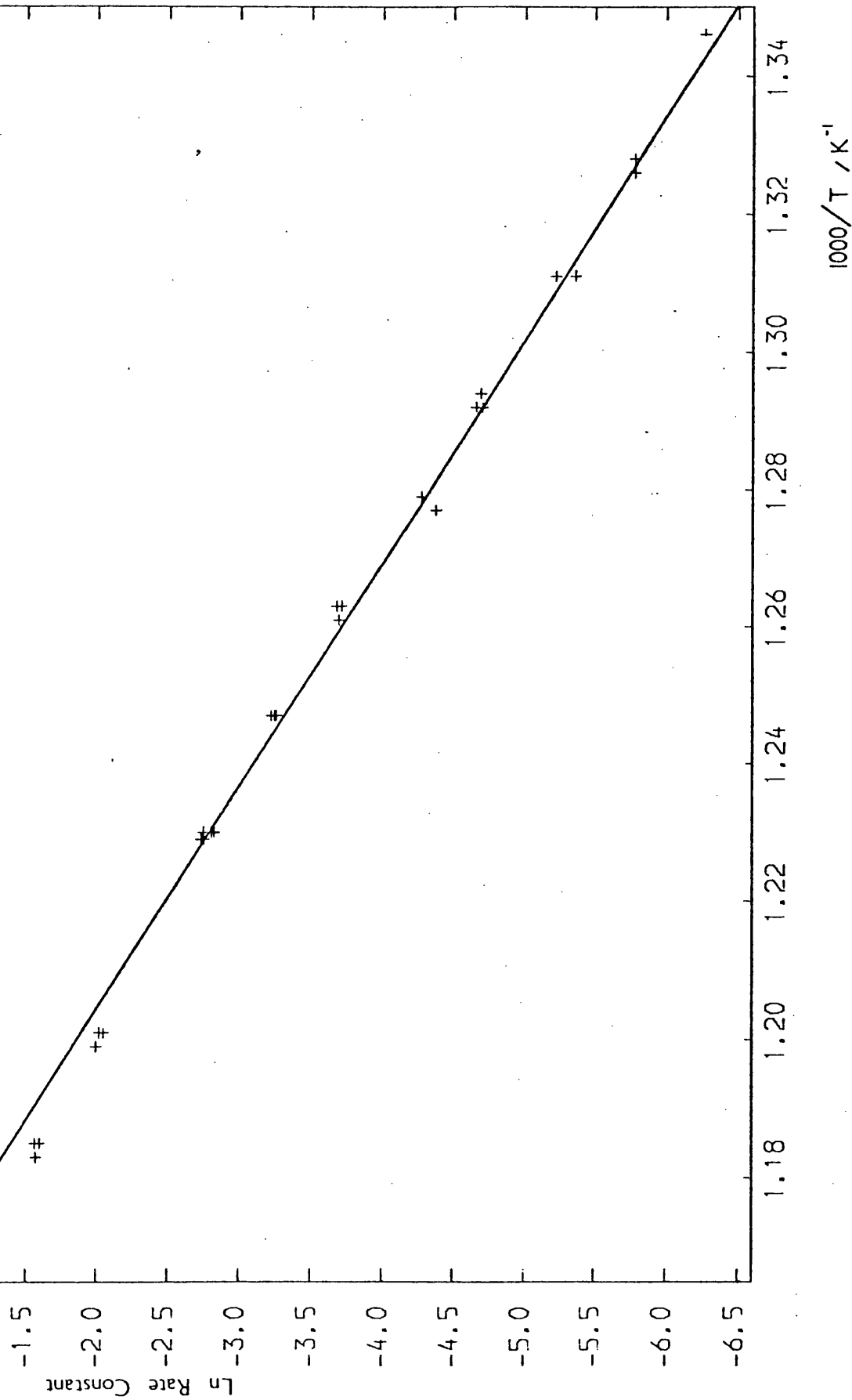
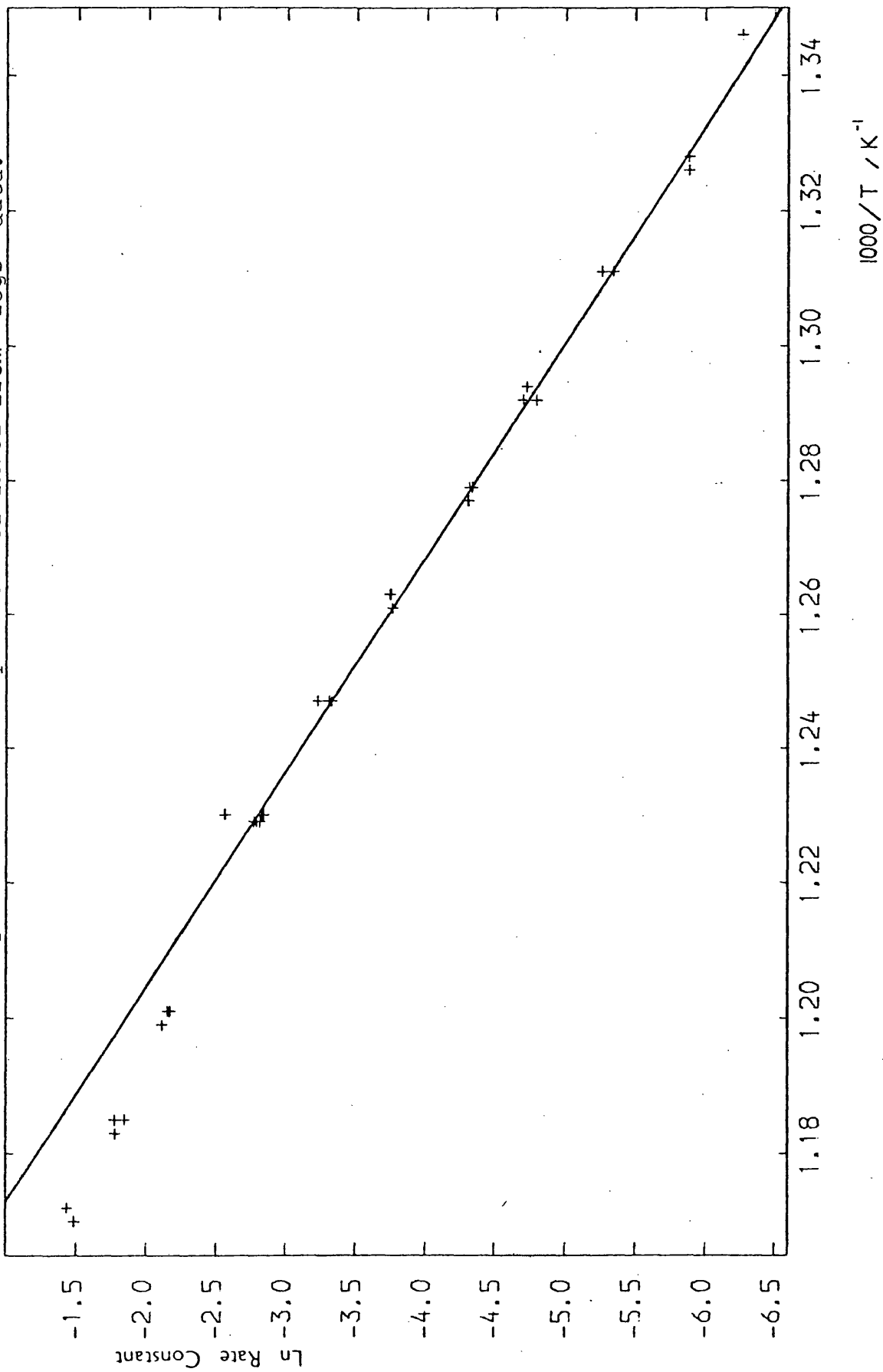


Fig. 2.9 Arrhenius plot for the decomposition of DMSCB from "logs" data.



series of experiments involving the same compound were carried out and this proved to be a consistent feature of the apparatus. The exact reason was not established, but was probably simply an artifact of the experimental system. The experiments described in the paragraphs above demonstrated that dead space was not responsible and it had been shown earlier (fig. 2.2) that the temperature gradient along the reaction vessel was small.

In the context of the work to follow however, the under estimation of Arrhenius parameters was not a serious problem, though the results obtained should be taken as a lower limit for the pyrolysis reaction concerned.

(vi) Product formation.

The leak-in and leak-out processes, inherent to the experimental system, made quantification of product formation difficult.

Owing to the leak in process, the measured maximum initial rate of formation of a product was an under-estimate of the true rate, the error being worse towards higher temperatures.

As products as well as reactants leaked out of the reaction vessel, the measured amount of product present in the system at any time was an under-estimate of the amount that had been formed. The error was worse with increasing time.

For version 1 of the apparatus, little could be done to solve the product problems, but a method was derived for version 4, with the aid of the micro computer and this will be described in chapter 5.

(vii) Fragmentation and Sensitivity Corrections.

Different species involved in a particular reaction may have coincident peaks in their mass spectra. Therefore it was sometimes necessary to correct the peak being used to follow a particular compound for the contribution from a second compound. In order to calculate the ratio between, say, two products, calibration was necessary. This was achieved by putting a mixture of the two products, in known proportions, into the mass spectrometer and reading off their peak heights. The ratio of these peak heights, when adjusted to correspond to a 1:1 mixture, was the sensitivity correction factor between the two products.

(viii) Interpolation of Data.

In version 1 of the apparatus, which used a four channel PP2, each channel was read every 3s. It was therefore difficult to compare directly, say channel 1 with channel 3, as their times were out of step by 1.5s.

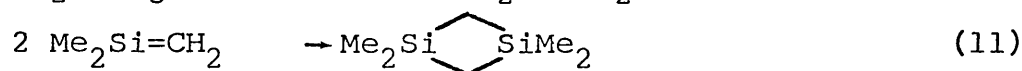
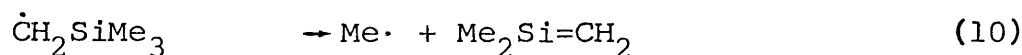
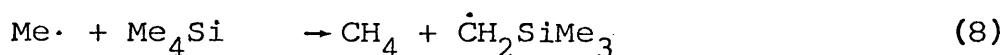
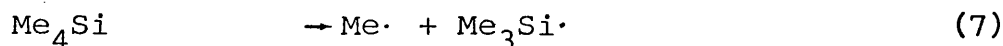
To correct for this, a computer routine was introduced at the processing stage which interpolated the data in 0.75s steps using a curve fitting method. Comparisons between channels were thus made easier.

CHAPTER THREE

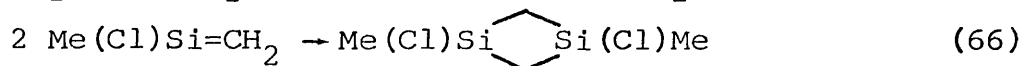
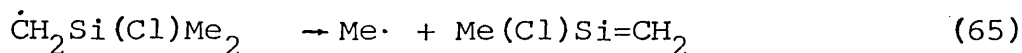
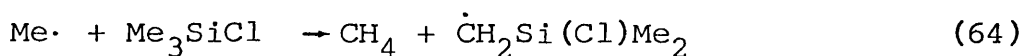
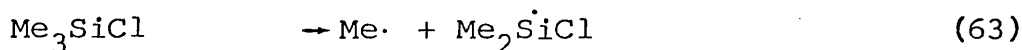
**PYROLYSIS OF
TRIMETHYLCHLOROSILANE**

3.1 Introduction

As discussed in Chapter 1, tetramethylsilane (TMS) has been shown to pyrolyse by a radical chain mechanism involving the formation of a reactive silaethene intermediate which then dimerises¹³.



Trimethylchlorosilane (3MCS) would be expected to decompose in an analogous way thus,



+ other reactions involving silicon-centred radicals.

The disilacyclobutane, if formed, could be useful as a precursor to polymeric materials containing $(-\text{Si}-\text{C}-)_n$ units.

3.2 Pyrolysis of 3MCS

Initial, qualitative experiments showed the major pyrolysis products to be hydrogen, methane and dimethyldichlorosilane (2M2CS). Small amounts of methyltrichlorosilane and tetrachlorosilane were also formed. There was no evidence for the formation of the dimeric product.

Some hydrogen chloride was produced, but this was thought to have come from the hydrolysis of the reactant

by background water inside the apparatus, a small peak at $m/e=147^+$, from a fragment of the hydrolysis product (hexamethyldisiloxane), being observed.

Many series of experiments were carried out to measure the activation energy for the decomposition of 3MCS. The majority of the measurements were made using version 1 of the apparatus, though the best quantitative results were finally obtained with version 4.

Typically, plots of \ln (peak height) vs time for the pyrolysis of this reactant were curved, as the example in fig. 3.1 demonstrates. The curvature was probably caused by some of the reactant adsorbing in the vicinity of the ion source and then desorbing back into the gas phase. These problems made it difficult to acquire consistently reliable kinetic data.

(i) Summary of Earlier Work.

As discussed in Chapter 1, the Arrhenius plot for the pyrolysis of TMS^{13} consisted of two linear regions, the higher temperature one being thought to correspond to the first order dissociation of the reactant. Thus, the initial pyrolyses of 3MCS were carried out at relatively high temperatures and first order decomposition rate constants were calculated, from the maximum slope of the \ln (peak height) vs time plots. The results from several series of experiments are shown in table 3.1 and the Arrhenius plot in fig. 3.2. A least squares fit over all the data between 1042 and 1112K gave $\log_{10} k = (14.15 \pm .33) - (310.6 \pm 6.9 \text{ KJ mol}^{-1}) / 2.303RT$.

Some experiments were carried out to measure the order of the pyrolysis reaction. For the process

Fig. 3.1 Typical plot of $\ln(\text{Peak Height})$ vs Time for the decomposition of 3MCS.

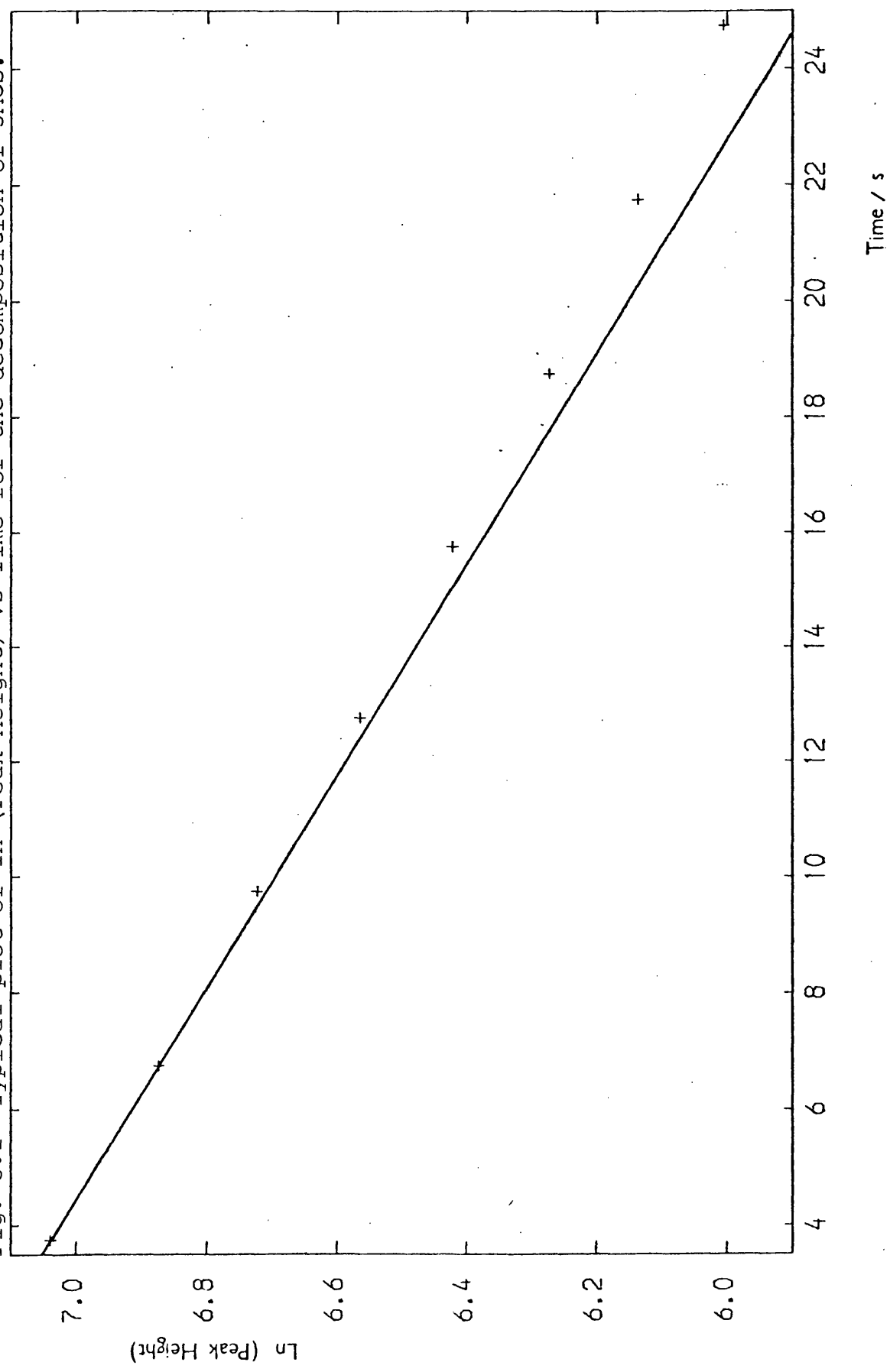
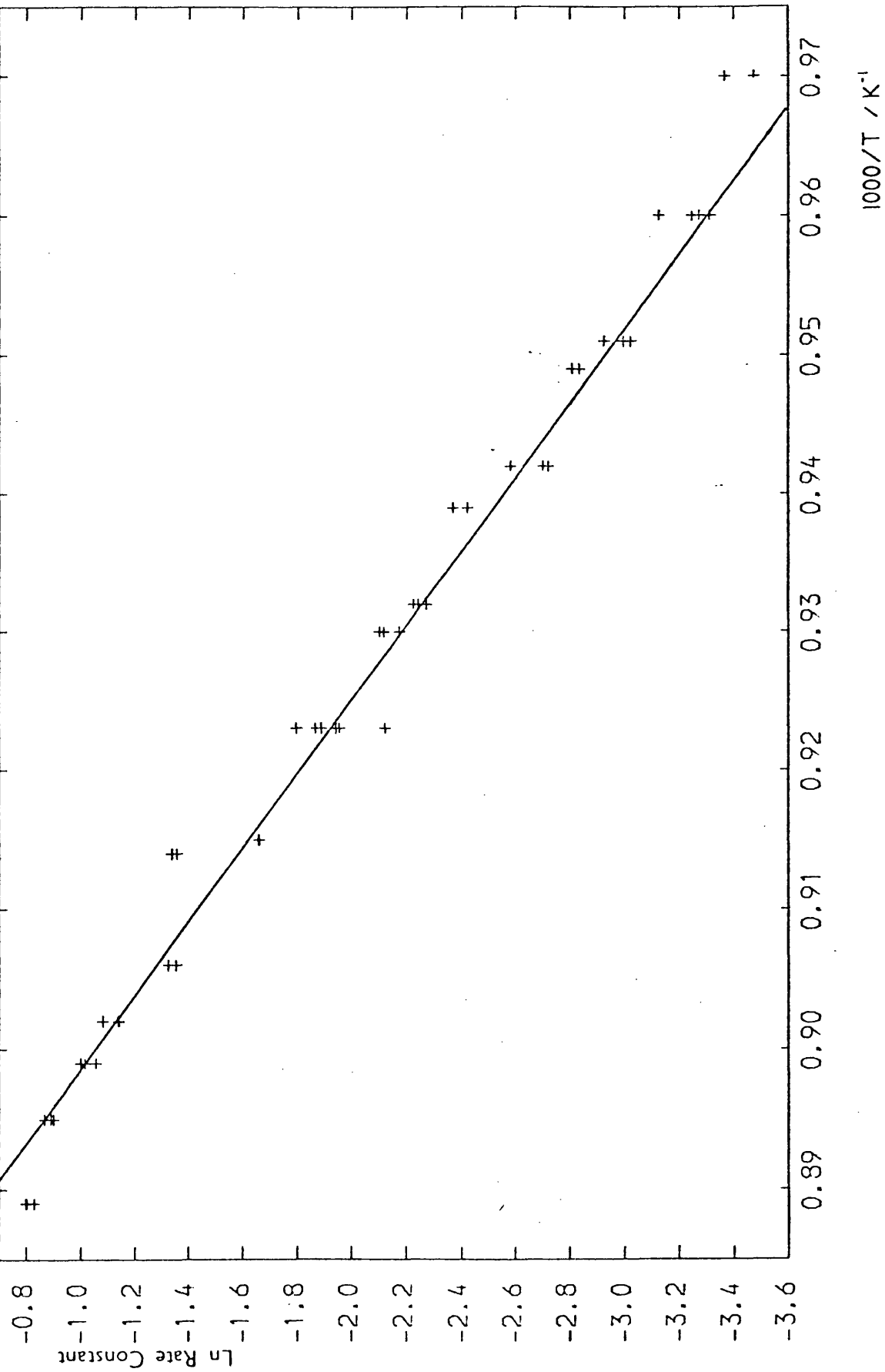


Table 3.1 Rate Constants for the pyrolysis of 3MCS (Corrected
for leak out).

Temp/K.	Rate Constant (k)/s ⁻¹	lnk.	Temp/K	Rate Constant (k)/s ⁻¹	lnk.
1031	.0311	-3.471	1084	.1665	-1.793
1031	.0345	-3.367	1084	.1550	-1.864
1042	.0389	-3.247	1084	.1438	-1.939
1042	.0364	-3.313	1084	.1421	-1.951
1042	.0378	-3.276	1084	.1202	-2.119
1042	.0439	-3.126	1093	.1903	-1.659
1052	.0487	-3.022	1093	.1910	-1.656
1052	.0500	-2.996	1094	.2580	-1.355
1052	.0536	-2.926	1094	.2624	-1.338
1054	.0588	-2.834	1094	.2629	-1.336
1054	.0603	-2.808	1104	.2584	-1.353
1054	.0603	-2.808	1104	.2662	-1.324
1062	.0658	-2.721	1109	.3198	-1.140
1062	.0756	-2.582	1109	.3204	-1.138
1062	.0670	-2.703	1109	.3389	-1.082
1065	.0939	-2.366	1112	.3621	-1.016
1065	.0889	-2.420	1112	.3472	-1.058
1073	.1030	-2.273	1112	.3678	-1.000
1073	.1079	-2.227	1117	.4069	-0.899
1073	.1059	-2.245	1117	.4203	-0.867
1075	.1207	-2.115	1117	.4106	-0.890
1075	.1138	-2.173	1125	.4368	-0.828
1075	.1225	-2.100	1125	.4503	-0.798
1084	.1518	-1.885	1126	.4490	-0.801

Fig. 3.2 Arrhenius plot for the decomposition of 3MCS.



A → Products

$$(\text{Initial Rate Decomposition}) = k [A_0]^n$$

where reactant A decomposes with rate constant k and order n, therefore,

$$\log (\text{Initial Rate}) = n \log [A_0] + \log k$$

thus, a plot of $\log (\text{Initial Rate})$ vs $\log A_0$, the initial amount of reactant, ought to be a straight line of slope n.

The results from two series of experiments, one at 1020K, the other at 1033K gave orders of $1.07 \pm .02$ and $1.26 \pm .04$ respectively. Table 3.2 shows the data and fig. 3.3 the plot for the former series and table 3.3 the data and fig. 3.4 the plot for the latter. The initial amount of reactant in each case was estimated by extrapolation of the peak height vs time plot back to zero time.

The difference between the two results obtained above could have been caused by a change in the surface condition of the reaction vessel, less radical species being removed from the gas phase in the second series of experiments.

For a non first order process, the rate constant for the decomposition of reactant is given by⁵⁶

$$k = \frac{1}{(n-1)t} \left[\frac{1}{(a-x)^{(n-1)}} - \frac{1}{a^{(n-1)}} \right] (\text{mol dm}^{-3})^{-(n-1)} \cdot \text{s}^{-1}$$

therefore

$$\frac{1}{(a-x)^{(n-1)}} = (n-1)kt + \frac{1}{a^{(n-1)}} \quad (\text{xiv})$$

where (a-x) is the amount of reactant decomposed and n is the order of the reaction.

A plot of $\frac{1}{(a-x)^{(n-1)}$ vs time t ought to give a straight line of slope $(n-1)k$.

Table 3.2 Initial Peak Height and Initial Rate, T=1029K

Initial Peak Height	ln(Height)	Initial Rate /Height . s ⁻¹	ln(Rate)
2044	7.623	36.7	3.603
2558	7.847	45.0	3.807
2590	7.859	46.0	3.829
3026	8.015	62.0	4.127
5086	8.534	92.0	4.522
6037	8.706	96.0	4.564
6046	8.707	110.0	4.701
6863	8.834	145.0	4.977
7516	8.925	143.0	4.963
8014	8.989	148.0	4.997
8412	9.037	165.0	5.106
8719	9.073	175.0	5.165
8921	9.096	181.0	5.199
9646	9.174	210.0	5.347
9939	9.204	207.0	5.333
10016	9.212	193.4	5.265
10155	9.226	205.0	5.323
11423	9.343	223.4	5.409
11727	9.370	234.0	5.455
13492	9.510	273.4	5.611
14327	9.570	290.0	5.670
15537	9.651	316.7	5.758

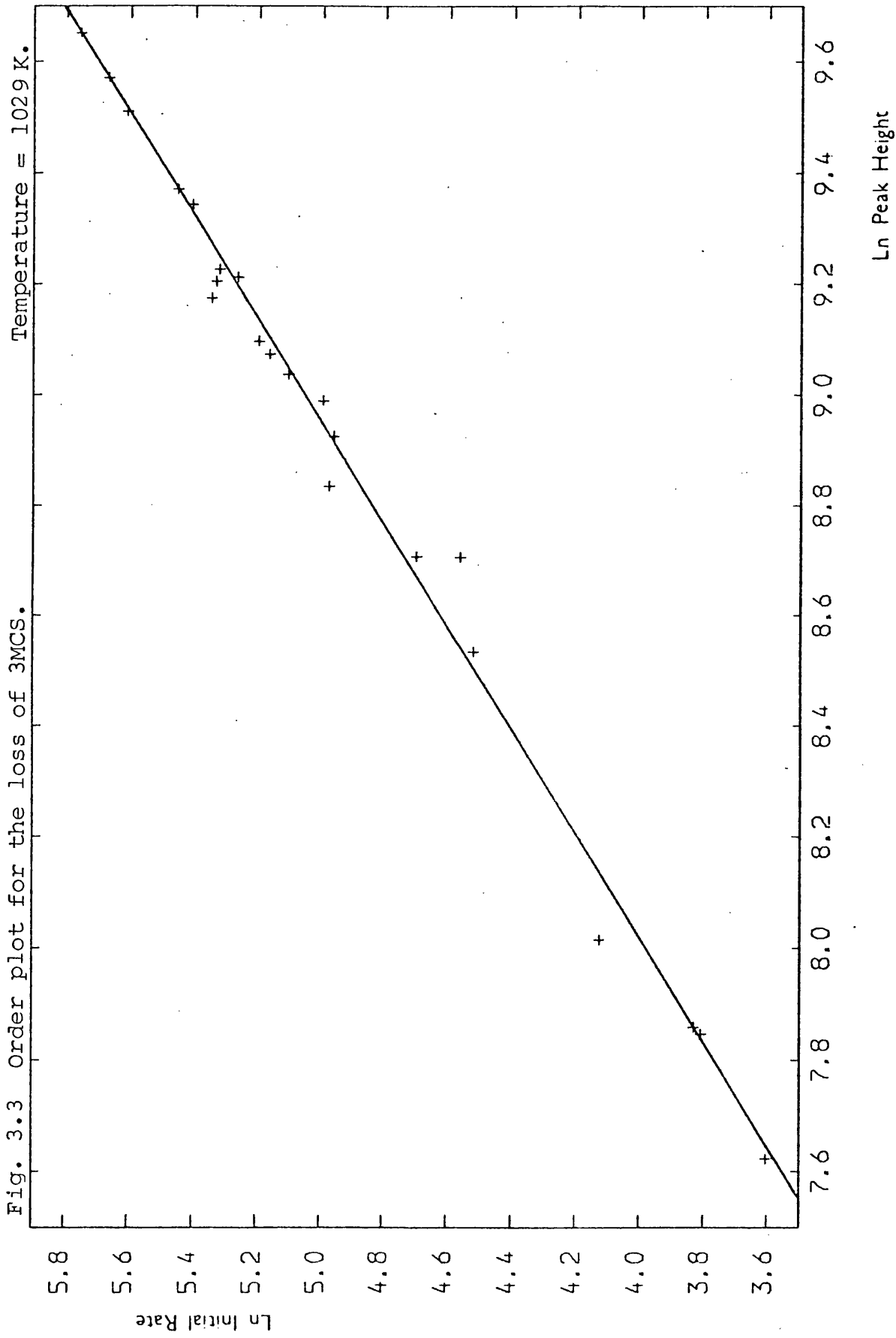
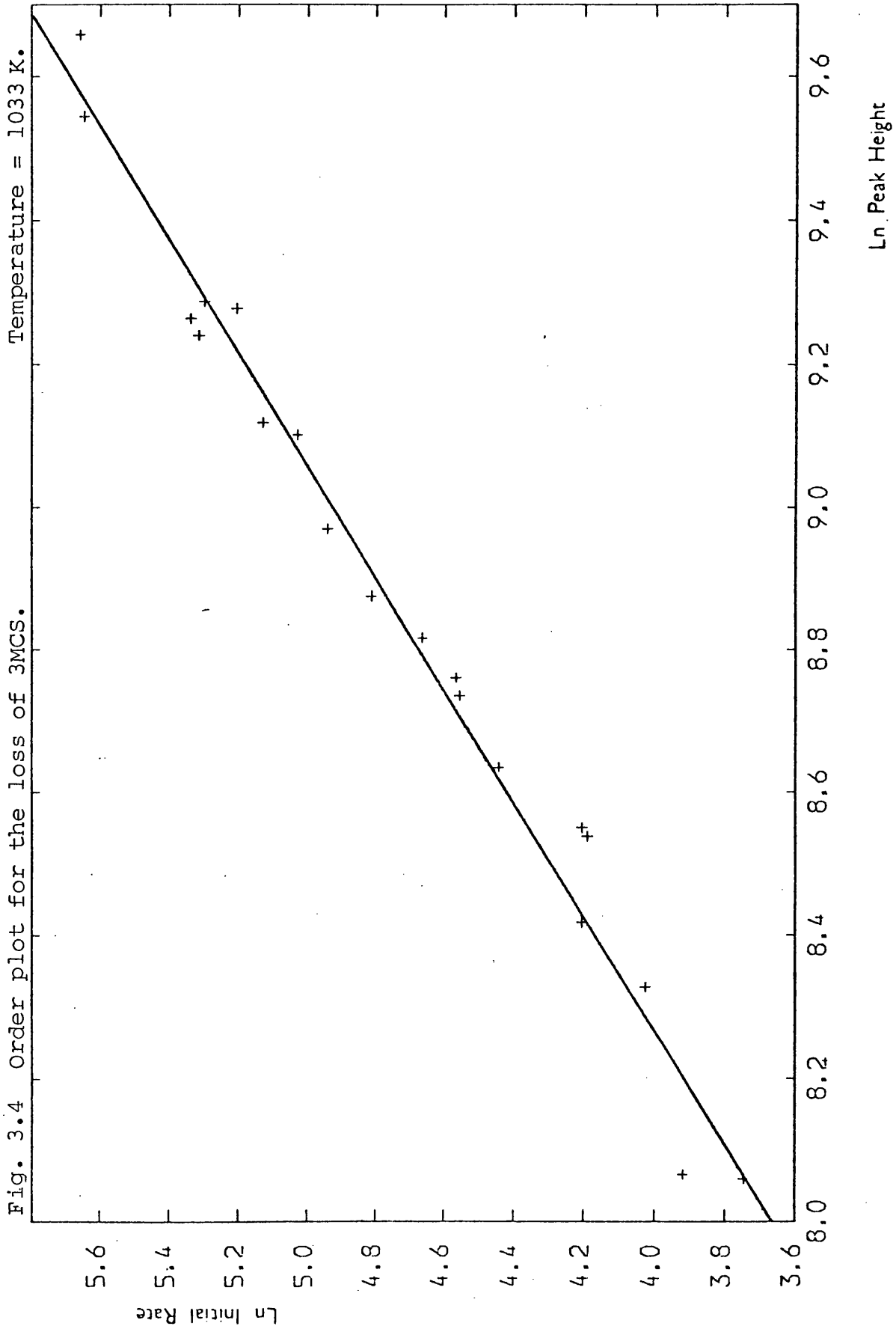


Table 3.3 Initial Peak Height and Initial Rate.

T=1033K.

Initial Peak Height	ln(Height)	Initial Rate /Height . s ⁻¹	ln(Rate)
3166	8.060	42.3	3.745
3184	8.066	50.3	3.918
4139	8.328	56.0	4.025
4527	8.418	67.0	4.205
5103	8.538	66.0	4.190
5165	8.550	67.0	4.205
5619	8.634	85.0	4.443
6218	8.735	95.0	4.554
6372	8.760	96.0	4.564
6743	8.816	106.0	4.663
7151	8.875	123.0	4.812
7867	8.970	140.0	4.942
8975	9.102	153.0	5.030
9125	9.119	169.0	5.130
10302	9.240	203.3	5.315
10550	9.264	208.0	5.338
10696	9.278	182.2	5.205
10809	9.288	200.0	5.298
13960	9.544	283.3	5.647
15640	9.658	286.7	5.658



3MCS was pyrolysed at 1094K and the reactant peak height data plotted according to eqn. xiv. A straight line was obtained with $n=1.2$, the plots with $n=1.1$ and with $n=1.3$ being curved, in opposite directions, away from a straight line (see figs. 3.5-3.7).

By the same method, the pyrolysis reaction at 1115K was found to have an order of about 1.1. This reduction in the order with increasing temperature was consistent with the pyrolysis of TMS.

No further work involving 3MCS was carried out using version 1 of the apparatus.

(ii) Summary of Later Work

The most recent experiments were carried out using version 4 of the apparatus, eight channels per second being used to monitor the reactant. This enabled six times as much data to be collected than for the previous experiments, so the behaviour of the reactant, especially in the early stages of the pyrolysis could be followed more closely than before.

The plots of $\ln(\text{Peak Height})$ vs time were curved, as they had been earlier, but a new processing method was now available. Decomposition rate constants were determined with the aid of the "Computer Comparison" routine which was described in section 4 of chapter 2. The calculated curve was fitted to the experimental peak height vs time curve to about 10% decomposition. At the relatively high temperatures used (1070-1149K), the pyrolysis was probably first order during this time.

A summary of the results from three series of experiments is shown in table 3.4 and the Arrhenius plot in fig. 3.8. A least squares fit over the more linear central section of the plot, between 1079 and 1130K, gave

Fig. 3.5 Decomposition of 3MCS plotted to order 1.1 .

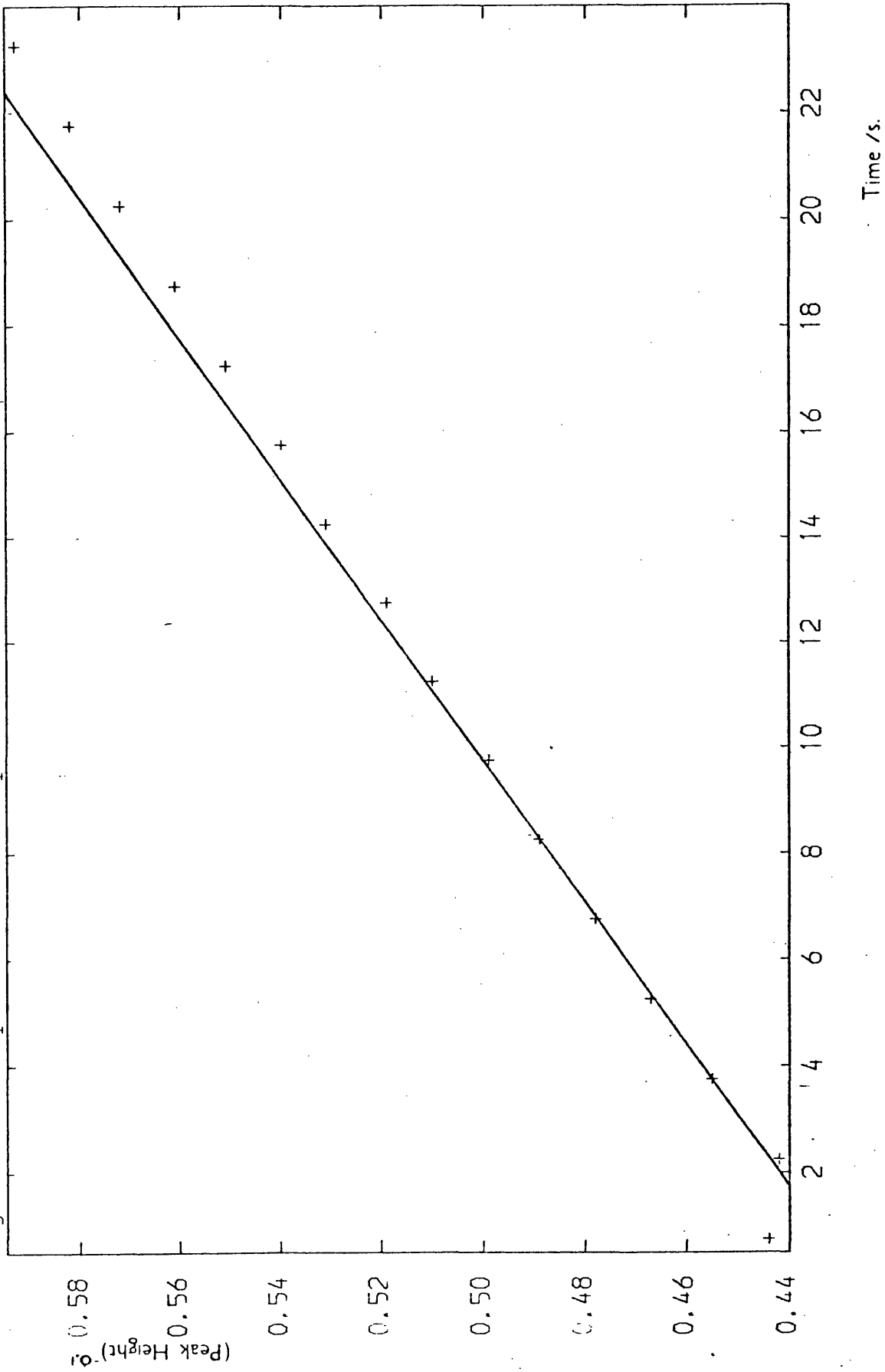


Fig. 3.6 Decomposition of 3MCS plotted to order 1.2 .

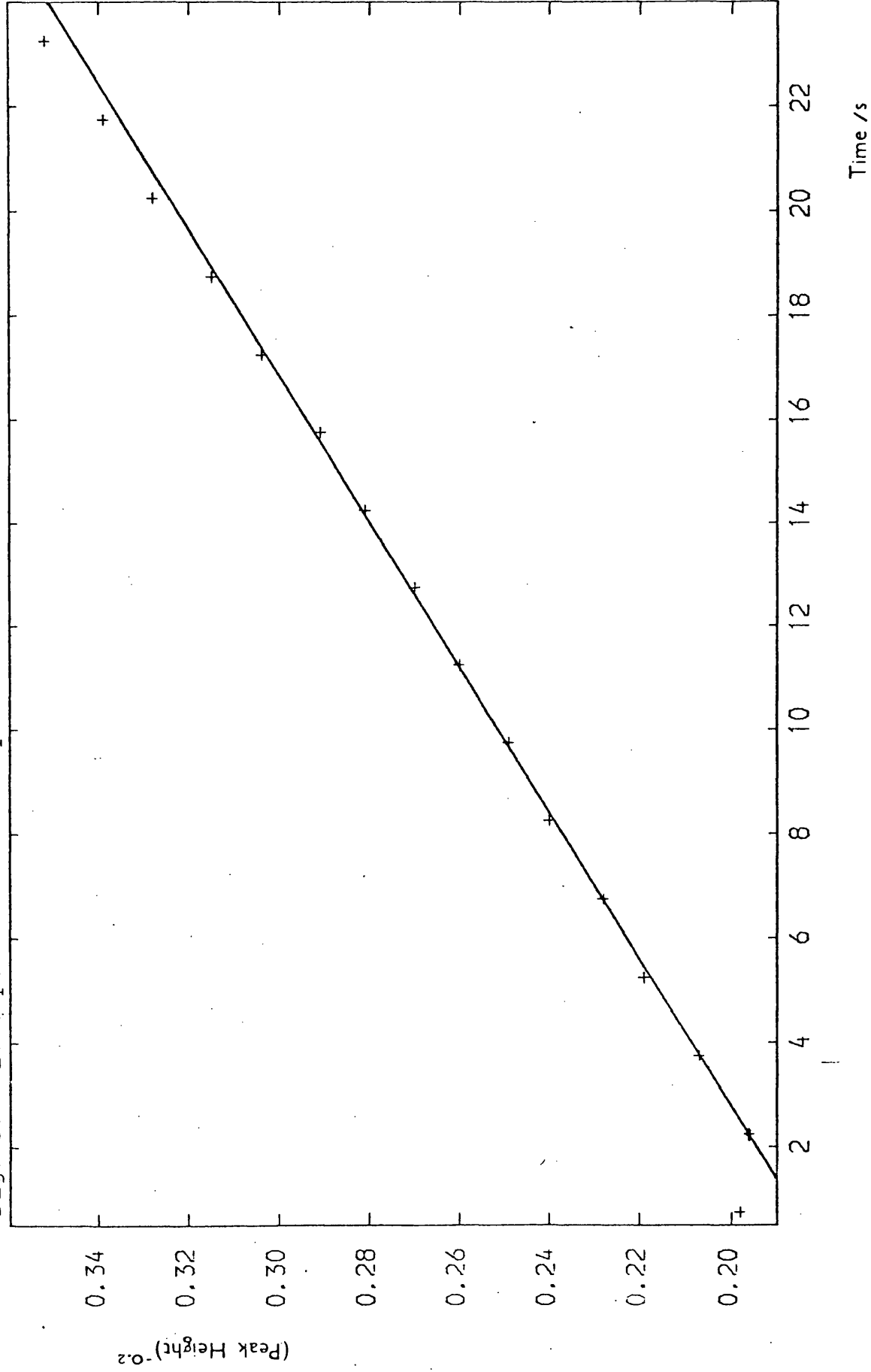


Fig. 3.7 Decomposition of 3MCS plotted to order 1.3 .

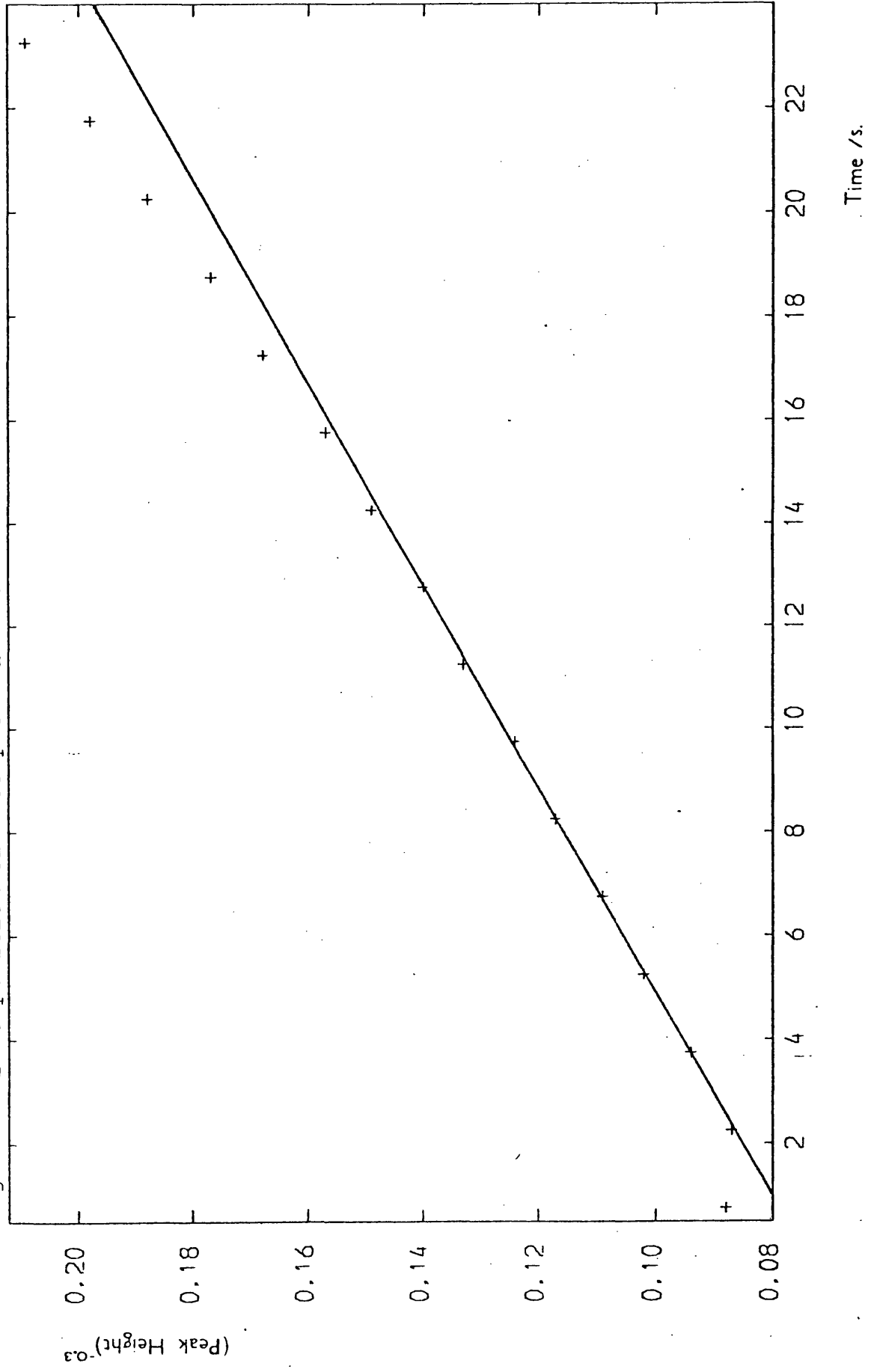


Table 3.4 Rate Constants for decomposition of 3MCS

Leak in Rate Const.= $1.1s^{-1}$, Leak out Rate Const.= $0.015s^{-1}$

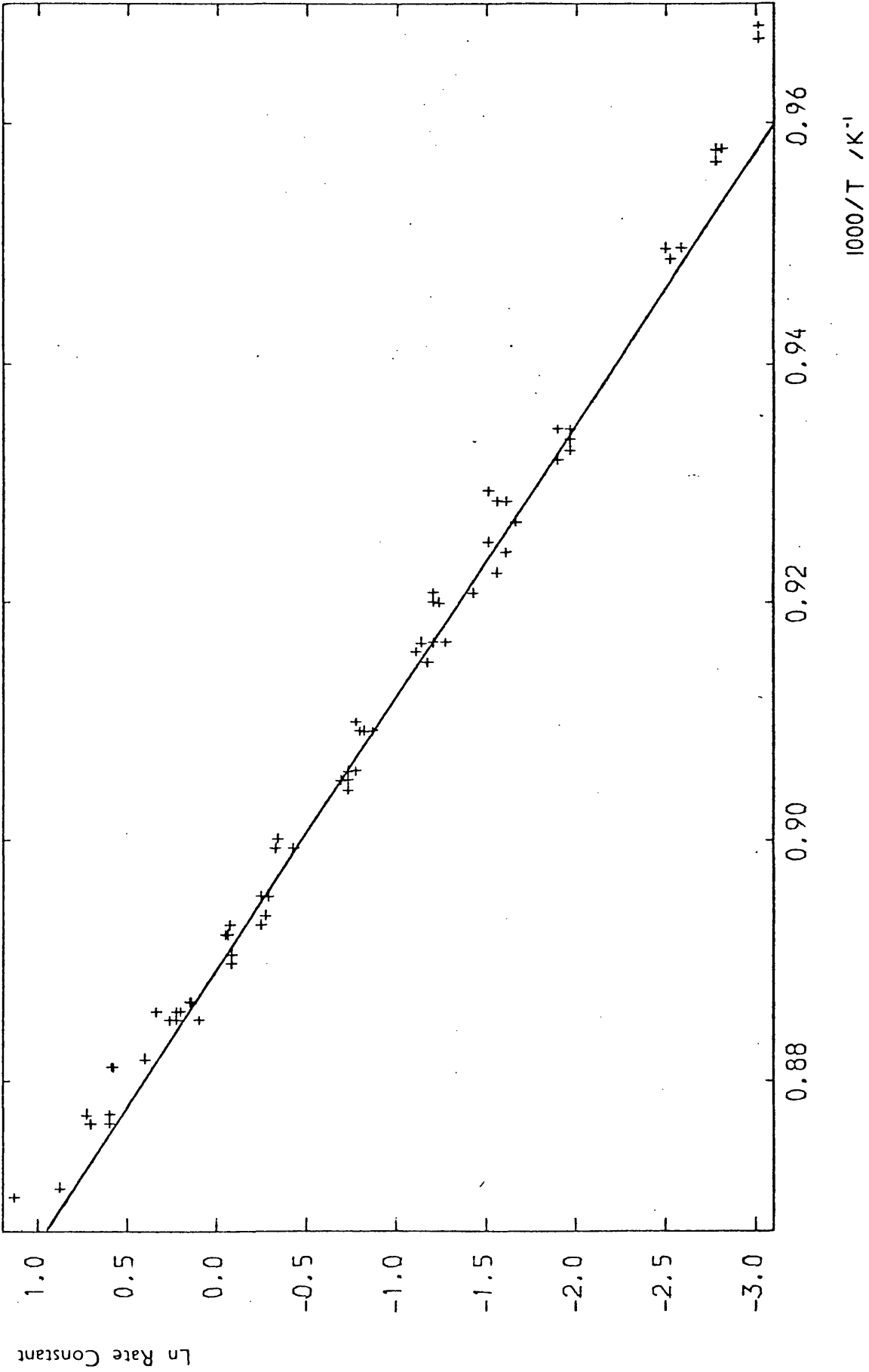
(see section 2.4)

Temp/K	Rate Constant (k)/s ⁻¹	lnk	Temp/K	Rate Constant (k)/s ⁻¹	lnk
1033	0.049	-3.016	1087	0.29	-1.238
1034	0.049	-3.016	1087	0.30	-1.204
1044	0.062	-2.781	1091	0.32	-1.139
1044	0.060	-2.813	1091	0.30	-1.204
1045	0.062	-2.781	1091	0.30	-1.204
1053	0.082	-2.501	1091	0.28	-1.273
1053	0.075	-2.590	1092	0.33	-1.109
1054	0.080	-2.526	1093	0.31	-1.171
1070	0.14	-1.966	1099	0.46	-0.777
1070	0.15	-1.897	1099	0.46	-0.777
1071	0.14	-1.966	1100	0.44	-0.821
1072	0.14	-1.966	1100	0.42	-0.868
1073	0.15	-1.897	1100	0.45	-0.799
1073	0.15	-1.897	1104	0.48	-0.734
1076	0.22	-1.514	1104	0.46	-0.777
1077	0.20	-1.609	1105	0.50	-0.693
1077	0.21	-1.561	1105	0.48	-0.734
1079	0.19	-1.661	1106	0.48	-0.734
1081	0.22	-1.514	1106	0.48	-0.734
1082	0.20	-1.609	1111	0.71	-0.343
1084	0.21	-1.561	1112	0.72	-0.329
1086	0.24	-1.427	1112	0.72	-0.329
1086	0.30	-1.204	1112	0.72	-0.329

(Table 3.4 continued)

Temp/K	Rate Constant (k)/s ⁻¹	lnk	Temp/K	Rate Constant (k)/s ⁻¹	lnk
1112	0.65	-0.431	1129	1.25	0.223
1117	0.75	-0.288	1130	1.10	0.095
1117	0.78	-0.249	1130	1.30	0.262
1119	0.76	-0.274	1130	1.25	0.223
1120	0.78	-0.249	1134	1.49	0.399
1120	0.93	-0.073	1135	1.78	0.577
1121	0.94	-0.062	1135	1.80	0.588
1121	0.95	-0.051	1140	2.07	0.728
1123	0.92	-0.083	1140	1.82	0.599
1124	0.92	-0.083	1141	2.03	0.708
1128	1.15	0.140	1141	2.02	0.703
1128	1.16	0.148	1141	1.82	0.599
1128	1.15	0.140	1141	1.82	0.599
1129	1.40	0.336	1148	2.40	0.876
1129	1.22	0.199	1149	3.1	1.131

Fig.3.8 Arrhenius plot for the decomposition of 3MCS.

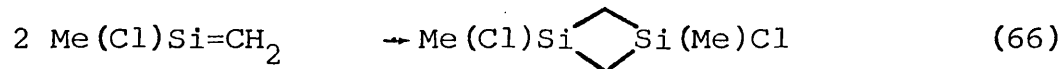
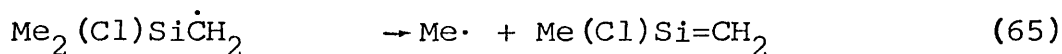
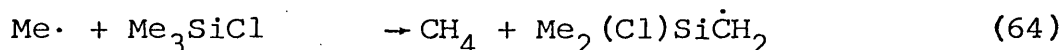
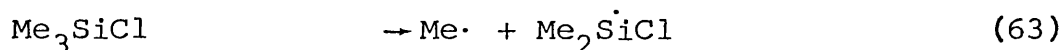


$$\log_{10}k = (17.03 \pm .34) - (366.5 \pm 7.2 \text{ KJ mol}^{-1}) / 2.303RT.$$

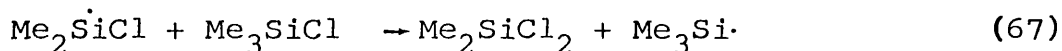
A value of at least 366.5 KJ mol⁻¹ could thus be assigned to the silicon-methyl bond dissociation energy.

3.3 Pyrolysis Mechanism.

In section 3.1 it was stated that, by analogy to the decomposition mechanism of TMS, the pyrolysis of 3MCS would be expected to proceed thus,

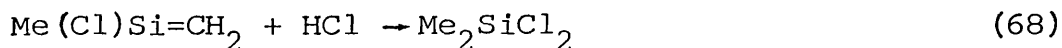


Exchange reactions of the type

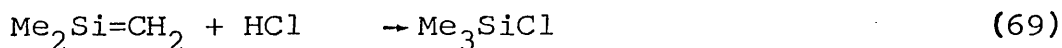


are also known⁵⁷, so this step should be included.

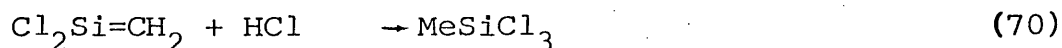
As no dimeric products were observed and there was always a quantity of hydrogen chloride formed (by hydrolysis) whenever 3MCS was put into the apparatus, the possibility for the reaction



was investigated. It was found that the addition reaction

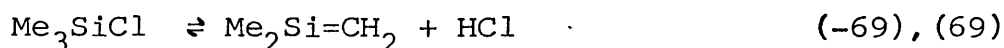


is a very efficient process with an activation energy of about 12 KJ mol⁻¹ and A-factor of 10^{7.5} dm³ mol⁻¹ s⁻¹. The addition reaction,



was also observed, though no kinetic measurements were made. It was concluded that reaction (68) could suppress reaction (66) to the extent that no dimer would be observed in the pyrolysis of 3MCS. A full description of the above work is included in chapter 4.

In view of the low activation energy for the addition reaction (69), the molecular elimination (-69) was an interesting possible step in the pyrolysis of 3MCS.



For this elimination,

$$\Delta H = D(\text{Si-Cl}) + D(\text{C-H}) - D(\text{H-Cl}) - D\pi(\text{Si}=\text{CH}_2)$$

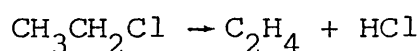
Using the following bond dissociation energies in KJ mol^{-1} ,
 $D(\text{Me}_3\text{Si-Cl}) = 472^{17}$, $D(\text{Me}_3\text{SiCH}_2\text{-H}) = 417^{17}$, $D(\text{H-Cl}) = 431^{19}$
 and $D\pi(\text{Si}=\text{CH}_2) = 163^{17}$,

$$\begin{aligned} \Delta H &= 472 + 417 - 431 - 163 \\ &= 295 \text{ KJ mol}^{-1}. \end{aligned}$$

The activation energy for reaction (69) was estimated to be about 12 KJ mol^{-1} , thus the activation energy for process (-69) is given by

$$E_{-69} = 295 + 12 = 307 \text{ KJ mol}^{-1}.$$

Assuming the A-factor for reaction (-69) to be similar to that for the process



where $\log A = 13.51^{58}$, then at lower pyrolysis temperatures, the elimination reaction (-69) could compete with the dissociation step (reaction 63).

For example at 1000K,

$$k_{63} = 6.75 \times 10^{-3} \text{ s}^{-1} \quad (\text{where } \log_{10} k = 17.0 - 367 \text{ KJ mol}^{-1} / 2.3 \text{ RT})$$

$$k_{-69} = 2.91 \times 10^{-3} \text{ s}^{-1} \quad (\text{where } \log_{10} k = 13.5 - 307 \text{ KJ mol}^{-1} / 2.3 \text{ RT})$$

The possibility for the elimination reaction was investigated qualitatively by co-pyrolysing 3MCS with hydrogen chloride, oxygen and hydrogen bromide.

(i) 3MCS + Hydrogen Chloride.

In the presence of excess hydrogen chloride, reaction (-69), a reversible process, would be suppressed so that the 3MCS would only decompose by the radical mechanism initiated by reaction (63). As this route leads to the formation of methane (by reaction 64) and the elimination reaction does not, then the rate of formation of this product in the presence of hydrogen chloride ought to be greater than for the pyrolysis of 3MCS alone.

Thus, 3MCS was pyrolysed (at 996K) both by itself and in a 1:1 mixture with hydrogen chloride. The rate of formation of methane, divided by the initial amount of 3MCS to allow for various initial pressures, was calculated for each experimental run. The results are shown in table 3.5. With hydrogen chloride there was an increase in the rate of formation of methane compared with the pyrolysis of 3MCS alone, though the difference was small.

It was also noted that more 2M2CS was formed in the pyrolysis with hydrogen chloride. This was evidence for reaction (68) (and hence for steps 63-65), but hydrogen was also produced, so some of the extra product was probably made by the reaction.

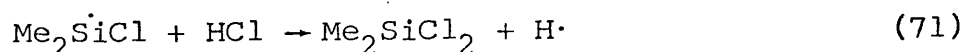


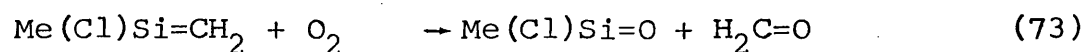
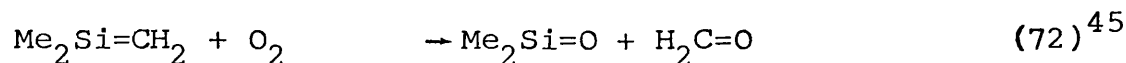
Table 3.5.

Comparison of initial rate of formation of methane from
3MCS with and without added HCl.

	Initial Amount 3MCS (Ao)	Initial Rate of Formation of Methane (R)	R/Ao
Pyrolysis of 3MCS alone	4322	59.3	1.37
	4444	58.4	1.31
	5178	63.5	1.23
	4169	51.7	1.24
Pyrolysis of 3MCS+HCl (1:1)	2246	34.9	1.55
	3483	53.4	1.53
	3735	60.2	1.61
	2009	30.7	1.53
	2311	33.2	1.44

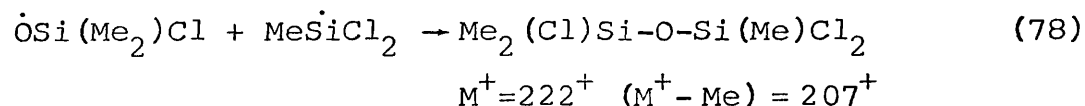
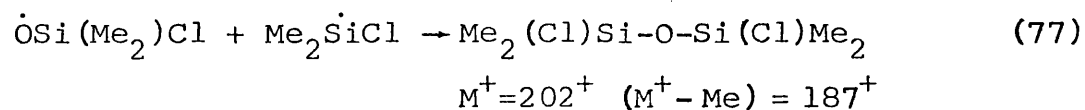
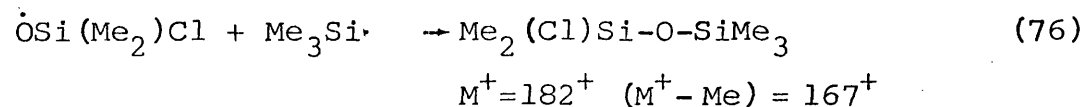
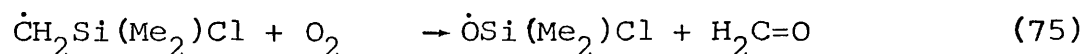
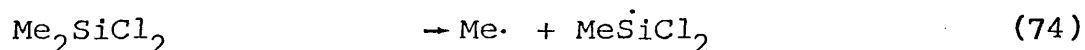
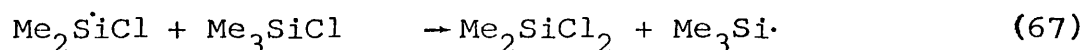
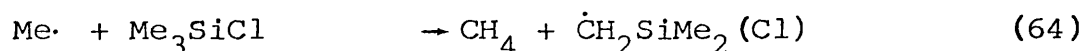
(ii) 3MCS + Oxygen

In the presence of oxygen it was anticipated that the following reactions would occur:-



The silanone (and silaethene) species would then combine with each other in various combinations to form a mixture of cyclic products.

The only new products observed however had groups of peaks at $m/e = 167^+$, 187^+ and 207^+ with the configurations for 1, 2 and 3 chlorine atoms respectively. The following sequence of reactions could account for these observations.

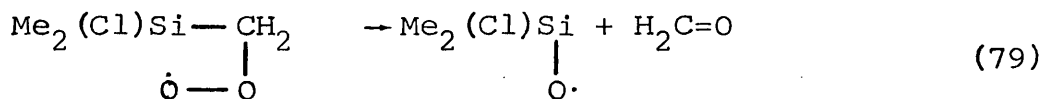
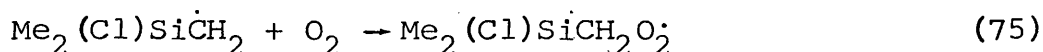


Although no evidence for the elimination reaction was obtained from the experiment with oxygen, the formation of

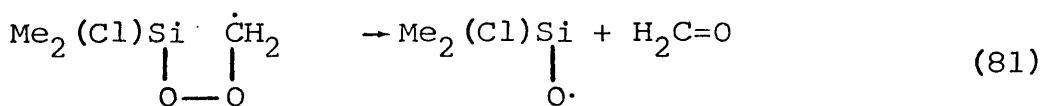
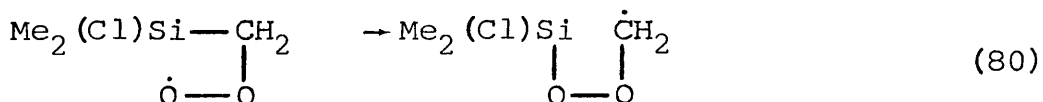
the radical $\dot{\text{O}}\text{Si}(\text{Me}_2)\text{Cl}$ was a strong indication that reaction (64) occurs and hence that the radical decomposition of 3MCS is analogous to that of TMS.

The mechanism of reaction (75) is interesting since the outcome is different to that of the carbon chemistry analogue.

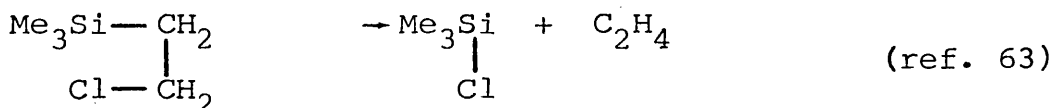
As silicon forms strong bonds to oxygen and has a greater tendency towards pentacovalency than does carbon, it is proposed that the following occurs⁶².



The latter step may be a direct elimination as shown, or it may occur as a two-step process of rearrangement followed by dissociation, thus



β -eliminations are well known in silicon chemistry, eg.

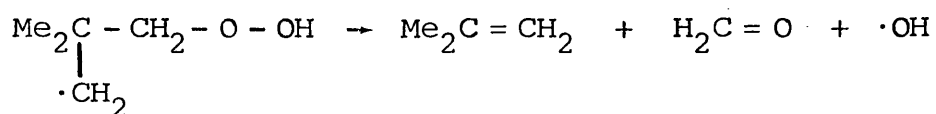
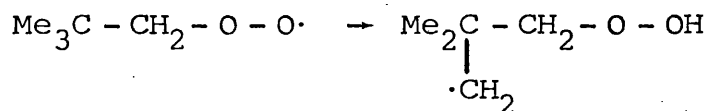


which supports the above scheme.

The reaction between a genuine (rather than a silicon containing) alkyl radical and oxygen can be illustrated as follows.

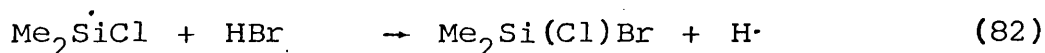


Instead of the end oxygen attacking the central atom, as in the silicon case above, there is an internal hydrogen abstraction followed by dissociation, thus⁶⁴

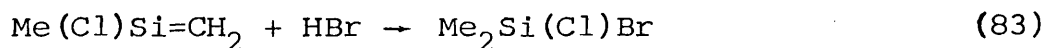


(iii) 3MCS + Hydrogen Bromide.

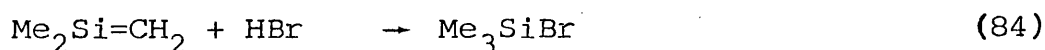
Above about 1000K, the products $\text{Me}_2\text{Si}(\text{Cl})\text{Br}$ and Me_3SiBr were observed. The former was probably produced by the reaction



with possibly some contribution from



The latter product was possibly from the addition reaction



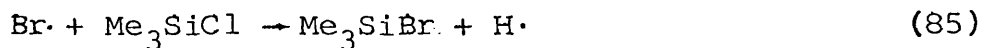
Some experiments were carried out at lower temperatures (713 - 941K) to try and eliminate the radical reactions. Trimethylbromosilane was clearly formed, but the data were too scattered for any quantitative conclusions to be made.

Based on the earlier estimate of the Arrhenius parameters for the elimination reaction, at 713K,

$$k_{\text{elim.}} = 1.0 \times 10^{-9} \text{ s}^{-1}$$

a negligible process. It seemed likely therefore, that there was a strong surface involvement in the production of the bromosilane. If, for example, there had been some

heterogenous formation of bromine atoms, then the reactions



may have occurred, although reaction (85) is endothermic by about 70 KJ mol⁻¹ 17.

3.4 Proposed Pyrolysis Mechanism

The mechanism shown in scheme 3.1 for the pyrolysis of 3MCS, which is analogous to that proposed for the pyrolysis of TMS, was computer simulated, the programme using Gear's method of numerical integration.

The rate constants for the loss of reactant and the "material balance", which was determined from the ratio

$$\frac{\text{(Amount of product formed)}}{\text{(Amount of reactant decomposed)}}$$

over a given time interval, were used to match the simulation to the experiment.

It was found that the temperature -independent step 14, proposed to take place at the walls of the reaction vessel, was necessary for the simulation to make sufficient methane. An initial amount of hydrogen chloride (3MCS:HCl 10:1), proposed to have come from the hydrolysis of the reactant, was also included in the mechanism. The Arrhenius parameters which had been measured earlier for the pyrolysis of 3MCS were used for the initial step.

The simulation broadly matched the experimental observations when the parameters shown in scheme 3.1 were used. A comparison between simulation and experiment is shown in table 3.6. The calculated formation of 2M2CS did not fit the experiment as well as the methane production

Scheme 3.1 Proposed Mechanism for the Pyrolysis of 3MCS.

		$\log_{10} A$	$E / \text{KJ mol}^{-1}$	
1	$\text{Me}_3\text{SiCl} \rightarrow \text{Me}\cdot + \text{Me}_2\dot{\text{S}}\text{iCl}$	17.00	366	(63)
2	$\text{Me}\cdot + \text{Me}_3\text{SiCl} \rightarrow \text{CH}_4 + \dot{\text{C}}\text{H}_2\text{Si}(\text{Cl})\text{Me}_2$	8.30	40	(64)
3	$\dot{\text{C}}\text{H}_2\text{Si}(\text{Cl})\text{Me}_2 \rightarrow \text{Me}\cdot + \text{Me}(\text{Cl})\text{Si}=\text{CH}_2$	15.00	190	(65)
4	$\text{Me}_2\dot{\text{S}}\text{iCl} + \text{Me}_3\text{SiCl} \rightarrow \text{Me}_2\text{SiCl}_2 + \text{Me}_3\text{Si}\cdot$	6.20	15	(67)
5	$\text{Me}_3\text{Si}\cdot + \text{Me}_2\text{SiCl}_2 \rightarrow \text{Me}_3\text{SiCl} + \text{Me}_2\dot{\text{S}}\text{iCl}$	6.20	15	(86)
6	$2 \text{Me}_2\dot{\text{S}}\text{iCl} + \text{M} \rightarrow (\text{Me}_2\dot{\text{S}}\text{iCl})_2 + \text{M}$	10.51	0	(87)
7	$2 \dot{\text{C}}\text{H}_2\text{Si}(\text{Cl})\text{Me}_2 + \text{M} \rightarrow (\text{Me}_2(\text{Cl})\text{Si}\dot{\text{C}}\text{H}_2)_2 + \text{M}$	9.00	0	(88)
8	$2 \text{Me}\cdot + \text{M} \rightarrow \text{C}_2\text{H}_6 + \text{M}$	10.51	0	(14)
9	$2 \text{Me}_3\text{Si}\cdot + \text{M} \rightarrow (\text{Me}_3\dot{\text{S}}\text{i})_2 + \text{M}$	10.51	0	(12)
10	$\text{Me}_2\text{SiCl}_2 \rightarrow \text{Me}\cdot + \text{Me}\dot{\text{S}}\text{iCl}_2$	17.00	366	(74)
11	$\text{Me}\cdot + \text{Me}_2\text{SiCl}_2 \rightarrow \text{CH}_4 + \dot{\text{C}}\text{H}_2\text{Si}(\text{Me})\text{Cl}_2$	8.30	40	(89)
12	$\dot{\text{C}}\text{H}_2\text{Si}(\text{Me})\text{Cl}_2 \rightarrow \text{Me}\cdot + \text{MeSiCl}_3$	15.00	190	(90)
13	$2 \dot{\text{C}}\text{H}_2\text{Si}(\text{Me})\text{Cl}_2 + \text{M} \rightarrow (\text{MeSiCl}_2\dot{\text{C}}\text{H}_2)_2 + \text{M}$	9.00	0	(91)
14	$\text{Me}\cdot \rightarrow \text{CH}_4$	$k = 50 \text{ s}^{-1}$		(92)
15	$\text{Me}_2\dot{\text{S}}\text{iCl} \rightarrow \text{WALLS}$	2.00	0	(93)
16	$\dot{\text{C}}\text{H}_2\text{Si}(\text{Cl})\text{Me}_2 \rightarrow \text{WALLS}$	2.00	0	(94)
17	$\text{Me}\cdot + \text{Me}_2\dot{\text{S}}\text{iCl} + \text{M} \rightarrow \text{Me}_3\text{SiCl} + \text{M}$	10.51	0	(95)
18	$\text{C}_2\text{H}_6 \rightarrow 2 \text{Me}\cdot$	17.00	369	(34)
19	$\text{Me}_3\text{Si}\cdot \rightarrow \text{Me}\cdot + \text{Me}_2\text{Si}\cdot$	14.51	255	(18)
20	$\text{Me}_2\dot{\text{S}}\text{iCl} \rightarrow \text{Me}\cdot + \text{Me}\dot{\text{S}}\text{iCl}$	14.51	255	(96)
21	$\text{Me}\cdot \rightarrow \text{WALLS}$	$k = 150 \text{ s}^{-1}$		(97)
22	$\text{Me}_2\dot{\text{S}}\text{iCl} + \text{WALLS} \rightarrow \text{Me}_2\text{SiCl}_2$	1.78	15	(98)
23	$\text{Me}_2\dot{\text{S}}\text{iCl} + \text{HCl} \rightarrow \text{Me}_2\text{SiCl}_2 + \text{H}\cdot$	7.00	15	(71)
24	$\text{H}\cdot + \text{Me}_3\text{SiCl} \rightarrow \text{H}_2 + \dot{\text{C}}\text{H}_2\text{Si}(\text{Cl})\text{Me}_2$	10.00	8	(99)
25	$\text{Me}(\text{Cl})\text{Si}=\text{CH}_2 + \text{HCl} \rightarrow \text{Me}_2\text{SiCl}_2$	7.51	10	(68)

Activation energies and A-factors based on data from
refs. 13 and 15

Table 3.6. Comparison between simulation and experiment for pyrolysis of 3MCS.

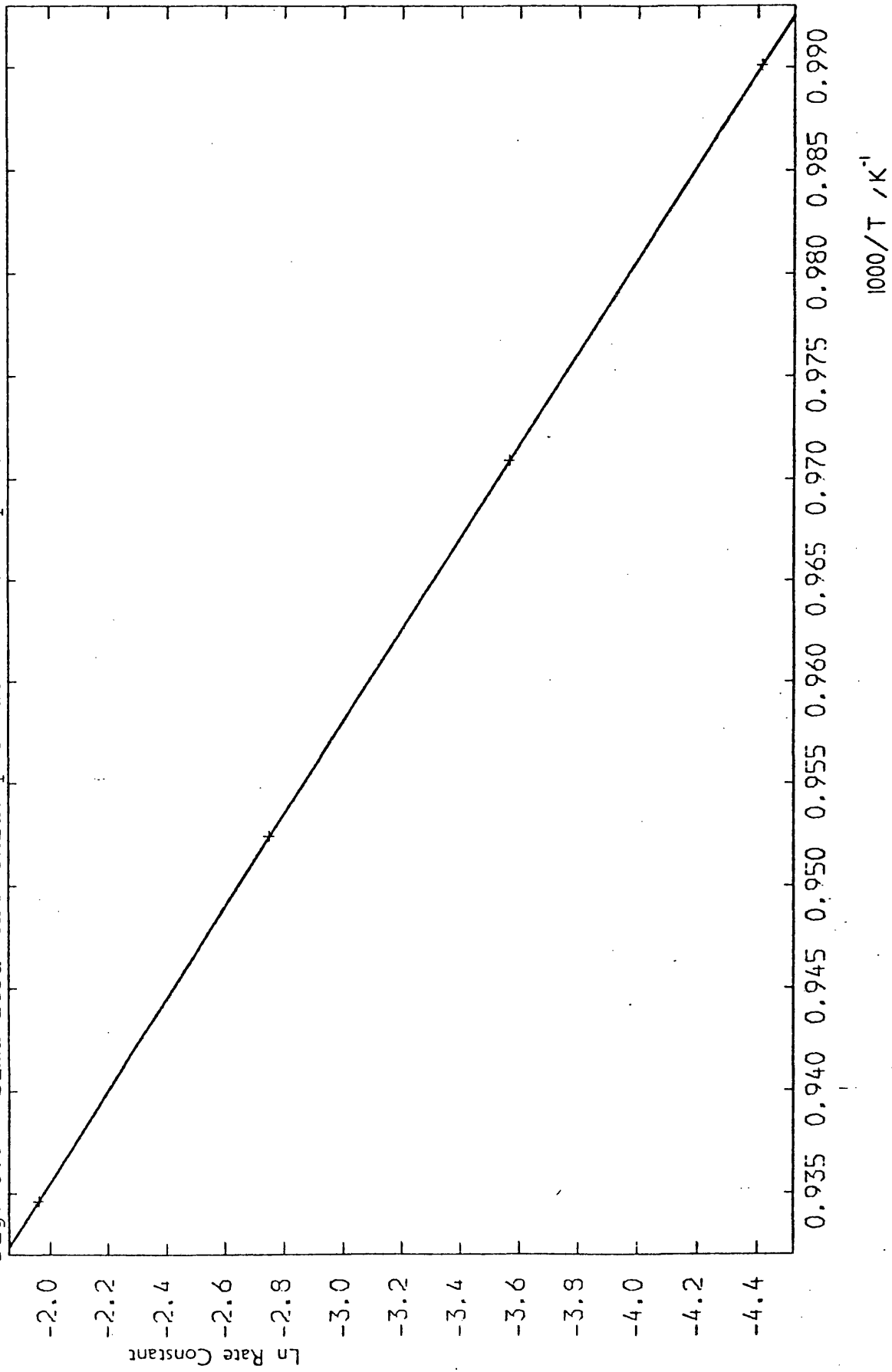
Temp /K	Rate Constant for decomp. 3MCS (Expt.) /s ⁻¹	Rate Constant for decomp. reactant (sim.) /s ⁻¹	$\frac{\Delta [\text{CH}_4]}{\Delta [3\text{MCS}]}$ Expt.	$\frac{\Delta [\text{CH}_4]}{\Delta [3\text{MCS}]}$ Sim.	$\frac{\Delta [\text{Me}_2\text{SiCl}_2]}{\Delta [3\text{MCS}]}$ Expt.	$\frac{\Delta [\text{Me}_2\text{SiCl}_2]}{\Delta [3\text{MCS}]}$ Sim.
1010	.0118	.0121	.33 at 1020K	.30	.07	.10
1030	.0274	.0283	.45 at 1045K	.33	.09	.09
1050	.0619	.0639	.53 at 1066K	.36	.10	.08
1070	.1356	.1404		.39		.06

did, but in earlier experiments, the gas-phase concentration of hydrogen chloride had been observed to increase during a pyrolysis reaction. (No quantitative measurements could be made since the source of the compound - hydrolysis of 3MCS, displacement from the walls of the reaction vessel or even reaction - was difficult to determine). Such an increase in the amount of hydrogen chloride would lead to "extra" 2M2CS via steps 23 and 25 of the proposed mechanism. The simulation did not take account of this process and would therefore underestimate the production of 2M2CS.

An Arrhenius plot using the simulated rate constants in table 3.6 is shown in fig. 3.9. From this $\log_{10} k = 17.06 - 367 \text{ KJ mol}^{-1} / 2.303 \text{ RT}$.

Thus, the proposed pyrolysis mechanism accounted for the experimental observations.

Fig. 3.9 "Simulated" Arrhenius plot for the decomposition of 3MCS.

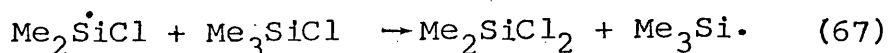


CHAPTER FOUR

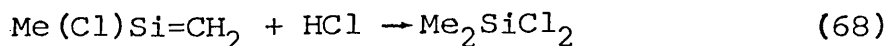
**PYROLYSIS OF
1,1-DIMETHYL-1-SILACYCLOBUTANE
AND OF
1,1-DICHLORO-1-SILACYCLOBUTANE**

4.1 Introduction

As discussed in chapter 3, the pyrolysis of trimethylchlorosilane produced dimethyldichlorosilane as the major silicon-containing product, partly by the radical abstraction reaction



and possibly by



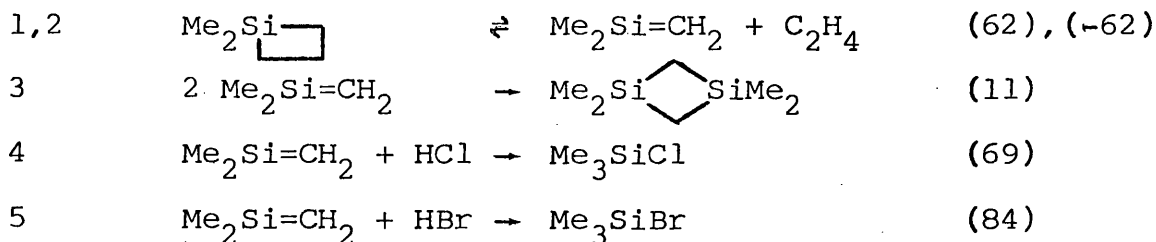
since a small amount of hydrogen chloride is inevitably present owing to hydrolysis.

A series of experiments was therefore devised to investigate the kinetics of addition of hydrogen halides to double bonded silaethene species.

It was known from the literature that the pyrolysis of 1,1-dimethylsilacyclobutane (DMSCB) produces a similar silaethene species to the one proposed to come from the thermolysis of trimethylchlorosilane. Steps 1-3 of scheme 4.1 show the established mechanism for the decomposition of DMSCB³⁹. Steps 4 and 5 were to be studied.

The work can be divided into three sections, experiments involving three-species mixtures, of DMSCB, hydrogen bromide and hydrogen chloride, and experiments using two-species mixtures of DMSCB and one of the hydrogen halides. Only the two-compound mixtures produced reliable, quantitative results, but a summary of all the work now follows.

Scheme 4.1. Pyrolysis of DMSCB.



4.2 Initial Observations.

Initial, qualitative experiments using mixtures of DMSCB and hydrogen chloride or hydrogen bromide showed clearly that the appropriate addition product was being formed, by reaction (4) or (5).

The rate of addition of hydrogen chloride to 1,1-dimethylsilaethene (DMSE) was such that the dimerisation reaction was suppressed until most of the halide had been used up. Typical concentration-time curves for a DMSCB:HCl (3:1) mixture are shown diagrammatically in fig. 4.1. The reaction demonstrated these features over a wide range of temperatures (743 - 813 K) and it was clear that very small proportions of hydrogen chloride would be necessary to enable a competitive reaction between dimerisation and addition to be studied.

The addition of hydrogen bromide to DMSE was apparently slower than that of the chloride to DMSE, the addition and dimerisation products being formed simultaneously. Typical concentration-time curves for a DMSCB:HBr (3:1) mixture are shown by fig. 4.2.

With the furnace temperature below that necessary

Fig.4.1 Typical Concentration-time curves for
DMSCB:HCl 3:1

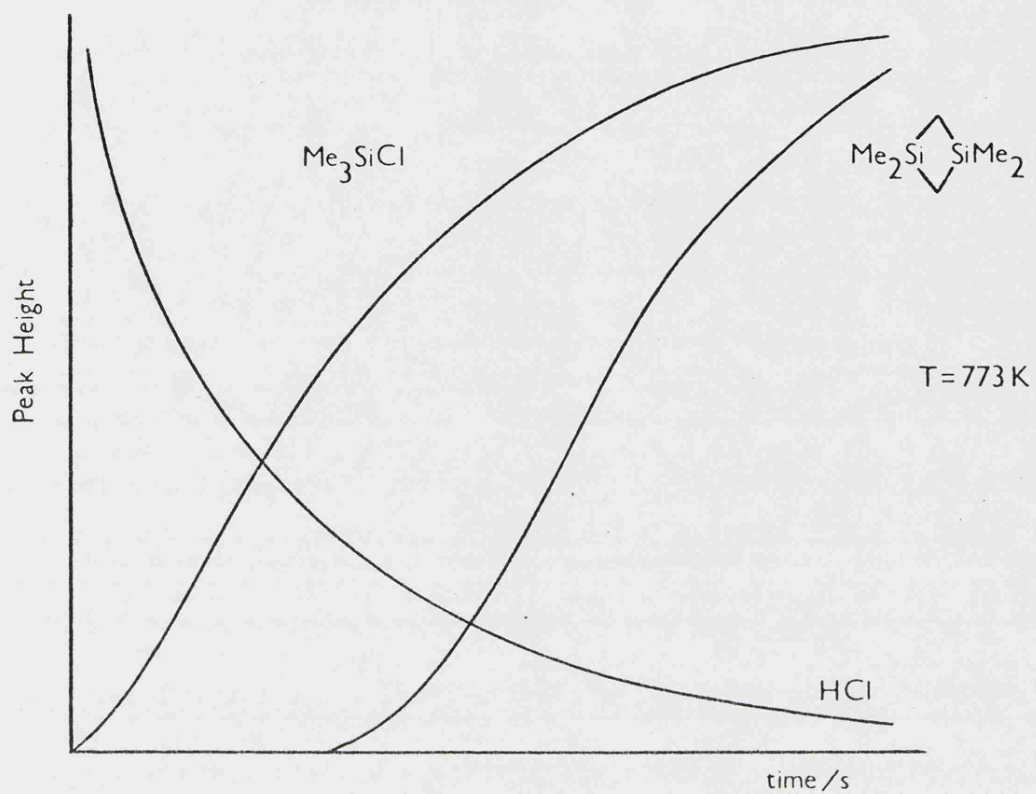
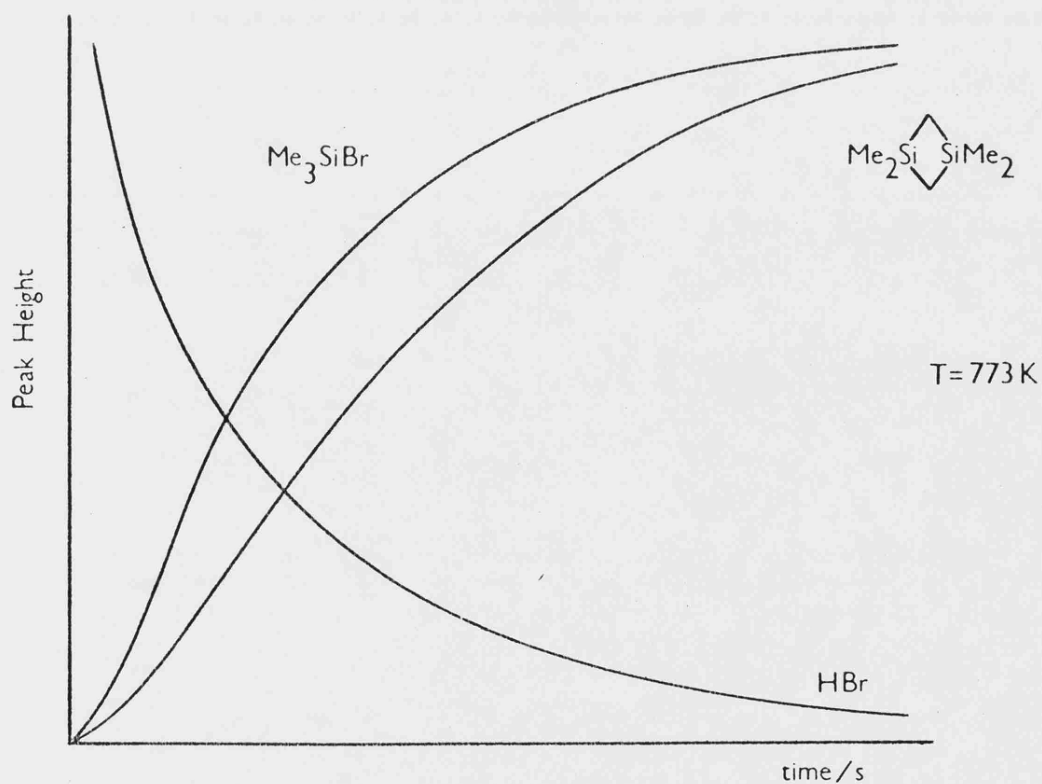


Fig.4.2 Typical Concentration-time curves for
DMSCB:HBr 3:1



for significant decomposition of DMSCB (about 723K), a comparison of the leak-in times (the times taken by compounds to expand into the reaction vessel) for DMSCB, hydrogen chloride and hydrogen bromide showed an anomaly in the behaviour of the halides. The mass spectrum peaks for DMSCB reached a maximum about 5s from tap 1 (fig. 2.1) being opened, which was a "normal" time for a compound of such molecular weight. The halide peaks however took up to about 15s to maximise. This delay was possibly due to the halides adsorbing to the walls of the reaction vessel, although adsorption inside the mass spectrometer itself could cause a delay in seeing the peaks, even if expansion into the reaction vessel was "normal".

After hydrogen halide had been introduced into the apparatus it was very difficult to remove. Even after considerable pumping out of the reaction vessel at elevated temperatures (>950K), peaks due to it were still visible in the spectrum, evidence that some adsorption at least occurs inside the mass spectrometer.

The introduction of hydrogen bromide into the system, besides producing its own characteristic peaks, also caused the peaks due to hydrogen chloride to increase. As there was no reason to suspect that the hydrogen bromide was contaminated with the chloride, it was concluded that the former displaced the latter already adsorbed in the apparatus.

4.3 DMSCB + Hydrogen Chloride + Hydrogen Bromide.

Three-component mixtures of proportions ranging from DMSCB:HBr:HCl 1:1:1 - 10:3:1 were tried. As no reliable quantitative conclusions were obtained from these experiments, only examples of the quality of the data collected are included, along with the methods of analysis which were attempted.

Only mixtures containing a very small proportion of hydrogen chloride (eg. 10:3:1) could be used, as the analysis methods required the simultaneous production of dimer and addition products. Greater proportions of hydrogen chloride suppressed the dimerisation reaction. Even a 10:3:1 mixture did not give an initial competition between addition and dimerisation, but the latter appeared to start soon enough for calculations to be attempted.

Some experiments were carried out using a mixture of DMSCB and hydrogen bromide only, with hydrogen chloride being produced (by desorption) as the mixture entered the reaction vessel/mass spectrometer. The results were then analysed as a three-component mixture, a valid approach as long as most of the hydrogen chloride came from inside the reaction vessel. This was believed to be the case as the relevant spectrum peaks initially rose and then decreased as if a reaction was occurring. Also, both of the addition products were formed.

For these series of experiments, four methods of analysis were attempted and an outline of each follows below.

(i) Based on reaction scheme 4.1, the following can be

derived

$$d[\text{Dimer}]/dt = k_3 [\text{Me}_2\text{Si}=\text{CH}_2]^2$$

$$d[\text{Me}_3\text{SiBr}]/dt = k_5 [\text{Me}_2\text{Si}=\text{CH}_2] \cdot [\text{HBr}]$$

$$\frac{d[\text{Me}_3\text{SiBr}]/dt}{(d[\text{Dimer}]/dt)^{1/2}} = \frac{k_5 [\text{Me}_2\text{Si}=\text{CH}_2] \cdot [\text{HBr}]}{k_3^{1/2} [\text{Me}_2\text{Si}=\text{CH}_2]} \quad (\text{xv})$$

For small t (ie. small extent of reaction),

$$[\text{Me}_3\text{SiBr}]/[\text{Dimer}]^{1/2} \cdot t^{1/2} = k_5 [\text{HBr}]/k_3^{1/2}$$

therefore,

$$[\text{Me}_3\text{SiBr}]/[\text{Dimer}]^{1/2} \cdot [\text{HBr}] = (k_5/k_3^{1/2}) \cdot t^{1/2} \quad (\text{xvi})$$

similarly,

$$[\text{Me}_3\text{SiCl}]/[\text{Dimer}]^{1/2} \cdot [\text{HCl}] = (k_4/k_3^{1/2}) \cdot t^{1/2}$$

A plot of the left hand side vs $t^{1/2}$ ought to give a straight line of slope $k_5/k_3^{1/2}$.

This was tried for both the hydrogen chloride and bromide addition reactions, but the data obtained at each temperature were too scattered for reliable straight lines to be drawn.

(ii) From eqn. (xvi) above,

$$[\text{Me}_3\text{SiBr}]/[\text{Dimer}]^{1/2} \cdot [\text{HBr}] \cdot t^{1/2} = k_5/k_3^{1/2}$$

therefore, assuming the activation energy for dimerisation to be zero, a plot of \ln (left hand side) vs $10^3/T$ ought to give a straight line of slope $-E/R$, where E is the activation energy of the addition step.

This method was tried for both of the addition reactions,

the ratio being calculated at the maximum peak height (concentration) of hydrogen halide. As figs. 4.3 and 4.4 show, from the results in table 4.1, both of the plots were very scattered, only having negative slopes over the temperature range ~834-872K. A least squares fit over the negative portion of the "hydrogen bromide" plot gives an activation energy of $62.5 \pm 18.4 \text{ kJ. mol}^{-1}$, and for the "hydrogen chloride" plot an activation energy of $31.2 \pm 19.7 \text{ kJ. mol}^{-1}$.

Owing to adsorption inside the apparatus, the gas-phase concentrations of the hydrogen halides at given times could not be reliably measured. It was also noted that the addition products, particularly the bromosilane, disappeared from the system more quickly than was expected by simple leak out. As both of the addition products were susceptible to hydrolysis, the bromide much more so than the chloride, then the interaction of the halosilanes with background water was a possible explanation of this observation.

In subsequent work, attempts were made to remove background water by passing trimethylchlorosilane through the apparatus prior to the reaction mixture being put in, but this was found not to have much effect.

Another possibility was that trimethylbromosilane was not thermally stable at the temperatures being used (774 - 872K), although this is unlikely since the bond dissociation energy $D(\text{Me}_3\text{Si-Br})$ has been derived as 401 kJ mol^{-1} ¹⁷ and the silicon-methyl bond strength will probably be about the same as that in trimethylchlorosilane (366 kJ mol^{-1}). Assuming the A-factor for the dissociation of trimethylbromosilane to be similar to that for the

Table 4.1

$$[\text{Me}_3\text{SiBr}] / [\text{HBr}] \cdot [\text{DIMER}]^{\frac{1}{2}} = P$$

$$[\text{Me}_3\text{SiCl}] / [\text{HCl}] \cdot [\text{DIMER}]^{\frac{1}{2}} = Q$$

t=time at which the halide peak reached a maximum/s.

Temp/K	$P/t^{\frac{1}{2}}$	$\ln(P/t^{\frac{1}{2}})$
771	.0342	-3.3755
773	.0343	-3.3726
773	.0322	-3.4358
795	.0214	-3.8444
795	.0340	-3.3814
795	.0208	-3.8728
812	.0152	-4.1865
811	.0145	-4.2336
813	.0139	-4.2759
835	.0150	-4.1997
833	.0112	-4.4918
834	.0125	-4.3820
853	.0157	-4.1541
853	.0179	-4.0230
852	.0161	-4.1290
872	.0180	-4.0174

Temp/k	$Q/t^{\frac{1}{2}}$ x10	$\ln(Q/t^{\frac{1}{2}})$
775	.0647	-5.0406
774	.0661	-5.0192
774	.0775	-4.8601
793	.0853	-4.7642
793	.0685	-4.9835
793	.0950	-4.6565
812	.0376	-5.5833
813	.0475	-5.3496
813	.0576	-5.1568
833	.0259	-5.9561
834	.0310	-5.7764
833	.0335	-5.6988
853	.0314	-5.7635
853	.0296	-5.8226
854	.0292	-5.8362
782	.0297	-5.8192
871	.0465	-5.3709
872	.0362	-5.6213

Fig. 4.3 $\ln \left(\frac{[\text{Me}_3\text{SiBr}]}{([\text{HBr}] [\text{Me}_2\text{Si}(\text{SiMe}_2)^{\frac{1}{2}} \cdot t^{\frac{1}{2}}])} \right) \text{ vs } 10^3 / T$

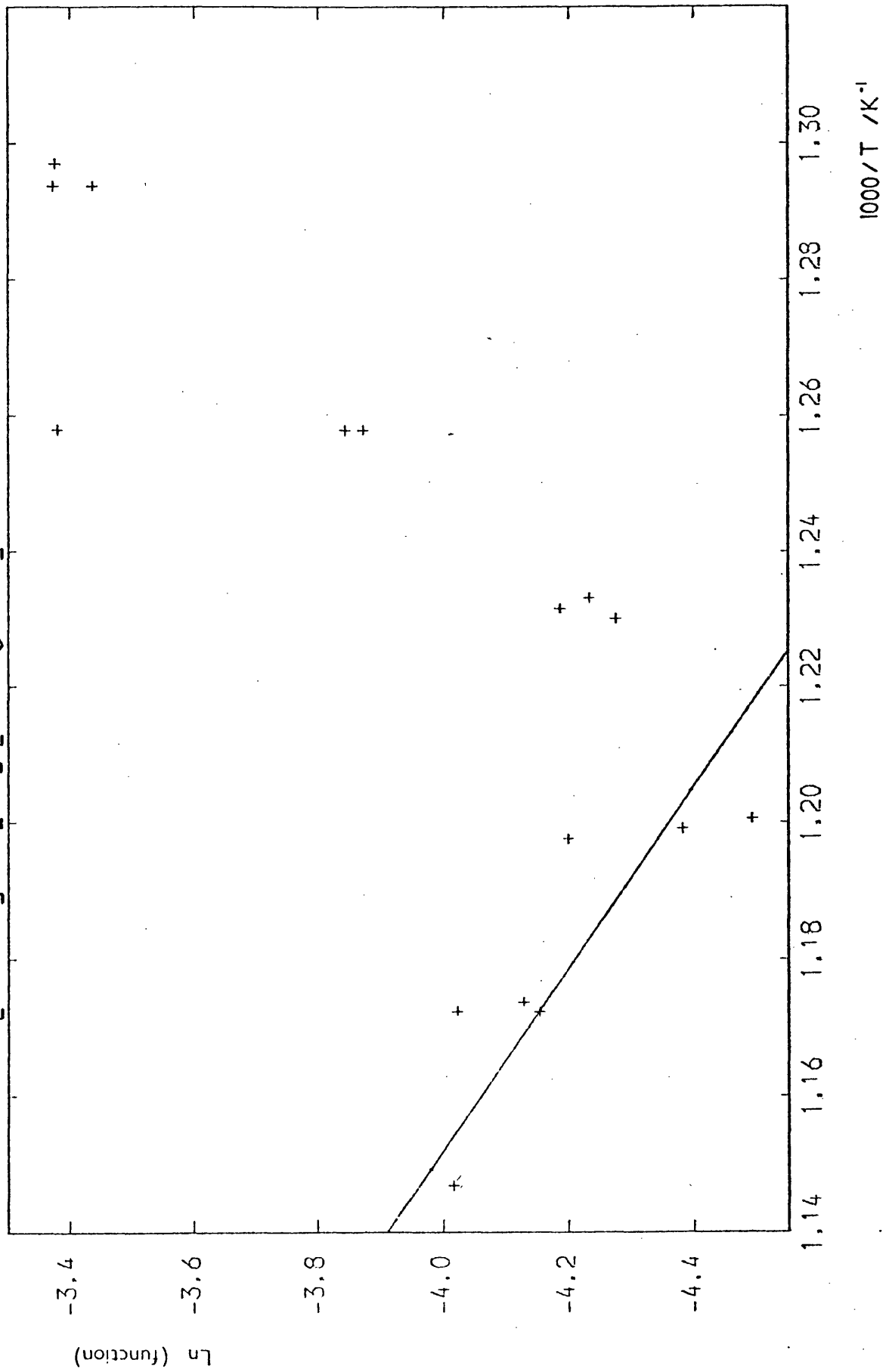
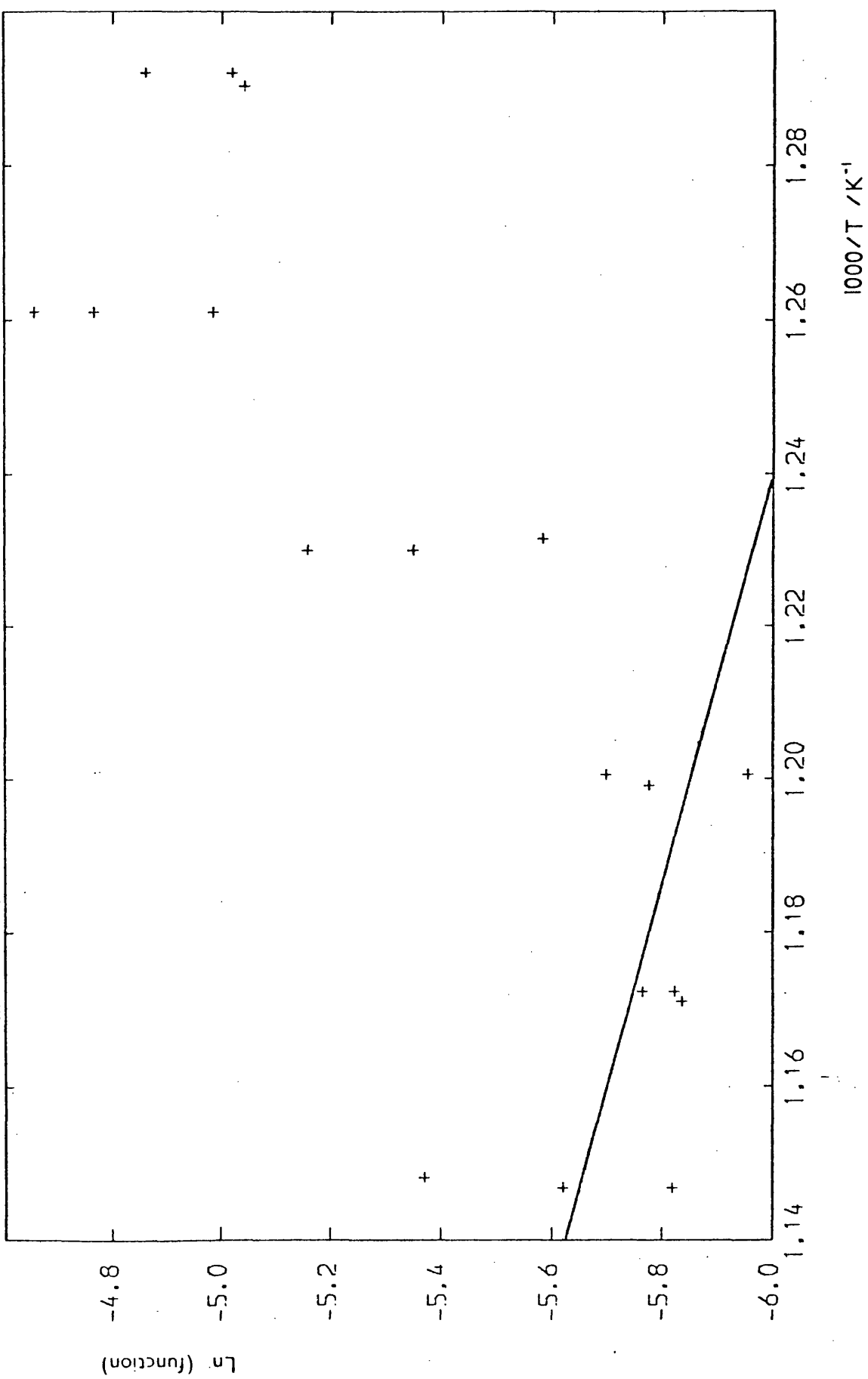


Fig. 4.4 $\ln \left(\frac{[\text{Me}_3\text{SiCl}]}{[\text{HCl}]} \left[\frac{\text{Me}_2\text{SiSiMe}_2}{t} \right]^{\frac{1}{2}} \right)$ vs $10^3/T$.



chloro- compound, then at 872K, the rate constant for the dissociation would be $k = 1.19 \times 10^{-5} \text{ s}^{-1}$, making it a negligible process.

(iii) From eqn. (xv), if the initial rates of product formation are used instead of their peak heights at a specific time, then the following can be derived.

$$(\text{Initial Rate Me}_3\text{SiCl})/(\text{Initial Rate Dimer})^{1/2} = (k_4/k_3^{1/2}) \cdot [\text{HCl}]_0$$

where $[\text{HCl}]_0$ is the initial concentration of hydrogen chloride. A plot of $\ln(\text{left hand side})$ vs $10^3/T$ ought to give a straight line of slope $-E/R$ where E is the activation energy of the addition step.

To allow for different initial amounts of reaction mixture, both sides of the above equation were divided by the initial amount of DMSCB (as estimated by extrapolation of the $\ln(\text{Peak Height})$ vs time plots back to zero time), it being assumed that the reaction mixture was of the same proportions throughout the series of experiments.

$$\text{ie. } [\text{HCl}]_0/[\text{DMSCB}]_0 = \text{Constant.}$$

As table 4.2 and fig. 4.5 show, the result for hydrogen chloride addition was a graph with a positive slope, corresponding to an activation energy of $(-)\ 157 \pm 22 \text{ KJ mol}^{-1}$.

(iv) Still for three-component mixtures, it is possible to compare the halogen species, the following derivation again referring to scheme 4.1.

$$d[\text{Me}_3\text{SiCl}]/dt = k_4[\text{Me}_2\text{Si}=\text{CH}_2] \cdot [\text{HCl}]$$

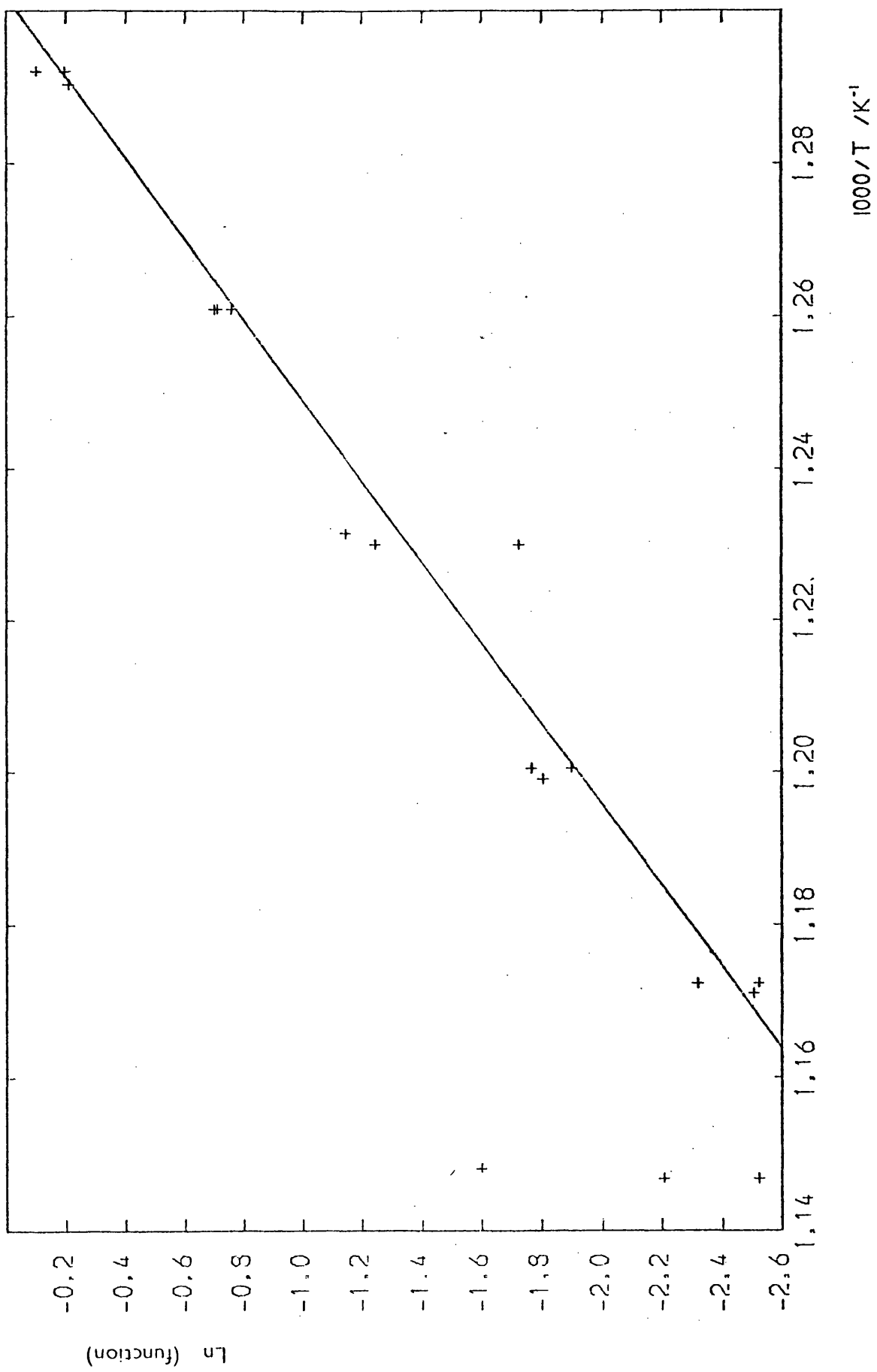
$$d[\text{Me}_3\text{SiBr}]/dt = k_5[\text{Me}_2\text{Si}=\text{CH}_2] \cdot [\text{HBr}]$$

$$\frac{[\text{Me}_3\text{SiCl}]}{[\text{Me}_3\text{SiBr}]} = \frac{k_4 \cdot t [\text{Me}_2\text{Si}=\text{CH}_2] [\text{HCl}] + C}{k_5 \cdot t [\text{Me}_2\text{Si}=\text{CH}_2] [\text{HBr}] + C}$$

Table 4.2 Comparison of Initial Rates.

Temp/K	Initial Rate Me ₃ SiCl (E)	Initial Rate Dimer (D)	Initial DMSCB (A _o)	$\frac{E}{D^{1/2}} \times 100$ A _o (F)	ln(F)
775	107.3	18.6	3063	.812	-0.2079
774	178.9	27.7	3759	.904	-0.1006
774	136.0	22.0	3526	.822	-0.1956
793	123.3	48.6	3555	.498	-0.6981
793	158.3	68.8	3873	.493	-0.7077
793	132.8	59.8	3660	.469	-0.7567
812	155.8	162.9	3828	.319	-1.1429
813	131.0	152.4	3683	.288	-1.2444
813	175.8	179.1	7383	.178	-1.7264
833	159.6	455.3	4380	.171	-1.7674
833	132.7	399.3	4441	.150	-1.9002
834	148.1	433.7	4325	.164	-1.8053
853	113.8	665.3	4475	.099	-2.3168
853	107.3	770.0	4824	.080	-2.5238
854	102.3	738.3	4609	.082	-2.5049
871	197.4	1269.0	2747	.202	-1.6009
872	88.3	1050.3	3399	.080	-2.5237
872	121.9	1115.0	3321	.110	-2.2080

Fig. 4.5 (Initial Rate $(\text{Me}_3\text{SiCl}) / (100 \times \text{Initial Rate } (\text{Me}_2\text{Si SiMe}_2)^{1/2} \times [\text{DMSCE}]_0)$) vs $10^3/T$.



where C is the constant of integration.

therefore

$$\frac{[\text{Me}_3\text{SiCl}] \cdot [\text{HBr}]}{[\text{Me}_3\text{SiBr}] \cdot [\text{HCl}]} = k_4/k_5 \quad (\text{xvii})$$

ie. a constant at any given temperature.

Table 4.3 shows the results which were obtained by this calculation at different times into the reaction, for five consecutive experimental runs at about 763K. The deviation from constancy at these and the other temperatures was too large for any reliable conclusions to be made.

The calculation was repeated using the initial rates of change of the species rather than their peak heights at a specific time. Column 8 of table 4.4 shows that there was no systematic variation with temperature. The main uncertainty was the measurement of the hydrogen halides.

(v) By assuming that the initial ratio $[\text{HBr}] : [\text{HCl}]$ was approximately the same as at $t=0$, ie. the proportion in the reaction mixture before pyrolysis, then eqn. (xvii) simplified to,

$$(\text{Initial Rate Me}_3\text{SiCl})/(\text{Initial Rate Me}_3\text{SiBr}) = k_4/k_5$$

A plot of \ln (left hand side) vs $10^3/T$ ought to give a straight line of slope $-(E_4-E_5)/R$.

As fig. 4.6 shows, from the data in column 7 of table 4.4, the resulting plot was scattered, it being possible to draw two lines through the points, corresponding to about 46 and to 8.8 KJ mol^{-1} , the latter being a least squares fit through the points in the region 856-772 K, missing the indicated point at 794K.

Table 4.3

Comparisons of $[\text{Me}_3\text{SiCl}] [\text{HBr}] / [\text{Me}_3\text{SiBr}] [\text{HCl}]$ at about 763K.

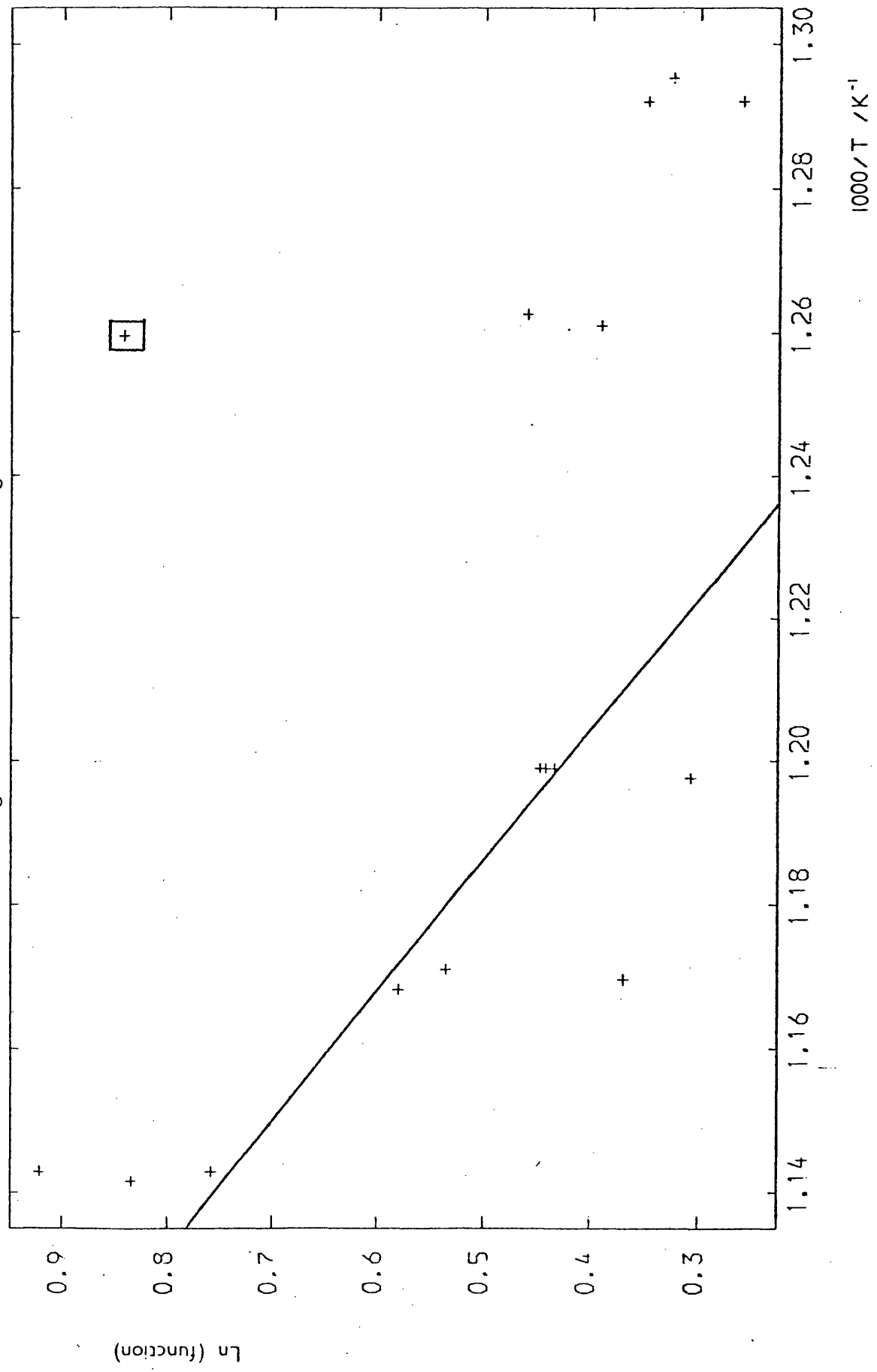
Time/s	$[\text{Me}_3\text{SiCl}] \cdot [\text{HBr}] / [\text{Me}_3\text{SiBr}] \cdot [\text{HCl}]$ at				
	761K	762K	763K	763K	764K
0.75	3.46	3.17	2.12	2.97	2.17
1.50	3.02	1.76	1.78	2.21	1.93
2.25	2.06	1.01	1.20	1.43	1.35
3.00	1.66	0.76	0.96	1.13	1.12
3.75	1.61	0.73	0.93	1.10	1.10
4.50	1.66	0.75	0.97	1.12	1.14
5.25	1.72	0.77	1.04	1.13	1.19
6.00	1.80	0.78	1.12	1.14	1.24
6.75	1.85	0.80	1.18	1.16	1.29

Table 4.4

Comparison of initial rates of halide species

Temp /K	Initial Rate [HCl] J	Initial Rate [HBr] K	Initial Rate [Me ₃ SiCl] L	Initial Rate [Me ₃ SiBr] M	L/M	$\ln \frac{L}{M}$	$\frac{L \cdot K}{M \cdot J}$
772	95.91	30.11	147.96	106.86	1.385	0.3254	0.435
774	119.78	31.66	179.63	138.52	1.297	0.2599	0.343
774	125.02	29.12	158.76	112.16	1.416	0.3475	0.330
792	100.09	31.52	160.27	101.14	1.585	0.4604	0.499
793	98.04	28.99	180.96	122.39	1.479	0.3911	0.437
794	118.31	35.32	251.36	108.16	2.324	0.8433	0.694
834	345.77	39.33	225.53	146.08	1.544	0.4343	0.176
834	356.00	38.67	223.08	142.61	1.564	0.4474	0.170
834	328.15	39.47	212.76	136.72	1.556	0.4422	0.187
835	356.00	37.49	176.76	130.08	1.359	0.3066	0.143
854	123.11	33.13	195.67	114.61	1.707	0.5349	0.459
855	208.89	33.37	176.40	122.00	1.446	0.3687	0.231
856	167.11	34.58	190.54	106.67	1.786	0.5801	0.370
875	236.74	35.70	268.75	125.95	2.134	0.7579	0.322
875	139.70	28.71	224.80	89.47	2.513	0.9213	0.516
876	140.45	33.62	277.10	120.36	2.302	0.8339	0.551

Fig. 4.6 Ln (Initial Rate Me_3SiCl / Initial Rate Me_3SiBr) vs $10^3/T$.



The negative slope of this plot suggested that E_4 was greater than E_5 , which was not reasonable since hydrogen chloride suppressed dimerisation but comparable amounts of hydrogen bromide did not.

4.4 DMSCB + Hydrogen Chloride (3:1)

No competitive reaction between the formation of addition product and dimer could be observed, thus the methods of analysis outlined in section 4.3 above, which required the simultaneous formation of the two products, could not be applied to this system.

The time, relative to the start of the reaction, for the onset of dimerisation was seen to vary with temperature, the dimer appearing as the hydrogen chloride was just about used up. This variation in onset time was used to determine an activation energy for the addition of hydrogen chloride to dimethylsilaethene (DMSE), relative to that for the self dimerisation of DMSE.

Table 4.5 shows the rate constants which were measured for the loss of the reactant (DMSCB) and the lower line of fig. 4.7 the resulting Arrhenius plot from which

$$\log_{10} k = (14.72 \pm .53) - (249.1 \pm 8.0 \text{ KJ mol}^{-1}) / 2.303 \text{ RT.}$$

These parameters are less than the established literature values (which are indicated by the upper line of fig. 4.7), but it had been found that the experimental system consistently returned low values, even when, as in these runs, the plots of $\ln(\text{peak height})$ vs time for the loss of reactant were straight over several experimental readings (in this series of experiments up to 20s at 813K). A comparison between the measured and literature rate constants is shown in table 4.6. The experiments were

Table 4.5

Rate constants for the loss of DMSCB in 3:1 mixture with hydrogen chloride.

Temp /K	Rate Constant k/s^{-1}	$k-k_L$ $/s^{-1}$	$\ln(k-k_L)$
744	.0031	.0011	-6.812
763	.0072	.0052	-5.259
763	.0073	.0053	-5.240
764	.0076	.0056	-5.185
773	.0100	.0080	-4.828
773	.0103	.0083	-4.792
774	.0105	.0085	-4.768
782	.0157	.0137	-4.290
782	.0148	.0128	-4.358
782	.0138	.0118	-4.440
793	.0218	.0198	-3.922
794	.0231	.0211	-3.859
794	.0223	.0203	-3.897
803	.0334	.0314	-3.461
803	.0334	.0314	-3.461
803	.0330	.0310	-3.474
812	.0506	.0486	-3.024
813	.0509	.0489	-3.018
813	.0498	.0478	-3.041

Fig. 4.7 Arrhenius plot for the decomposition of DMSCB.

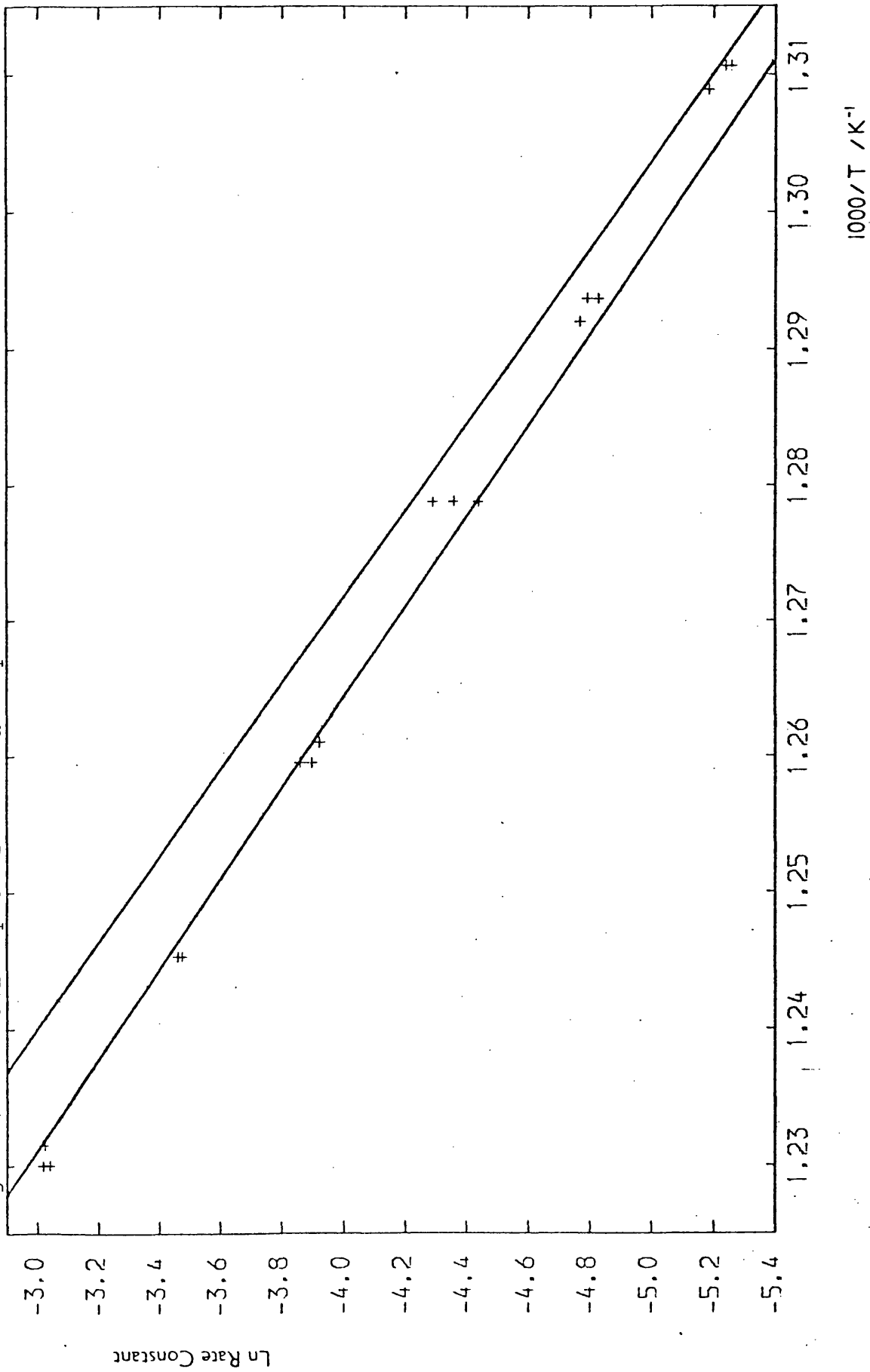


Table 4.6

Comparison between literature and measured rate constants
for the decomposition of DMSCB.

Temp. /K	Experimental rate constant from measured Arrhenius parameters / s ⁻¹	Literature rate constant / s ⁻¹	$\frac{k_{\text{measured}}}{k_{\text{literature}}}$ x 100
744	.0017	.0019	89.5
782	.0120	.0149	80.5
813	.0519	.0689	75.3

Table 4.7

On-set time of dimer (Me₂Si \diamond SiMe₂) and comparison between
experimental and calculated times for 30% loss of reactant.

Temp.	Initial DMSCB	Expt. time for a 30% loss /s	Calc. time for a 30% loss /s	On-set Dimer /s	Calc. time for 30% decomp. /s
763	4795	53.8	55.1	69.0	78.9
763	4233	55.3	55.1	70.6	78.9
764	4365	50.9	53.2	53.0	75.1
773	3935	36.7	38.2	42.0	48.2
773	4185	35.7	38.2	32.4	48.2
774	4447	35.1	36.8	39.6	45.9
782	4462	23.2	26.9	25.9	31.4
782	4508	25.1	26.9	27.2	31.4
782	4041	26.1	26.9	27.5	31.4
793	4263	16.3	17.5	16.8	19.2
794	4399	15.5	16.8	15.4	18.4
794	3974	16.1	16.8	16.4	18.4
803	3701	10.7	11.9	10.0	12.6
803	3988	10.8	11.9	10.6	12.6
803	3745	10.8	11.9	10.2	12.6
812	4297	7.1	8.4	6.1	8.8
813	4453	7.1	8.1	6.8	8.5
813	3233	7.3	8.1	7.4	8.5

carried out using "version 1" of the apparatus and no interactive, computer-aided comparisons between experimental and calculated curves could be made. (See chapter 2, sections 2 and 4.)

As the reaction mixture had to "leak" into the reaction vessel at the start of the pyrolysis and because material, including reactant, also leaked out of the reaction vessel, calculation of the amount of decomposition which had occurred was difficult.

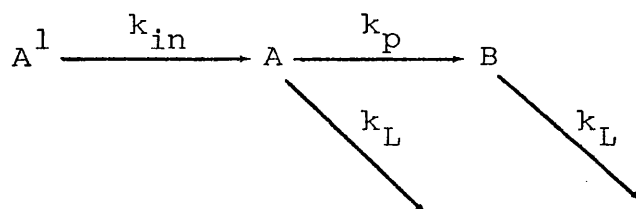
A computer model (using a main-frame computer) was set up, based on scheme 4.2, to simulate the experimental system. The formulae to calculate the concentrations of A and B at any time are⁵³,

$$A = A_0^1 k_{in} / (k_{in} - k_p) \left[e^{-(k_p + k_L)t} - e^{-k_{in}t} \right]$$

$$B = A_0^1 \left[e^{-k_L t} + k_p \cdot e^{-k_{in}t} / (k_{in} - k_p) - k_{in} \cdot e^{-(k_p + k_L)t} / (k_{in} - k_p) \right]$$

where A_0^1 is the initial amount of reactant A^1 .

Scheme 4.2 Model of Experimental System.



k_{in} is the "leak in" rate constant.

k_L is the "leak out" rate constant.

k_p is the pyrolysis rate constant.

It was assumed that "leak in" and "leak out" were first order processes. The leak-out rate constant was measured as 0.002 s^{-1} and k_{in} was estimated to be 0.6 s^{-1} .

The observed Arrhenius parameters were used to calculate k_p .

To check the computer model, the rate constants were set as above, and with A_0 set at 4000, the times for a 30% loss of the reactant (by reaction and by "leak-out") were calculated corresponding to each of the temperatures used in the series of experiments.

The real times for a 30% loss of DMSCB were then determined for each of the experimental runs, the initial amount of reactant being taken as the extrapolation of the $\ln(\text{peak height})$ vs time plots back to zero time. (see table 4.7).

A plot of the experimental times for 30% loss of reactant against the calculated times was a good straight line through the origin, indicating that the model could reproduce the experimental conditions (fig. 4.8).

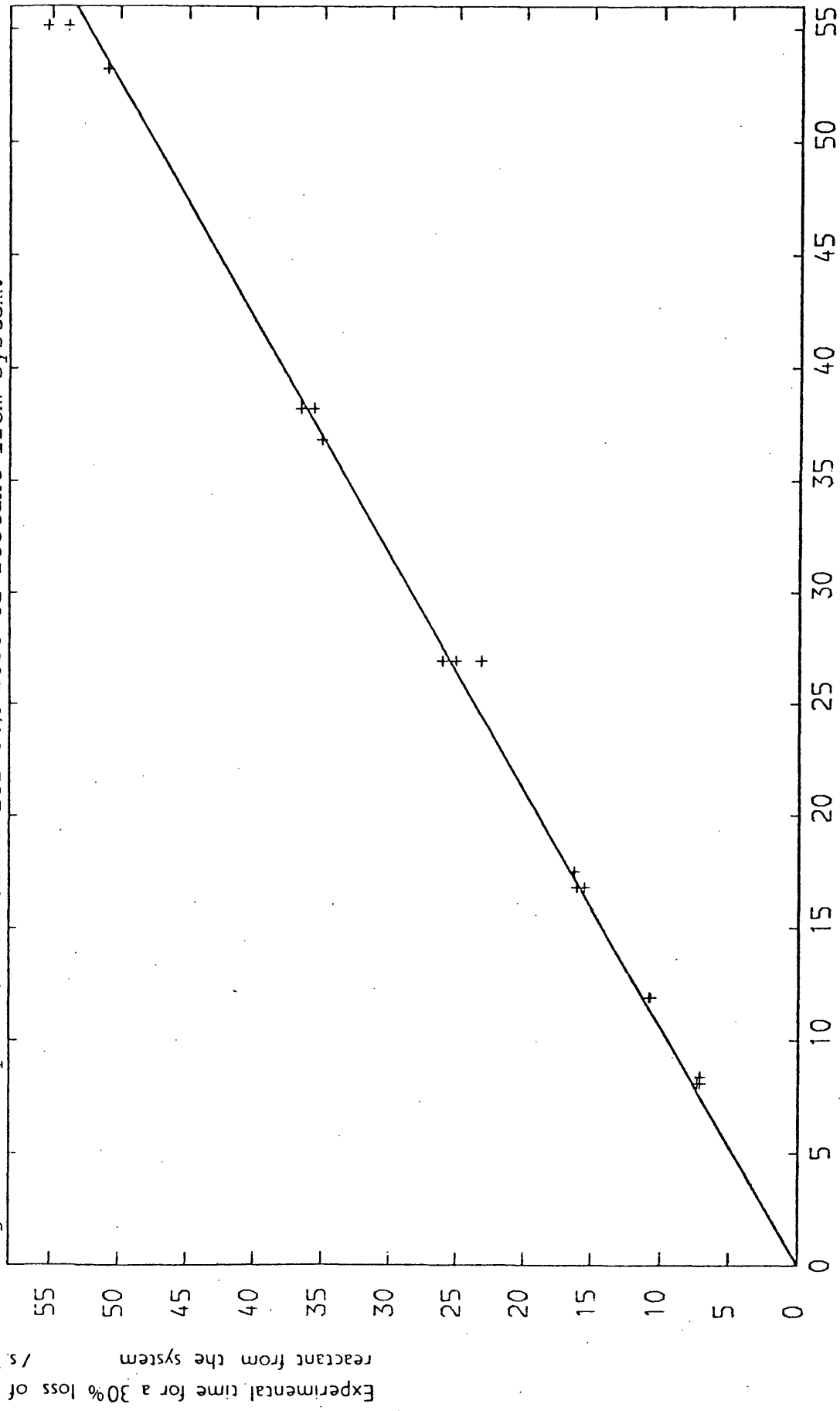
The same computer model was re-run, but with the leak-out rate constant set to zero, enabling the time for 30% decomposition (ie. pyrolysis only) to be calculated.

The experimental "onset times" of dimerisation were determined by extrapolation of the steep part of the peak height vs time curves back to the time axis. An example is given as fig. 4.9.

A plot of the dimer onset time vs the time calculated for 30% decomposition at each temperature was a good straight line through the origin (fig. 4.10). This was taken as an indication that the activation energy for the addition of hydrogen chloride to DMSE was about the same as (if not equal to) the activation energy for dimerisation.

If the addition step has an activation energy

Fig. 4.8 Comparison of times for 30% loss of reactant from system.



Calculated time for a 30% loss of reactant from the system /s.

Experimental time for a 30% loss of reactant from the system /s.

Fig. 4.9 Production of $\text{Me}_2\text{Si}(\text{SiMe}_2)_2$ at 783 K.

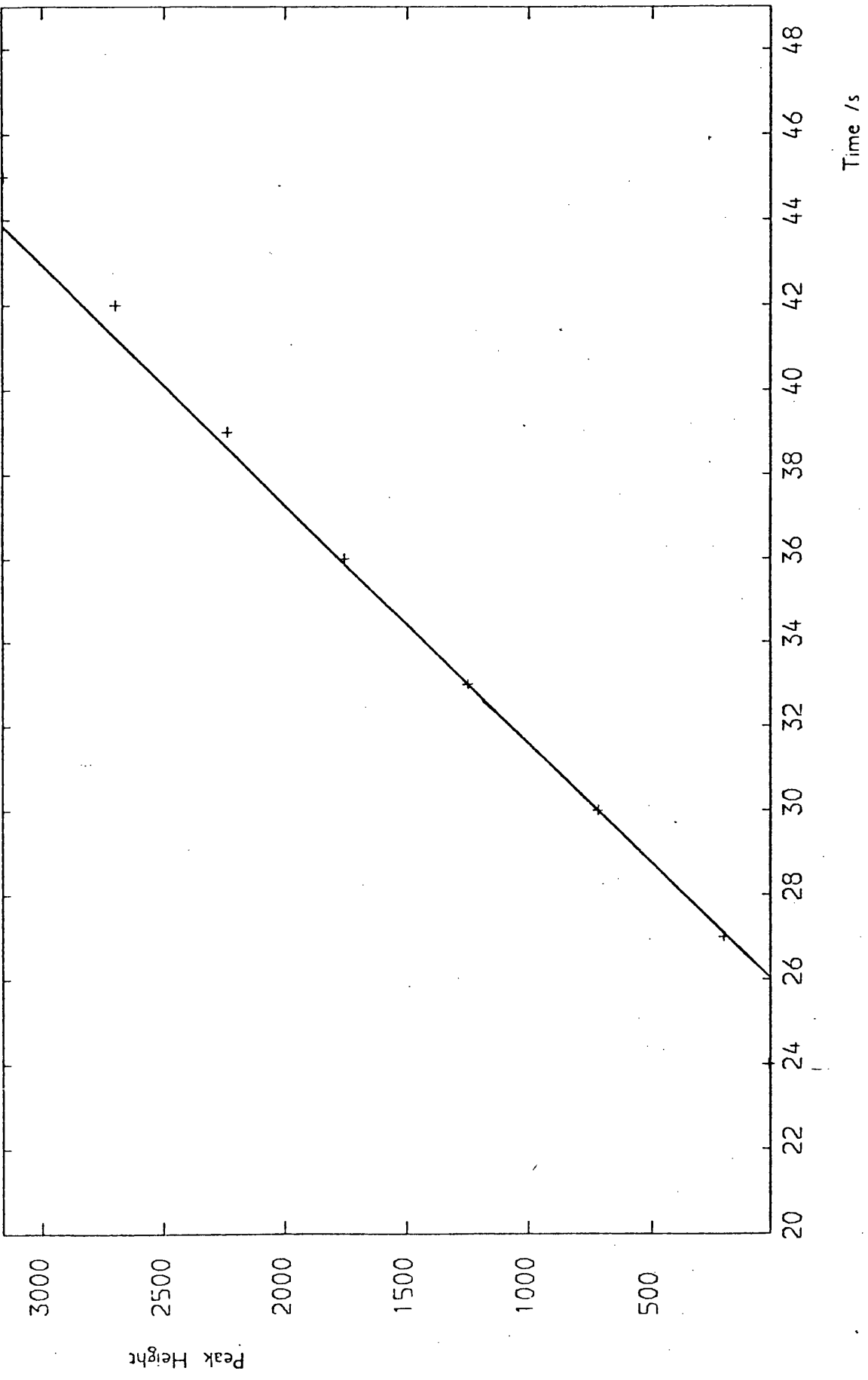
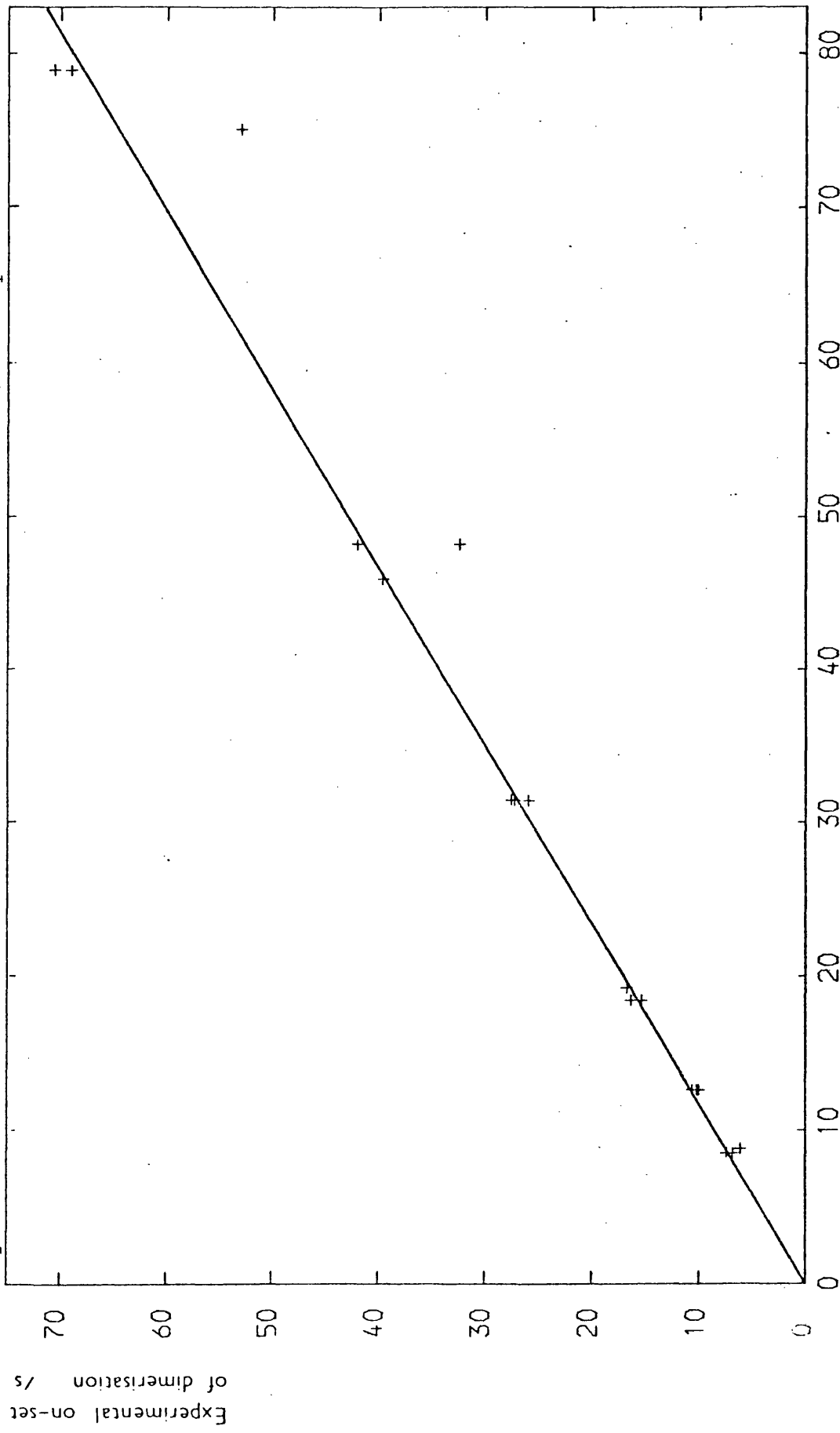


Fig. 4.10 On-set of dimerisation vs Calculated time for 30% decomposition reactant.



Calculated time for
30% decomposition /s

significantly higher than that of dimerisation, then at lower temperatures, the dimer would appear sooner relative to the start of the reaction and the above plot would be curved.

The above series of experiments was repeated, again using a DMSCB:HCl 3:1 mixture. Rate constants for the loss of DMSCB were given by $\log_{10}k = (15.24 \pm .20) - (255.9 \pm 2.9 \text{ KJ mol}^{-1}) / 2.303 \text{ RT}$. A table of rate constants and the Arrhenius plot appeared in chapter 2.

Up to 814K, data were collected at temperatures coincident with those of the earlier series. A comparison of the mean dimer on-set times between the two series (fig. 4.11) showed that they were essentially the same.

As previously, calculations of the times for 30% loss and decomposition of reactant were made, using the experimentally determined rate constants in the computer model. The results were plotted as for the earlier experiments (table 4.8 and figs. 4.12 and 4.13). The conclusions were the same.

4.5 Test of proposed mechanism.

A computer simulation of the mechanism shown in scheme 4.3, which takes account of leak-in and leak-out processes, was then carried out. The leak in rate constant k_1 was set at 0.7 s^{-1} and the leak out rate constants k_6 - k_{11} at 0.0012 s^{-1} . The reaction rate constants k_2 - k_4 were set at the literature values. The value of k_5 was then varied in an attempt to match the calculated (from the simulation) times for the onset of dimerisation with those observed experimentally

Fig. 4.11 Comparison of mean times for the on-set of dimerisation.

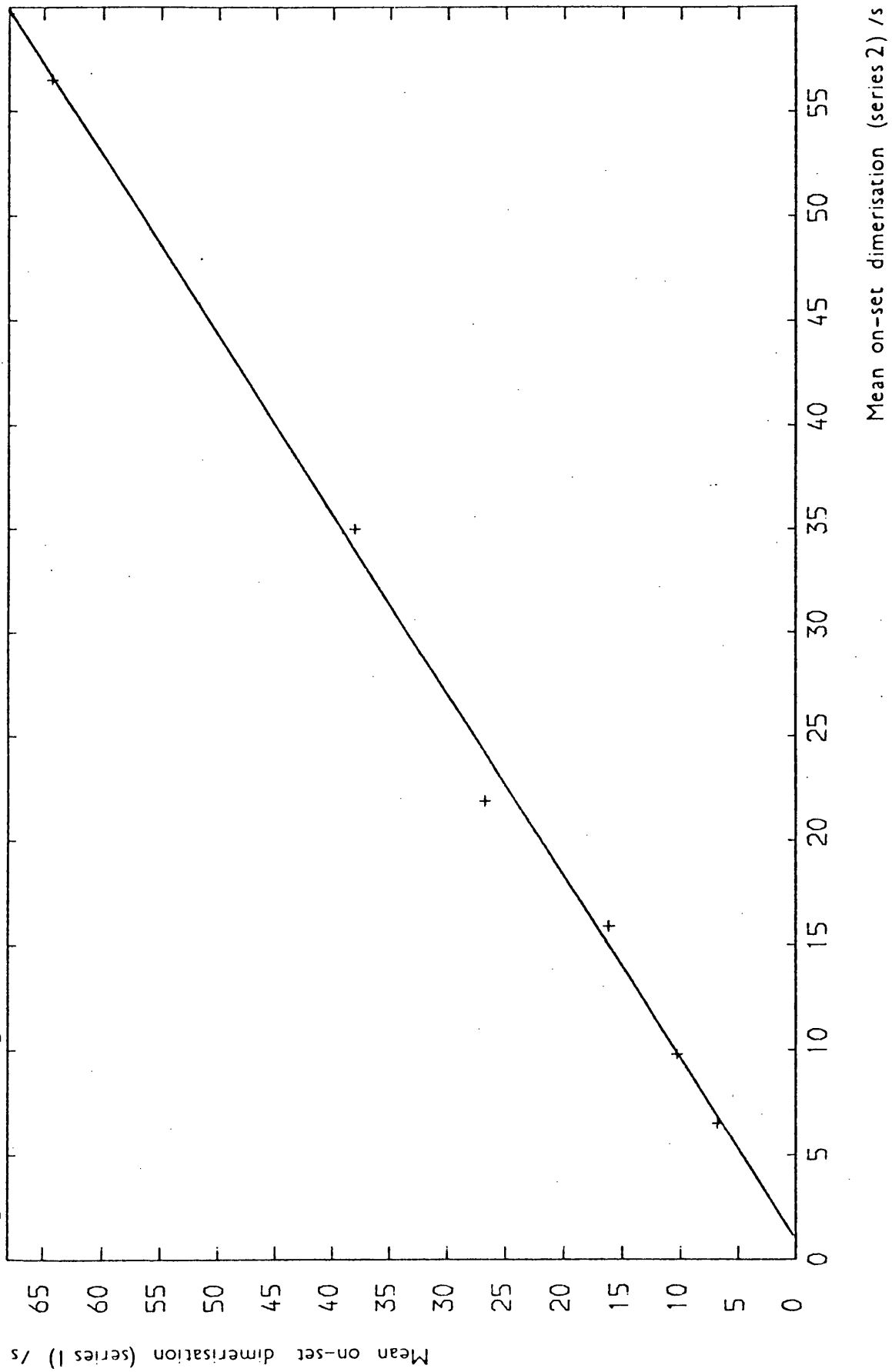
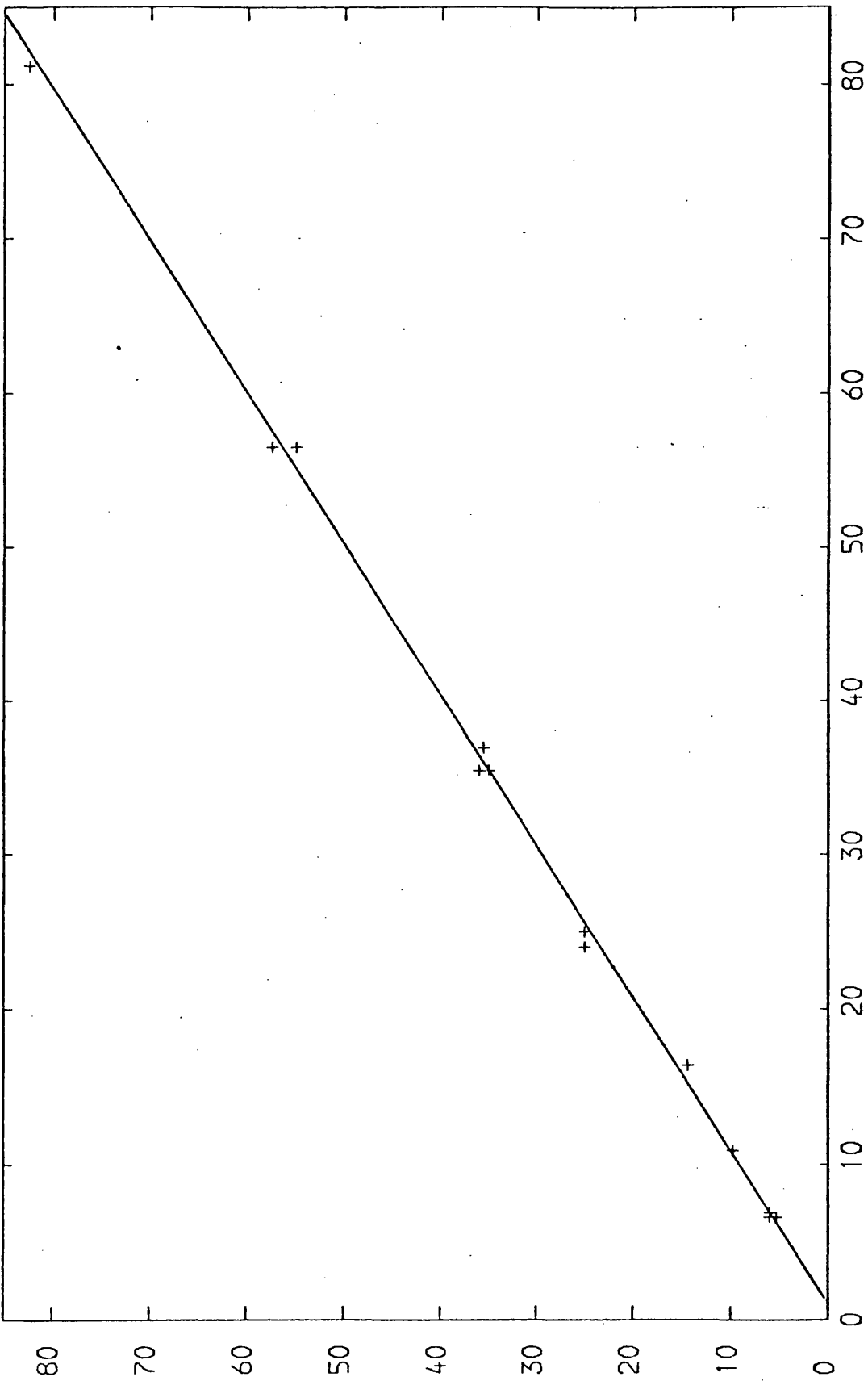


Table 4.8

On-set time of dimer and comparison between experimental and calculated time for 30% loss of reactant.

Temp /K	Initial DMSCB	Expt. time for 30% loss/s	Calc. time for 30% loss/s	On-set Dimer /s	Calc. time for 30% Decomp/s
754	1161	82.5	81.15	100.5	111.7
763	1410	55.0	56.5	52.5	69.6
763	1431	57.5	56.5	60.5	69.6
773	1683	35.5	36.9	33.2	42.0
774	1209	36.0	35.4	34.8	40.0
774	1582	35.0	35.4	37.0	40.0
782	1306	25.0	25.0	21.5	27.2
782	1417	25.0	25.0	21.0	27.2
783	1496	25.0	24.0	22.5	25.9
792	1488	14.5	16.4	15.8	17.2
802	1497	9.8	10.9	10.5	11.2
802	1307	9.8	10.9	8.8	11.2
802	1395	9.8	10.9	10.2	11.2
813	1287	6.0	6.9	6.6	7.1
813	1496	6.0	6.9	7.0	7.1
814	1247	6.0	6.6	6.5	6.8
814	1330	5.3	6.6	5.8	6.8

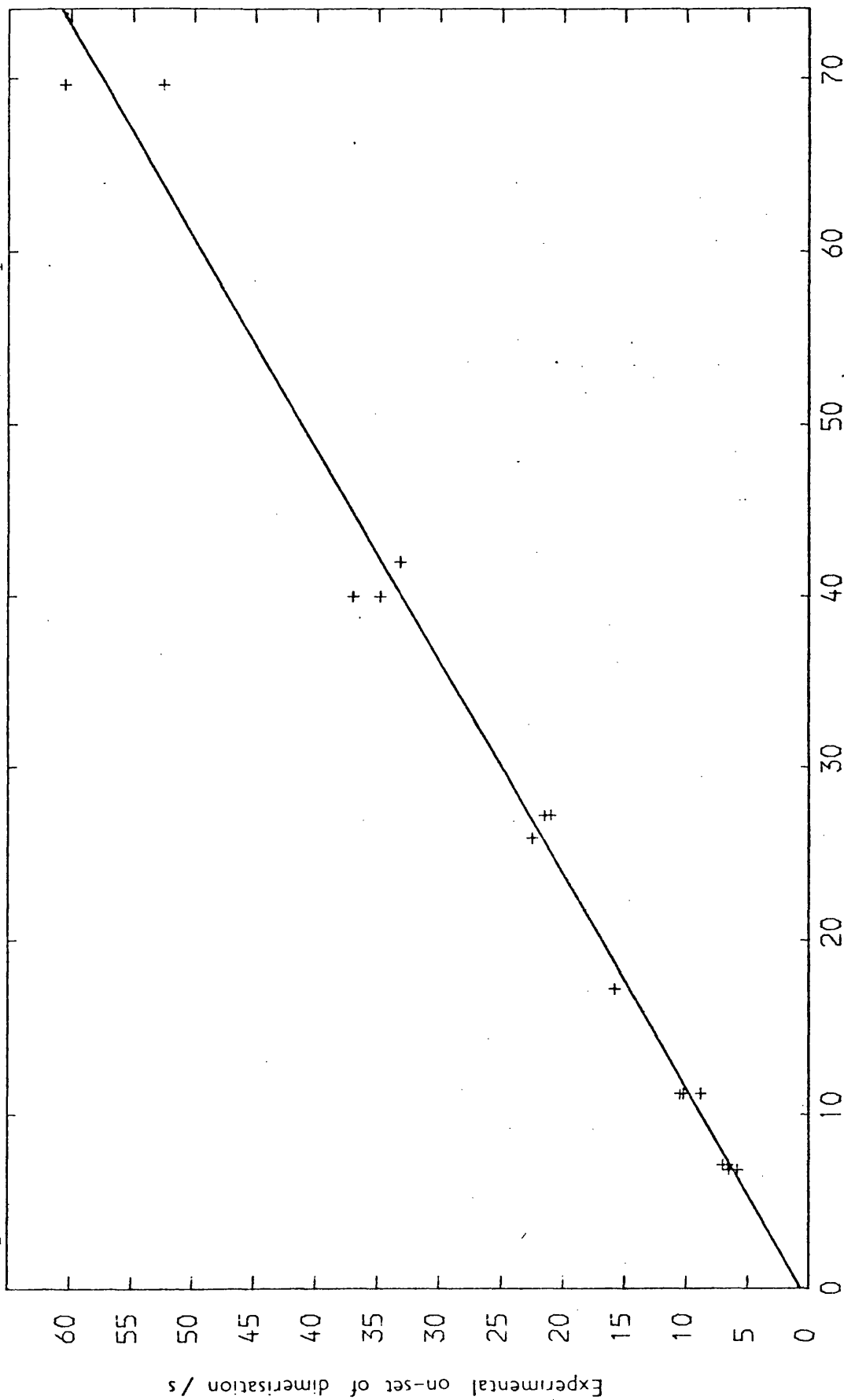
Fig. 4.12 Comparison of times for 30% loss of reactant from the system.



Calculated time for a 30% loss of reactant from the system /s

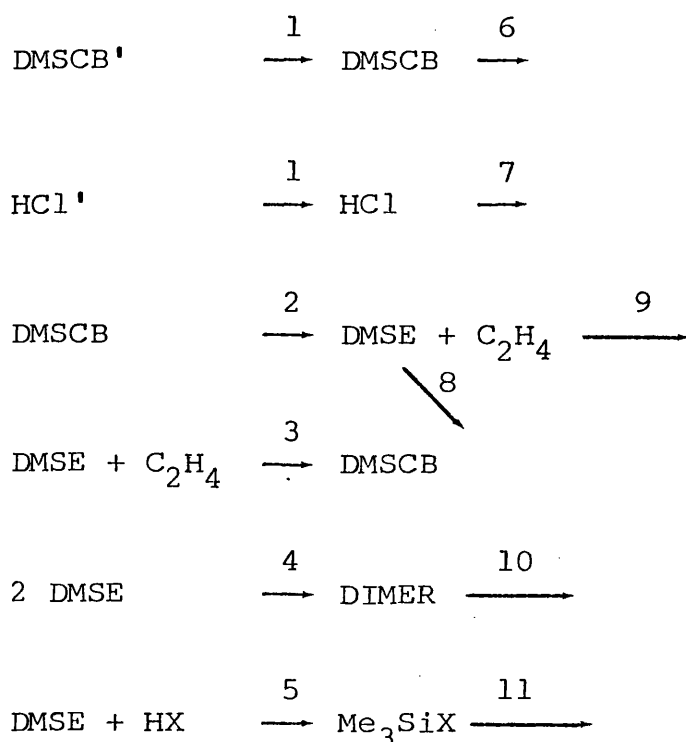
Experimental time for a 30% loss of reactant from the system /s

Fig. 4.13 On-set of dimerisation vs Calculated time for 30% decomposition reactant.



Calculated time for 30% decomposition / s.

Scheme 4.3



where X = Br or Cl and DIMER = $\text{Me}_2\text{Si} \begin{array}{c} \diagup \\ \diagdown \end{array} \text{SiMe}_2$

The computer simulation program used Gear's method of numerical integration to solve simultaneously a series of differential equations which described the rate of change of every species in scheme 4.3.

The formation of the dimer in the simulated reaction demonstrated the same features as in the experiment, the onset time having a temperature dependence. The simulated scheme best fitted the experimental data when the activation energy for the addition step was given by

$$\log_{10} k = (7.5 \pm .3) - (12 \pm 5 \text{ KJ mol}^{-1}) / 2.303 \text{ RT.}$$

This supported the conclusion from the experimental work alone that the activation energy for the addition reaction is similar to that for dimerisation. A comparison between the simulated and experimental data appears in table 4.9.

One simulation was tried with the dimerisation step

Table 4.9a

Comparison between simulated and experimental data for

DMSCB + HCl (3:1).

Temp. /K	Experimental on-set time of dimerisation /s	Simulation on-set time of dimerisation when addition step parameters were as indicated in the table below /s.					
		1	2	3	4	5	6
773	39.6 - 42.0	47.7	42.3	26.7	30.0	47.5	43.5
783	25.9 - 27.5	29.7	25.5	15.2	16.5	29.2	26.0
793	15.4 - 16.8	18.0	15.2	8.0	8.4	18.4	15.8
803	10.0 - 10.6	11.8	9.0	4.1	4.5	12.0	9.6
813	6.1 - 7.4	7.7	5.6	2.5	2.7	7.6	6.0

Table 4.9b

The above sets of simulation on-set times were obtained

using the following values for k_{addition} and $k_{\text{dimerisation}}$.

Set	Rate Constant for addition given by /s ⁻¹	Rate Constant for dimerisation given by /s ⁻¹
1	$k = 10^{7.5} e^{-7/RT}$ &	$k = 10^{6.55}$ @
2	$k = 10^{7.5} e^{-12/RT}$	$k = 10^{6.55}$
3	$k = 10^{7.5} e^{-17/RT}$	$k = 10^{6.55}$
4	$k = 10^{7.2} e^{-12/RT}$	$k = 10^{6.55}$
5	$k = 10^{7.8} e^{-12/RT}$	$k = 10^{6.55}$
6	$k = 10^{8.2} e^{-22/RT}$	$k = 10^{7.2} e^{-10/RT}$

@ Literature value

& Activation energies are in KJ mol⁻¹

given an activation energy of 10 KJ mol^{-1} . The A-factor was set at $10^{7.2} \text{ s}^{-1}$, so that the rate constant at 793K was equal to $10^{6.55} \text{ s}^{-1}$, the temperature-independent, literature value. The activation energy for the addition step was set at 22 KJ mol^{-1} (ie. 12 KJ greater than that for dimerisation), the A-factor being increased to $10^{8.2} \text{ s}^{-1}$ so that the rate constant for this step at 793K was unchanged.

The formation of the dimer reproduced the characteristic behaviour of the system, the onset times being close to the experimental values. A comparison between this simulation and experiment is also shown in table 4.9.

The conclusions were therefore, that the activation energy for the addition of DMSE to hydrogen chloride is about 12 KJ mol^{-1} greater than that for the self dimerisation of DMSE and that the dimerisation step itself could have a small activation energy.

4.6 DMSCB + Hydrogen Bromide.

Mixtures in the proportion DMSCB:HBr 2:1 and 3:1 were used for these series of experiments. No temperature dependent variation in the on-set time of dimerisation was observed for either series, the dimer and addition product being formed simultaneously. The latter quickly decomposed again, either by hydrolysis or because it was not thermally stable at the temperature used. Calculations involving this species were therefore impracticable.

Only the 2:1 mixture produced any quantitative conclusions and a summary of these experiments now follows.

DMSCB:HBr (2:1)

The pyrolyses were carried out over the temperature

range 793-853K in approximately 10K steps. Higher temperatures than for previous experiments were used in an effort to reduce the amount of adsorption within the reaction vessel. No significant improvement was found however.

The rate constants for the decomposition of DMSCB over the range 793-813K were similar to those measured for the loss of this reactant in the second series of DMSCB/HCl(3:1) experiments. As the rate constants above 813K could not be reliably determined, because they were greater than 0.06 s^{-1} (see chapter 2), it was assumed that the Arrhenius parameters for these DMSCB/HBr experiments were about the same as for the earlier work with hydrogen chloride and that $\log_{10}k=15.24-256 \text{ KJ mol}^{-1}/2.303 \text{ RT}$.

Owing to the aforementioned adsorption problems, particularly of hydrogen bromide, the methods of analysis outlined earlier could again not be successfully applied.

The function $\ln(V_{\text{Dim}}/k.A_0)$ was plotted against $10^3/T$. The maximum initial rate of dimerisation (V_{Dim}) was calculated from the interpolated experimental data and the initial amount of DMSCB (A_0) was determined by extrapolation of $\ln(\text{Peak Height})$ vs time plots back to zero time. The decomposition rate constant k was calculated from the observed Arrhenius parameters. The resulting plot, of the data in table 4.10, is shown in fig. 4.14.

Similarly curved plots could be drawn from data derived by computer simulation of the mechanism shown by scheme 4.3, using the same numerical integration program as for simulation of the DMSCB/hydrogen chloride system.

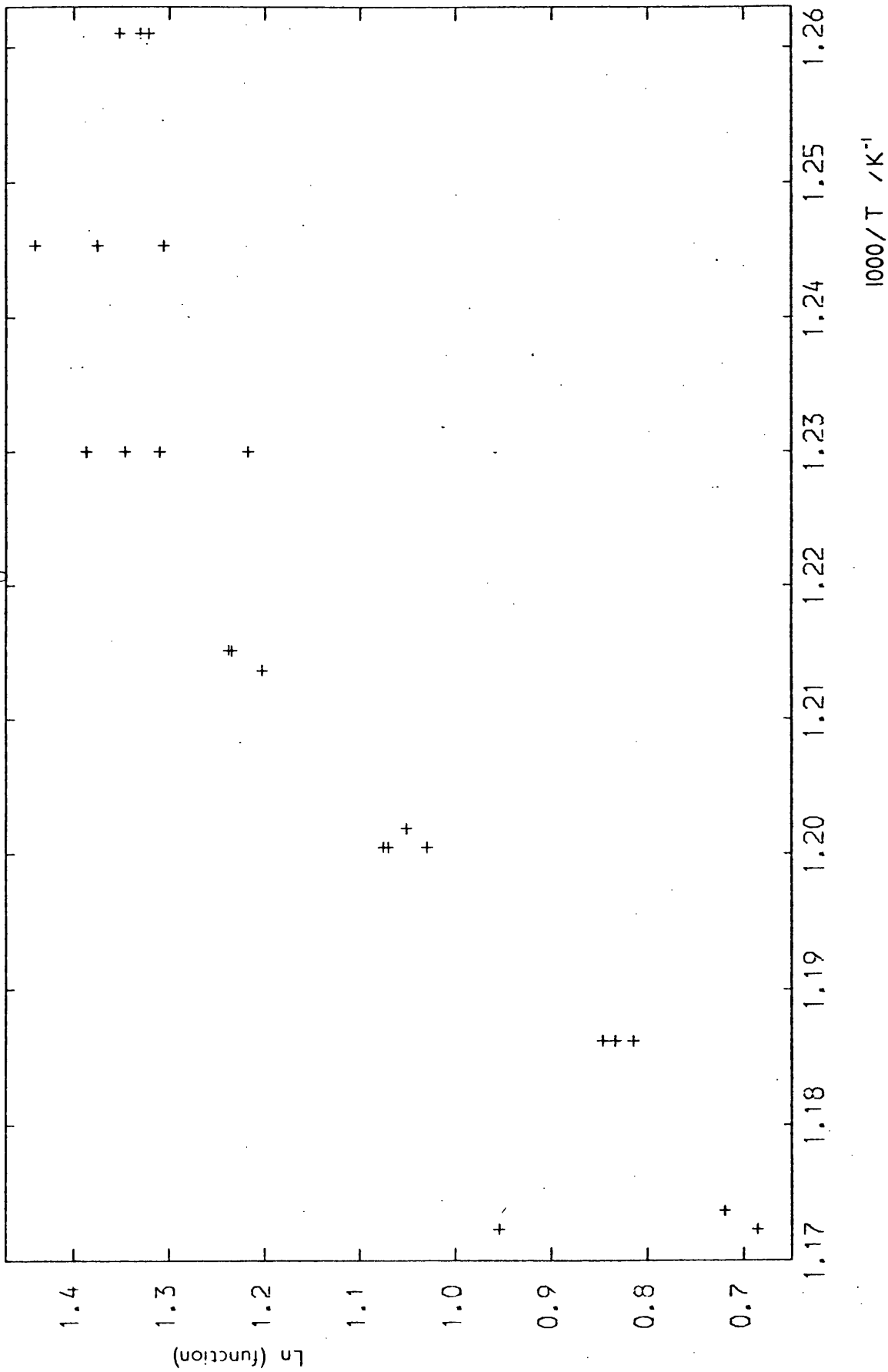
The calculated curves could not be expected to match

Table 4.10

Calculation of $\ln(V_{\text{Dim}}/k \cdot A_{\text{O}})$ for DMSCB + HBr (2:1).

Temp/K	Initial DMSCB A_{O}	Rate Constant k/s^{-1}	Rate Dimerisation V_{Dim}	$\frac{10 \times V_{\text{Dim}}}{k \cdot A_{\text{O}}}$ (F)	$\ln(F)$
793	1643	.0238	14.8	3.785	1.331
793	1532	.0238	14.1	3.867	1.353
793	1457	.0238	13.0	3.749	1.322
803	1312	.0386	18.7	3.693	1.306
803	1969	.0386	30.1	3.960	1.376
803	1939	.0386	31.6	4.222	1.440
813	1277	.0619	29.3	3.707	1.310
813	1615	.0619	40.0	4.001	1.387
813	1378	.0619	32.8	3.845	1.347
813	1286	.0619	26.9	3.379	1.218
823	1806	.0981	60.9	3.437	1.235
823	1747	.0981	59.1	3.449	1.238
824	1627	.1026	55.6	3.331	1.203
832	1691	.1470	71.1	2.860	1.051
833	1861	.1537	80.0	2.797	1.029
833	1696	.1537	76.4	2.931	1.075
833	1835	.1537	82.2	2.915	1.070
843	1420	.2382	77.8	2.300	0.833
843	1642	.2382	91.1	2.329	0.846
843	1356	.2382	72.9	2.257	0.814
852	1682	.3504	120.9	2.051	0.719
853	1799	.3655	170.7	2.596	0.954
853	1788	.3655	129.8	1.986	0.686

Fig. 4.14 \ln (Initial Rate Dimerisation / $k \cdot A_0$) vs $10^3 / T$.

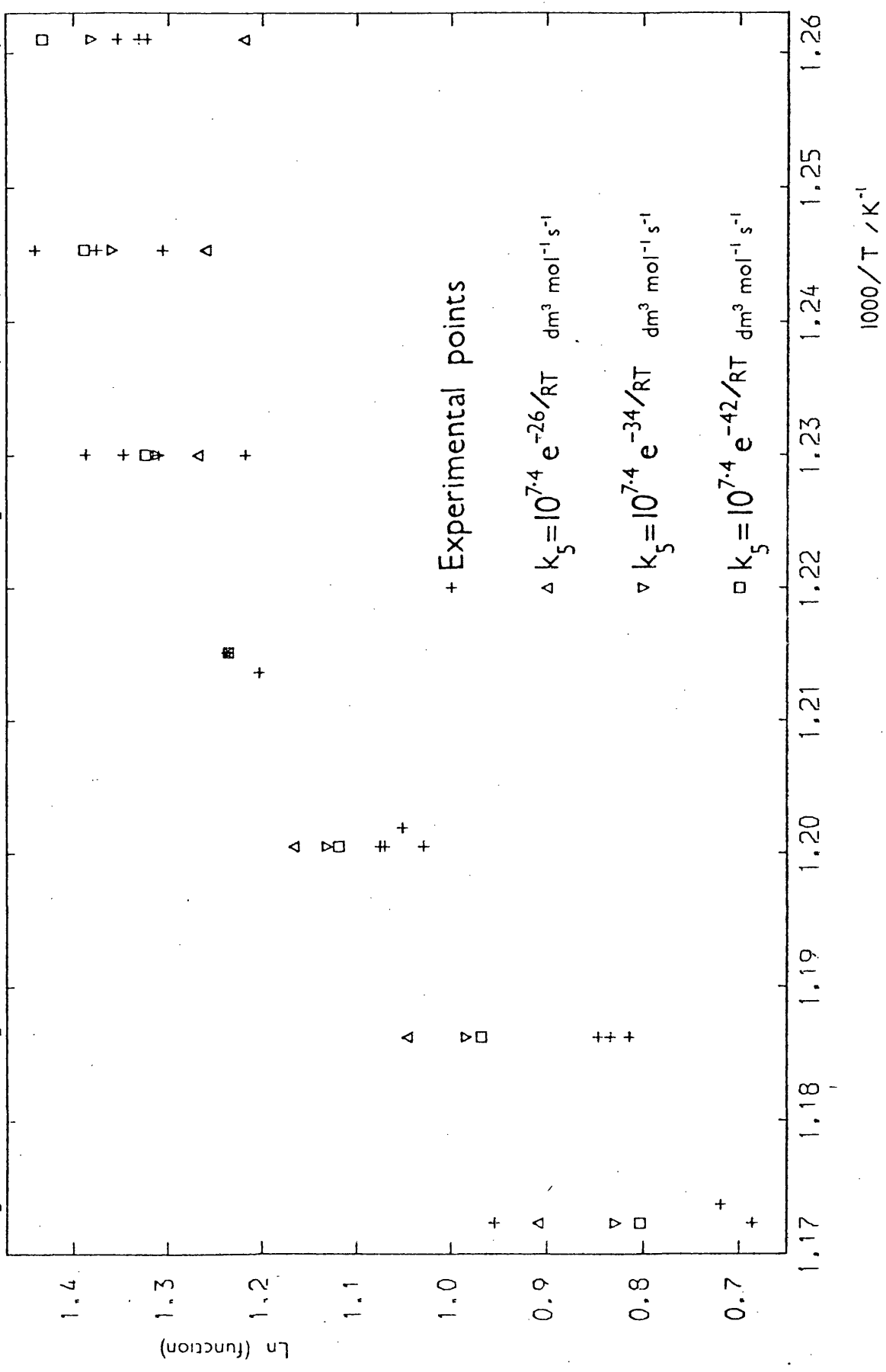


the experimental plot numerically, since the latter had not been corrected for the sensitivity difference between DMSCB and the dimer, and the simulation procedure assumed equal sensitivity between the two species. The calculated plot was therefore superimposed onto the experimental by the addition of a constant to the \ln of the calculated function, such that the point at 823K matched the experimental value.

The best fit to the experimental data in the temperature range 793-823K was given by $\log_{10} k_5 = (7.4 \pm 0.3) - (34 \pm 8 \text{ kJ mol}^{-1}) / 2.303 RT$. Comparisons between simulations and experiment are shown in fig. 4.15. Other combinations of A and E may have fitted equally well, but it was reasonable to assume that the A-factor for the addition of hydrogen bromide to DMSE ought to be about the same as for the addition of hydrogen chloride. The initial rate of the dimerisation reaction tended to be under estimated towards higher temperatures which is why it was decided to concentrate on fitting the simulated data to the lower half of the experimental temperature range. This could also explain the steeper slope of the experimental curve (compared to the simulated) at the higher temperatures.

Plots of $\ln(V_{\text{Dim}}/k.A_0)$ (experimental) against the same function for the simulated data were drawn. A straight line would have indicated a good correlation between simulation and experiment. The experimental data however were too scattered for any use to be made of these plots, it being possible to draw a straight line through all of them. Table 4.11 summarises the simulated data used and figs. 4.16-4.18 show the resulting plots.

Fig. 4.15 Comparisons between simulations and experiment. (Ln (function) vs $10^3/T$)



1.4

Ln (function)

1.3

1.2

1.1

1.0

0.9

0.8

0.7

1.17

1.18

1.19

1.20

1.21

1.22

1.23

1.24

1.25

1.26

$1000/T / \text{K}^{-1}$

Table 4.11.

DMSCB + HBr (2:1) Simulated data for various step 5 parameters.

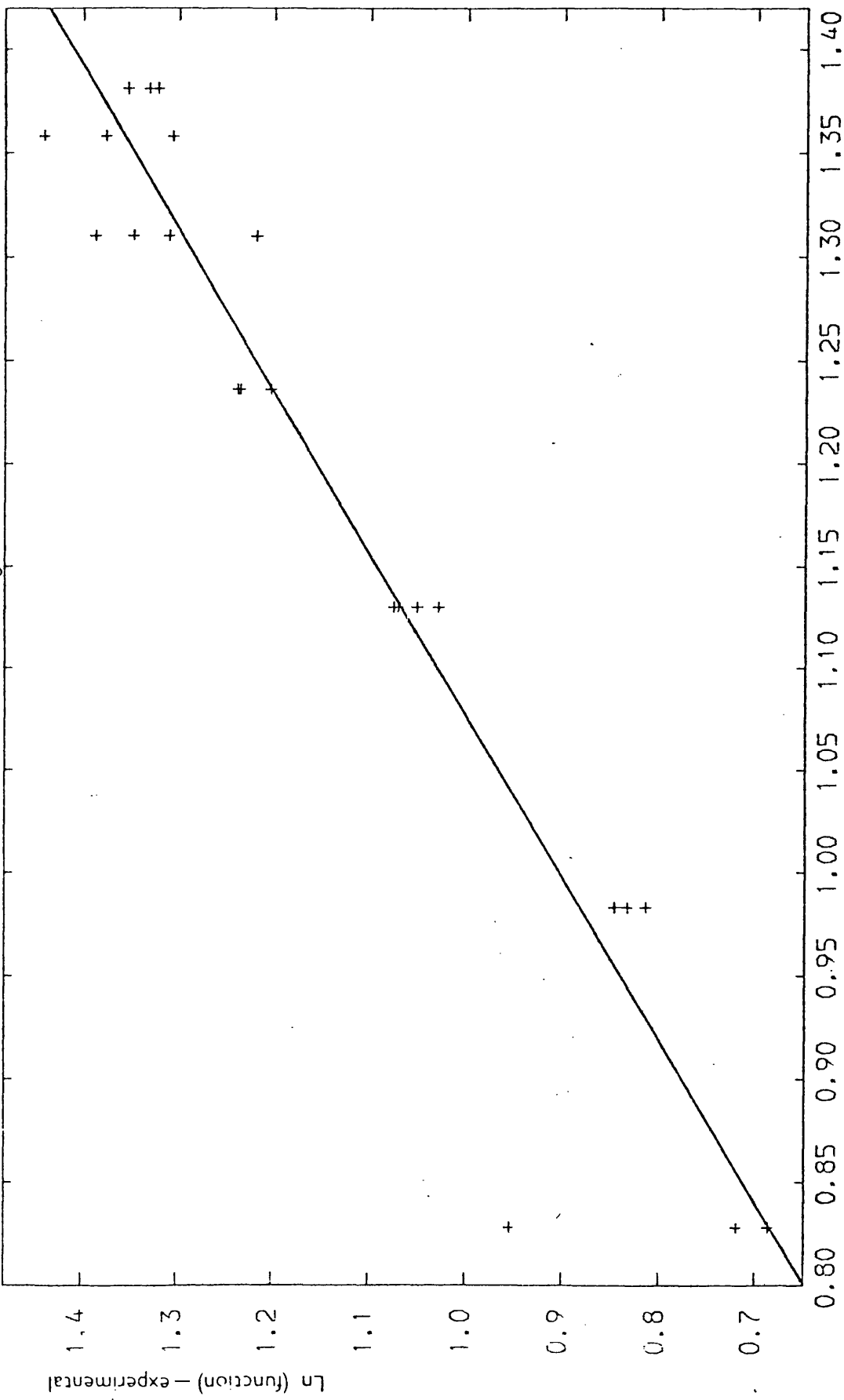
$A_0 = 1000$

Temp /K	Rate Constant k_1/s^{-1}	Maximum Rate Dimerisation V_{Dim}	$\frac{10 \times V_{Dim}}{k \cdot A_0}$ (F)	$\ln(F)$	$\ln(F)$ corrected
$\log_{10} k_5 = 7.4 - 34 \text{ KJ mol}^{-1} / 2.303 \text{ RT}$					(+.129)
793	.0260	9.09	3.496	1.252	1.381
803	.0426	14.56	3.418	1.229	1.358
813	.0689	22.45	3.258	1.181	1.310
823	.1103	33.36	3.025	1.107	1.236
833	.1744	47.45	2.721	1.001	1.130
843	.2730	64.15	2.350	0.854	0.983
853	.4228	85.01	2.011	0.699	0.828
$\log_{10} k_5 = 7.4 - 42 \text{ KJ mol}^{-1} / 2.303 \text{ RT}$					(+.060)
793	.0260	10.25	3.942	1.372	1.432
803	.0426	16.09	3.777	1.329	1.389
813	.0689	24.38	3.539	1.264	1.324
823	.1103	35.76	3.242	1.176	1.236
833	.1744	50.30	2.884	1.060	1.120
843	.2730	67.70	2.480	0.908	0.968
853	.4228	88.89	2.102	0.743	0.803
$\log_{10} k_5 = 7.4 - 26 \text{ KJ mol}^{-1} / 2.303 \text{ RT}$					(+.336)
793	.0260	6.29	2.419	0.884	1.220
803	.0426	10.74	2.521	0.925	1.261

(Table 4.11 continued)

Temp /K	Rate Constant k_1/s^{-1}	Maximum Rate Dimerisation V_{Dim}	$\frac{10 \times V_{Dim}}{k \cdot A_O}$ (F)	$\ln(F)$	$\ln(F)$ corrected
813	.0689	17.50	2.540	0.932	1.269
823	.1103	27.12	2.459	0.900	1.236
833	.1744	40.00	2.294	0.830	1.167
843	.2730	55.48	2.032	0.709	1.046
853	.4228	74.95	1.773	0.573	0.909

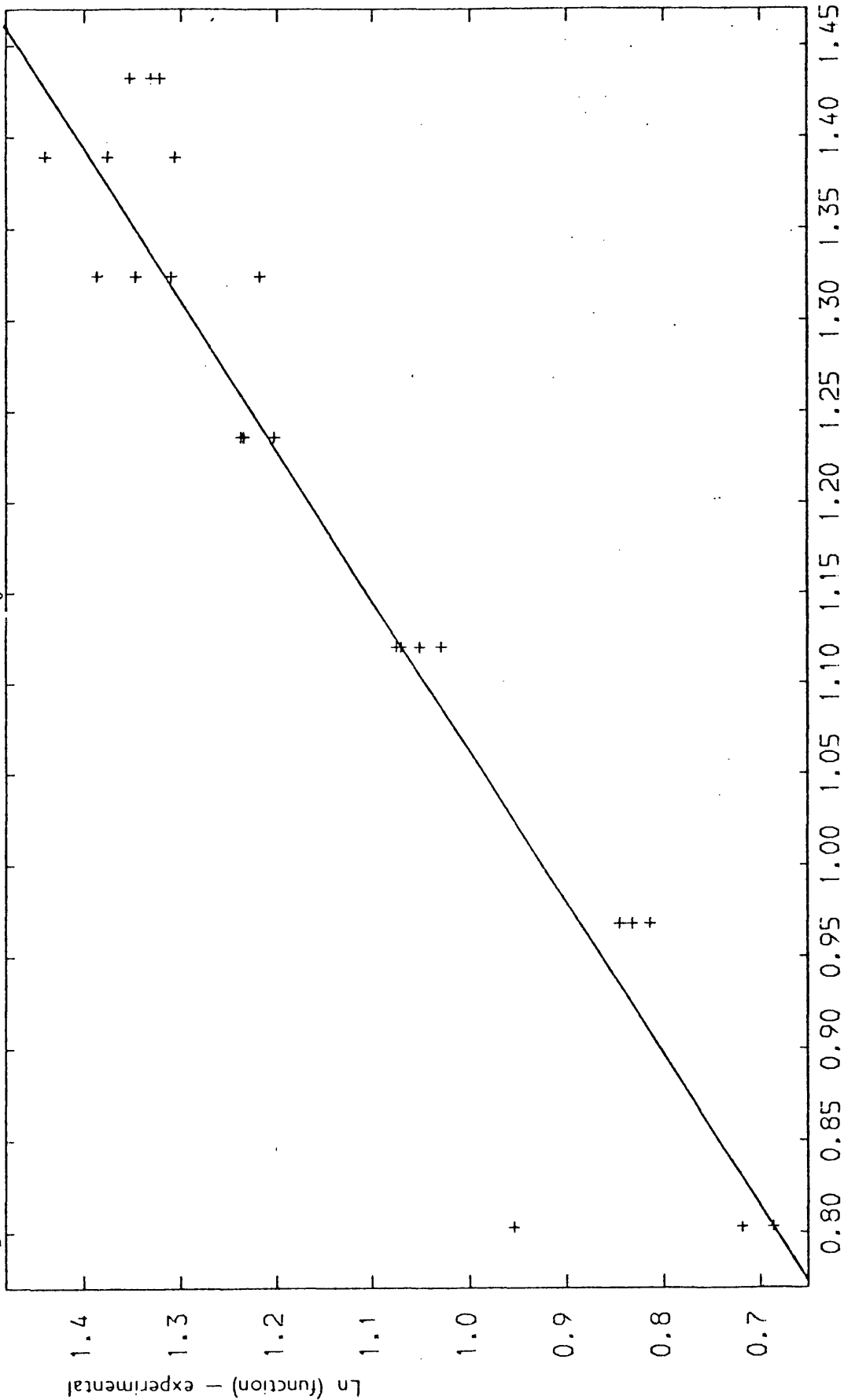
Fig. 4.16 $\ln(\text{Initial Rate Dimerisation}/k \cdot A_0)$: Experimental vs Calculated.



Ln (function) — calculated

$$k_5 = 10^{7.4} e^{-34/RT} \text{ dm}^3 \text{ mol}^{-1} \text{ s}^{-1}$$

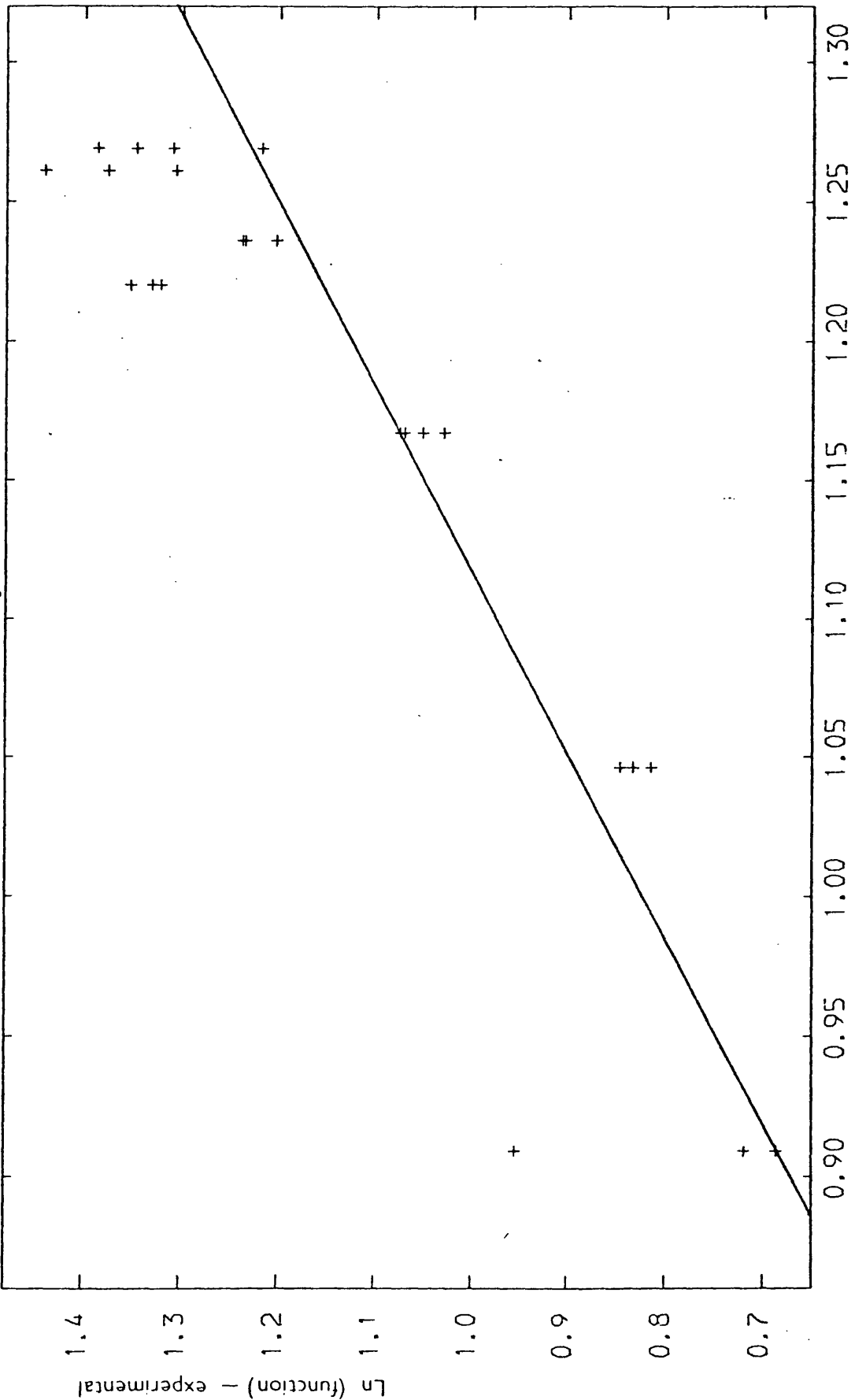
Fig. 4.17 $\ln(\text{Initial Rate Dimerisation}/k_5 A_0)$: Experimental vs Calculated.



$\ln(\text{function}) - \text{calculated}$

$$k_5 = 10^{7.4} e^{-42/RT} \text{ dm}^3 \text{ mol}^{-1} \text{ s}^{-1}$$

Fig. 4.18 $\ln(\text{Initial Rate Dimerisation}/k_5 A_0)$: Experimental vs Calculated.



$\ln(\text{function}) - \text{calculated}$

$$k_5 = 10^{7.4} e^{-26/RT} \text{ dm}^3 \text{ mol}^{-1} \text{ s}^{-1}$$

The hydrogen-bromine bond dissociation energy, $D(\text{H-Br})$, is 366 KJ mol^{-1} ¹⁹. Assuming an A-factor for unimolecular dissociation of $10^{14.1}$, then at 853K, the highest temperature used in the above experiments, the rate constant for the gas-phase pyrolysis of hydrogen bromide would be $5 \times 10^{-9} \text{ s}^{-1}$, making this a negligible process.

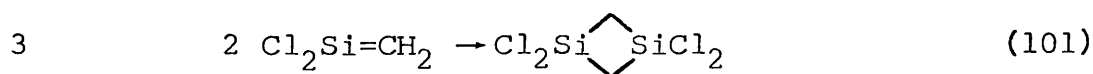
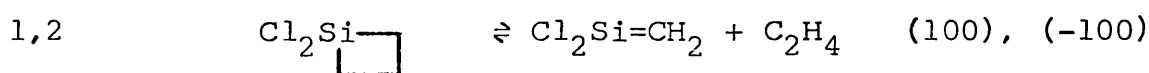
Also, no bromine was observed during the experiments, indicating that no significant surface (or gas phase) decomposition of the hydrogen bromide occurred during the pyrolysis reaction.

4.7 Pyrolysis of 1,1-dichlorosilacyclobutane (DCSCB).

The pyrolysis of this compound was expected to proceed in an analogous way to that of DMSCB, producing a silaethene species which would then dimerise. The mechanism is illustrated in scheme 4.4. It was hoped to show that hydrogen chloride would readily add to 1,1-dichlorosilaethene (DCSE) as it does to 1,1-dimethylsilaethene. A fast addition reaction between hydrogen chloride and 1-methyl, 1-chlorosilaethene, as a step in the pyrolysis mechanism of trimethylchlorosilane, would then be a "safe" assumption.

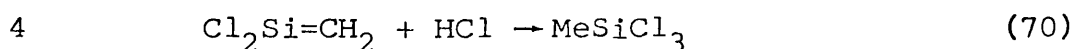
However, owing to the now familiar problems of adsorption within the reaction vessel and/or ion source, which were generally worse for the DCSCB system than for the DMSCB, it was not possible in the time available, to obtain any quantitative results regarding the addition of hydrogen chloride to DCSE. Nevertheless, some observations were made and the pyrolysis parameters for DCSCB were measured. A summary of the results follows below.

Scheme 4.4 Pyrolysis mechanism of DCSCB



Initial, quantitative experiments showed that DCSCB pyrolyses from about 775K. A group of spectrum peaks, starting at $m/e=224^+$ and with the proportions for a species with 4 chlorine atoms, confirmed the production of the dimeric compound and therefore of the silaethene.

Pyrolysis of DCSCB in the presence of hydrogen chloride produced groups of peaks at $m/e=133^+$ and 148^+ , probably due to the ions $(\text{SiCl}_3)^+$ and $(\text{MeSiCl}_3)^+$ respectively. This was confirmation for the addition reaction between the silaethene and hydrogen chloride.



However, the reaction seemed slower than for dimethylsilaethene + hydrogen chloride, the formation of the dimer not being totally suppressed in a DCSCB:HCl (3:1) mixture.

4.8 Decomposition Parameters for DCSCB.

Samples of DCSCB were pyrolysed, using version 1 of the apparatus, over the temperature range 770-877K. The rate constants obtained (by the "Swinbourne" method outlined in chapter 2) are in table 4.12 and the resulting Arrhenius plot is in fig. 4.19. A least squares fit over all the points gave $\log_{10}k = (12.85 \pm .14) - (231.4 \pm 2.2 \text{ KJ mol}^{-1}) / 2.303 \text{ RT}$.

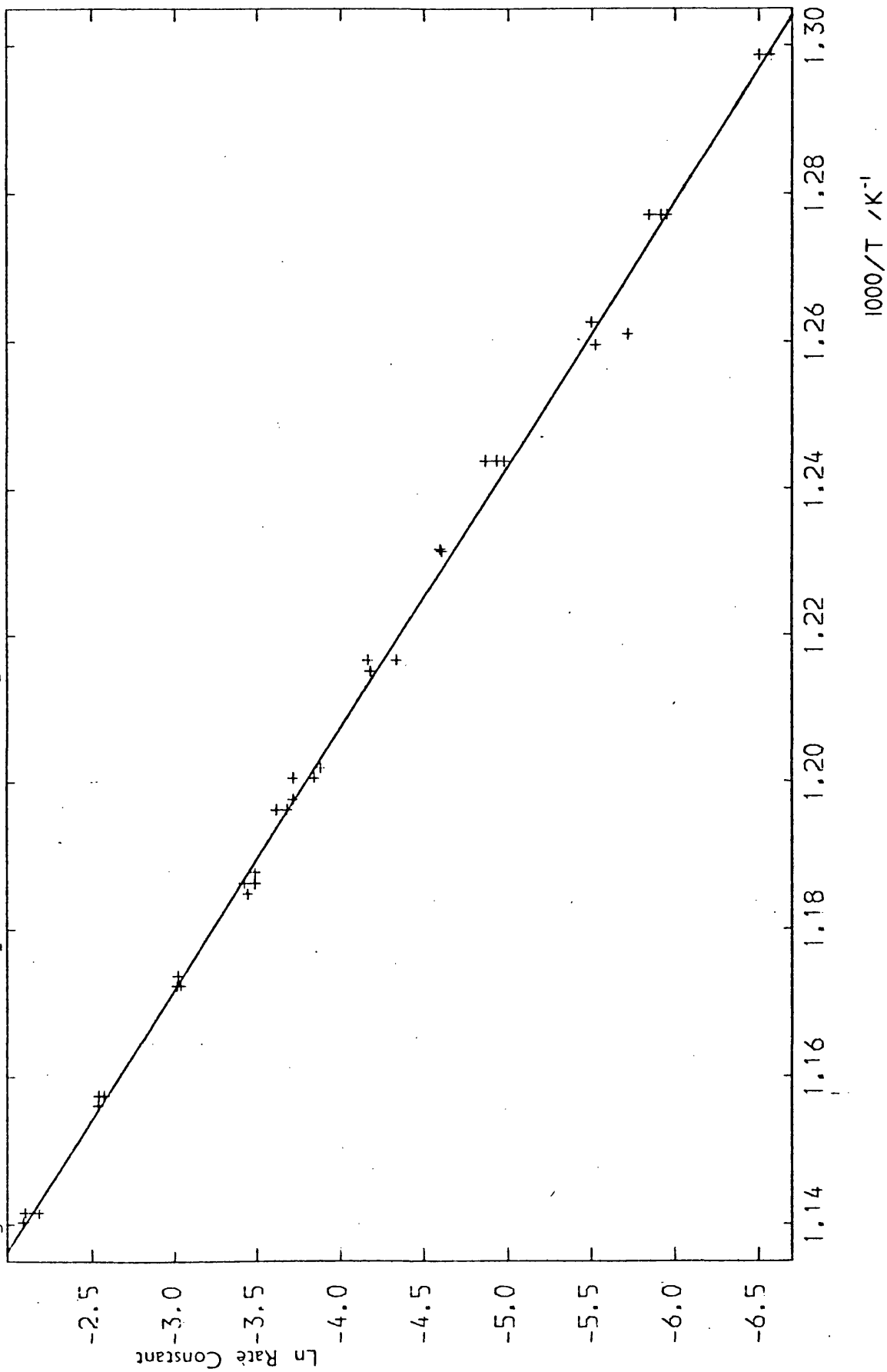
The activation energy for the pyrolysis of DCSCB was expected to be similar to that for DMSCB, it being generally accepted that the initial step of the decomposition involves the breaking of a carbon-carbon bond away from the substituted

Table 4.12

Rate Constants for the pyrolysis of DCSCB (Corrected for leak out).

Temp /K	Rate Constant for the decomposition of DCSCB k/s ⁻¹	lnk	Temp /K	Rate Constant for the decomposition of DCSCB k/s ⁻¹	lnk
770	.0014	-6.571	833	.0215	-3.840
770	.0015	-6.502	835	.0243	-3.717
783	.0026	-5.952	836	.0269	-3.616
783	.0029	-5.843	836	.0252	-3.681
783	.0027	-5.915	842	.0305	-3.490
792	.0041	-5.497	843	.0305	-3.490
793	.0033	-5.714	843	.0306	-3.487
794	.0040	-5.522	843	.0326	-3.423
804	.0069	-4.976	844	.0319	-3.445
804	.0072	-4.934	852	.0488	-3.020
804	.0077	-4.867	853	.0491	-3.014
812	.0100	-4.605	853	.0480	-3.037
812	.0101	-4.595	864	.0760	-2.577
822	.0131	-4.335	864	.0785	-2.545
822	.0155	-4.167	865	.0786	-2.543
823	.0153	-4.180	876	.1122	-2.188
832	.0207	-3.878	876	.1214	-2.109
833	.0243	-3.717	877	.1228	-2.097

Fig. 4.19 Arrhenius plot for the decomposition of DCSCB.



silicon. The activation energy obtained above was therefore rather small. A possible explanation for this was that the "back reaction" (step 2 of scheme 4.4) was more important for the DCSCB system than for that of the DMSCB.

Several series of pyrolysis reactions were therefore carried out using a DCSCB:HCl (1:1) mixture, the hydrogen chloride being present to remove the silaethene species by addition and thus preventing the back reaction from occurring.

The initial series of experiments returned an activation energy of 188 kJ mol^{-1} , but the two subsequent sets yielded values closer to those expected. The rate constants from these later experiments are combined in table 4.13 and the Arrhenius plot is in fig. 4.20. A least squares fit through all the points up to 843K gave $\log_{10}k = (14.73 \pm .47) - (259.5 \pm 7.3 \text{ kJ mol}^{-1})/2.303 \text{ RT}$.

This result compares well with the activation energy of $255.9 \text{ kJ mol}^{-1}$ and A-factor of $10^{15.24}$ obtained earlier for the pyrolysis of DMSCB. The A-factor for the decomposition of the dichloro-compound may be reduced owing to unimolecular fall off, an effect which did not apply to DMSCB to the same extent.

A recent experiment in this laboratory involving the pyrolysis of DCSCB in a flow system, with analysis by gas chromatography, yielded decomposition rate constants given by $\log_{10}k = (15.56 \pm .30) - (263.8 \pm 4.8 \text{ kJ mol}^{-1})/2.303 \text{ RT}^{59}$, which within experimental error were the same as the literature values for DMSCB pyrolysis.

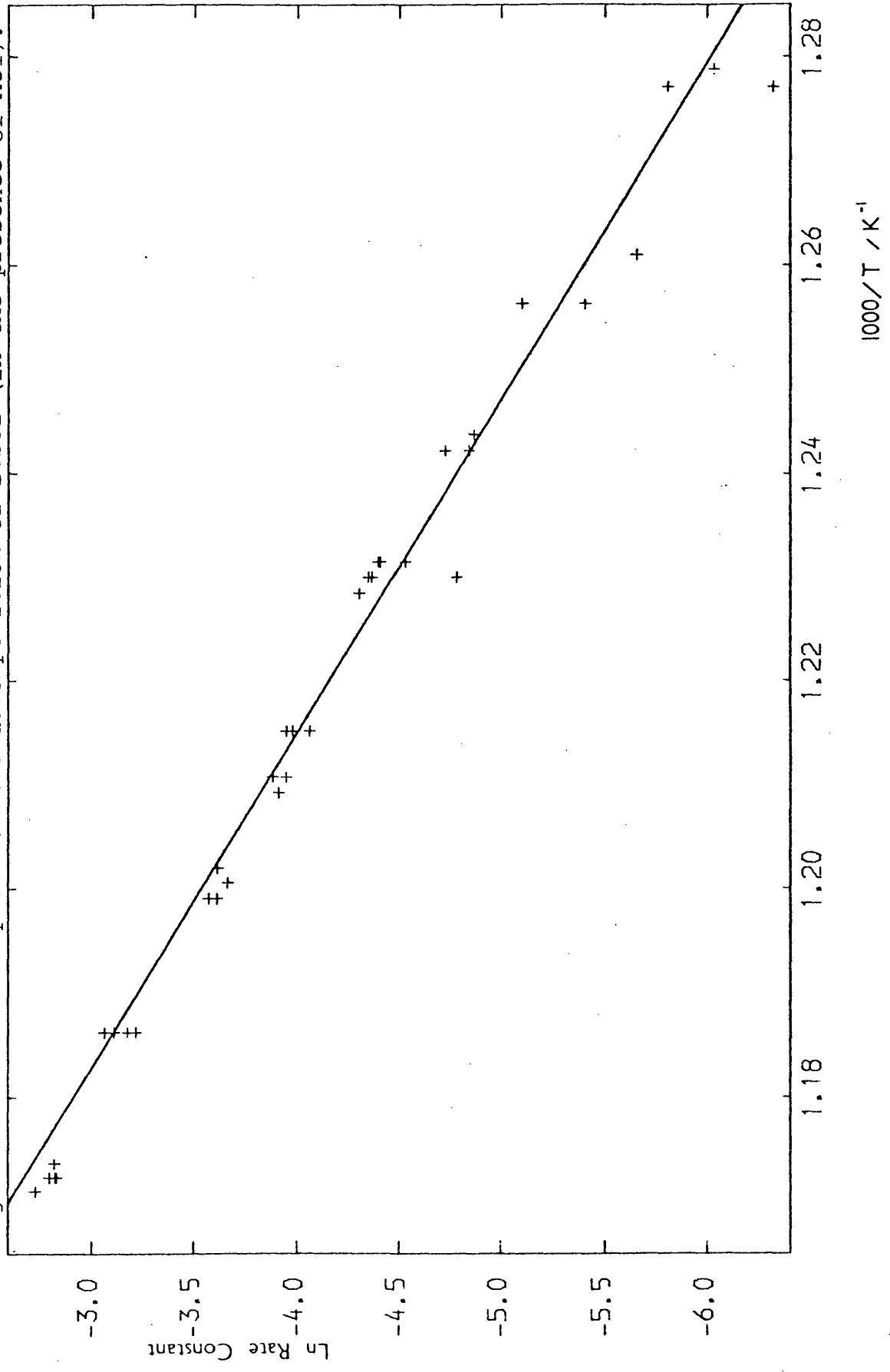
Also, a mixture of DMSCB and DCSCB was pyrolysed in a sealed tube and the products qualitatively analysed by G.C. mass spectrometry. Ethene and the expected dimeric products, formed by the following reactions, were found to

Table 4.13

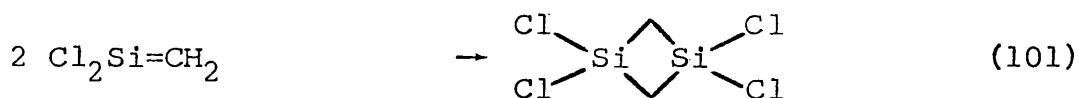
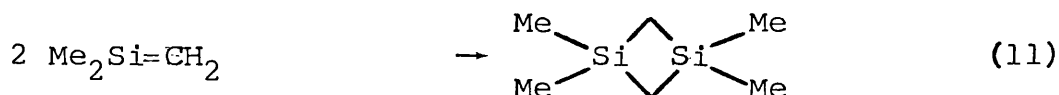
Rate Constants for the decomposition of DCSCB in presence
of HCl. (Corrected for leak out).

Temp /K	Rate Constant for the decomposition of DCSCB k/s^{-1}	lnk	Temp /K	Rate Constant for the decomposition of DCSCB k/s^{-1}	lnk
782	.0024	-6.032	823	.0187	-3.979
783	.0018	-6.320	823	.0193	-3.948
783	.0030	-5.809	826	.0193	-3.948
793	.0035	-5.655	826	.0206	-3.883
796	.0045	-5.404	827	.0200	-3.912
796	.0061	-5.100	832	.0270	-3.612
804	.0077	-4.867	833	.0257	-3.661
805	.0089	-4.722	834	.0270	-3.612
805	.0079	-4.841	834	.0281	-3.572
812	.0122	-4.406	843	.0468	-3.062
812	.0108	-4.528	843	.0402	-3.214
812	.0123	-4.398	843	.0446	-3.110
813	.0084	-4.780	843	.0418	-3.175
813	.0127	-4.366	852	.0594	-2.824
813	.0129	-4.351	853	.0608	-2.800
814	.0135	-4.305	853	.0592	-2.827
823	.0185	-3.990	853	.0587	-2.835
823	.0172	-4.063	854	.0650	-2.733

Fig. 4.20 Arrhenius plot for the decomposition of DCSCB (in the presence of HCl).



be present.

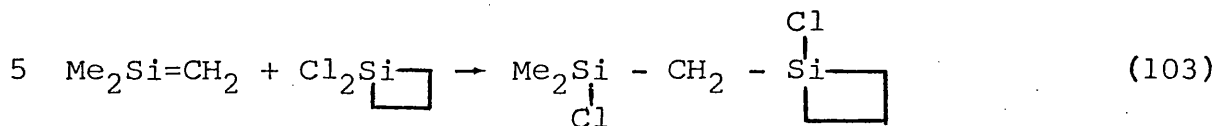
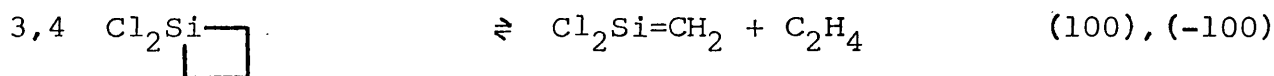
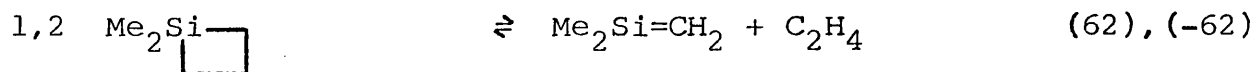


There were also some minor products which remained unidentified. Among these was a compound having mass spectrum peaks at m/e 92^+ and 94^+ , in the proportions for a species with one chlorine atom. The fragment ion which produced these peaks was probably $(\text{Cl}(\text{Me})\text{SiCH}_2)^+$, which initiated speculation about the parent compound. The mechanism shown in scheme 4.5 was proposed, involving the insertion of DMSE into a silicon-chlorine bond of DCSCB, as indicated by step 5. The insertion product would contain the unit $(\text{Cl}(\text{Me})\text{SiCH}_2-)$, so peaks at m/e 92^+ and 94^+ , similar to those observed above, would be expected in the mass spectrum of this compound.

If the insertion of DMSE into a silicon-chlorine

Scheme 4.5

Proposed mechanism for the co-pyrolysis of DCSCB and DMSCB.



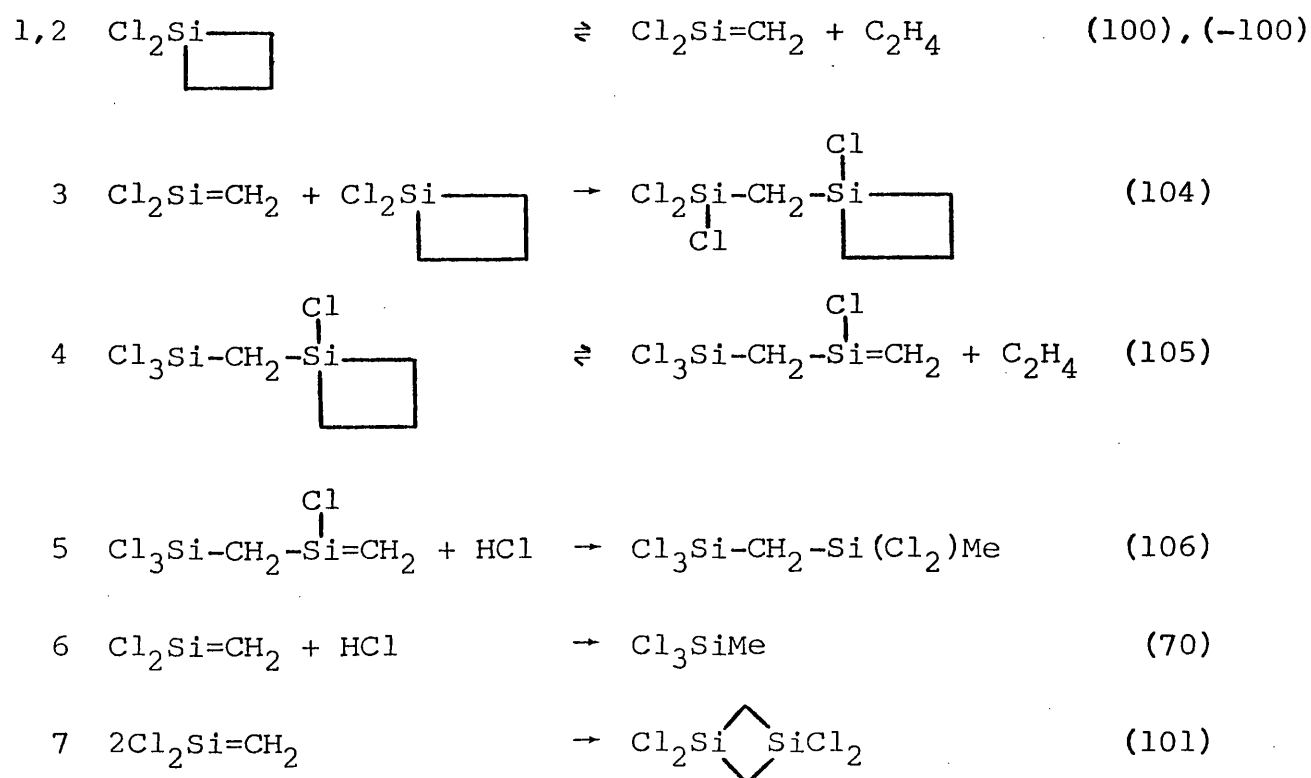
+ Self- and cross-dimerisation steps.

bond occurred, then DCSE would be expected to undergo a similar reaction. During the pyrolysis of DCSCB in the Q8 apparatus a group of peaks at m/e 245⁺ was observed with configuration for a species with five (or at least several) chlorine atoms. The mechanism proposed in scheme 4.6 could have accounted for this observation.

The product formed by step 5 would have the necessary fragment peaks at m/e 245⁺, arising from the loss of the methyl group. The hydrogen chloride was assumed to be present owing to a small amount of hydrolysis of the reactant. The same product would be formed by the insertion of DCSE into a silicon-chlorine bond of methyltrichlorosilane, the product of step 6. The co-pyrolysis of DCSCB and methyltrichlorosilane however did not produce a significant enhancement of the peaks at m/e 245⁺.

Scheme 4.6

Proposed mechanism for the pyrolysis of DCSCB.



CHAPTER FIVE

**PYROLYSIS OF
DIMETHYLCHLOROSILANE
AND OF
METHYLDICHLOROSILANE**

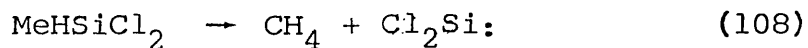
5.1 Introduction

As discussed in chapter 1, the pyrolysis of trimethylsilane has been shown to proceed via a radical chain mechanism and not by the formation of methane and dimethylsilylene¹³. A relatively high activation energy for the reverse of the latter process was offered² as an explanation as to why the radical route is favoured.

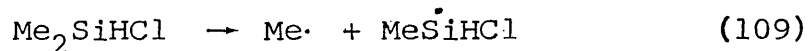
It was therefore of interest to investigate the thermal decomposition of dimethylchlorosilane (DMCS) and of methylchlorosilane (MDCS) to see if the chlorinated silylenes would be formed, by



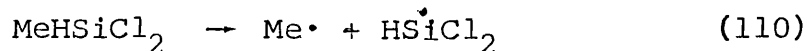
and



or whether the pyrolysis would follow a radical chain mechanism analogous to that proposed for trimethylsilane, with the breaking of a silicon-methyl bond as the initial step thus:-



and



For these chlorinated compounds, the elimination of hydrogen chloride was also a possibility.



and



The pyrolyses were carried out using version 4 of the apparatus. For both compounds it was very difficult to obtain conclusive, quantitative results, owing to adsorption and other effects at the walls of the reaction vessel. For example, hydrogen continued to diffuse from the walls, even after pumping out the reaction vessel at the end of an experimental run. Also, some abstraction reactions by radicals were thought to take place at the walls. The dichloro-compound was the more troublesome of the two.

An attempt was made to measure the Arrhenius parameters for product formation from both compounds, a new computer-aided analysis method being introduced.

5.2 Pyrolysis of DMCS

This compound was pyrolysed over the temperature range 994-1042K. The products observed were hydrogen, methane and dimethyldichlorosilane (the same products as for the pyrolysis of trimethylchlorosilane). Some hydrogen chloride was also present, but this could have been produced by hydrolysis of the reactant.

The mass peak of the dimethyldichlorosilane ($m/e=128^+$) was too small to follow accurately, so the larger peak at $m/e=113^+$, corresponding to the ion MeSiCl_2^+ was used. Some methyldichlorosilane (MDCS) may also have been formed, which would likewise have had a major peak at $m/e=113^+$. The ratio of the peaks at $m/e=113^+$ and 114^+ for the pyrolysis mixture however was about the same as for a sample of dimethyldichlorosilane, as was the ratio of the peaks at $m/e=113^+$ and 128^+ , which suggested that the dimethyl-compound was the major chlorinated product.

Three series of experiments were carried out in which the decomposition of the DMCS was followed. The plots of $\ln(\text{peak height})$ vs time were straight to around 20-30% reaction, so these were used to determine the rate constants rather than the computer comparison routine described in chapter 2.

At the temperatures used to measure the leak out rate constant (about 500K) the DMCS was lost from the gas phase by adsorption to the walls of the reaction vessel as well as by the leak out process. This made determination of the leak out rate constant difficult, apparent values in the range $0.001-0.015 \text{ s}^{-1}$ being obtained, depending on the amount of adsorption. By repeating the measurement several times and discarding the first two or three values, a rate constant of about 0.003 s^{-1} was obtained and this was taken to be due to the leak out process.

Table 5.1 shows a summary of the pyrolysis rate constants obtained (corrected for leak out) from all the experiments and fig. 5.1 shows the resulting Arrhenius plot. The rate constants for the individual series of experiments ranged from $\log_{10}k=11.28-245 \text{ KJ mol}^{-1}/2.3 \text{ RT}$ to $\log_{10}k=13.13-285 \text{ KJ mol}^{-1}/2.3 \text{ RT}$. The Arrhenius plots were generally good straight lines up to a rate constant of about 0.2 s^{-1} . Above this value they curved away from a straight line, the rate constants being under-estimated.

The overall Arrhenius parameters, obtained from a least squares fit of all the points in fig. 5.1 up to a rate constant of 0.2 s^{-1} were given by $\log_{10}k=(11.35 \pm .21) - (246.9 \pm 4.1 \text{ KJ mol}^{-1})/2.303 \text{ RT}$.

At the pyrolysis pressures used, the DMCS may have

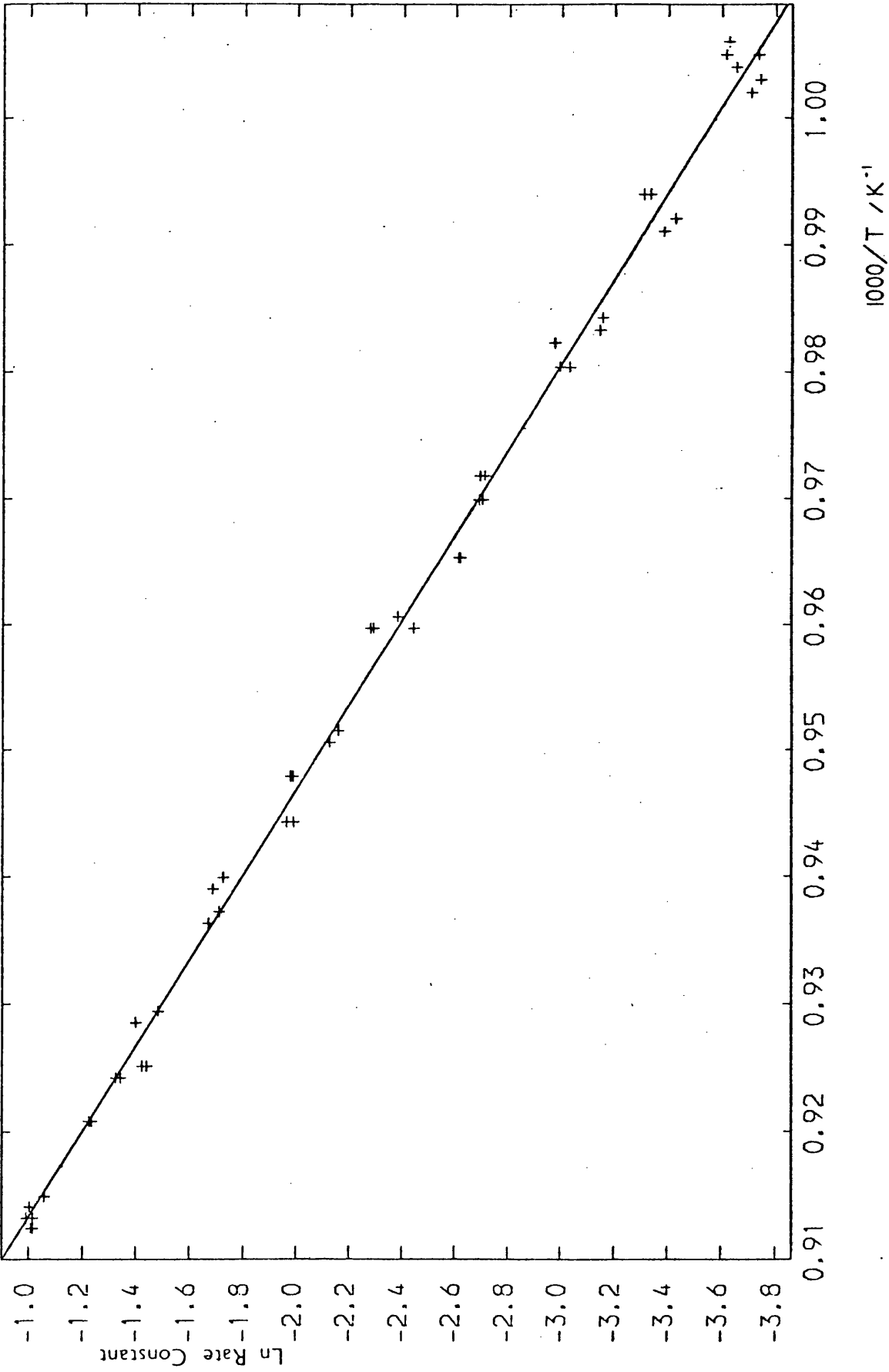
Table 5.1

Rate constants for the pyrolysis of DMCS.

k is corrected for leak out ($k_L = .003 \text{ s}^{-1}$).

Temp /K	Rate Constant k/s^{-1}	lnk	Temp /K	Rate Constant k/s^{-1}	lnk
994	.0266	-3.627	1042	.1024	-2.279
995	.0269	-3.616	1051	.1158	-2.156
995	.0239	-3.734	1052	.1195	-2.124
996	.0259	-3.654	1055	.1372	-1.986
997	.0237	-3.742	1055	.1384	-1.978
998	.0245	-3.709	1059	.1406	-1.962
1006	.0366	-3.308	1059	.1368	-1.989
1006	.0357	-3.333	1064	.1785	-1.723
1008	.0325	-3.427	1065	.1855	-1.685
1009	.0339	-3.384	1067	.1812	-1.708
1016	.0427	-3.154	1068	.1887	-1.668
1017	.0431	-3.144	1076	.2271	-1.482
1018	.0510	-2.976	1077	.2468	-1.399
1018	.0512	-2.972	1081	.2410	-1.423
1020	.0483	-3.030	1081	.2372	-1.439
1020	.0501	-2.994	1082	.2615	-1.341
1029	.0678	-2.691	1082	.2660	-1.324
1029	.0666	-2.709	1086	.2913	-1.233
1031	.0681	-2.687	1086	.2941	-1.224
1031	.0672	-2.700	1093	.3472	-1.058
1036	.0735	-2.611	1094	.3668	-1.003
1036	.0730	-2.617	1095	.3711	-0.991
1041	.0925	-2.381	1095	.3619	-1.016
1042	.0869	-2.443	1096	.3622	-1.016
1042	.1013	-2.290	1096	.3645	-1.009

Fig. 5.1 Arrhenius plot for the decomposition of DMCS.



been slightly into the unimolecular fall off region, but as all the experiments were carried out at approximately the same initial pressure, then plotting all the data onto one graph should not present any problem. In any case, the activation energy should not be affected by a small degree of fall off and any difference in initial pressure between individual series of experiments would simply produce a displacement in position on the Arrhenius plot. If the temperature ranges of the different series of experiments overlap, as the above did, then a least squares fit of the combined Arrhenius data would still yield the correct activation energy, leaving only the A-factor in doubt.

5.3 Formation of Products from DMCS.

After correcting the relevant experimental data for the sensitivity difference between methane and DMCS, rate constants for the formation of methane were calculated from $k = (\text{initial rate of formation methane}) / (\text{initial amount DMCS})$ where the initial amount of reactant was determined by extrapolation of the $\ln(\text{peak height})$ vs time plots back to zero time.

The combined results from two series of experiments are shown in table 5.2 and the Arrhenius plot in fig. 5.2.

The curvature of the plot suggested that the rate of formation of methane was being under-estimated, particularly towards the higher temperatures. This problem had been observed before with the slower, four-channel data logging devices, but for these more recent experiments the methane peak height was recorded every 0.5s.

Some of the rate constants calculated (in table 5.2) for methane formation were slightly larger than the reactant

Table 5.2

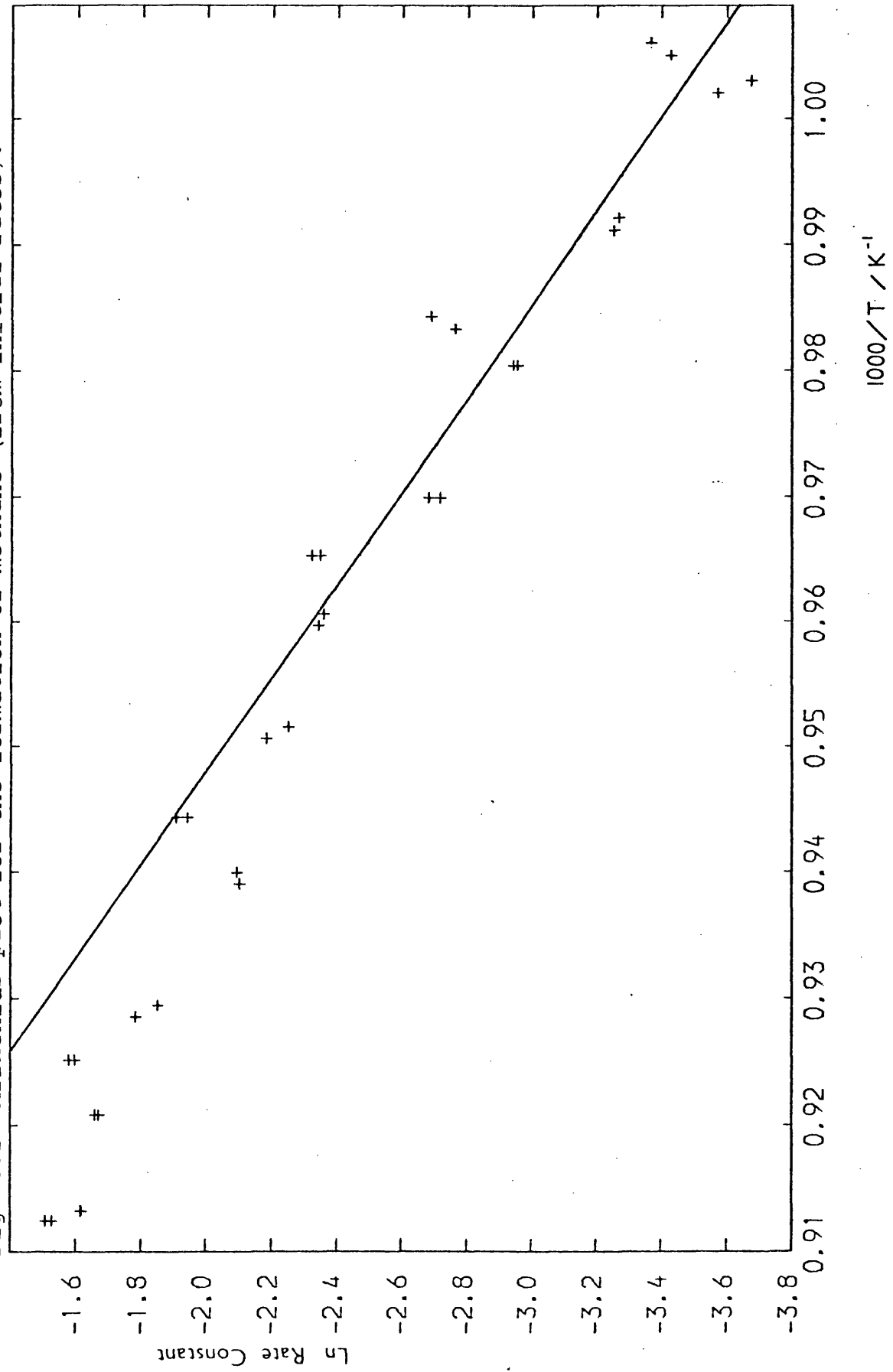
Comparison of the initial rate of formation of methane with
the initial amount of DMCS.

Temp /K	Rate Constant Loss DMCS/s ⁻¹	Initial DMCS (A ₀)	Initial Rate CH ₄ (R)	R/A ₀ (F)	ln(F)
994	.0266	6404	221.4	.0346	-3.365
995	.0269	6416	208.5	.0325	-3.427
997	.0237	5739	145.7	.0254	-3.674
998	.0245	5772	162.3	.0281	-3.571
1008	.0325	5683	216.4	.0381	-3.268
1009	.0339	5762	222.7	.0387	-3.253
1016	.0427	6144	418.8	.0682	-2.686
1017	.0431	5876	371.9	.0633	-2.760
1020	.0483	5792	302.1	.0522	-2.954
1020	.0501	5897	311.5	.0528	-2.941
1031	.0681	5468	362.5	.0663	-2.714
1031	.0672	5584	383.3	.0686	-2.679
1036	.0735	6664	654.2	.0982	-2.321
1036	.0730	6488	620.8	.0957	-2.347
1041	.0925	4095	387.5	.0946	-2.358
1042	.0869	4227	406.3	.0961	-2.342
1051	.1158	4128	435.4	.1055	-2.249
1052	.1195	4742	534.8	.1128	-2.182
1059	.1406	6412	919.6	.1434	-1.942
1059	.1368	6040	895.8	.1483	-1.908
1064	.1785	4914	606.3	.1234	-2.093
1065	.1855	4587	561.2	.1224	-2.101
1076	.2271	4976	781.3	.1570	-1.851

Table 5.2 continued

Temp /K	Rate Constant Loss DMCS/s ⁻¹	Initial DMCS (A ₀)	Initial Rate CH ₄ (R)	R/A ₀ (F)	ln(F)
1077	.2468	4854	816.7	.1683	-1.782
1081	.2410	5808	1178.1	.2028	-1.595
1081	.2372	5472	1129.2	.2064	-1.578
1086	.2913	4993	950.0	.1903	-1.659
1086	.2941	4825	908.0	.1882	-1.670
1095	.3731	5214	1035.4	.1986	-1.617
1095	.3619	4828	960.4	.1989	-1.615
1096	.3622	6236	1383.7	.2219	-1.506
1096	.3645	5960	1295.9	.2174	-1.526

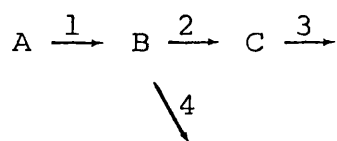
Fig. 5.2 Arrhenius plot for the formation of methane (from initial rates).



decomposition rate constants at the same temperature. A small error in the sensitivity correction factor between methane and DMCS could have accounted for this.

A least squares fit of the points in fig. 5.2 up to 1042K gave $\log_{10}k = (10.27 \pm 1.00) - (224.8 \pm 19.6 \text{ KJ mol}^{-1}) / 2.303 \text{ RT}$. An error in the sensitivity correction would lead to an error in the A-factor, but not in the activation energy. The estimation of A_0 and the measurement of the initial rate of methane production were the two major difficulties with the above method.

As discussed in chapter 2, if the leak in and leak out processes were assumed to be first order, then the experimental system could be represented by a reaction scheme such as



where k_1 and k_2 were the leak in and pyrolysis rate constants respectively, k_3 was the sum of the leak out and reaction rate constants for the loss of C and k_4 was the rate constant for the loss of B by leak out and by reaction to products other than C. The concentrations of species B and C for such a scheme can be calculated⁵³, the full equations being,

$$B = A_0 k_1 \left[\left[e^{-k_1 t} / (K - k_1) \right] + \left[e^{-Kt} / (k_1 - K) \right] \right] \quad (\text{xviii})$$

$$C = A_0 k_1 k_2 \left[\left[e^{-k_1 t} / (K - k_1) (k_3 - k_1) \right] + \left[e^{-Kt} / (k_1 - K) (k_3 - K) \right] + \left[e^{-k_3 t} / (k_1 - k_3) (K - k_3) \right] \right] \quad (\text{xiv})$$

where $K = (k_2 + k_4)$.

If the ratio C / B is taken, the common factor $A_0 \cdot k_1$ cancels, removing the two "unknown" parameters from the calculation.

An interactive computer program was written which enabled a plot of $[\text{CH}_4]/[\text{DMCS}]$ vs time to be displayed. (The ratio was corrected for the sensitivity difference between the two species). A similar curve was then calculated, using eqns. (xviii) and (xiv) above, which was superimposed onto the experimental plot. With k_3 set at 0.002 s^{-1} , the measured leak out rate constant of methane, the values of k_2 and k_4 were varied by trial and error to find the best fit (by eye) of the calculated curve to the experimental data. The only limitation was that the sum of k_2 and k_4 should equal the experimentally observed rate constant for the loss of DMCS.

At each temperature, a very good fit to the experimental data was obtained with k_4 set at 0.003 s^{-1} , the leak out rate constant for DMCS, and k_2 set as shown in table 5.3. The calculated rate constants for the formation of methane were essentially the same as those for the observed decomposition of DMCS. Fig. 5.3 shows the Arrhenius plot for methane formation derived from the calculated rate constants in table 5.3. A least squares fit over all the points gave

$$\log_{10} k_{\text{CH}_4} = (11.38 \pm 0.13) - (247.4 \pm 2.6 \text{ KJ mol}^{-1}) / 2.303 \text{ RT.}$$

Within experimental error, the Arrhenius parameters for the decomposition of DMCS were the same as for the formation of methane.

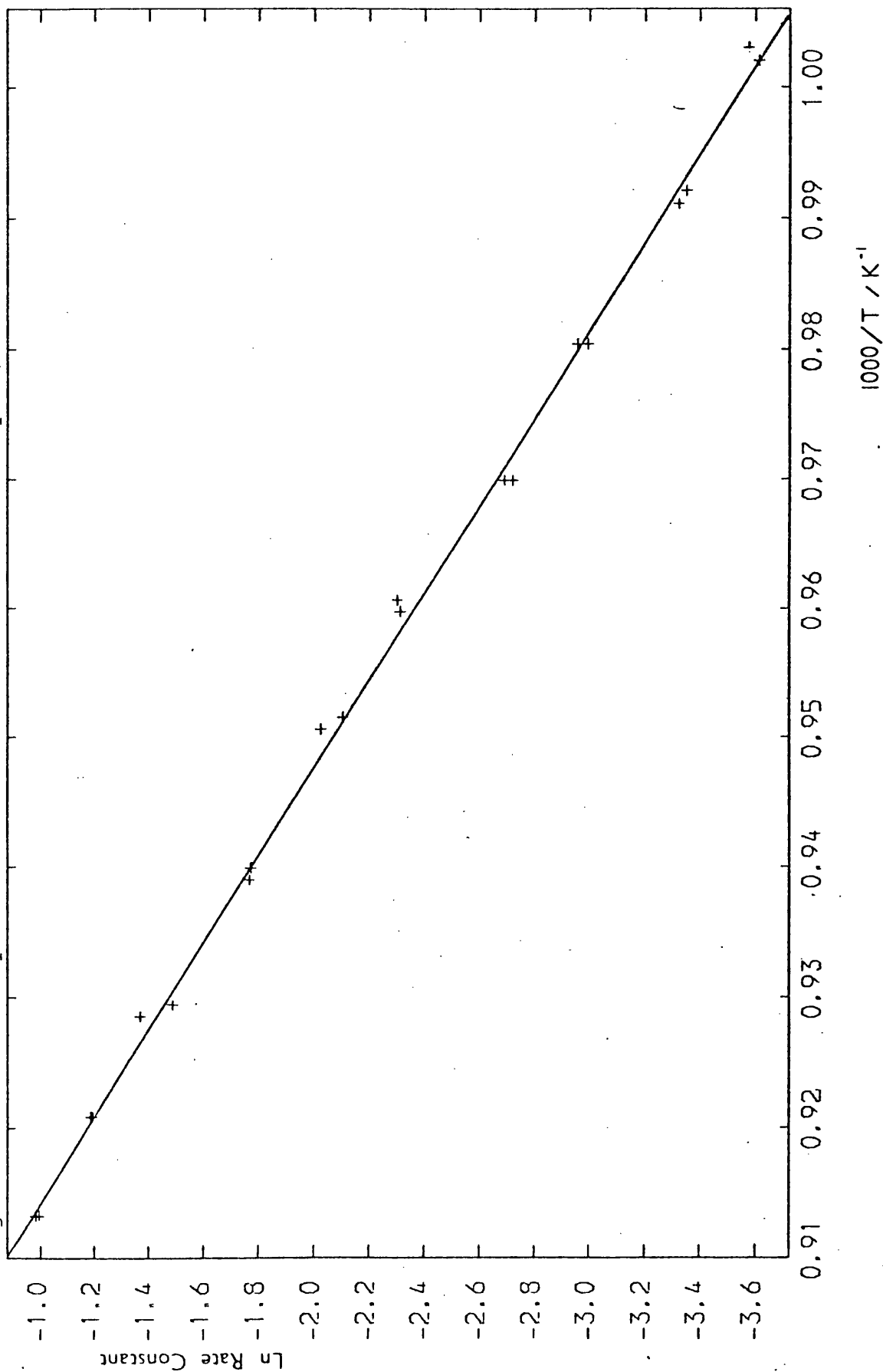
The above "C/B" method was also applied to the formation of dimethyldichlorosilane. For the calculation, k_3 , the rate constant for the loss of "C", was set by $\log_{10} k_3 = 17.0 - 370 \text{ KJ mol}^{-1} / 2.3 \text{ RT}$, the approximate Arrhenius parameters for the decomposition of this product.

Table 5.3

Formation of methane by "C/B" method.

Temp /K	Experimental Total Rate Constant for loss DMCS/s ⁻¹	Calculated Rate Constant for formation of methane, k ₂ /s ⁻¹	lnk ₂	Calculated Total Rate Constant for loss DMCS (k ₂ + k ₄)/s ⁻¹
997	.0267	.028	-3.576	.031
998	.0275	.027	-3.612	.030
1008	.0355	.035	-3.352	.038
1009	.0369	.036	-3.324	.039
1020	.0513	.050	-2.996	.053
1020	.0531	.052	-2.957	.055
1031	.0711	.066	-2.718	.069
1031	.0702	.068	-2.688	.071
1041	.0955	.100	-2.303	.103
1042	.0899	.099	-2.313	.102
1051	.1188	.122	-2.104	.125
1052	.1225	.132	-2.025	.135
1064	.1815	.170	-1.772	.173
1065	.1885	.171	-1.766	.174
1076	.2301	.226	-1.487	.229
1077	.2498	.254	-1.370	.257
1086	.2943	.303	-1.194	.306
1086	.2971	.305	-1.187	.308
1095	.3741	.375	-0.981	.378
1095	.3649	.370	-0.994	.373

Fig. 5.3 Arrhenius plot for the formation of methane (by "C/B" method).



The values of k_2 and k_4 which were necessary to obtain the best fit to the experimental data are shown in table 5.4 and the Arrhenius plot in fig. 5.4. From a least squares fit of the points in the temperature range 1008-1095K, the rate constants for the formation of dimethyldichlorosilane were given by $\log_{10}k = (11.19 \pm 0.19) - (247.1 \pm 3.8 \text{ KJ mol}^{-1}) / 2.303 \text{ RT}$.

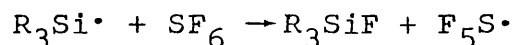
An attempt was made to apply the "C/B" method to hydrogen production. The results are shown in table 5.5 and the Arrhenius plot, from which $\log_{10}k = (13.41 \pm 0.16) - (286.8 \pm 3.1 \text{ KJ mol}^{-1}) / 2.303 \text{ RT}$, in fig. 5.5.

It was more difficult to "tune in" the PP2 to hydrogen than it was to tune it to higher mass species. Also, even after pumping out the reaction vessel at the end of an experimental run, hydrogen was seen to be desorbing in significant quantities from the walls. The above result for the formation of this product is therefore not reliable.

No reliable quantitative measurements concerning the production of hydrogen chloride could be made owing to its adsorption within the apparatus.

5.4 Co-pyrolysis of DMCS and Sulphur Hexafluoride.

For the reaction,



$$\Delta H = D(\text{F}_5\text{S}-\text{F}) - D(\text{R}_3\text{Si}-\text{F})$$

Using the bond dissociation energies $D(\text{F}_5\text{S}-\text{F}) = 381 \text{ KJ mol}^{-1}$ ⁶⁰ and $D(\text{F}_4\text{Si}-\text{F}) = 669 \text{ KJ mol}^{-1}$ ¹⁷, then

$$\Delta H = 381 - 669 = -288 \text{ KJ mol}^{-1}.$$

Table 5.4

Formation of Me₂SiCl₂ by "C/B" method.

Temp /K	Experimental Total Rate Constant for the loss of DMCS/s ⁻¹	Calculated Rate Constant for the formation of Me ₂ SiCl ₂ k ₂ /s ⁻¹	lnk ₂	Value of k ₄ used for calculation /s ⁻¹	k ₂ + k ₄ /s ⁻¹
997	.0267	.020	-3.912	.007	.027
998	.0275	.020	-3.912	.008	.028
1008	.0355	.025	-3.689	.010	.035
1009	.0369	.026	-3.650	.011	.037
1020	.0513	.135	-3.352	.018	.053
1020	.0531	.034	-3.381	.019	.053
1031	.0711	.043	-3.147	.029	.072
1031	.0702	.044	-3.124	.029	.073
1041	.0955	.069	-2.674	.024	.093
1042	.0899	.067	-2.703	.024	.091
1051	.1188	.185	-2.465	.040	.125
1052	.1225	.086	-2.453	.040	.126
1064	.1815	.110	-2.207	.080	.190
1065	.1885	.112	-2.189	.080	.192
1076	.2301	.153	-1.877	.100	.253
1077	.2498	.168	-1.784	.100	.268
1086	.2943	.205	-1.585	.150	.355
1086	.2971	.208	-1.570	.150	.358
1095	.3741	.260	-1.347	.220	.480
1095	.3649	.250	-1.386	.240	.490

Fig. 5.4 Arrhenius plot for the formation of Me_2SiCl_2 (by "C/B" method).

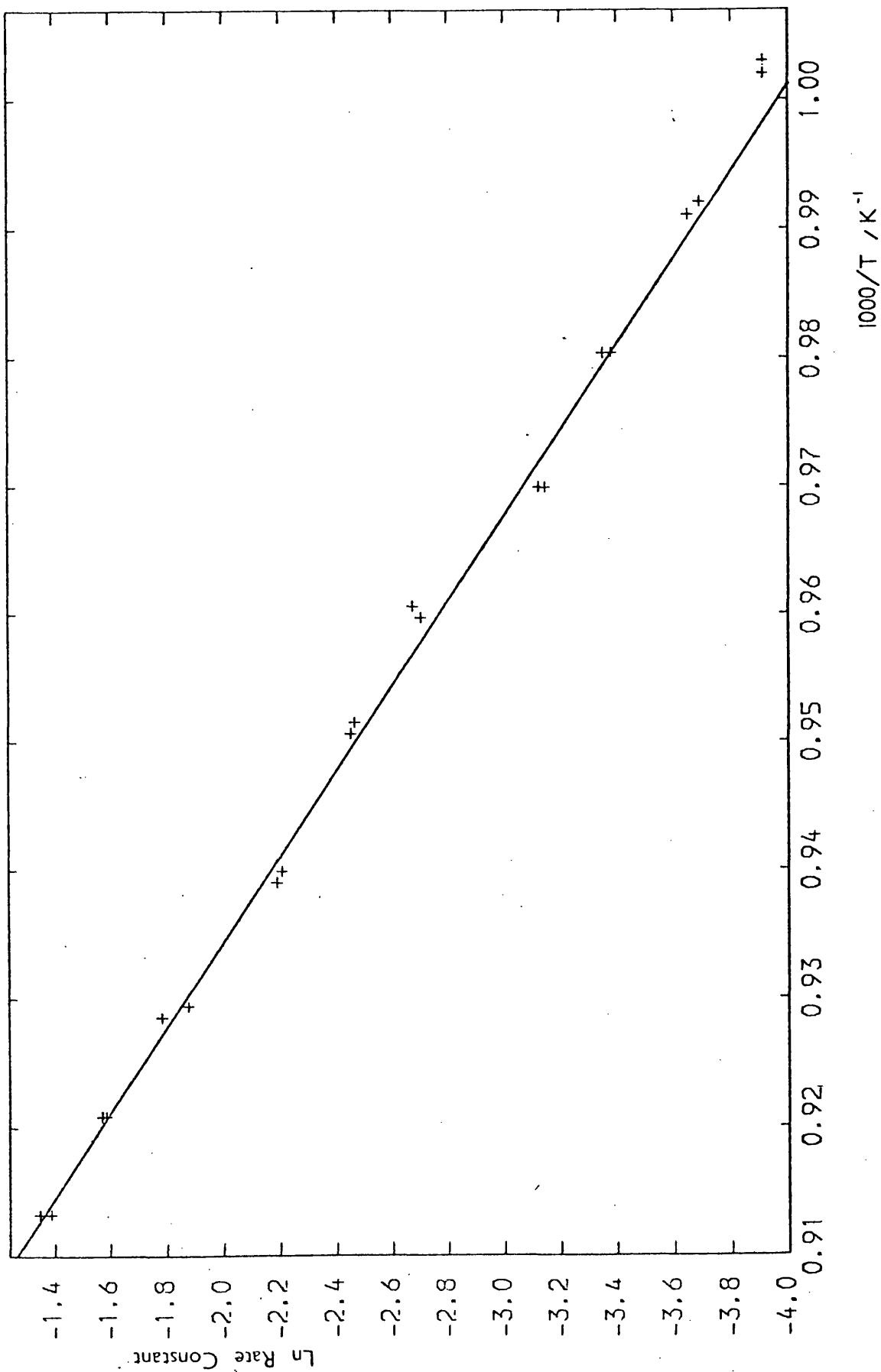


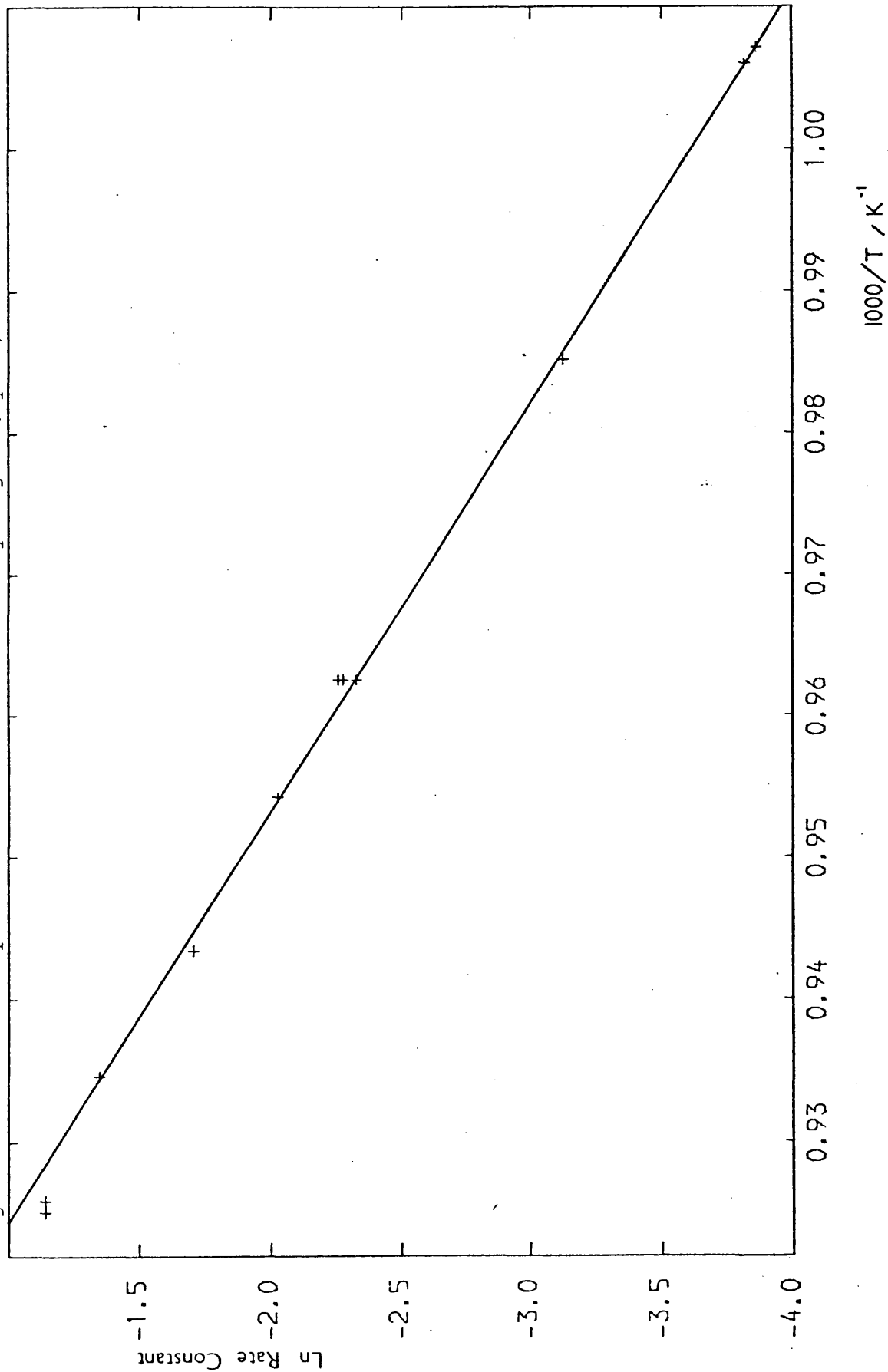
Table 5.5

Formation of hydrogen by the "C/B" method.

Temp. /K	Experimental Total Rate Constant for the loss of DMCS. /s ⁻¹	Calculated Rate Const. for the formation of H ₂ k ₂ / s ⁻¹	ln k ₂	Calculated Total Rate Constant for the loss of DMCS (k ₂ + k ₄) /s ⁻¹
993	.0170	.021	-3.863	.024
994	.0177	.022	-3.817	.025
1015	.0318	.044	-3.124	.047
1015	.0313	.044	-3.124	.047
1039	.0631	.103	-2.273	.106
1039	.0647	.105	-2.254	.108
1039	.0676	.098	-2.323	.101
1048	.0922	.132	-2.025	.135
1048	.0902	.132	-2.025	.135
1060	.1238	.182	-1.704	.185
1060	.1258	.182	-1.704	.185
1070	.1682	.260	-1.347	.263
1070	.1697	.260	-1.347	.263
1080	.2318	.320	-1.139	.323
1081	.2274	.320	-1.139	.323

The experimental rate constants for the loss of reactant as measured for this series, were generally smaller than for previous series. However, the Arrhenius parameters for methane production agreed with earlier measurements. The calculated decomposition rate constants for this series are in good agreement with those measured in previous experiments.

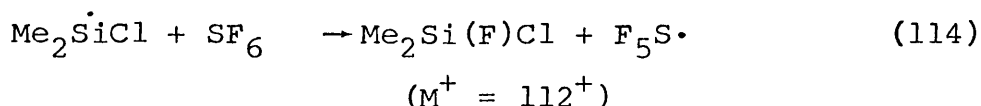
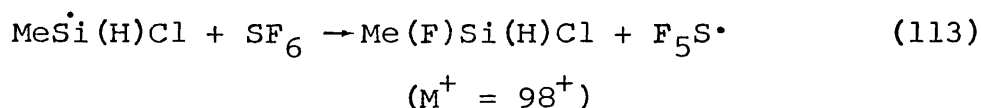
Fig. 5.5 Arrhenius plot for the formation of hydrogen (by "C/B" method).



Therefore, sulphur hexafluoride could be a good trap for silicon radicals.

DMCS was pyrolysed at about 1030K in the presence of excess sulphur hexafluoride. A new group of peaks, with the configuration for a species containing one chlorine atom, was formed at $m/e = 97^+$. A similar group may also have been formed at $m/e = 112^+$, though the peaks were small, making their ratios difficult to determine with any certainty.

The following reactions involving silicon-centred radicals were proposed.



The mass spectra of both these products would be expected to have strong peaks at $m/e = 97^+$.

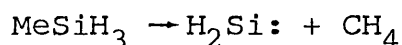
Assuming the A-factor for the unimolecular dissociation of sulphur hexafluoride to be about $10^{14.5} \text{ s}^{-1}$, then at 1030K, the decomposition rate constant would be $k = 1.5 \times 10^{-5} \text{ s}^{-1}$, which would make an exchange reaction involving fluorine atoms an unlikely explanation for the formation of the observed products.

5.5 Proposed Pyrolysis Mechanism

As discussed in section 5.1, there were three possible pyrolysis mechanisms to consider, a radical chain, initiated by the breaking of a silicon-methyl bond, the formation of a silylene and methane, or the formation of a silylene and hydrogen chloride. The results of the experiments with

sulphur hexafluoride suggested a radical mechanism, but the possibility for silylene elimination was considered as outlined below.

Davidson and Ring¹¹ have estimated rate constants given by $\log_{10}k = 13.6 - 290 \text{ KJ mol}^{-1}/2.303 \text{ RT s}^{-1}$ for the reaction



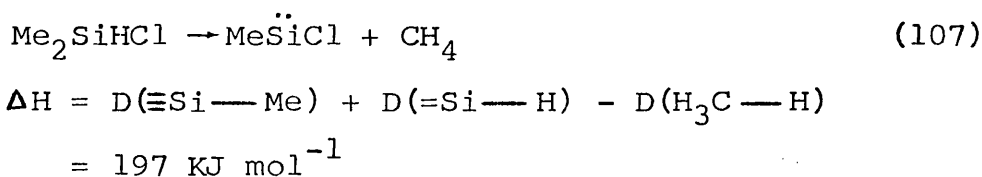
Using the bond dissociation energies $D(\equiv\text{Si}-\text{Me}) = 367 \text{ KJ mol}^{-1}$, $D(=\text{Si}-\text{H}) = 268 \text{ KJ mol}^{-1}$ ¹⁷ and $D(\text{H}_3\text{C}-\text{H}) = 438 \text{ KJ mol}^{-1}$ ¹⁸, then ΔH for the above reaction is given by

$$\begin{aligned} \Delta H &= D(\equiv\text{Si}-\text{Me}) + D(=\text{Si}-\text{H}) - D(\text{H}_3\text{C}-\text{H}) \\ &= 367 + 268 - 438 = 197 \text{ KJ mol}^{-1}. \end{aligned}$$

The activation energy of the reverse, silylene insertion reaction is thus

$$E_{\text{rev}} = 290 - 197 = 93 \text{ KJ mol}^{-1}.$$

Similarly, for the reaction



Assuming methylchlorosilylene to be less reactive than silylene itself, since the former could be stabilised by the overlap of the p-orbitals of the chlorine with the d-orbitals of the silicon, then the activation energy for the above decomposition of DMCS would be

$$E = 197 + \gg 93$$

therefore

$$E \gg 290 \text{ KJ mol}^{-1}$$

The rate constants for the pyrolysis of methylsilane¹¹ were estimated to be into the unimolecular fall off region such that $k = 0.14 k_{\infty}$, where k_{∞} was the high pressure limiting rate constant. Thus, the high pressure A-factor for the elimination of a silylene and methane from both methylsilane and DMCS would be

$$A = 10^{13.6}/0.14 = 10^{14.5} \text{ s}^{-1}.$$

The rate constants for the elimination reaction could thus be estimated and compared, in table 5.6, with the experimentally observed rate constants for the formation of methane.

If the Arrhenius parameters for the elimination are

Table 5.6

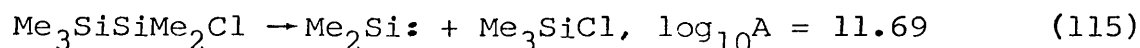
Comparison of observed rate constants for methane formation with those estimated for the elimination.

T/K	$k_{+\text{CH}_4}/\text{s}^{-1}$ Experiment	$k_{+\text{CH}_4}/\text{s}^{-1}$ Estimated	$k_{+\text{CH}_4}/\text{s}^{-1}$ 50% Fall off
1000	.029	.225	.112
1080	.260	2.975	1.488

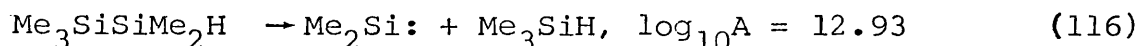
as estimated above ($\log_{10}k = 14.5 - 290 \text{ KJ mol}^{-1}/2.3 \text{ RT}$) then the rate constants for this process would be about ten times bigger than the observed rate constants. (Even allowing for 50% unimolecular fall off did not bring the estimated values in line with those measured.) However, the 290 KJ mol^{-1} measured by Davidson and Ring¹¹ may not be correct. As pointed out in chapter 1, the result was

quoted with error limits of $\pm 30 \text{ KJ mol}^{-1}$, the uncertainty being an indication of the difficulties encountered in measuring the Arrhenius parameters of a minor process. The activation energy for the elimination of methane from methylsilane could thus be as high as 320 KJ mol^{-1} . Owing to the greater stability of chlorinated silylenes, the activation energy for the elimination of methane from DMCS could therefore be in excess of this. A value of 330 KJ mol^{-1} , together with the A-factor calculated above would make the elimination a minor process compared to the observed rate constants, those for the silylene formation being $k = .0018 \text{ s}^{-1}$ at 1000K and $k = .0346 \text{ s}^{-1}$ at 1080K .

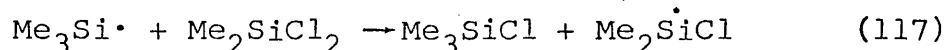
Apart from the uncertainty in the activation energy, there is evidence that A-factors for silylene elimination from chlorosilanes are smaller than for similar reactions involving non-chlorinated silanes⁴. For example,



but for

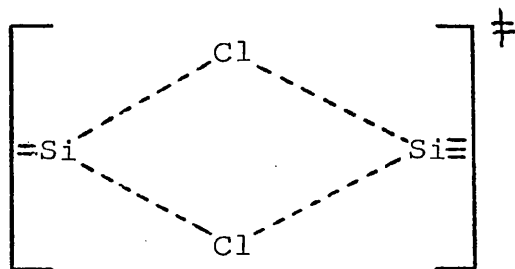


A-factors for reactions involving the abstraction of chlorine atoms from alkyl chlorides have been determined to be in the range $\log_{10}A = 7.3 - 7.7$, whereas that for the reaction



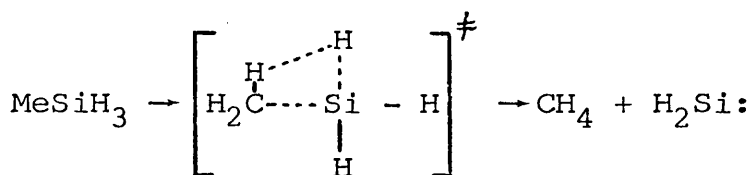
has been estimated⁵⁷ as $\log_{10}A = 6.2$.

The low values of A for the elimination (115) above and for the abstraction (117) were attributed to a tight transition state of the type

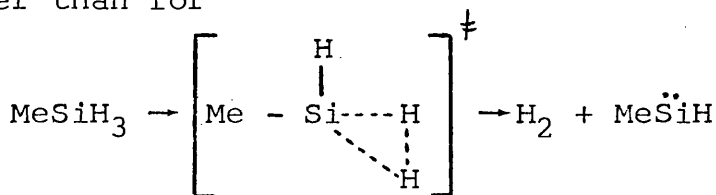


The loss in entropy to form such a species would be greater than for the case if the chlorines were replaced by methyl or hydrogen since the stronger attraction between silicon and chlorine than between silicon and carbon or hydrogen would lead to a tighter transition state.

The same type of argument was used¹¹ to explain why the elimination of methane from methylsilane had a lower A-factor than for the elimination of hydrogen, the loss in entropy on forming the transition state for



being greater than for



owing to the loss of internal rotation by the methyl group.

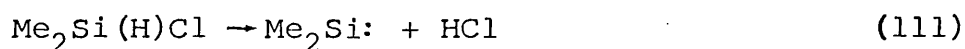
Although the silicon-chlorine bond is not directly involved in the elimination of methane from DMCS, it is possible that the presence of the halide has sufficient influence on the entropy of the transition state to cause a lowering of the A-factor relative to that for the analogous elimination from methylsilane.

For an activation energy of 290 kJ mol^{-1} , the A-factor would have to be reduced to about 10^{13} s^{-1} to make silylene

formation a minor process.

Thus, the elimination of methane from DMCS could not be completely ruled out, but there was however strong evidence in favour of a radical decomposition. Apart from the co-pyrolyses with sulphur hexafluoride, from which the species $\text{Me}(\text{H})\dot{\text{Si}}\text{Cl}$ and $\text{Me}_2\dot{\text{Si}}\text{Cl}$ were shown to be present, an elimination reaction could not easily explain the formation of hydrogen or of dimethyldichlorosilane. The experimentally determined activation energy of about 247 kJ mol^{-1} for the formation of methane, less than all the estimates above for silylene elimination, also pointed towards a radical mechanism.

The other possible elimination reaction was also considered.



$$\Delta H = D(\text{Si}-\text{Cl}) + D(=\text{Si}-\text{H}) - D(\text{H}-\text{Cl})$$

Using the bond dissociation energies $D(\equiv\text{Si}-\text{Cl}) = 472 \text{ kJ mol}^{-1}$ ¹⁷, $D(\text{H}-\text{Cl}) = 435 \text{ kJ mol}^{-1}$ ¹⁸, and $D(=\text{Si}-\text{H})$ as above, then

$$\Delta H = 472 + 268 - 435 = 305 \text{ kJ mol}^{-1}$$

The activation energy for the insertion of a silylene into hydrogen chloride has been estimated as 28 kJ mol^{-1} ⁶¹. Thus, for the elimination of hydrogen chloride from DMCS, the activation energy would be

$$E = 305 + 28 = 333 \text{ kJ mol}^{-1}.$$

Assuming the same A-factor as for the elimination of hydrogen from methylsilane, which was determined by

Davidson and Ring¹¹ to be $10^{14.1} \text{ s}^{-1}$ (or $10^{14.95} \text{ s}^{-1}$ when corrected for fall off), then rate constants for the elimination of hydrogen chloride from DMCS could be estimated and compared with the experimental values for the loss of the reactant, This is done in table 5.7, from which it is clear that the elimination would be a minor process, especially if the pyrolysis was into the unimolecular fall off region, in which case the estimated rate constants would be even smaller. As for the elimination of methane the A-factor for HCl formation could be reduced from the above owing to the presence of the chlorine atom, which in this case is directly involved in the formation of the transition state.

Table 5.7

Comparison of estimated rate constants for the elimination of HCl with those for the loss of the reactant.

T/K	$k_{\text{exp}}/\text{s}^{-1}$	$k_{+\text{HCl}}$ Estimated
1000	.0284	.0036
1080	.2560	.0698

To see if a radical decomposition could explain the observed results, in view of the uncertainties regarding the activation energy and A-factor for the elimination of methane, the radical mechanism for the pyrolysis of DMCS shown in scheme 5.1, which is analogous to those proposed for the decomposition of trimethylsilane¹³ and of trimethylchlorosilane (chapter 3), was computer-simulated, the programme using Gear's method of numerical integration.

The Arrhenius parameters used for the initial step,

Scheme 5.1 Proposed pyrolysis mechanism of DMCS.

			$\log_{10} A$	$E/\text{KJ mol}^{-1}$	
1	Me_2SiHCl	$\rightarrow \text{Me}\cdot + \text{MeSiHCl}$	17.00	367	(109)
2	$\text{MeSiHCl} + \text{HCl}$	$\rightarrow \text{MeSiHCl}_2 + \text{H}\cdot$	7.00	15	(118)
3	$\text{Me}\cdot + \text{Me}_2\text{SiHCl}$	$\rightarrow \text{CH}_4 + \text{Me}_2\text{SiCl}$	8.11	30	(119)
4	$\text{H}\cdot + \text{Me}_2\text{SiHCl}$	$\rightarrow \text{H}_2 + \text{Me}_2\text{SiCl}$	10.00	8	(120)
5	$\text{Me}_2\text{SiCl} + \text{HCl}$	$\rightarrow \text{Me}_2\text{SiCl}_2 + \text{H}\cdot$	7.00	15	(71)
6	$\text{Me}\cdot + \text{Me}_2\text{SiHCl}$	$\rightarrow \text{CH}_4 + \dot{\text{C}}\text{H}_2\text{SiMeHCl}$	8.40	42	(121)
7	$\text{H}\cdot + \text{Me}_2\text{SiHCl}$	$\rightarrow \text{H}_2 + \dot{\text{C}}\text{H}_2\text{SiMeHCl}$	10.00	8	(122)
8	$\dot{\text{C}}\text{H}_2\text{SiMeHCl}$	$\rightarrow \text{H}_2\text{C}=\text{SiHCl} + \text{Me}\cdot$	15.00	190	(123)
9	$\text{H}_2\text{C}=\text{SiHCl} + \text{HCl}$	$\rightarrow \text{MeSiHCl}_2$	7.51	10	(124)
10	MeSiHCl	$\rightarrow \text{WALLS}$	$k = 100 \text{ s}^{-1}$		(125)
11	Me_2SiCl	$\rightarrow \text{WALLS}$	$k = 100 \text{ s}^{-1}$		(93)
12	$\dot{\text{C}}\text{H}_2\text{SiMeHCl}$	$\rightarrow \text{WALLS}$	$k = 100 \text{ s}^{-1}$		(126)
13	$2 \text{ Me}\cdot + \text{M}$	$\rightarrow \text{C}_2\text{H}_6 + \text{M}$	10.51	0	(14)
14	$2 \text{ H}\cdot + \text{M}$	$\rightarrow \text{H}_2 + \text{M}$	10.51	0	(127)
15	$2 \text{ MeSiHCl} + \text{M}$	$\rightarrow (\text{MeSiHCl})_2 + \text{M}$	10.51	0	(128)
16	$2 \text{ Me}_2\text{SiCl} + \text{M}$	$\rightarrow (\text{Me}_2\text{SiCl})_2 + \text{M}$	10.51	0	(87)
17	$2 \dot{\text{C}}\text{H}_2\text{SiMeHCl} + \text{M}$	$\rightarrow (\dot{\text{C}}\text{H}_2\text{SiMeHCl})_2 + \text{M}$	9.00	0	(129)
18	Me_2SiHCl	$\rightarrow \text{CH}_4$	$k = .017 \text{ s}^{-1}$		(130)
19	Me_2SiCl	$\rightarrow \text{Me}\cdot + \text{MeSiCl}$	14.51	255	(96)
20	$\text{Me}_2\text{SiCl} + \text{Me}_2\text{SiHCl}$	$\rightarrow \text{Me}_2\text{SiCl}_2 + \text{Me}_2\text{SiH}$	6.20	15	(131)
21	$\text{MeSiHCl} + \text{Me}_2\text{SiHCl}$	$\rightarrow \text{MeSiHCl}_2 + \text{Me}_2\text{SiH}$	6.20	15	(132)
22	$\text{Me}_2\text{SiCl} + \text{Me}_2\text{SiHCl}$	$\rightarrow \text{Me}_2\text{SiHCl} + \dot{\text{C}}\text{H}_2\text{SiMeHCl}$	10.40	75	(133)
23	$\text{MeSiHCl} + \text{Me}_2\text{SiHCl}$	$\rightarrow \text{H}_2\text{SiMeCl} + \text{Me}_2\text{SiCl}$	10.00	45	(134)
24	$\text{MeSiHCl} + \text{Me}_2\text{SiHCl}$	$\rightarrow \text{H}_2\text{SiMeCl} + \dot{\text{C}}\text{H}_2\text{SiMeHCl}$	10.40	75	(135)
25	$\text{Me}\cdot + \text{WALLS}$	$\rightarrow \text{CH}_4$	$k = 200 \text{ s}^{-1}$		(136)
26	MeSiHCl	$\rightarrow \text{Me}\cdot + \text{HSiCl}$	14.51	255	(137)

Activation energies and A-factors based on data in chapters 3 and 4, and in refs. 13 and 57

involving the breaking of a silicon-methyl bond, were consistent with the values determined earlier for the equivalent step in the pyrolysis of trimethylchlorosilane. Also consistent with that mechanism, an initial amount of hydrogen chloride, proposed to have come from the hydrolysis of the reactant, was included in the DMCS simulation. An initial ratio of DMCS : HCl 3 : 1 was used.

In order to match the experimentally observed results, the simulated mechanism required two temperature-independent reaction steps (18 and 25), proposed to take place at the walls of the reaction vessel. The range of decomposition Arrhenius parameters measured over several series of experiments did however suggest that there was a significant (and variable) surface involvement. The steps in the simulation which involved simply the loss of chlorinated radicals to the walls of the reaction vessel were given the same rate constant as the equivalent steps in the trimethylchlorosilane scheme.

With the parameters set as shown in scheme 5.1, the simulation broadly matched the experiment as far as the decomposition of reactant and formation of methane were concerned. But as table 5.8 indicates, the simulated production of dimethyldichlorosilane and of hydrogen fell well below the observed levels.

The simulation only allowed for the gas-phase production of hydrogen, whereas experimentally there was evidence for a strong surface involvement in its production, possibly from the decomposition of polymer, which could account for the failings of the calculated mechanism.

The simulation's under-production of dimethyldichlorosilane was harder to explain, but if it was assumed that some of the chlorinated radical species underwent a surface reaction to produce this product, then sufficient quantities could be formed to account for the experimental observations.

An Arrhenius plot for the decomposition of reactant, based on the simulated data in table 5.8 is shown in fig. 5.6. The plot is rather curved but then, a range of Arrhenius parameters were measured experimentally. The line drawn gives $\log_{10}k = 11.08 - 242.2 \text{ KJ mol}^{-1}/2.3 \text{ RT}$.

Table 5.8

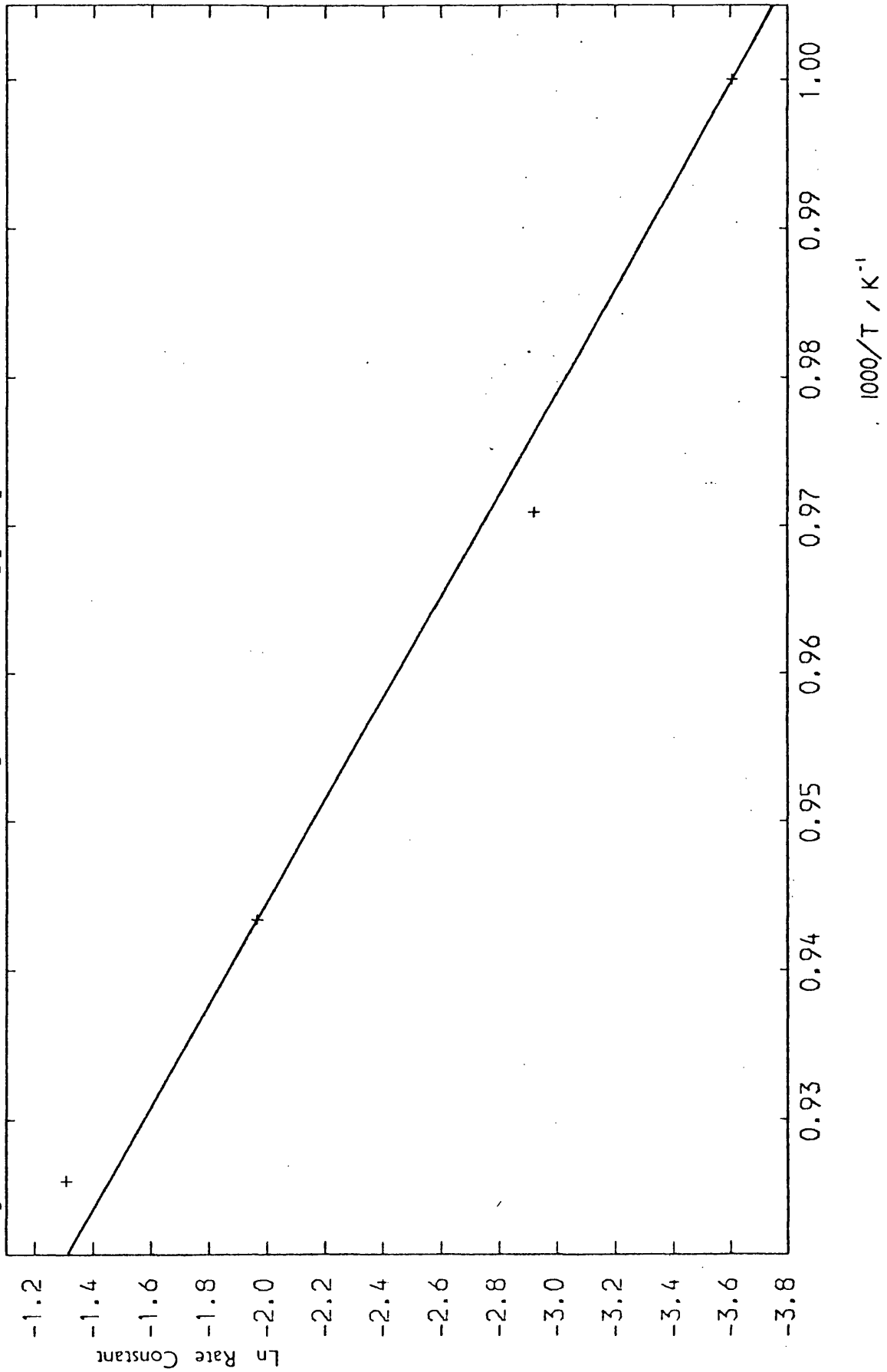
Comparisons between simulation and experiment.

Temp /K	Experimental Rate Constant for decomposition DMCS / s ⁻¹	Simulated Rate Constant for decomposition of reactant /s ⁻¹	$\frac{V_{\text{CH}_4-}}{V_{\text{DMCS}}}$ Expt. (Sim)	$\frac{V_{\text{Me}_2\text{SiCl}_2}}{V_{\text{DMCS}}}$ Expt. (Sim)	$\frac{V_{\text{H}_2-}}{V_{\text{DMCS}}}$ Expt. (Sim)
1000	.0273	.0272	1.0 (.93)	.35 (.02)	.95 (.02)
1030	.0660	.0540			
1060	.1519	.14			
1080	.2579	.27	1.0 (1.16)	.68 (.05)	1.35 (.003)

5.6 Pyrolysis of MDCS

Five series of experiments were carried out in which the decomposition of MDCS was followed. The overall temperature range covered was 992 - 1139K.

Fig. 5.6 "Simulated" Arrhenius plot for the pyrolysis of DMCS.



The products observed were methane, methyltrichlorosilane, hydrogen and hydrogen chloride, although as for DMCS, this last product could have been formed by hydrolysis of the reactant. The methyltrichlorosilane (mass peak $M^+ = 148^+$) was followed by monitoring the peak at $m/e = 133^+$, corresponding to the ion ($SiCl_3^+$). Trichlorosilane, if formed, would also have had a peak at $m/e = 133^+$, but the ratio of $133^+/148^+$ was approximately as measured for a sample of methyltrichlorosilane.

As for DMCS, the leak out rate constant for DMCS was difficult to determine owing to adsorption within the reaction vessel and/or ion source, but an average value of about 0.003 s^{-1} was obtained.

The plots of $\ln(\text{peak height})$ vs time for the loss of DMCS were generally straight over 20 - 30% decomposition and so were used to determine the pyrolysis rate constants.

The individual Arrhenius plots were straight up to a rate constant of about 0.2 s^{-1} and gave parameters ranging from $\log_{10}k = 10.36 - 228.6 \text{ KJ mol}^{-1}/2.3 \text{ RT}$ to $\log_{10}k = 11.77 - 258.4 \text{ KJ mol}^{-1}/2.3 \text{ RT}$.

A summary of all the rate constants measured appears in table 5.9 and the Arrhenius plot up to 1084K in fig. 5.7. A least squares fit of all the points up to a rate constant of 0.2 s^{-1} gave $\log_{10}k = (11.10 \pm .20) - (244.1 \pm 4.0 \text{ KJ mol}^{-1})/2.303 \text{ RT}$.

This compound would have been further into the unimolecular fall off region than the DMCS was, although the Arrhenius parameters were, within experimental error, the same.

Table 5.9

Rate Constants for the decomposition of MDCS (corrected for leak out).

Temp. /K	Rate Constant for the decomposition of MDCS k/s^{-1}	ln k	Temp. /K	Rate Constant for the decomposition of MDCS k/s^{-1}	ln k
992	.0142	-4.255	1022	.0480	-3.037
992	.0148	-4.213	1022	.0472	-3.053
1000	.0205	-3.887	1025	.0421	-3.168
1001	.0215	-3.840	1025	.0494	-3.008
1002	.0205	-3.887	1025	.0520	-2.957
1003	.0196	-3.932	1025	.0507	-2.982
1004	.0256	-3.665	1026	.0420	-3.170
1004	.0231	-3.768	1029	.0492	-3.012
1007	.0321	-3.439	1030	.0515	-2.966
1007	.0341	-3.379	1033	.0588	-2.834
1007	.0333	-3.402	1033	.0575	-2.856
1008	.0356	-3.335	1036	.0573	-2.860
1008	.0322	-3.436	1038	.0574	-2.858
1008	.0310	-3.474	1038	.0741	-2.602
1014	.0294	-3.527	1038	.0746	-2.596
1014	.0327	-3.420	1038	.0709	-2.647
1015	.0293	-3.530	1038	.0728	-2.620
1015	.0337	-3.390	1039	.0731	-2.616
1016	.0300	-3.507	1039	.0757	-2.581
1018	.0384	-3.260	1041	.0693	-2.669
1018	.0399	-3.221	1043	.0716	-2.637
1022	.0463	-3.073	1048	.0782	-2.549
1022	.0463	-3.073	1048	.0861	-2.452

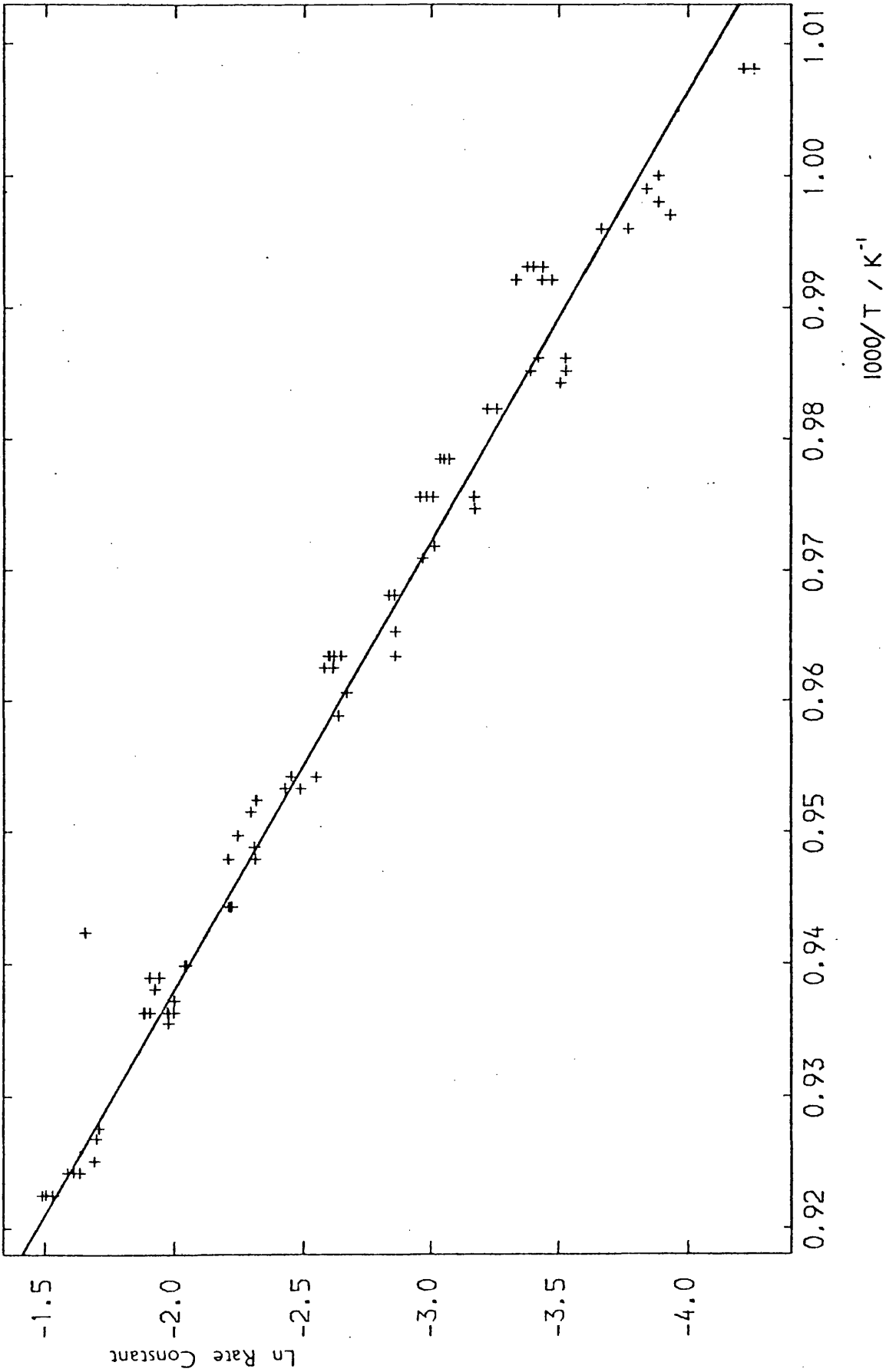
(table 5.9 continued)

Temp. /K	Rate Constant for the decomposition of MDCS k/s^{-1}	ln k	Temp. /K	Rate Constant for the decomposition of MDCS k/s^{-1}	ln k
1049	.0832	-2.487	1069	.1386	-1.976
1049	.0883	-2.427	1078	.1815	-1.707
1050	.0988	-2.315	1079	.1830	-1.698
1050	.0987	-2.316	1081	.1847	-1.689
1051	.1010	-2.293	1082	.1914	-1.653
1053	.1063	-2.242	1082	.1954	-1.633
1053	.1062	-2.242	1082	.2045	-1.587
1054	.0995	-2.308	1082	.1999	-1.610
1055	.1101	-2.206	1084	.2253	-1.490
1055	.0992	-2.311	1084	.2168	-1.529
1059	.1086	-2.220	1084	.2223	-1.504
1059	.1100	-2.207	1087	.2420	-1.419
1059	.1094	-2.213	1088	.2450	-1.407
1064	.1292	-2.046	1088	.2483	-1.393
1064	.1302	-2.039	1091	.2338	-1.453
1065	.1434	-1.942	1091	.2388	-1.449
1065	.1489	-1.905	1091	.2614	-1.342
1066	.1461	-1.924	1091	.2402	-1.426
1067	.1355	-1.999	1092	.2557	-1.364
1068	.1385	-1.977	1093	.2639	-1.332
1068	.1358	-1.997	1099	.2955	-1.219
1068	.1487	-1.906	1100	.2964	-1.216
1068	.1525	-1.881	1101	.3353	-1.093
1068	.1519	-1.885	1102	.3178	-1.146
1068	.1391	-1.973	1102	.3183	-1.145

(table 5.9 continued)

Temp. /K	Rate Constant for the decomposition of MDCS k/s^{-1}	ln k	Temp. /K	Rate Constant for the decomposition of MDCS k/s^{-1}	ln k
1102	.3416	-1.074	1116	.4022	-0.911
1102	.3325	-1.101	1117	.4131	-0.884
1103	.3272	-1.117	1123	.4817	-0.730
1103	.3273	-1.117	1123	.4794	-0.735
1103	.3564	-1.032	1124	.4641	-0.768
1103	.3461	-1.061	1124	.4679	-0.760
1103	.3555	-1.034	1138	.6263	-0.468
1115	.3956	-0.927	1139	.6259	-0.469
1115	.3994	-0.918			

Fig. 5.7 Arrhenius plot for the decomposition of MDCS.



5.7 Formation of products from DMCS.

The Arrhenius parameters for the formation of methane and of methyltrichlorosilane were determined by the C/B method outlined earlier. Generally the fit of the model to the experimental data was considerably worse than for the DMCS experiments.

It was found that at the lower temperatures, the rate constants for the formation of methane were about a fifth the size of those for the decomposition of the reactant. At the higher temperatures they were about a third the size of the decomposition rate constants. This was in contrast to the pyrolysis of DMCS, where the methane formation matched the decomposition of the reactant.

The rate constants obtained for the formation of methane are shown in table 5.10 and the resulting Arrhenius plot in fig. 5.8. A least squares fit over all the points up to 1084K gave $\log_{10}k = (11.73 \pm .13) - (267.6 \pm 2.6 \text{ KJ mol}^{-1}) / 2.303 \text{ RT}$.

The calculated rate constants for the formation of methyltrichlorosilane are shown in table 5.11 and the Arrhenius plot in fig. 5.9. A least squares fit over all the points gave $\log_{10}k = (8.49 \pm .16) - (201.3 \pm 3.3 \text{ KJ mol}^{-1}) / 2.303 \text{ RT}$.

No reliable quantitative information could be obtained for the formation of hydrogen or hydrogen chloride.

Table 5.10

Formation of methane by "C/B" method.

Temp/K	Experimental Total Rate Constant for loss of MDCS /s	Calculated Total Rate Constant for loss of MDCS ($k_2 + k_4$)/s ⁻¹	Calculated Rate Constant for formation of methane (k)/s ⁻¹	lnk
1007	.0411	.043	.007	-4.962
1007	.0391	.043	.007	-4.962
1008	.0426	.045	.007	-4.962
1025	.0577	.068	.013	-4.343
1025	.0590	.068	.013	-4.343
1025	.0564	.068	.012	-4.423
1038	.0811	.082	.019	-3.963
1039	.0827	.084	.019	-3.963
1039	.0801	.084	.019	-3.963
1053	.1132	.115	.030	-3.507
1053	.1133	.120	.030	-3.507
1055	.1171	.120	.030	-3.507
1068	.1589	.154	.044	-3.124
1068	.1595	.153	.043	-3.147
1068	.1557	.163	.043	-3.147
1084	.2293	.230	.070	-2.659
1084	.2238	.226	.066	-2.718
1084	.2323	.228	.068	-2.688
1101	.3423	.335	.105	-2.254
1102	.3395	.330	.100	-2.303
1102	.3486	.360	.100	-2.303

Fig. 5.8 Arrhenius plot for the formation of methane (by "C/B" method).

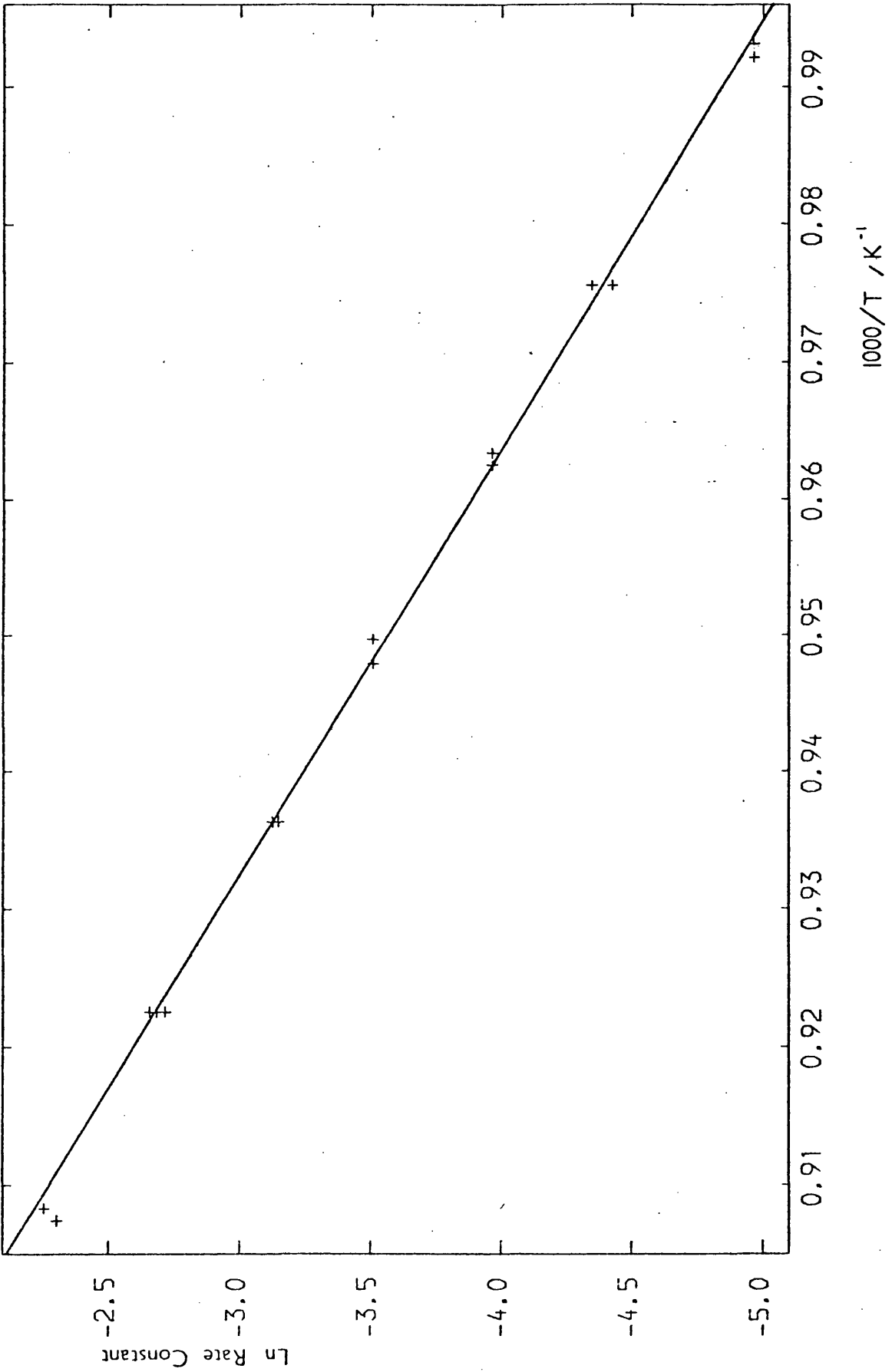
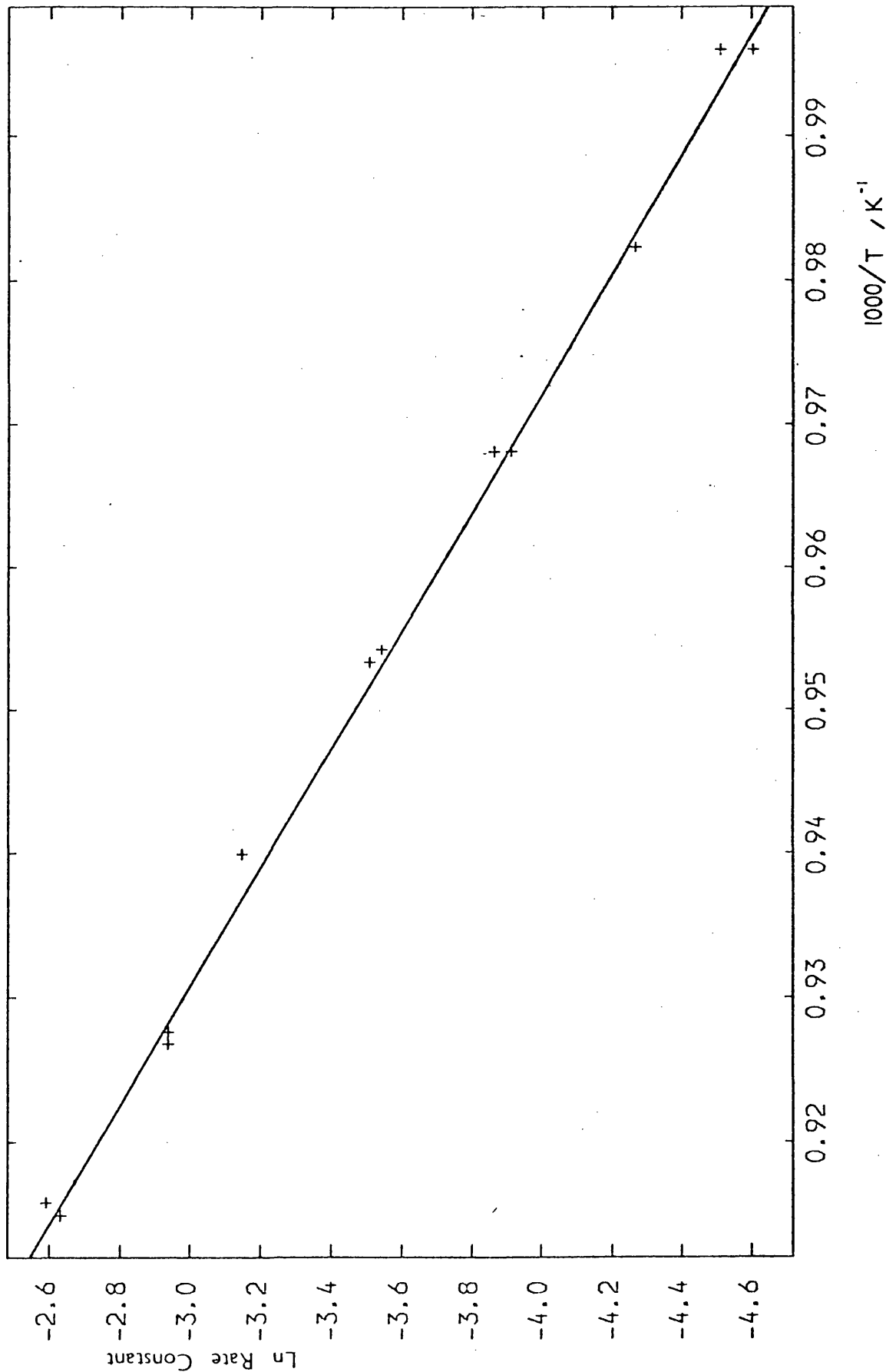


Table 5.11Formation of MeSiCl₃ by C/B method.

Temp/K	Experimental Total Rate Constant for loss MDCS /s ⁻¹	Calculated Total Rate Constant for loss MDCS (k ₂ + k ₄)/s ⁻¹	Calculated Rate Constant for formation of MeSiCl ₃ (k)/s ⁻¹	lnk
1004	.0261	.026	.011	-4.510
1004	.0286	.031	.010	-4.605
1018	.0429	.045	.014	-4.269
1018	.0414	.044	.014	-4.269
1033	.0605	.064	.020	-3.912
1033	.0618	.065	.021	-3.863
1048	.0891	.094	.029	-3.541
1049	.0913	.100	.030	-3.507
1064	.1322	.143	.043	-3.147
1078	.1845	.193	.053	-2.938
1079	.1860	.193	.053	-2.938
1092	.2587	.269	.075	-2.590
1093	.2669	.269	.072	-2.631

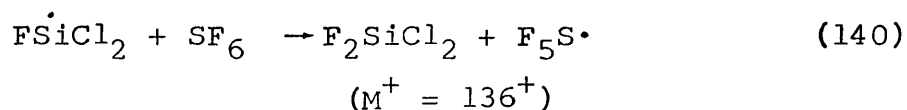
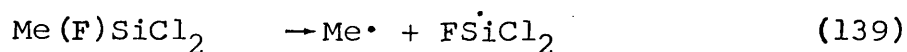
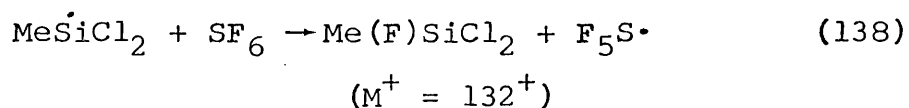
Fig. 5.9 Arrhenius plot for the formation of MeSiCl_3 (by "C/B" method).



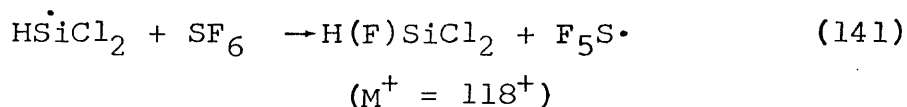
5.8 Co-pyrolysis of MDCS and Sulphur Hexafluoride.

As was discussed in section 5.4, the co-pyrolysis of DMCS and sulphur hexafluoride, the sulphur compound could be a good trap for silicon radicals.

MDCS was pyrolysed at about 1030K in the presence of excess sulphur hexafluoride. Two groups of peaks, both with the configuration for a species with two chlorine atoms, were formed, one at $m/e = 132^+$ and the other at $m/e = 136^+$. The following radical reactions were proposed.



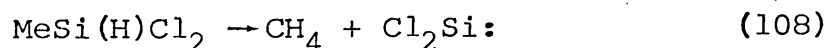
The silicon product from the reaction



would have strong mass-spectrum peaks at $m/e = 117^+$ from the ion $\text{F}\dot{\text{Si}}\text{Cl}_2^+$. But this ion would also be formed from $\text{Me}(\text{F})\text{SiCl}_2$, so the presence of the radical $\text{H}\dot{\text{Si}}\text{Cl}_2$ in the pyrolysis mixture could not be established.

5.9 Proposed Pyrolysis Mechanism

The thermochemistry for the formation of silylenes from MDCS would be the same as for their formation from DMCS. Thus, for the reaction



$$\begin{aligned} \Delta H &= D(\equiv\text{Si}-\text{Me}) + D(=\text{Si}-\text{H}) - D(\text{H}_3\text{C}-\text{H}) \\ &= 197 \text{ KJ mol}^{-1} \end{aligned}$$

and the activation energy for the process would be given by

$$E = 197 + \gg 93$$

thus

$$E \gg 290 \text{ KJ mol}^{-1}$$

Similarly, the activation energy for the reaction



would be given by $E = 333 \text{ KJ mol}^{-1}$

As for DMCS, rate constants for methane elimination could be estimated from the above activation energy and the A-factor from the methylsilane work¹¹. This time, no corrections for fall off were necessary since methylsilane and MDCS have equal numbers of atoms. A comparison between the observed rate constants for methane formation and those estimated from $\log_{10}k = 13.6 - 290 \text{ KJ mol}^{-1}/2.303 \text{ RT}^{11}$ is shown in table 5.12. Similar to DMCS, the estimated values were somewhat greater than the observed. However, if it was assumed that the activation energy was 330 KJ mol^{-1} , for the reasons outlined earlier, then the estimated rate constants became small relative to the observed values. Again, it could be argued that the A-factor may be less than $10^{13.6} \text{ s}^{-1}$ because of the chlorine atoms in the molecule.

Table 5.12

Comparison between rate constants for the formation of methane and those estimated for the elimination.

T/K	k_{+CH_4}/s^{-1} Experiment	k_{+CH_4}/s^{-1} $k = 10^{13.6} e^{-290/RT}$	k_{+CH_4}/s^{-1} $k = 10^{13.6} e^{-330/RT}$
1000	.0056	.028	.0002
1080	.0612	.375	.0044

Calculated rate constants for the elimination of hydrogen chloride from MDCS, based on $\log_{10} k = 14.1 - 333 \text{ KJ mol}^{-1}/2.3RT$, are compared in table 5.13 with the measured rate constants for the loss of the reactant. This elimination would be a minor process, especially if the A-factor were less than $10^{14.1} \text{ s}^{-1}$, which, as outlined above, seems likely since a chlorine atom would be directly involved in the formation of the transition state.

Table 5.13

Comparison between decomposition rate constants and those estimated for the elimination of HCl

T/K	k/s^{-1} Experiment	k_{+HCl}/s^{-1} Estimated
1000	.0223	.0005
1080	.1966	.0099

The experimentally determined activation energy for the formation of methane was less than the value estimated for silylene elimination, which suggested that a radical mechanism was involved.

Further support for radicals came from the experiments

involving sulphur hexafluoride, which were described in the section above.

Thus the mechanism for the pyrolysis of MDCS shown in scheme 5.2, which is analogous to that proposed for the decomposition of DMCS, was computer-simulated, the programme using Gear's method of numerical integration

Previous work in this laboratory had shown that, in the Q8 apparatus, the decomposition of methylsilane was into the unimolecular fall off region such that the rate constants measured were about $0.14k_{\infty}$, where k_{∞} was the high pressure limiting value. As MDCS has the same number of atoms as methylsilane, the same amount of fall off was assumed. Therefore, the A-factor for the initial step of the simulated mechanism was set at $0.14 \times 10^{17} \text{ s}^{-1}$, where 10^{17} s^{-1} was the value of the A-factor determined earlier for the decomposition of trimethylchlorosilane. The A-factors of the other unimolecular steps in the mechanism were similarly reduced. The activation energy used for the initial step was consistent with the silicon-methyl bond strength determined earlier. The other parameters used were taken from the literature as indicated.

Also consistent with the proposed decomposition mechanism of DMCS, an initial amount of hydrogen chloride, proposed to have come from the hydrolysis of the reactant, was included in the simulation. An initial ratio MDCS:HCl 3:1 was set.

In order to match the experimentally observed results for the formation of methane, one temperature-independent step (number 18) was required in the simulated mechanism. Comparisons between simulation and experiment are shown in table 5.14.

Scheme 5.2 Proposed pyrolysis mechanism of MDCS.

		$\log_{10} A$	E/KJ mol^{-1}	
1	$\text{MeSiHCl}_2 \rightarrow \text{Me}\cdot + \dot{\text{Si}}\text{HCl}_2$	16.15	367	(110)
2	$\dot{\text{Si}}\text{HCl}_2 + \text{HCl} \rightarrow \text{HSiCl}_3 + \text{H}\cdot$	7.00	15	(142)
3	$\text{Me}\cdot + \text{MeSiHCl}_2 \rightarrow \text{CH}_4 + \text{Me}\dot{\text{Si}}\text{Cl}_2$	8.11	30	(143)
4	$\text{H}\cdot + \text{MeSiHCl}_2 \rightarrow \text{H}_2 + \text{Me}\dot{\text{Si}}\text{Cl}_2$	10.00	8	(144)
5	$\text{Me}\dot{\text{Si}}\text{Cl}_2 + \text{HCl} \rightarrow \text{MeSiCl}_3 + \text{H}\cdot$	7.00	15	(145)
6	$\text{Me}\cdot + \text{MeSiHCl}_2 \rightarrow \text{CH}_4 + \dot{\text{C}}\text{H}_2\text{SiHCl}_2$	8.40	42	(146)
7	$\text{H}\cdot + \text{MeSiHCl}_2 \rightarrow \text{H}_2 + \dot{\text{C}}\text{H}_2\text{SiHCl}_2$	10.00	8	(147)
8	$\dot{\text{C}}\text{H}_2\text{SiHCl}_2 \rightarrow \text{CH}_2=\text{SiCl}_2 + \text{H}\cdot$	13.15	198	(148)
9	$\text{CH}_2=\text{SiCl}_2 + \text{HCl} \rightarrow \text{MeSiCl}_3$	6.65	10	(70)
10	$\dot{\text{Si}}\text{HCl}_2 \rightarrow \text{WALLS}$	$k = 100 \text{ s}^{-1}$		(149)
11	$\text{Me}\dot{\text{Si}}\text{Cl}_2 \rightarrow \text{WALLS}$	$k = 100 \text{ s}^{-1}$		(150)
12	$\dot{\text{C}}\text{H}_2\text{SiHCl}_2 \rightarrow \text{WALLS}$	$k = 100 \text{ s}^{-1}$		(151)
13	$2 \text{ Me}\cdot + \text{M} \rightarrow \text{C}_2\text{H}_6 + \text{M}$	10.51	0	(14)
14	$2 \text{ H}\cdot + \text{M} \rightarrow \text{H}_2 + \text{M}$	10.51	0	(127)
15	$2 \dot{\text{Si}}\text{HCl}_2 + \text{M} \rightarrow (\dot{\text{Si}}\text{HCl}_2)_2 + \text{M}$	10.51	0	(152)
16	$2 \text{ Me}\dot{\text{Si}}\text{Cl}_2 + \text{M} \rightarrow (\text{Me}\dot{\text{Si}}\text{Cl}_2)_2 + \text{M}$	10.51	0	(153)
17	$2 \dot{\text{C}}\text{H}_2\text{SiHCl}_2 + \text{M} \rightarrow (\dot{\text{C}}\text{H}_2\text{SiHCl}_2)_2 + \text{M}$	9.00	0	(154)
18	$\text{MeSiHCl}_2 + \text{WALLS} \rightarrow \text{CH}_4$	$k = .005 \text{ s}^{-1}$		(155)
19	$\text{MeSiHCl}_2 \rightarrow \text{H}\cdot + \text{Me}\dot{\text{Si}}\text{Cl}_2$	15.51	375	(156)
20	$\text{Me}\dot{\text{Si}}\text{Cl}_2 + \text{MeSiHCl}_2 \rightarrow \text{MeSiCl}_3 + \text{Me}\dot{\text{Si}}\text{HCl}$	6.20	15	(157)
21	$\dot{\text{Si}}\text{HCl}_2 + \text{MeSiHCl}_2 \rightarrow \text{HSiCl}_3 + \text{Me}\dot{\text{Si}}\text{HCl}$	6.20	15	(158)
22	$\text{MeSiHCl}_2 + \text{WALLS} \rightarrow \text{HCl}$	$k = .0132 \text{ s}^{-1}$		(159)
23	$\text{Me}\dot{\text{Si}}\text{Cl}_2 + \text{MeSiHCl}_2 \rightarrow \text{MeSiHCl}_2 + \dot{\text{C}}\text{H}_2\text{SiHCl}_2$	10.40	75	(160)
24	$\text{H}\dot{\text{Si}}\text{Cl}_2 + \text{MeSiHCl}_2 \rightarrow \text{H}_2\text{SiCl}_2 + \text{Me}\dot{\text{Si}}\text{Cl}_2$	10.00	45	(161)
25	$\text{H}\dot{\text{Si}}\text{Cl}_2 + \text{MeSiHCl}_2 \rightarrow \text{H}_2\text{SiCl}_2 + \dot{\text{C}}\text{H}_2\text{SiHCl}_2$	10.40	75	(162)
26	$\text{Me}\dot{\text{Si}}\text{Cl}_2 \rightarrow \text{Me}\cdot + \dot{\text{Si}}\text{Cl}_2$	14.51	255	(163)

Activation energies and A-factors based on data in chapters 3 and 4, and in refs. 13 and 57.

As for the DMCS, the simulation underestimated the production of chlorosilane product. But again, if it was assumed that some of the chlorinated radicals produced methyltrichlorosilane via the surface, then the simulation could match the experiment.

An Arrhenius plot for the decomposition of reactant, based on the simulated data in table 5.14 is shown in fig. 5.10. The line drawn gives $\log_{10}k = 11.00 - 242 \text{ KJ mol}^{-1} / 2.303 \text{ RT}$.

5.10 Discussion of the proposed mechanisms for DMCS and MDCS

The radical mechanisms proposed for the pyrolysis of DMCS and of MDCS broadly accounted for the experimental observations, though they could not be taken as proof that silylene formation from these compounds did not occur to a small extent. A small proportion of the methane formed at each temperature could have come from an elimination reaction.

For the pyrolysis of methylsilane in the same apparatus¹¹, no secondary bimolecular insertion reactions by silylene into the parent compound occurred, making the decomposition a "clean" first order process. It was reasonable to assume therefore that no bimolecular insertions would occur (none were observed) in the pyrolysis of MDCS or DMCS and that the formation of an elimination product would match the loss of the reactant.

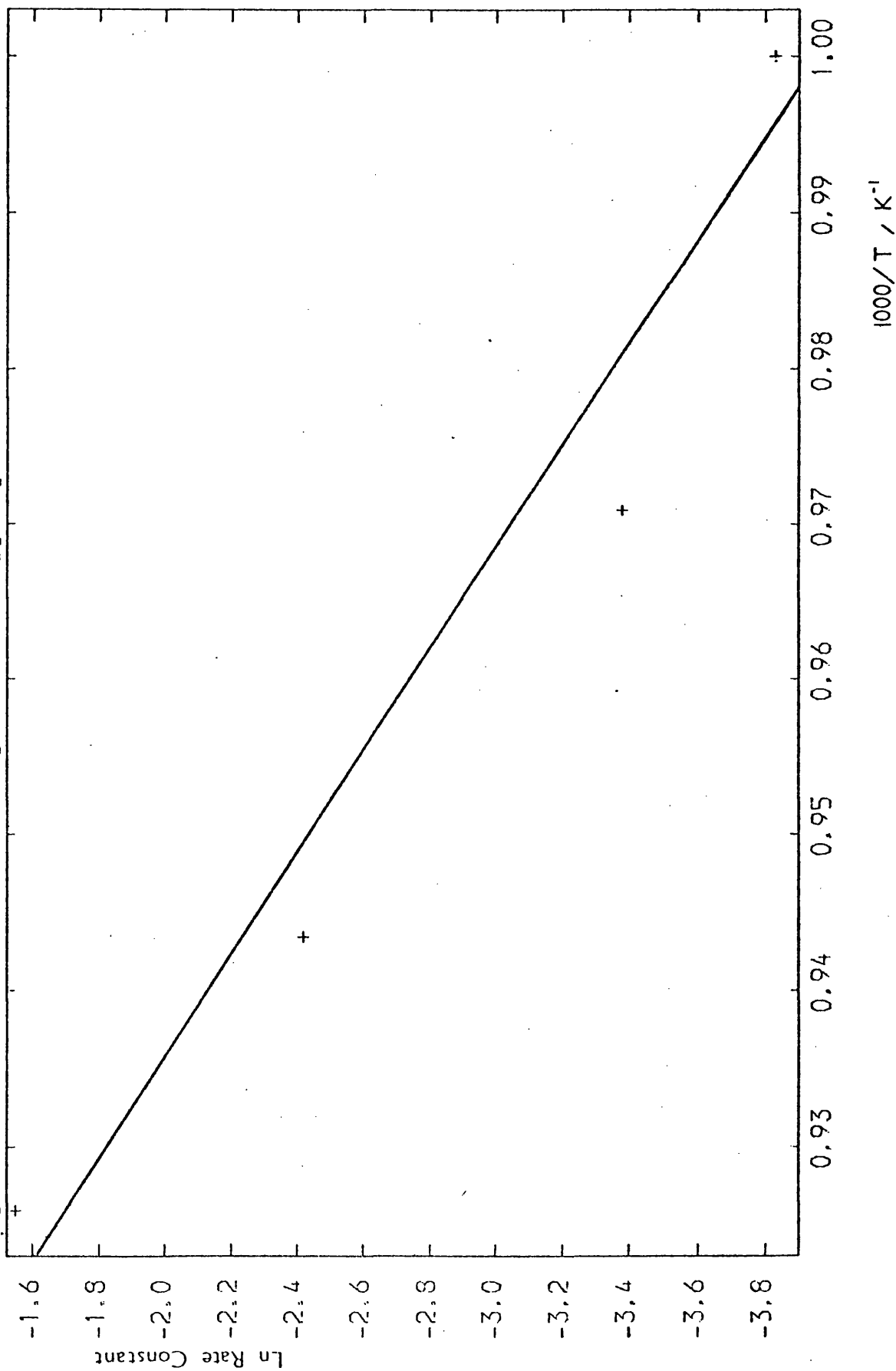
The experimental rate constants for the formation of methane from the pyrolysis of MDCS were only about a quarter the size of those for the decomposition of the reactant. A radical chain mechanism for the pyrolysis of this compound was therefore more easily justified than for the pyrolysis of DMCS. But, in view of the fact that a

Table 5.14

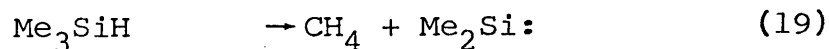
Comparison between simulation and experiment for the decomposition of MDCS.

Temp. /K	Experimental Rate Constant for the decomposition of MDCS. /s ⁻¹	Simulation Rate Constant for the decomposition of reactant. /s ⁻¹	$\frac{V_{CH_4}}{V_{MDCS}}$		$\frac{V_{MeSiCl_3}}{V_{MDCS}}$	
			Expt.	(Sim.)	Expt.	(Sim.)
1000	.0223	.0217	.25	(.28)	.42	(.04)
1030	.053	.034				
1060	.118	.089				
1080	.197	.213	.31	(.42)	.29	(.11)

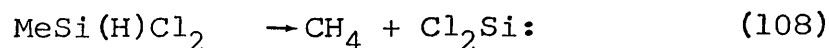
Fig. 5.10 "Simulated" Arrhenius plot for the pyrolysis of MDCS.



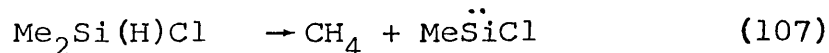
radical mechanism had been proposed for the pyrolysis of trimethylsilane, then a similar mechanism for DMCS would seem logical since, as far as silylene elimination is concerned, it is between the two. That is, if the reactions



and



are not favoured as the main decomposition route, then the reaction



should not be either.

Experimentally, less methane was formed from the decomposition of MDCS than from DMCS. The proposed pyrolysis mechanism for DMCS involved a chain in methyl radicals (which easily abstract hydrogen atoms to become methane), whereas that for MDCS only involves a chain in hydrogen atoms. Both mechanisms however require some surface production of methane in order to match the experiment.

Although silylene eliminations from DMCS and MDCS cannot be excluded, it could prove difficult to match a competitive silylene and radical mechanism to the observed rate constants for reactant loss and product formation. The main problem would be to sufficiently slow down the chain part of the mechanism without using ridiculously large rate constants for the losses of species to the walls of the reaction vessel. In the proposed mechanisms for DMCS and MDCS, the rate constants for the "loss steps" were similar to those used in the simulation of the 3MCS pyrolysis.

CHAPTER SIX

DISCUSSION

Consistent and reliable kinetic data concerning the pyrolysis of chlorosilanes were difficult to obtain, the work being complicated by the adsorption of reactants, intermediates and products within the apparatus. The problems tended to be worse for compounds containing silicon-hydrogen as well as silicon-chlorine bonds.

For the pyrolysis of trimethylchlorosilane (3MCS) however, the loss of silicon-centred and other radicals to the walls of the reaction vessel (together with relatively low initial pressures) did, in the end, allow the Arrhenius parameters for the non-chain dissociation of the compound to be measured, which led to a new value of 366 kJ mol^{-1} for the silicon-methyl bond dissociation energy.

Davidson et al¹³ measured a value of $355 \pm 6 \text{ kJ mol}^{-1}$ for the same type of bond in tetramethylsilane (TMS). This work, which was outlined in chapter 1, involved pyrolysing TMS in a flow system, the production of methane being used to monitor the reaction. The rate constants for the formation of the product could, however, have been greater than those for the decomposition of the reactant, since some of the observed methane may have come from the break-up of surface polymer. The error would have been greater at the lower of the temperatures used, where less methane was produced from the TMS. Thus the slope of the Arrhenius plot for methane formation would have been less than that for the decomposition of the reactant. The result does however fix a lower limit to the silicon-methyl bond dissociation energy in TMS. In the temperature range used to obtain the final value, it was thought that the

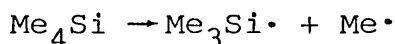
decomposition was a non-chain process, the activation energy being equal to the bond strength.

Walsh¹⁷ has derived a value of 374 KJ mol⁻¹ for the silicon-methyl bond dissociation energy in TMS, the figure being obtained from a combination of kinetic and thermochemical (heats of formation) data. For the reaction



$$\Delta H_f^0 (\text{Me}_3\text{Si}\cdot) = \Delta H_f^0 (\text{Me}_3\text{SiH}) - \Delta H_f^0 (\text{H}\cdot) + D(\text{Me}_3\text{Si}-\text{H})$$

and for



$$D(\text{Me}_3\text{Si}-\text{Me}) = \Delta H_f^0 (\text{Me}_3\text{Si}\cdot) + \Delta H_f^0 (\text{Me}\cdot) - \Delta H_f^0 (\text{Me}_4\text{Si})$$

By adding the two equations,

$$D(\text{Me}_3\text{Si}-\text{Me}) = D(\text{Me}_3\text{Si}-\text{H}) - \Delta H_f^0 (\text{H}\cdot) + \Delta H_f^0 (\text{Me}\cdot) + (\Delta H_f^0 (\text{Me}_3\text{SiH}) - \Delta H_f^0 (\text{Me}_4\text{Si})).$$

The bond dissociation energy $D(\text{Me}_3\text{Si}-\text{H})$ was determined kinetically by the "iodine equilibrium" method which was described in chapter 1. The heat of formation of trimethylsilane was calculated from literature enthalpies of formation of TMS and silane, it being assumed that there is a constant increment to ΔH_f^0 when a methyl group is replaced by hydrogen. (This is reasonable since the methylsilanes have been shown to obey simple additivity rules^{10, 28, 35, 38.})

Thus,

$$\begin{aligned} D(\text{Me}_3\text{Si}-\text{Me}) &= 378^{17} - 218^{58} + 144^{58} + (-163^{17} + 232^{17}) \\ &= 373 \text{ KJ mol}^{-1}. \end{aligned}$$

Apart from the experimental error in the kinetic measurement, estimated to be $\pm 12.5 \text{ kJ mol}^{-1}$, the above derived bond energy is dependent on the difference $(\Delta H_f^0 (\text{Me}_3\text{SiH}) - \Delta H_f^0 (\text{Me}_4\text{Si}))$. Two independent sets of data, both of which have been shown to be internally consistent³⁸, are those comprising the CATCH tables²⁶ and those determined by Potzinger et al^{28b} from appearance potential measurements. The relevant values from these two data sets, together with the numbers adopted by Walsh are shown in table 6.1. The silicon-methyl bond strength is also derived in each case. A lack of reliable absolute values for the heats of formation of silicon compounds is

Table 6.1

Derived silicon-methyl bond dissociation energy using different ΔH_f^0 values.

	$\Delta H_f^0 (\text{Me}_3\text{SiH})$ /KJ mol ⁻¹	$\Delta H_f^0 (\text{Me}_4\text{Si})$ /KJ mol ⁻¹	$\Delta \Delta H_f^0$ /KJ mol ⁻¹	$D(\text{Me}_3\text{Si}-\text{Me})$ /KJ mol ⁻¹
Potzinger et al ^{28b}	-124	-177	53	357
Walsh ¹⁷	-163	-232	69	373
CATCH	-157	-236	79	383

thus highlighted. The problems encountered in measuring such values were explained in chapter 1 and until more corroborative data have been made available derivations such as above should be used cautiously. For example, it is best to use heats of formation which are all taken from the same data set, preferably one which shows internal consistency. By mixing the Potzinger et al and CATCH enthalpies in table 6.1, values for $D(\text{Me}_3\text{Si}-\text{Me})$ ranging

from 318 - 416 KJ mol⁻¹ can be obtained. By comparison, the values quoted in the table show reasonable agreement both amongst themselves and with the experimental values discussed above.

The discussion so far has compared the silicon-methyl bond dissociation energy in 3MCS, obtained as described in chapter 3, with estimates for the same type of bond in TMS. This is a valid exercise, since it seems likely that a chlorine ligand has no significant effect on D(Si—Me). The small substituent effects found in silicon chemistry are illustrated in table 6.2, where the silicon-hydrogen bond strength is shown to be essentially unchanged by methyl or chlorine ligands. This is in contrast to carbon chemistry, where carbon-hydrogen bonds are affected by the other substituents on the central atom. Values for the analogous carbon-centred molecules are also included in the table.

Table 6.2

Comparison of D(Si—H) with analogous D(C—H).

Measured Si—H Bond Energy ¹⁷		Analogous C—H Bond Energy	
Bond	D/KJ mol ⁻¹	Bond	D/KJ mol ⁻¹
H ₃ Si - H	378	H ₃ C - H	439
Me ₃ Si - H	378	Me ₃ C - H	385
Cl ₃ Si - H	382	Cl ₃ C - H	402

From their electron impact studies of the methylsilanes, Potzinger et al found that D(Si—C) (and D(Si—H)) were unchanged by the number of methyl groups attached to the

silicon, again illustrating that substituent effects are small. Once more this is in contrast to carbon chemistry as table 6.3 illustrates.

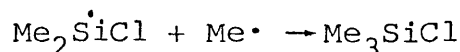
Table 6.3

Comparison of $D(\equiv\text{Si}-\text{C})$ with analogous $D(\equiv\text{C}-\text{C})$

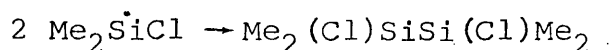
Bond	D/KJ mol ⁻¹ 28b	Bond	D/KJ mol ⁻¹ 58
Me ₃ Si—Me	355 ± 17	Me ₃ C—Me	343
Me ₂ HSi—Me	355 ± 17	Me ₂ HC—Me	352
MeH ₂ Si—Me	355 ± 17	MeH ₂ C—Me	356
H ₃ Si—Me	355 ± 17	H ₃ C—Me	368

Davidson et al determined the A-factor for the pyrolysis of TMS to be $10^{17.6} \text{ s}^{-1}$, the result being based on the formation of methane. If, as suggested above, some of the observed product had come from the decomposition of surface polymer, then the A-factor could have been overestimated. The value $A = 10^{17.0} \text{ s}^{-1}$, obtained in chapter 3 for the pyrolysis of 3MCS, is perhaps more reliable, since it was determined directly from the decomposition of the reactant.

It would be interesting to derive an A-factor for the reverse of this process, that is, for the reaction



because then, an A-factor for the recombination



could be calculated. At present there is some uncertainty concerning the size of this parameter for the self-recombination of silicon-centred radicals, estimates ranging

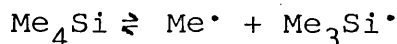
from $10^6 - 10^{11} \text{ dm}^3 \text{ mol}^{-1} \text{ s}^{-1}$.

The above derivation cannot be attempted at present owing to a lack of reliable thermodynamic data for the chlorosilanes. Ring and O'Neal however have recently published a set of "Group Additivity" tables for the methylsilanes which contain sufficient data to calculate³⁸ the entropy change for the process,



An estimate of the A-factor for this reaction can thus be made.

Consider the reversible dissociation



The A-factor for the forward unimolecular process is given by⁵⁸,

$$A_f = (ekT/h) \exp(\Delta S^\ddagger/R) \text{ s}^{-1}$$

whereas that for the reverse bimolecular reaction is⁵⁸,

$$A_r = (e^2kT/h) \exp(\Delta S^\ddagger/R) \text{ dm}^3 \text{ mol}^{-1} \text{ s}^{-1}$$

where $e = 2.718$, k is the Boltzmann constant, T is the temperature, h is Planck's constant, ΔS^\ddagger is the entropy change to form the transition state and R is the gas constant. Dividing the two equations,

$$A_f/A_r = e^{-1} \exp(\Delta S^0/R)/V \text{ (mol dm}^{-3}\text{)}$$

where ΔS^0 is the standard entropy change for the process left to right. V is the standard volume of an ideal gas and is needed to correct for the difference between first and second order units. Thus,

$$A_r = A_f \cdot V/e \cdot \exp(\Delta S^0/R) \text{ dm}^3 \text{ mol}^{-1} \text{ s}^{-1} \quad (\text{xx})$$

For the decomposition of both TMS and 3MCS, the entropy change ΔS^\ddagger on forming the transition state is essentially due to the lengthening of a silicon-methyl bond, therefore the A-factors for the two forward processes are probably about equal. As the A-factor for the pyrolysis of 3MCS was thought to be more reliable than that for the decomposition of TMS, the former was used in the calculation of A_r .

Since A-factors are somewhat temperature-dependent and the value of $A = 10^{17.0} \text{ s}^{-1}$ for the decomposition of 3MCS was obtained over the range 1033 - 1149K, then in order to apply the above expression for A_r , it was necessary to calculate ΔS for the reaction at a similarly high temperature. Thus, entropies at 1000K were derived as outlined below.

(i) Entropy of Me_4Si , (Data from ref. 38).

Point group = Td, with four internal three-fold rotations.

Thus, the external symmetry number $\sigma_{\text{ext}} = 12$ and the internal symmetry number $\sigma_{\text{int}} = 3^4$.

Groups: $4(\text{C} - (\text{Si})(\text{H})_3) + (\text{Si} - (\text{C})_4)$

$$S^0 \text{ (intrinsic)} = 4(127) + (-84) = 424 \text{ J mol}^{-1} \text{ K}^{-1}$$

$$S^0 \text{ (real, free rotor)} = 424 - R \ln 12 - 4R \ln 3 = 367 \text{ J mol}^{-1} \text{ K}^{-1}.$$

$$C_p^0 \text{ (real, free rotor)} = 4(25.9) + 21.6 = 125.2 \text{ J mol}^{-1} \text{ K}^{-1}.$$

$$C_p^0 \text{ (real, hindered rotor)} = 125.2 - 4(3.8) = 110.0 \text{ J mol}^{-1} \text{ K}^{-1}.$$

$$\text{Similarly, } C_p \text{ (real, hindered rotor)}_{1000\text{K}} = 274.3 \text{ J mol}^{-1} \text{ K}^{-1}.$$

$$C_p \text{ (mean)} = (110.0 + 274.3)/2 = 192.2 \text{ J mol}^{-1} \text{ K}^{-1}.$$

$$\begin{aligned} S \text{ (real, free rotor)}_{1000\text{K}} &= 367 + (192.2 \ln(1000/298)) \\ &= 600 \text{ J mol}^{-1} \text{ K}^{-1} \end{aligned}$$

(ii) Entropy of Me₃Si•

Point group = C_{3v}, with $\sigma_{\text{ext}} = 3$ and $\sigma_{\text{int}} = 3^3$.

There are no group additivity schemes for silicon radicals, but the entropy of the above can be estimated from that of Me₃SiH.

Me₃SiH C_{3v}, $\sigma_{\text{ext}} = 3$, $\sigma_{\text{int}} = 3^3$, the same as for the radical.

Groups: 3(C - (Si)(H)₃) + (Si - (H)(C)₃)

By the same method as was used to calculate the entropies and heat capacities of TMS above,

$$S^0 \text{ (free rotor)} = 343 \text{ J mol}^{-1} \text{ K}^{-1}.$$

$$C_p^0 \text{ (hindered rotor)} = 95 \text{ J mol}^{-1} \text{ K}^{-1}.$$

$$C_p \text{ (hindered rotor)}_{1000\text{K}} = 228 \text{ J mol}^{-1} \text{ K}^{-1}$$

In converting from the molecule to the radical by removal of the silicon-hydrogen bond, there is a loss of 3 vibrational degrees of freedom. (A negative entropy change). These correspond to one silicon-hydrogen stretching mode and two (C—Si—H) bending modes. The silicon-hydrogen stretch frequency is high enough (2130 cm⁻¹) not to contribute significantly to the entropy or heat capacity. The bending mode has been assigned a frequency of 690 cm⁻¹ and does therefore contribute, by an amount determined from⁵⁸

$$C_{\text{vib}}/R = x^2 e^x / (e^x - 1)^2$$

and

$$S^0/R = -\ln(1 - e^{-x}) + x/(e^x - 1)$$

where $x = (ch\bar{\nu}/kT) = (1.44 \bar{\nu}/T)$ with $\bar{\nu}$ in cm^{-1} and T in K.

The odd electron increases the entropy of the radical by an amount $R \ln 2$, but does not contribute significantly to the heat capacity⁵⁸.

The external and internal symmetry numbers of Me_3SiH and $\text{Me}_3\text{Si}\cdot$ are the same. Thus, the entropy of the the radical is given by,

$$S_{\text{radical}}^0 = S_{\text{molecule}}^0 - S_{\text{vibration}}^0 + R \ln 2$$

At 300K, $x = 3.3$ for (C—Si—H) bending, which corresponds⁵⁸ to an entropy of $1.3 \text{ J mol}^{-1} \text{ K}^{-1}$.

Thus,

$$\begin{aligned} S^0(\text{Me}_3\text{Si}\cdot) &= S^0(\text{Me}_3\text{SiH}) - 2 S^0(\text{Vib}) + R \ln 2 \\ &= 343 - 2(1.3) + 5.8 \\ &= 346 \text{ J mol}^{-1} \text{ K}^{-1}. \end{aligned}$$

A value of $x = 3.3$ corresponds to a heat capacity of $3.4 \text{ J mol}^{-1} \text{ K}^{-1}$ ⁵⁸. Thus,

$$\begin{aligned} C_p^0(\text{Me}_3\text{Si}\cdot) &= C_p^0(\text{Me}_3\text{SiH}) - 2 C_p^0(\text{Vib}) \\ &= 95 - 2(3.4) \\ &= 88 \text{ J mol}^{-1} \text{ K}^{-1} \end{aligned}$$

Similarly,

$$\begin{aligned} C_p(\text{Me}_3\text{Si}\cdot)_{1000\text{K}} &= 228 - 2(7.5) \\ &= 213 \text{ J mol}^{-1} \text{ K}^{-1} \end{aligned}$$

Thus,

$$C_p(\text{mean}) = (88 + 213)/2 = 150.5 \text{ J mol}^{-1} \text{ K}^{-1}$$

and

$$\begin{aligned} S(\text{Me}_3\text{Si}\cdot)_{1000\text{K}} &= 346 + (150.5 \ln (1000/298)) \\ &= 528 \text{ J mol}^{-1} \text{ K}^{-1} \end{aligned}$$

(iii) Entropy of $\cdot\text{CH}_3$ ⁵⁸

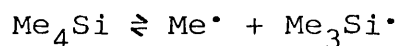
$$S^0 = 194 \text{ J mol}^{-1} \text{ K}^{-1}$$

$$C_{p(298\text{K})} = 36.8, \quad C_{p(1000\text{K})} = 60.7 \text{ J mol}^{-1} \text{ K}^{-1}$$

Therefore, $C_p(\text{mean}) = 48.8 \text{ J mol}^{-1} \text{ K}^{-1}$

Thus $S_{1000\text{K}} = 253 \text{ J mol}^{-1} \text{ K}^{-1}$.

An A-factor for the reverse of the process



can now be calculated.

From above,

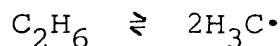
$$\begin{aligned} \Delta S_{1000\text{K}} &= 253 + 528 - 600 \\ &= 181 \text{ J mol}^{-1} \text{ K}^{-1}. \end{aligned}$$

(without the heat capacity corrections, $\Delta S^0_{(298\text{K})} = 173 \text{ J mol}^{-1} \text{ K}^{-1}$)

From eqn. (xx) above,

$$\begin{aligned} A_r &= 10^{17.0} \times 82.1/e^{\cdot} \exp(188/R) \\ &= 10^{9.89} \text{ dm}^3 \text{ mol}^{-1} \text{ s}^{-1} \end{aligned}$$

An A-factor for the dissociation



has been determined as $10^{17.45} \text{ s}^{-1}$ at a mean temperature of

800K⁵⁸. The entropies of ethane and methyl radicals at this temperature can be calculated as 309 and 239 J mol⁻¹ K⁻¹ respectively. Thus,

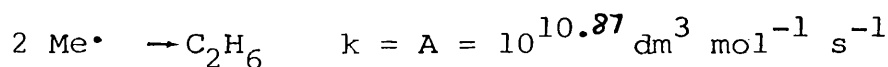
$$\begin{aligned}\Delta S_{800K} &= 2(239) - 309 \\ &= 169 \text{ J mol}^{-1} \text{ K}^{-1}.\end{aligned}$$

Hence

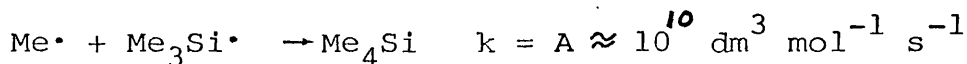
$$\begin{aligned}A_r &= 10^{17.45} \times 65.64 / e^{-1} \exp(169/R) \\ &= 10^{10.87} \text{ dm}^3 \text{ mol}^{-1} \text{ s}^{-1}.\end{aligned}$$

which is in fair agreement with other estimates in the literature⁶⁵ of $10^{10.3} \text{ dm}^3 \text{ mol}^{-1} \text{ s}^{-1}$.

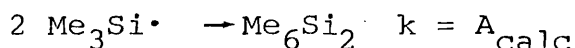
Thus for,



and for



Rate constants for the combination



can be calculated since A-factors obey a geometric mean rule.

Thus,

$$\log_{10}(A_{\text{calc}}/2) + (1/2) = 10$$

therefore

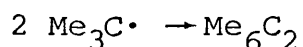
$$\log_{10} A_{\text{calc}} = 9$$

and
$$A_{\text{calc}} = 10^9 \text{ dm}^3 \text{ mol}^{-1} \text{ s}^{-1}$$

Some measurements of the same combination in

solution have given values of $\log_{10}A = 9.3^{66}$, 9.7^{67} , 9.5^{68} and 11.3^{69} . The value calculated above seems at first sight a little small, but in view of the uncertainties in the rather indirect calculation, the agreement with the lower of the experimental values above is not unreasonable.

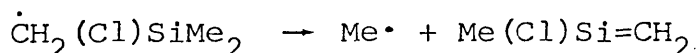
It would be interesting to compare the A-factor for the combination of two trimethylsilyl radicals with that for the reaction



but even here there is some uncertainty. For example, values of $\log_{10}A = 6.6^{70}$ and of $\log_{10}A = 9.2^{71}$ have been reported.

The anticipated pyrolysis mechanism of 3MCS was apparently prevented by the presence of background hydrogen chloride, a hydrolysis product. The decomposition was expected to be analogous to that of TMS, with a disilacyclobutane being formed. Such a product was not observed, although evidence was obtained for the formation of a silaethene.

The co-pyrolysis experiments involving 3MCS and oxygen, whilst not producing any positive results for the investigation in hand (that of the elimination of hydrogen chloride from 3MCS), did however indicate the presence of the radical $\dot{\text{C}}\text{H}_2(\text{Cl})\text{SiMe}_2$, which would be formed if the "TMS mechanism" were occurring. As this radical was produced, then it was reasonable to assume that the process

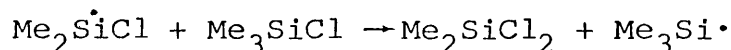


occurred, giving the silaethene shown. No disilacyclobutane

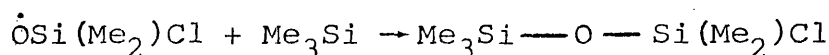
(from the self-dimerisation of the silaethene) was observed however, dimethyldichlorosilane (2M2CS) being the major silicon-containing product. An addition reaction between the silaethene and background hydrogen chloride was proposed to account for these observations.

Strong evidence in favour of this explanation was obtained from the work described in chapter 4. Clearly, the addition of hydrogen chloride to 1,1-dimethylsilaethene is a very efficient process, indeed, a rather unconventional method of analysis was necessary to determine an activation energy.

In the pyrolysis of 3MCS, some 2M2CS was also formed by the exchange reaction



Evidence for this process was again provided by the co-pyrolysis experiments between 3MCS and oxygen, the product of the combination



being observed, which indicated the presence of the radical $\text{Me}_3\dot{\text{Si}}$. Similarly the radicals $\text{Me}_2\dot{\text{Si}}\text{Cl}$ and $\text{Me}\dot{\text{Si}}\text{Cl}_2$ were shown to be present.

No firm conclusions could be made regarding the possible elimination of hydrogen chloride from 3MCS. The co-pyrolysis experiments involving the chlorosilane with oxygen produced no evidence for the process, whilst those involving 3MCS and hydrogen halide were inconclusive. The lack of positive evidence indicates that if the elimination does occur, then it is a minor process compared with the

dissociation into radicals, a fact which had been predicted by consideration of the appropriate thermochemistry.

Inclusion of the elimination process in the proposed reaction scheme for the pyrolysis of 3MCS would have made little (if any) difference to the value determined for the silicon-methyl bond dissociation energy.

The pyrolysis of dimethylchlorosilane (DMCS) and of methylchlorosilane (MDCS) was best explained by a radical chain mechanism. The alternative mode of decomposition, that of silylene formation, could not easily account for the formation of the dichloro- product from DMCS or of the trichloro- product from MDCS and it could also not account for the formation of hydrogen, seen in the pyrolysis of both compounds.

The best evidence for the presence of radicals came from the co-pyrolysis of each of the chlorosilanes with sulphur hexafluoride. As was discussed in chapter 5, the hexafluoride was thermally stable at the temperatures used and the abstraction of a fluorine atom from it by a silicon radical is a convincingly exothermic process, the silicon-fluorine bond being one of the strongest formally single bonds known¹⁷. Sulphur hexafluoride is thus recommended as a useful compound for the "trapping" of silicon-centred radicals present in a pyrolysis system.

The observed activation energies for the formation of methane from and for the decomposition of, the two chlorosilanes were less than those estimated for silylene elimination. This, together with the small amount of

methane produced in the pyrolysis of MDCS was further evidence for a radical mechanism.

The final Arrhenius parameters obtained earlier for the pyrolysis of the various chlorosilanes are summarised in table 6.3 and those for the two addition reactions studied, in table 6.4.

Table 6.3

Summary of Arrhenius parameters obtained earlier.

Pyrolysis of	$\log_{10}A$	E /KJ mol ⁻¹	Formation of	$\log_{10}A$	E /KJ mol ⁻¹
Me ₃ SiCl	17.03 ± .34	366.5 ± 7.2			
Me ₂ Si(H)Cl	11.35 ± .21	246.9 ± 4.1	CH ₄	11.38 ± .13	247.4 ± 2.6
			Me ₂ SiCl ₂	11.19 ± .19	247.1 ± 3.8
			H ₂	13.41 ± .16	286.8 ± 3.1
MeSi(H)Cl ₂	11.10 ± .20	244.1 ± 4.0	CH ₄	11.73 ± .13	267.6 ± 2.6
			MeSiCl ₃	8.49 ± .16	201.3 ± 3.3
Me ₂ Si <input type="checkbox"/>	14.72 ± .53	249.1 ± 8.0	@		
	15.24 ± .20	255.9 ± 2.9			
Cl ₂ Si <input type="checkbox"/>	12.86 ± .14	231.4 ± 2.2			
	14.73 ± .47	259.5 ± 7.3	£		
	15.56 ± .30	263.8 ± 4.8	&		

@ Literature values 15.64/261.5³⁹

£ In the presence of excess hydrogen chloride

& Work in this laboratory using stirred flow system.

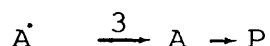
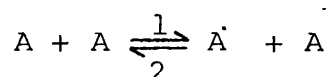
Table 6.4

Arrhenius parameters obtained for the addition reactions.

Addition	$\log_{10} A$	$E / \text{KJ mol}^{-1}$
$\text{Me}_2\text{Si}=\text{CH}_2 + \text{HCl}$	$7.5 \pm .3$	12 ± 5
$\text{Me}_2\text{Si}=\text{CH}_2 + \text{HBr}$	$7.4 \pm .3$	34 ± 8

Some of the decomposition reactions studied may have been in the unimolecular fall off region. The extent to which this was so can be estimated as outlined below.

The Lindemann theory describes the unimolecular decomposition of molecule A as follows,



Applying a steady state approximation to "hot" species \dot{A} ,

$$d[\dot{A}]/dt = k_1[A]^2 - k_2[\dot{A}][A] - k_3[\dot{A}] = 0$$

Therefore,

$$[\dot{A}] = k_1[A]^2 / (k_3 + k_2[A])$$

For the production of product P

$$d[P]/dt = k_3[\dot{A}]$$

therefore

$$d[P]/dt = k_3 k_1 [A]^2 / (k_3 + k_2[A]) \quad (\text{xxi})$$

At high pressure, $k_2[A] \gg k_3$, so

$$d[P]/dt = (k_3 k_1 / k_2) [A] = k_{\infty} [A]$$

Therefore, by dividing the top and bottom of eqn (xxi) by $k_2 [A]$

$$\begin{aligned} d[P]/dt &= k_{\infty} [A] / (1 + (k_3/k_2 [A])) \\ &= k_{\text{exp}} [A] \end{aligned}$$

where k_{exp} is the observed first order rate constant.

Therefore

$$k_{\text{exp}} = k_{\infty} / (1 + (k_3/k_2 [A])) \quad (\text{xxii})$$

When

$$k_{\text{exp}} = 0.5 k_{\infty}, \quad (\text{at pressure } p_{1/2})$$

then,

$$k_3 = k_2 [A]$$

and

$$[A] = k_3 / k_2 = p_{1/2} \quad (\text{xxiii})$$

For a pyrolysis reaction, the fall off pressure ($p_{1/2}$) is related to the number of atoms (N) in the reactant molecule. A linear plot of $\log_{10} p_{1/2}$ vs N has been produced⁷² from which the approximate value of $p_{1/2}$ for any decomposition reaction can be predicted. Using this plot in conjunction with eqn. (xxii), the pressure corresponding to any value of the ratio ($k_{\text{exp}}/k_{\infty}$) can be estimated. For example, "Estimate the pressure at which ($k_{\text{exp}}/k_{\infty} = 0.9$)".

From eqn. (xxii)

$$k_{\text{exp}} = 0.9 k_{\infty} \text{ when } k_3/k_2 [A] = 0.1$$

That is, when

$$[A] = (k_3/k_2) \times 10$$

or at pressure $p = p_{1/2} \times 10$

The value of $p_{1/2}$ for the appropriate number of atoms can be read off from the above graph.

This method was used to produce fig. 6.1, which is a plot of $\log_{10} p$ vs N for $(k_{\text{exp}}/k_{\infty}) = 0.9$ and 0.98 , the positions of the lines being calculated from the plot of $\log_{10} p_{1/2}$ vs N^{72} , which is also shown.

For most of the pyrolyses, a reaction vessel pressure of approximately 0.3 mm Hg was used. Fig. 6.1 can thus be used to estimate the amount of fall off involved in the decomposition of each compound. It should be remembered however that owing to the simple method used to produce these graphs, they can only serve as a rough guide.

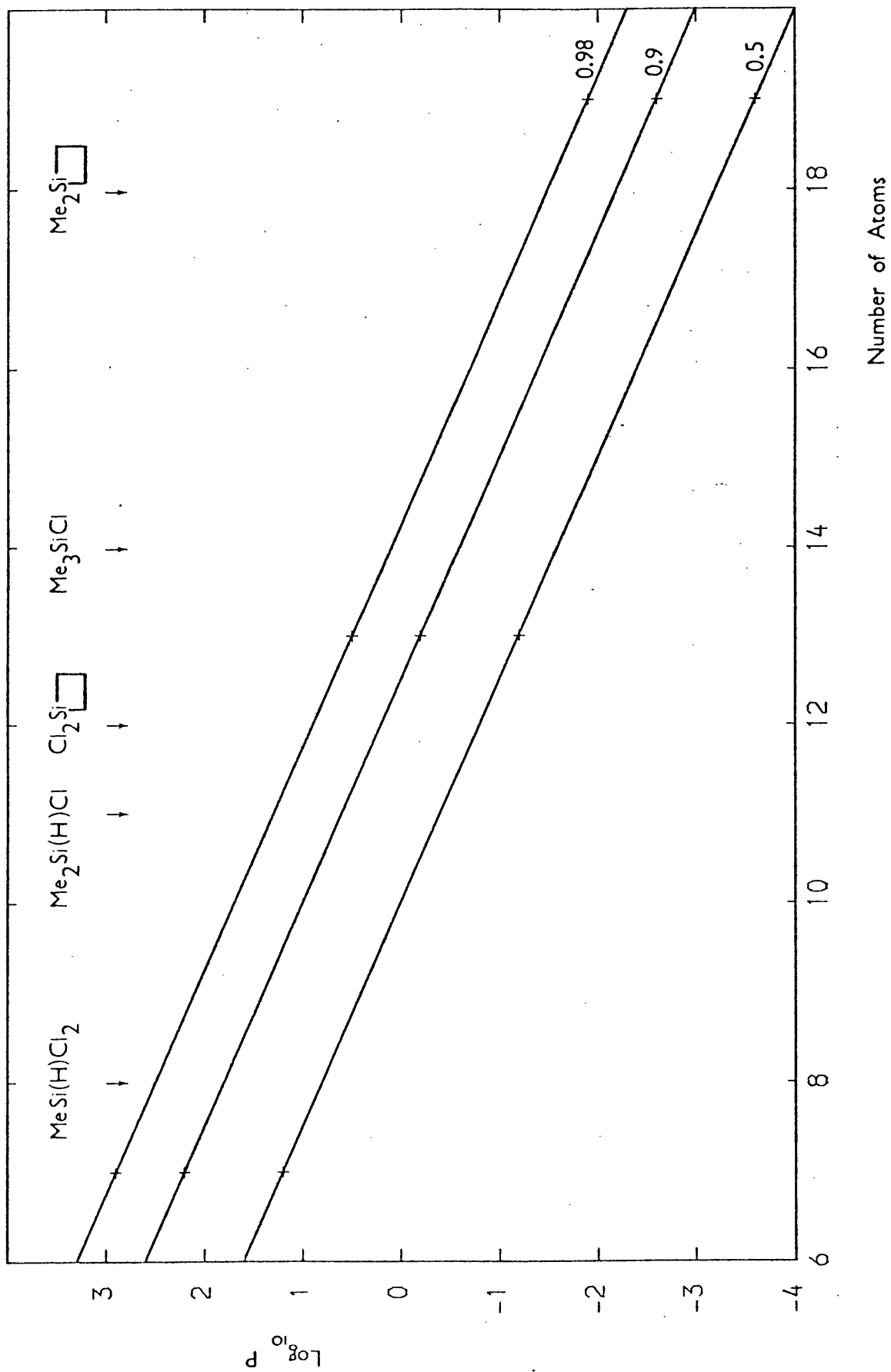
It is clear that the pyrolysis of 1,1-dimethylsilacyclobutane (DMSCB) was probably unaffected. For the 3MCS however, the measured rate constants would have been about 0.9 of the high pressure values. This would make the high pressure A-factor for the pyrolysis

$$10^{17.0}/0.9 = 10^{17.05} \text{ s}^{-1},$$

which represents an insignificant increase from the measured value since the experimental uncertainty was $\pm 0.34 \log_{10} A$ units.

From fig. 6.1, it seems that the pyrolysis of DMCS

Fig. 6.1 "Fall off plot" : $\log_{10} P_{0.5}$, $\log_{10} P_{0.9}$, and $\log_{10} P_{0.98}$ vs Number of atoms.



could have been further into the fall off region than was thought at the time, the experimental rate constants possibly being as low as $0.5 k_{\infty}$. (Slightly higher pressures of around 0.5 mm Hg were used for the pyrolysis of DMCS and MDCS.)

The conclusion about the type of mechanism i.e. radicals rather than silylene elimination, is unaffected by this late realisation, but the computer model of the pyrolysis could have been modified by reducing the A-factors of all the unimolecular steps by up to a half. In fitting the simulation to the observed results, one problem was to slow down the chain sufficiently whilst still using reasonable rate constants for losses of radical species to the walls of the reaction vessel. A justifiable reduction in the unimolecular A-factors could have greatly simplified this task. However, since several arbitrary steps would still have been necessary, to account for the significant surface involvement which occurred in the pyrolysis and because the exact amount of fall off was not known, such a modification to the model was thought to be inappropriate since, even with the parameters used it broadly matched the experimental observations.

As predicted from the work involving methylsilane¹¹, the pyrolysis of MDCS would have been well into the fall off region, but from working the above calculation backwards, the rate constants could have been as low as $0.07k_{\infty}$ and not $0.14k_{\infty}$ as assumed. Again, as for DMCS, the conclusion regarding the mode of decomposition is unchanged, but the computer model could have been further modified. This was thought to be inappropriate however for

the same reasons as outlined in the paragraph above.

Finally, the rate constants for the pyrolysis of 1,1-dichlorosilacyclobutane (DCSCB) could have been about $0.6k_a$. The decomposition of this compound ought to have the same Arrhenius parameters as for the pyrolysis of DMSCB, since it is now generally accepted that the initial step involves the breaking of a carbon-carbon rather than of a silicon-carbon bond and the former would be unaffected by the substituents attached to the silicon.

The series of pyrolyses involving DMSCB which yielded Arrhenius parameters closest to the literature values³⁹ produced rate constants given by

$$\log_{10}k = 15.24 \pm .2 - (255.9 \pm 2.9 \text{ KJ mol}^{-1})/2.303 \text{ RT.}$$

A similar activation energy was found for the pyrolysis of DCSCB, the rate constants being given by

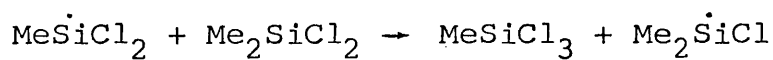
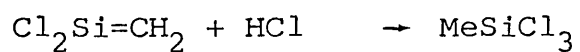
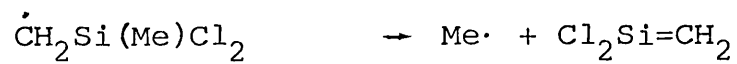
$$\log_{10}k = 14.73 \pm .47 - (259.5 \pm 7.3 \text{ KJ mol}^{-1})/2.303 \text{ RT.}$$

Correcting this A-factor for the estimated degree of fall off gives a value of $10^{14.95} \text{ s}^{-1}$, which is in reasonable agreement with the value for DMSCB.

Tetramethylsilane, trimethylchlorosilane and the members of the series $\text{Me}_n(\text{Cl}_{3-n})\text{SiH}$ have been shown to pyrolyse by dissociation into radicals, mechanisms analogous to that proposed for the thermolysis of TMS accounting for the experimental observations.

It would be interesting to investigate the pyrolysis mechanism of dimethyldichlorosilane to see if it follows the same pattern thus,





+ termination steps.

The pyrolysis of 1,1-dichlorosilacyclobutane, described in chapter 4, demonstrated the existence of the intermediate 1,1-dichlorosilaethene, so the above mechanism would seem likely.

APPENDIX

COMPUTER PROGRAMS

The program "Q8MC" was used both to collect and to process data from the mass spectrometer.

Program "PROG.ZSM" is the collection of machine code routines which controlled the interface to the mass spectrometer. The listing is divided up into sections which correspond to the flow diagram shown in fig. 2.5. PROG.ZSM was "called" from program Q8MC.

The determination of rate constants for product formation, using the "C/B" method described in chapter 5, was carried out using programs such as "CCALC2".

```

5 ?CHR$(17)
10 ?::?:?:?:?
15 ?"      Q8 Data Collection & Processing"
20 ?"          Program"
25 ?::?:?:?:?"Version 5 --for eight data channels,"
30 ?::?"using machine code routine for reading"
35 ?::?"data":?:?:?:?"Run with patched BASIC"
40 ?"-----"
45 ?::?:?:?:?"          Written by C.E.Dean May '81."
50 ?::?
55 Z=GET(200):IF Z=0 GOTO 60
60 ?::?:?:?:?:?:?:?:?:?:?:?:?:?:?:?:?:?:?:?:?:?:?
65 GOTO 160
70 CLEAR
72 REM TAKE IN DATA FROM Q8
75 DIM Z(3000)
80 INPUT"Name of data file":A$
85 CREATE#10,A$
90 QUOTE#10,34
95 N=100:REM Number of scans.
100 N=N*8
105 ?"Start Q8"
107 REM CALL MACHINE CODE ROUTINE
110 CALL &3A0F,VARADR(Z(1)),N
115 A=(256*PEEK(&3BB3))+PEEK(&3BB2)
120 A=A*2
125 INPUT"Temp/C, Pressure, Scan/s";TEMP,PRES,SCAN
130 PRINT#10,TEMP,PRES,SCAN
135 ?"Writing data to disc"
140 FOR I=1 TO A
145 PRINT#10,Z(I)
150 NEXT I
155 CLOSE#10
160 ?"Type a P to process"
165 ?" or an R to record a run"
170 INPUT A$
175 IF A$="P" GOTO 190
180 IF A$="R" GOTO 70
185 GOTO 160
187 REM START OF PROCESSING ROUTINES
190 CLEAR
195 CALL "RESOLUTION",0,2:GRAPH0
200 DIM P(8,10),T(8,10),PEAK(800),TIME(800)
205 DIM F(20),LPEAK(800),K(800),T9(800)
207 REM READ IN DATA
210 INPUT"Name of data file":D$
215 IF LOOKUP(D$)(>)0 THEN 230
220 ?"No file of that name! Try again"
225 GOTO 210
230 OPEN#10,D$
235 ON EOF GOTO 285
240 INPUT#10,TEMP,PRES,SCAN
245 FOR J=1 TO 10
247 REM CALCULATE THE START TIME
250 INPUT#10,P1,T1,P2,T2,P3,T3,P4,T4,P5,T5,P6,T6,P7,T7,P8,T8
255 P(1,J)=P1:T(1,J)=T1/100:P(2,J)=P2:T(2,J)=T2/100
260 P(3,J)=P3:T(3,J)=T3/100:P(4,J)=P4:T(4,J)=T4/100
265 P(5,J)=P5:T(5,J)=T5/100:P(6,J)=P6:T(6,J)=T6/100

```

```
270 P(7,J)=P7:T(7,J)=T7/100:P(8,J)=P8:T(8,J)=T8/100
275 NEXT J
280 GOTO 290
285 ?"Less than 10 data points."
290 BASES=4
295 M=8:N=BASES+(0.1/SCAN)
300 N1=INT(N+1)
305 NA=INT(N)
310 F=N-NA
315 TSTART=T(M,NA)+((T(M,N1)-T(M,NA))*F)
320 INPUT"Process which channel":C
322 REM READ IN DATA AND SUBTRACT AVERAGE BASELINES
325 IF C=18 GOTO 1865
330 IF C>8 GOTO 320
335 IF C<=0 GOTO 320
340 OPEN#10,D#
345 NUMBER=0
350 ON EOF GOTO 545
355 INPUT#10,TEMP,PRES,SCAN
360 I=0
365 INPUT#10,P1,T1,P2,T2,P3,T3,P4,T4,P5,T5,P6,T6,P7,T7,P8,T8
370 I=I+1
375 G=I-1
380 NUMBER=NUMBER+1
385 IF C=1 GOTO 425
390 IF C=2 GOTO 440
395 IF C=3 GOTO 455
400 IF C=4 GOTO 470
405 IF C=5 GOTO 485
410 IF C=6 GOTO 500
415 IF C=7 GOTO 515
420 IF C=8 GOTO 530
425 PEAK(I)=P1:TIME(I)=T1/100
430 IF TIME(I)<TIME(G) THEN TIME(I)=TIME(I)+250
435 GOTO 365
440 PEAK(I)=P2:TIME(I)=T2/100
445 IF TIME(I)<TIME(G) THEN TIME(I)=TIME(I)+250
450 GOTO 365
455 PEAK(I)=P3:TIME(I)=T3/100
460 IF TIME(I)<TIME(G) THEN TIME(I)=TIME(I)+250
465 GOTO 365
470 PEAK(I)=P4:TIME(I)=T4/100
475 IF TIME(I)<TIME(G) THEN TIME(I)=TIME(I)+250
480 GOTO 365
485 PEAK(I)=P5:TIME(I)=T5/100
490 IF TIME(I)<TIME(G) THEN TIME(I)=TIME(I)+250
495 GOTO 365
500 PEAK(I)=P6:TIME(I)=T6/100
505 IF TIME(I)<TIME(G) THEN TIME(I)=TIME(I)+250
510 GOTO 365
515 PEAK(I)=P7:TIME(I)=T7/100
520 IF TIME(I)<TIME(G) THEN TIME(I)=TIME(I)+250
525 GOTO 365
530 PEAK(I)=P8:TIME(I)=T8/100
535 IF TIME(I)<TIME(G) THEN TIME(I)=TIME(I)+250
540 GOTO 365
545 TPEAK=0
550 FOR I=1 TO BASES
```

```

555 TPEAK=TPEAK+PEAK(I)
560 NEXT I
565 AVBASE=INT((TPEAK/BASES)+0.5)
570 ??:?:?"Av Baseline=";AVBASE
575 FPEAK=BASES+1
580 FOR I=FPEAK TO NUMBER
585 PEAK(I)=AVBASE-PEAK(I)
590 J=I-BASES
595 PEAK(J)=PEAK(I)
600 TIME(J)=(TIME(I)-TSTART)
605 TIME(J)=INT((TIME(J)*1000)+0.5):TIME(J)=TIME(J)/1000
610 NEXT I
615 NUMBER=NUMBER-BASES
620 ?CHR$(19)
625 INPUT"Printer list Y/N";A$
630 IF A$(">")"Y" GOTO683
635 PRINTER 4,4
640 INPUT"Is Printer on? Y/N";A$
645 IF A$(">")"Y" GOTO 685
650 LPRINT:LPRINT:LPRINT:LPRINT:LPRINT
655 LPRINT"PEAK HT.      TIME"
660 FOR I=1 TO NUMBER
665 LPRINT PEAK(I),TIME(I):NEXT I
670 LPRINT:LPRINT:LPRINT:LPRINT:LPRINT
675 LPRINT:LPRINT:LPRINT
680 GOTO 705
683 ?CHR$(19)
685 ??:?:?:?"PEAK HT.      TIME"
690 FOR I=1 TO NUMBER
695 ?PEAK(I),TIME(I):NEXT I
700 ??:?:?:?:?:?
705 ?"You have a choice,PLOT,LOGS,"
710 ?"RESTART,ARRH,RORP or STOP"
715 INPUT B$
720 IF B$="PLOT" THEN GOTO 755
725 IF B$="LOGS" THEN GOTO 845
730 IF B$="ARRH" THEN GOTO 1515
735 IF B$="RORP" THEN CALL "CLEAR":GOTO 160
740 IF B$="RESTART" THEN GOTO 320
745 IF B$="STOP" THEN GRAPH0:?CHR$(12):STOP
750 ?"Illegal responce! Use capital letters.":?:?:?:GOTO 705
754 REM PLOT ROUTINE "PK HT vs TIME"
755 ??:?:?:?:?
760 INPUT "How many points ";N
765 IF N>NUMBER THEN N=NUMBER
770 MAX=PEAK(1):MIN=PEAK(1)
775 FOR I=1 TO N
780 IF MAX<PEAK(I) THEN MAX=PEAK(I)
785 IF MIN>PEAK(I) THEN MIN=PEAK(I)
790 NEXT I
795 IF MIN<0 THEN ?"-ve peak at beginning"
800 KX=315/TIME(N):KY=190/(MAX-MIN)
805 GOSUB 1200
810 FOR I=1 TO N
815 X=TIME(I)*KX:Y=(PEAK(I)-MIN)*KY
820 CALL "PLOT",X,Y,3
825 NEXT I
830 INPUT"Replot ? Y/N",A$

```

```
835 IF A$="Y" GOTO 755
840 CALL "CLEAR":GRAPH0:GOTO 705
844 REM LOGS ROUTINE; PLOTS "Ln PK HT vs TIME"
845 ??:?:?:?:?
850 FOR I=1 TO NUMBER
855 IF PEAK(I)=0 THEN LPEAK(I)=0:GOTO865
860 LPEAK(I)=LOG(PEAK(I))
865 NEXT I
870 INPUT"Do you want printer listing? Y/N",A$
875 IF A$("<")"Y" GOTO 927
880 INPUT"Is printer on? Y/N",A$
885 IF A$("<")"Y" GOTO 927
890 PRINTER 4,4
895 LPRINT:LPRINT:LPRINT:LPRINT:LPRINT
900 LPRINT"Ln pk. ","Time"
905 FOR I=1 TO NUMBER
910 LPRINT LPEAK(I),TIME(I)
915 NEXT I
920 LPRINT:LPRINT:LPRINT:LPRINT:LPRINT
925 GOTO 955
927 ?CHR$(19)
930 ?:"Ln pk. ","Time"
935 FOR I=1 TO NUMBER
940 ?LPEAK(I),TIME(I)
945 NEXT I
950 ??:?:?
955 INPUT"Plot which points";N3,N4
960 IF N4>NUMBER THEN N4=NUMBER
965 IF N3=>NUMBER GOTO 955
970 MAX=0:MIN=30
975 FOR I=N3 TO N4
980 IF MAX<LPEAK(I) THEN MAX=LPEAK(I)
985 IF MIN>LPEAK(I) THEN MIN=LPEAK(I)
990 NEXT I
995 KX=315/(TIME(N4)-TIME(N3))
1000 KY=190/(MAX-MIN)
1005 GOSUB 1200
1010 FOR I=N3 TO N4
1015 X=(TIME(I)-TIME(N3))*KX
1020 Y=(LPEAK(I)-MIN)*KY
1025 CALL "PLOT",X,Y,3
1030 NEXT I
1035 INPUT"Do you want least squares fit? Y/N",A$
1040 IF A$("<")"Y" GOTO 1160
1045 ?:"Points"N3"to"N4"are plotted"
1050 ?:"INPUT"Fit between which points";M1,M2
1055 IF M2>NUMBER THEN M2=NUMBER
1060 IF M1=>NUMBER GOTO 1045
1065 INPUT"Miss out how many points";F
1070 IF F=0 GOTO 1100
1075 FOR I=1 TO F
1080 INPUT"Miss point number=";F(I)
1085 IF F(I)>M2 THEN F(I)=0
1090 IF F(I)<M1 THEN F(I)=0
1095 NEXT I
1100 GOSUB 1230:REM L.S.F ROUTINE
1102 REM PLOT L.S.F. LINE
1105 X1=0:Y1=(GRAD*TIME(N3))+INCT
```

```
1110 Y1=(Y1-MIN)*KY
1115 X2=315
1120 Y2=(GRAD*TIME(N4))+INCT
1125 Y2=(Y2-MIN)*KY
1130 CALL "PLOT",X1,Y1,-2
1135 CALL "LINE",X2,Y2,-2
1140 ?" K =" ; -GRAD "+/-" ; A1 "s(-1)"
1145 ?"Intercept=" ; EXP(INCT) "+/-" EXP(B1)
1150 INPUT "Try another line? Y/N",A#
1155 IF A#="Y" GOTO 1185
1160 INPUT "Replot LOGS? Y/N",A#
1165 IF A#="Y" GOTO 955
1170 INPUT "Save K, T, P Y/N",A#
1175 IF A#="Y" GOTO 1405
1180 CALL "CLEAR":GRAPH0:GOTO 705
1185 CALL "PLOT",X1,Y1,-2
1190 CALL "LINE",X2,Y2,-2
1195 GOTO 1045
1200 GRAPH1:CALL "RESOLUTION",0,2
1205 CALL "PLOT",318,0,1
1210 CALL "LINE",0,0
1215 CALL "LINE",0,191
1220 RETURN
1225 END
1227 REM "LEAST SQUARES FIT" ROUTINE
1230 FOR I=M1 TO M2
1235 T9(I)=TIME(I):K(I)=LPEAK(I)
1240 NEXT I
1245 N1=((M2-M1)+1)-F
1250 S1=0:S2=0:S3=0:S4=0
1255 FOR I=M1 TO M2
1260 IF F=0 GOTO 1280
1265 FOR J=1 TO F
1270 IF I=F(J) GOTO 1300
1275 NEXT J
1280 S1=S1+T9(I)
1285 S2=S2+K(I)
1290 S3=S3+T9(I)*K(I)
1295 S4=S4+T9(I)*T9(I)
1300 NEXT I
1305 C1=N1*S4-S1*S1
1310 GRAD=(N1*S3-S1*S2)/C1
1315 INCT=(S2*S4-S1*S3)/C1
1320 IF N1-2=0 GOTO 1390
1325 Z1=0
1330 FOR I=M1 TO M2
1335 IF F=0 GOTO 1355
1340 FOR J=1 TO F
1345 IF I=F(J) GOTO 1365
1350 NEXT J
1355 D1=GRAD*T9(I)+INCT-K(I)
1360 Z1=Z1+D1*D1
1365 NEXT I
1370 A1=SQR(N1*Z1/((N1-2)*C1))
1375 B1=SQR(S4*Z1/((N1-2)*C1))
1380 RETURN
1385 END
1390 A1=0:B1=0
```

```
1395 RETURN
1400 END
1402 REM ROUTINE TO SAVE K & T ON SEPARATE FILE FOR ARR.H. PLOT
1405 K1=-GRAD:T1=TEMP:P1=PRES
1410 INPUT"Name of Arrh data file";R#
1415 IF LOOKUP(R#)=0 GOTO 1485
1420 RENAME "LOCAL",R#
1425 OPEN#10,"LOCAL"
1430 CREATE#10,R#
1435 QUOTE#10,34
1440 ON EOF GOTO 1460
1445 INPUT#10,K,T,P
1450 PRINT#10,K,T,P
1455 GOTO 1445
1460 ERASE "LOCAL"
1465 PRINT#10,K1,T1,P1
1470 CLOSE#10
1475 CALL "CLEAR":GRAPH0
1480 GOTO 705
1485 CREATE#10,R#
1490 QUOTE#10,34
1495 PRINT#10,K1,T1,P1
1500 CLOSE#10
1505 CALL "CLEAR":GRAPH0
1510 GOTO 705
1512 REM ARR.H. PLOT ROUTINE
1515 CLEAR
1520 DIM K(200),T9(200)
1525 INPUT"Name of Arrh data file ";R#
1530 IF LOOKUP(R#)=0 THEN ?"No file":GOTO 1525
1535 OPEN#10,R#
1540 NUMBER=0
1545 KL=0.002
1550 ?"K Leak=";KL
1555 ?"SET AT LINE 6555"
1560 ON EOF GOTO 1590
1565 INPUT#10,K1,T1,P
1570 NUMBER=NUMBER+1
1575 K(NUMBER)=LOG(K1-KL)
1580 T9(NUMBER)=1000/(T1+273.0)
1585 GOTO 1565
1590 FOR J=1 TO (NUMBER-1)
1595 FOR L=(J+1) TO NUMBER
1600 IF T9(L)>T9(J) GOTO 1620
1605 B=T9(L):C=K(L)
1610 T9(L)=T9(J):K(L)=K(J)
1615 T9(J)=B:K(J)=C
1620 NEXT L
1625 NEXT J
1630 INPUT"Plot which points";N3,N4
1635 IF N4>NUMBER THEN N4=NUMBER
1640 MAX=-100:MIN=100
1645 FOR J=N3 TO N4
1650 IF K(J)>MAX THEN MAX=K(J)
1655 IF K(J)<MIN THEN MIN=K(J)
1660 NEXT J
1665 KX=315/(T9(N4)-T9(N3))
1670 KY=190/(ABS(MAX-MIN))
```

```
1675 GOSUB 1200
1680 FOR J=N3 TO N4
1685 X=(T9(J)-T9(N3))*KX
1690 Y=ABS((K(J)-MIN)*KY)
1695 CALL "PLOT",X,Y,3
1700 NEXT J
1705 INPUT"Do you want least squares fit Y/N",A#
1710 IF A#(">")"Y" GOTO 1835
1715 ?:"Points"N3"to"N4"are plotted"
1720 ?:"INPUT"Fit between which points";M1,M2
1725 IF M2>NUMBER THEN M2=NUMBER
1730 IF M1)= NUMBER GOTO 1715
1735 INPUT"Miss out how many points";F
1740 IF F=0 GOTO 1770
1745 FOR J=1 TO F
1750 INPUT"Miss point number:";F(J)
1755 IF F(J)>M2 THEN F(J)=0
1760 IF F(J)<M1 THEN F(J)=0
1765 NEXT J
1770 GOSUB 1245
1771 REM PLOT L.S.F. LINE
1775 X1=0
1780 Y1=(GRAD*T9(N3))+INCT
1785 Y1=ABS(Y1-MIN)*KY
1790 X2=315
1795 Y2=(GRAD*T9(N4))+INCT
1800 Y2=ABS(Y2-MIN)*KY
1805 CALL "PLOT",X1,Y1,-2
1810 CALL "LINE",X2,Y2,-2
1815 ?"E=";(-GRAD*8.314)" +/- "(A1*8.314)"KJ. mol (-1)"
1820 ?"Log A=";INCT/2.303"+/-"B1/2.303
1825 INPUT"Try another line Y/N",A#
1830 IF A#="Y" GOTO 1850
1835 INPUT"Replot Arrh graph? Y/N",A#
1840 IF A#="Y" GOTO 1630
1845 CALL "CLEAR":GRAPH0:GOTO 705
1850 CALL "PLOT",X1,Y1,-2
1855 CALL "LINE",X2,Y2,-2
1860 GOTO 1715
1863 REM PROCESS ALL 8 Q8 CHANNELS
1865 ON EOF GOTO 1915
1870 I=0:BASES=32
1875 OPEN#10,D#
1880 INPUT#10,TEMP,PRES,SCAN
1885 I=I+1
1890 INPUT#10,PEAK(I),TIME(I)
1895 TIME(I)=TIME(I)/100
1900 IF TIME(I)<TIME(I-1) THEN TIME(I)=TIME(I)+250
1905 NUMBER=I
1910 GOTO 1885
1915 GOTO 545
1917 REM LIST Q8 DATA ON PRINTER
1920 INPUT"Name of data file";A#
1925 IF LOOKUP(A#)=0 GOTO 1935
1930 GOTO 1940
1935 ?"No file. Try again":GOTO 1910
1940 OPEN#10,A#
1942 PRINTER 4,4
```

```
1945 ON EOF GOTO 2010
1950 INPUT#10,TEMP,PRES,SCAN
1953 LPRINT CHR$(31)
1955 LPRINT TAB(10)"FILE NAME = ";A$
1960 LPRINT:LPRINT
1962 LPRINT CHR$(30)
1965 LPRINT "Temperature="TEMP"C";" Pressure=";PRES;
1966 LPRINT TAB(32)" Scan="SCAN"s"
1970 LPRINT:LPRINT
1972 LPRINT CHR$(29)
1975 LPRINT TAB(5);"CH 1";TAB(22);"CH 2";TAB(39);"CH 3";
1976 LPRINT TAB(56);"CH 4";
1980 LPRINT TAB(73);"CH 5";TAB(90);"CH 6";TAB(107);"CH 7";
1981 LPRINT TAB(124);"CH 8"
1985 LPRINT
1990 INPUT#10,P1,T1,P2,T2,P3,T3,P4,T4,P5,T5,P6,T6,P7,T7,P8,T8
1995 LPRINT P1;TAB(8);T1;TAB(18);P2;TAB(25);T2;TAB(35);P3;
1996 LPRINT TAB(42);T3;TAB(52);P4;TAB(59);T4;
2000 LPRINT TAB(69);P5;TAB(76);T5;TAB(86);P6;TAB(93);T6;
2001 LPRINT TAB(103);P7;TAB(110);T7;TAB(120);P8;TAB(126);T8
2005 GOTO 1990
2010 LPRINT:LPRINT:LPRINT:LPRINT:LPRINT:LPRINT
2015 GOTO 1920
```

*H BASIC CODE SUPPORT

SAVVAR	EQU	10FH	
BBUFV	EQU	118H	
	ORG	BBUFV	
	DEFW	BASEND	
	ORG	03A0FH	
<hr/>			
	EXX		
	POP	BC	1
	EXX		
<hr/>			
	POP	HL	2
	LD	(STOR1), HL	
<hr/>			
	LD	B, 0	
	LD	C, 0	3
	LD	(COUNT), BC	
<hr/>			
	LD	A, 0FH	
	OUT	(03H), A	
	OUT	(05H), A	
	OUT	(07H), A	
	OUT	(0AH), A	
	OUT	(0BH), A	
	LD	B, 04H	4
RSI:	LD	HL, RSI1	
	PUSH	HL	
	RETI		
RSI1:	DJNZ	RSI	
<hr/>			
	LD	A, 4FH	
	OUT	(05H), A	
	OUT	(07H), A	
	OUT	(0AH), A	
	LD	A, 07H	
	OUT	(05H), A	
	OUT	(07H), A	
	OUT	(0AH), A	
	LD	A, 0FH	
	OUT	(02), A	
	LD	A, 07H	
	OUT	(02), A	
	XOR	A	
	OUT	(00), A	
	LD	A, 255	
	OUT	(03H), A	5
	OUT	(0BH), A	
	LD	A, 01H	
	OUT	(03H), A	
	LD	A, 80H	
	OUT	(0BH), A	
	LD	A, 183	
	OUT	(03H), A	
	OUT	(0BH), A	
	LD	A, 254	
	OUT	(03H), A	
	LD	A, 7FH	
	OUT	(0BH), A	
	LD	A, INTADR MOD 256	
	OUT	(03H), A	
	LD	A, INTAR MOD 256	
	OUT	(0BH), A	

```

LD      A, 0
OUT     (0CH), A
LD      A, 7FH
OUT     (0CH), A
OUT     (0DH), A
OUT     (0EH), A
OUT     (0FH), A
LD      A, 250
OUT     (0CH), A
LD      A, 05H
OUT     (0DH), A
LD      A, 64H
OUT     (0EH), A
LD      A, 250
OUT     (0FH), A
-----
IM2
LD      A, INTADR/256
LD      I, A
EI
-----
IN      A, (04H)
IN      A, (05H)
IN      A, (08H)
IN      A, (0EH)
-----
LOOP:  IN      A, (0FH)
LD      B, A
LD      A, 250
SUB     B
LD      (TIME1), A
JR      LOOP
-----
RPORTS: IN      A, (0EH)
LD      B, A
LD      A, 64H
SUB     B
LD      (TIME2), A
IN      A, (0FH)
LD      B, A
LD      A, 250
SUB     B
LD      B, A
LD      A, (TIME1)
CP      B
JR      Z, READ
LD      A, B
LD      (TIME1), A
IN      A, (0EH)
TIME:  LD      B, A
LD      A, 64H
RPT:   SUB     B
LD      (TIME2), A
-----
READ:  IN      A, (08H)
AND     0FH
LD      (STOR), A
IN      A, (08H)
AND     240
SRL     A
SRL     A
SRL     A
SRL     A

```

6

7

8

9

10

11

```

LD      H, 0AH
LD      E, A
CALL    MULT
LD      A, (STOR)
ADD     A, L
LD      (STOR), A
IN      A, (05H)
AND     0FH
LD      E, A
LD      H, 64H
CALL    MULT
LD      A, (STOR)
ADD     A, L
JR      NC, SKIP
INC     H
SKIP:   LD      L, A
LD      (STOR), HL
IN      A, (05H)
AND     240
SRL     A
SRL     A
SRL     A
SRL     A
LD      H, 0AH
LD      E, A
CALL    MULT
LD      H, 64H
LD      E, L
CALL    MULT
LD      DE, (STOR)
ADD     HL, DE
LD      A, H
LD      B, L
LD      HL, (STOR1)
CALL    SAVVAR
-----
LD      HL, (STOR1)
IN      A, (04H)
SLA     A
JR      C, TIME
INC     HL
INC     HL
LD      A, (HL)
ADD     A, 80H
LD      (HL), A
JR      SKIP4
TIME:   INC     HL
SKIP4:  INC     HL
INC     HL
LD      (STOR1), HL
-----
LD      A, (TIME1)
LD      E, A
LD      H, 64H
CALL    MULT
LD      A, (TIME2)
ADD     A, L
JR      NC, SKIP3
INC     H

```

12

13

SKIP3:	LD	B, A	
	LD	A, H	
	LD	HL, (STOR1)	
	CALL	SAVVAR	
	LD	HL, (STOR1)	
	INC	HL	
	INC	HL	14
	INC	HL	
	INC	HL	
	LD	(STOR1), HL	
	EX	AF, AF	
	EXX		
	XOR	A	
	DEC	BC	
	CP	C	
	JR	NZ, CONT	
	CP	B	
	JR	NZ, CONT	15
	EX	AF, AF	
	EXX		
	LD	HL, (COUNT)	
	INC	HL	
	LD	(COUNT), HL	
STOP:	POP	HL	
	RETI		
CONT:	EX	AF, AF	
	EXX		
	LD	HL, (COUNT)	16
	INC	HL	
	LD	(COUNT), HL	
	LD	A, 0	
	CP	H	
	JR	NZ, CONT1	
	LD	A, 20H	17
	CP	L	
	JR	NZ, CONT1	
	CALL	OPEN	
CONT1:	EI		
	RETI		
MULT:	LD	B, 00H	
	LD	D, 00H	
	LD	L, D	
SKIP2:	ADD	HL, HL	18
	JR	NC, SKIP1	
	ADD	HL, DE	
SKIP1:	DJNZ	SKIP2	
	RET		
OPEN:	LD	A, 90H	
	OUT	(0), A	20
	RET		
	ORG	03BASH	
INTADR:	DEFW	STOP	
INTAR:	DEFW	RPORTS	
STOR:	DEFS	2H	
STOR1:	DEFS	2H	
TIME1:	DEFS	1H	
TIME2:	DEFS	1H	
COUNT:	DEFS	2H	

BASEND: DEFB 0

```

10 DIM P1(1000),P2(1000),TIME(1000),R(1000),C(1000)
20 INPUT"Sensitivity factor prod/reactant=",G
30 INPUT"Reactant gain= ",G1
40 INPUT"Product gain= ",G2
50 ?"Names of data files --- reactant first."
60 INPUT A$,B$
70 IF LOOKUP(A$)=0 THEN 50
80 IF LOOKUP(B$)=0 THEN 50
100 OPEN#10,A$
110 INPUT#10,TEMP,PRES,SCAN
120 J=0
130 ON EOF GOTO 190
140 J=J+1
150 INPUT#10,P1(J),TIME(J)
160 P1(J)=P1(J)/G1
170 TIME(J)=TIME(J)/100
180 GOTO 140
190 N3=J
200 OPEN#10,B$
210 INPUT#10,TEMP,PRES,SCAN
220 I=0
230 ON EOF GOTO 280
240 I=I+1
250 INPUT#10,P2(I),T9
260 P2(I)=P2(I)/G2
270 GOTO 240
280 N3=N3-2
290 R(1)=0
300 FOR I=1 TO N3
310 IF P1(I)=0 THEN R(I)=0:GOTO 330
320 R(I)=P2(I)/P1(I)
330 NEXT I
340 INPUT "Plot which points" :N1,N2
350 IF N2>N3 THEN N2=N3
360 MAX=0:MIN=10000
370 FOR I=N1 TO N2
380 IF R(I)<MIN THEN MIN=R(I)
390 IF R(I)>MAX THEN MAX=R(I)
400 NEXT I
410 GRAPH1:CALL "RESOLUTION",0,2
420 GOSUB 940
430 KX=315/(TIME(N2)-TIME(N1))
440 KY=190/(MAX-MIN)
450 GOSUB 1050
460 FOR I=N1 TO N2
470 X=(TIME(I)-TIME(N1))*KX
480 Y=(R(I)-MIN)*KY
490 CALL "PLOT",X,Y,-3
500 NEXT I
510 INPUT "k1=",K1
520 INPUT "k3=",K3
530 INPUT"K4=",K4
540 INPUT "k2=",K2
550 K=K2+K4
560 FOR I=N1 TO N2
570 T=TIME(I)
580 X=EXP(-K1*T)/((K-K1)*(K3-K1))
590 Y=EXP(-K*T)/((K1-K)*(K3-K))

```

```
600 Z=EXP(-K3*T)/(K1-K3)*(K-K3)
610 U=K2*(X+Y+Z)
620 X1=EXP(-K1*T)/(K-K1)
630 Y1=EXP(-K*T)/(K1-K)
640 V=X1+Y1
650 IF V=0 THEN C(I)=0:GOTO 570
660 C(I)=(U/V)*S
670 X=(TIME(I)-TIME(N1))*KX
680 Y=(C(I)-MIN)*KY
690 CALL "PLOT",X,Y,-2
700 NEXT I
710 D2=0:D1=0
720 INPUT"Shift curve Y/N":A$
730 IF A$="Y" GOTO 830
740 INPUT"New k2 Y/N":A$
750 IF A$="Y" THEN GOSUB 990 ELSE GOTO 770
760 GOTO 540
770 INPUT"Change other parameters Y/N":A$
780 IF A$="Y" THEN GOSUB 980 ELSE GOTO 800
790 GOTO 510
800 INPUT"New experimental plot Y/N":A$
810 IF A$="Y" GOTO 340
820 CALL "CLEAR":GRAPH0:90HR$(12):GOTO 50
830 INPUT"R/L, number ",D$,D
840 IF D=0 GOTO 720
850 D1=D2
860 GOSUB 990
870 IF D$="L" THEN D2=D2-D ELSE D2=D2+D
880 FOR I=N1 TO N2
890 X=((TIME(I)-TIME(N1))*KX)+D2
900 Y=(C(I)-MIN)*KY
910 CALL "PLOT",X,Y,-2
920 NEXT I
930 GOTO 830
940 CALL "PLOT",0,190,3
950 CALL "LINE",0,0
960 CALL "LINE",315,0
970 RETURN
980 D1=D2
990 FOR I=N1 TO N2
1000 X=((TIME(I)-TIME(N1))*KX)+D1
1010 Y=(C(I)-MIN)*KY
1020 CALL "PLOT",X,Y,-2
1030 NEXT I
1040 RETURN
1050 FOR I=1 TO 4
1060 Z=0.5*I
1070 Y=((Z*5)-MIN)*KY
1080 CALL "PLOT",0,Y,-2
1090 CALL "LINE",5,Y
1100 NEXT I
1110 FOR I=1 TO 20
1120 Z=1.0*I
1130 X=(Z-TIME(N1))*KX
1140 CALL "PLOT",X,0,-2
1150 CALL "LINE",X,3,-2
1160 NEXT I
1170 RETURN
```

REFERENCES

- 1 S. J. Hart, "Silicones and Industry", Murray, London, 1960.
R. J. H. Voorhoeve, "Organohalosilanes : Precursors to silicones", Elsevier, Amsterdam, 1967.
- 2 I. M. T. Davidson, J. Organomet. Chem., 1970, 24, 97.
- 3 I. M. T. Davidson, Quart. Rev., 1971, 25.
- 4 I. M. T. Davidson and M. E. Delf, J.C.S. Faraday I, 1976, 72, 1912.
- 5 I. M. T. Davidson and N. A. Ostah, J. Organomet. Chem., 1981, 206, 149.
- 6 M. Bowrey and J. H. Purnell, J. Amer. Chem. Soc., 1970, 92, 2594.
- 7 P. John and J. H. Purnell, J.C.S. Faraday I, 1973, 69, 1455.
- 8 W. H. Atwell and D. R. Weyenberg, Agnew. Chem. Int. Ed., 1969, 8, 469.
- 9 K. Shiina and M. Kumada, J. Org. Chem., 1958, 23, 139.
- 10 I. M. T. Davidson, J. Organomet. Chem., 1979, 170, 365.
- 11 I. M. T. Davidson and M. A. Ring, J.C.S. Faraday I, 1980, 76, 1520.
- 12 I. M. T. Davidson and A. V. Howard, J.C.S. Faraday I, 1975, 71, 69.
- 13 A. C. Baldwin, I. M. T. Davidson and M. D. Reed, J.C.S. Faraday I, 1978, 74, 2171.
- 14 I. M. T. Davidson, "Reaction Kinetics", Spec. Period. Rep., Chem. Soc., London, 1975.
- 15 C. G. Newman, H. E. O'Neal, M. A. Ring, F. Leska and N. Shipley, Internat. J. Chem. Kinetics, 1979, 11, 1167.
- 16 I. M. T. Davidson and C. A. Lambert, J.C.S. Chem. Comm., 1969, 1276.

- 17 R. Walsh, *Acc. Chem. Res.*, 1981, 14, 246.
- 18 S. W. Benson, "Thermochemical Kinetics", Wiley, New York, First Ed., 1968.
- 19 "Handbook of Chemistry and Physics", C.R.C. Press, Cleveland, 1974.
- 20 P. S. Neudorfl and O. P. Strausz, *J. Phys. Chem.*, 1978, 82, 241.
- 21 S. W. Benson, "Foundations of Chemical Kinetics", McGraw-Hill, New York, 1960, p. 349.
- 22 F. G. R. Gimblett, "Introduction to Kinetics of Chemical Chain Reactions", McGraw-Hill, New York, 1970.
- 23 S. W. Benson and G. N. Spokes, *J. Amer. Chem. Soc.*, 1967, 89, 2525.
S. W. Benson, D. M. Golden and G. N. Spokes, *Agnew. Chem. Int. Ed.*, 1973, 12, 534.
- 24 H. E. Gunning, M. A. Nay, O. P. Strausz and G. N. C. Woodall, *J. Amer. Chem. Soc.*, 1965, 87, 179.
- 25 S. W. Benson and D. M. Golden, *Chem. Rev.*, 1969, 69, 125.
- 26 B. S. Iseard and J. B. Pedley, "CATCH Tables for Silicon Compounds", University of Sussex, 1972.
- 27 I. M. T. Davidson and I. L. Stephenson, *J. Organomet. Chem.*, 1967, 7, 24.
- 28 a) F. W. Lampe and P. Potzinger, *J. Phys. Chem.*, 1970, 74, 719.
b) J. Krause, P. Potzinger and A. Ritter, *Z. Naturforsch.*, 1975, 30a, 347
- 29 B. G. Gowenloch and J. Stephenson, *J. Organomet. Chem.*, 1968, 13, 13.
- 30 L. D. Nichols, W. C. Steele and F. G. A. Stone, *J. Amer. Chem. Soc.*, 1962, 84, 4441.
W. C. Steele and F. G. A. Stone, *J. Amer. Chem. Soc.*, 1962, 84, 3599.
- 31 S. R. Gunn and L. G. Green, *J. Phys. Chem.*, 1961, 65, 779.

- 32 T. L. Allen, J. Phys. Chem., 1959, 31, 1039.
- 33 S. W. Benson and M. Luria, J. Amer. Chem. Soc., 1975, 97, 704.
S. W. Benson and M. Luria, J. Amer. Chem. Soc., 1975, 97, 3337.
S. W. Benson and M. Luria, J. Amer. Chem. Soc., 1975, 97, 3342.
- 34 M. J. Agarunov and S. N. Hajiev, J. Organomet. Chem., 1970, 22, 305.
- 35 D. Quane, J. Phys. Chem., 1971, 75, 2480.
- 36 Nat. Bur. Stand. (U.S) Tech. Note, 1968, 270.
- 37 I. M. T. Davidson, J. Organomet. Chem., 1979, 170, 365.
- 38 H. E. O'Neal and M. A. Ring, J. Organomet. Chem., 1981, 213, 419.
- 39 M. C. Flowers and L. E. Gusel'nikov, J.C.S. (B), 1968, 419.
- 40 L. E. Gusel'nikov, K. S. Konobeyevsky, N. S. Nametkin and V. M. Vdovin, Doklady Akad. Nauk SSSR, 1977, 235, 1086.
- 41 P. Boudjouk and L. H. Sommer, J.C.S. Chem. Comm., 1973, 54.
- 42 L. E. Gusel'nikov, N. S. Nametkin, R. L. Ushakova and V. M. Vdovin, Doklady Chem., 1971, 201, 1056.
- 43 D. N. Roark and L. H. Sommer, J.C.S. Chem. Comm., 1973, 167.
- 44 I. M. T. Davidson and I. T. Wood, J.C.S. Chem. Comm., 1982, 550.
- 45 I. M. T. Davidson, C. E. Dean and F. T. Lawrence, J.C.S. Chem. Comm., 1981, 52.
- 46 E. Bastian, P. Potzinger, A. Ritter, H.-P. Schuchmann, C. V. Sonntag and G. Weddle, Ber. Bunsenges. Phys. Chem., 1980, 84, 56.
- 47 R. Ahlrichs and R. Heinzmann, J. Amer. Chem. Soc., 1977, 99, 7452.
- 48 D. M. Hood and H. F. Schaefer III, J. Chem. Phys., 1978, 68, 2985.

- 49 M. S. Gordon, Chem. Phys. Let., 1978, 54, 9.
- 50 T. J. Barton, C. C. Chang, O. L. Chapman, J. Kolc, L. A. Lowe, M. L. Tumej and M. E. Tung, J. Amer. Chem. Soc., 1976, 98, 7844.
- 51 R. M. Irwin, J. Laane and J. R. Ohlsen, 173rd A.C.S. Nat. Meeting, New Orleans, U.S.A., 1977, Phys. 204.
- 52 I. M. T. Davidson, P. Potzinger and B. Reimann, Ber. Bunsenges. Phys. Chem., 1982, 86, 13.
- 53 N. M. Rodiguin and E. N. Rodiguina, "Consecutive Reactions", Van Nostrand, London, 1964.
- 54 G. Pannetier and P. Souchay, "Chemical Kinetics", Elsevier, Amsterdam, 1967.
- 55 E. S. Swinbourne, "Analysis of Kinetic Data", Nelson, London, 1971.
- 56 K. J. Laidler, "Reaction Kinetics, Vol. 1", Pergamon Press, Oxford, 1970.
- 57 I. M. T. Davidson and J. I. Matthews, J.C.S. Faraday I, 1981, 77, 2277.
- 58 S. W. Benson, "Thermochemical Kinetics", Wiley, New York, second edition, 1976.
- 59 P. Ciampa, I. M. T. Davidson, I. Rowland and R. J. Scampton, Unpublished results.
- 60 T. Kiang and R. N. Zare, J. Amer. Chem. Soc., 1980, 102, 4024.
- 61 I. M. T. Davidson, F. T. Lawrence and N. A. Ostah, J.C.S. Chem. Comm., 1980, 859.
- 62 I. M. T. Davidson and J. F. Thompson, J.C.S. Faraday I, 1976, 72, 1088.
- 63 I. M. T. Davidson, M. R. Jones and C. Pett, J.C.S. (B), 1967, 937.
- 64 R. R. Baldwin, M. W. M. Hisham and R. W. Walker, J.C.S. Faraday I, 1982, 78, 1615.

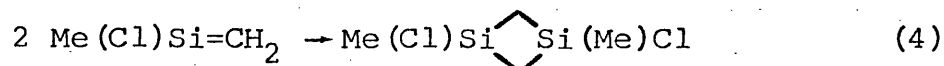
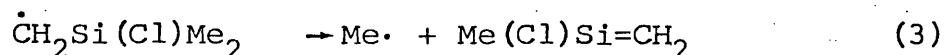
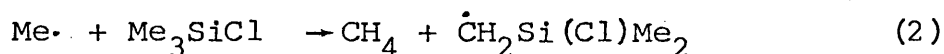
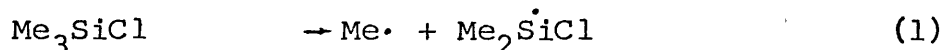
- 65 A. B. Trenwith, *Trans. Far. Soc.*, 1966, 62, 1538.
P. D. Pacey and J. H. Purnell, *J.C.S. Faraday I*, 1972, 68, 1472.
A. Burcat, R. W. Crossley, K. Scheller and B. G. Skinner, *Internat. J. Chem. Kinetics*, 1973, 5, 345.
- 66 P. T. Frangopol and K. U. Ingold, *J. Organomet. Chem.*, 1970, 25, C9.
- 67 K. U. Ingold and G. B. Watts, *J. Amer. Chem. Soc.*, 1972, 94, 491.
- 68 K. Y. Choo, P. P. Gaspar and A. D. Haizlip, *J. Amer. Chem. Soc.*, 1972, 94, 9032.
- 69 P. Cadman, G. M. Tilsey and A. F. Trotman-Dickenson, *J.C.S. Faraday I*, 1972, 68, 1849.
- 70 S. W. Benson and R. Hiatt, *Internat. J. Chem. Kinetics*, 1973, 5, 385.
R. S. Konar, R. M. Marshall and J. H. Purnell, *Internat. J. Chem. Kinetics*, 1973, 5, 1007.
- 71 R. M. Marshall, J. H. Purnell and P. D. Storey, *J.C.S. Faraday I*, 1976, 72, 85.
- 72 P. J. Robinson and K. A. Holbrook, "Unimolecular Reactions", Wiley, London, 1972, p239.

The Pyrolysis of some Methylchlorosilanes.

by

Christopher E. Dean

By analogy with the established mechanism for the low pressure pyrolysis of tetramethylsilane (TMS)¹, the decomposition of trimethylchlorosilane (3MCS) would be expected to proceed thus,

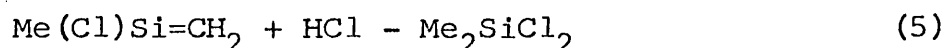


+ termination and other reactions involving silicon-centred radicals.

The dimeric product, if formed, could be useful as a precursor to long chain polymers containing $(-\text{Si}-\text{C}-)_n$ units.

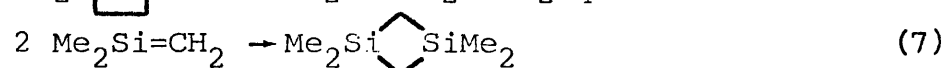
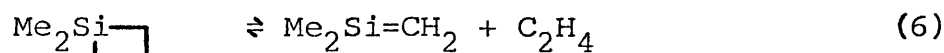
Thus, 3MCS was pyrolysed, at low pressure in a static system, using quadrupole mass spectrometry as the principal method of analysis. First order Arrhenius parameters given by $\log_{10} k = (17.03 \pm .34) - (366.5 \pm 7.2 \text{ KJ mol}^{-1})/2.303RT$ were measured for the decomposition, the activation energy being assigned to the silicon-methyl bond strength.

The dimeric product proposed above however, was not formed, dimethyldichlorosilane (2M2CS) being the major silicon-containing product. Since a small quantity of hydrogen chloride was invariably present in the experimental system, owing to some hydrolysis of the reactant by background water, it was suggested that the addition process,



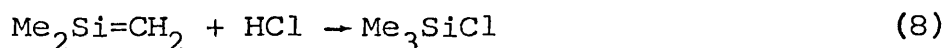
could prevent reaction (4). A series of experiments was devised to test this idea and it was shown to be a possible explanation.

The decomposition of 1,1-dimethyl-1-silacyclobutane (DMSCB) is well known².



From the co-pyrolysis of DMSCB with hydrogen chloride³ it was

found that the addition



is a very efficient process, reaction (7) being suppressed until most of the hydrogen chloride had been used up.

Since no competition between processes (7) and (8) could be observed, an unusual analysis method was devised, which involved a comparison of the "on-set time" for reaction (7) with the calculated amount of DMSCB decomposed. Computer simulation of the co-pyrolysis mechanism yielded values of $\log_{10} k_7 = (7.5 \pm .3) - (12 \pm 5 \text{ KJ mol}^{-1})/2.303 \text{ RT}$. The addition of hydrogen bromide to 1,1-dimethylsilaethene was also investigated.

Finally, the decomposition of dimethylchlorosilane (DMCS) and of methylchlorosilane (MDCS), was shown to proceed via a radical route, consistent with the proposed pyrolysis mechanism of trimethylsilane¹.

The co-pyrolysis of DMCS and of MDCS with sulphur hexafluoride provided evidence for the presence of silicon radicals, the hexafluoride being a good "trap" for such species.

- 1 A. C. Baldwin, I. M. T. Davidson and M. D. Reed, J. Chem. Soc. Faraday I, 1978, 74, 2171.
- 2 M. C. Flowers and L. E. Gusel'nikov, J. Chem. Soc. (B), 1968, 419.
- 3 I. M. T. Davidson, C. E. Dean and F. T. Lawrence, J. Chem. Soc. Chem. Comm., 1981, 52.